TENSION STIFFENING EFFECT IN GFRP REINFORCED CONCRETE ELEMENTS

A Thesis submitted for the degree of

Doctor of Philosophy in the faculty of engineering of

The University of Sheffield

by

Harsha Sooriyaarachchi

BSc.Eng.(SL), MEng. (Tokyo)

Department of Civil and Structural Engineering
The University of Sheffield
July 2006

.....To My Parents

ABSTRACT

The deflection of Glass Fibre Reinforced Polymer Reinforced Concrete (GFRP RC) is often the governing criterion for design. The lack of fundamental research particularly on the tension stiffening behaviour of GFRP RC has hindered both the development of fundamental equations to predict deflection and the use of nonlinear Finite Element (FE) analysis for predicting the structural behaviour of GFRP RC. This thesis investigates the tension stiffening effect of GFRP RC in an effort to improve the predictability of GFRP RC deformation behaviour. The study adopts a holistic approach for tension stiffening which considers the bond as the building block for tension stiffening modelling and tension stiffening as being a macroscopic representation of bond modelling.

In this study tension stiffening is experimentally evaluated first against more generic variables like concrete strength, reinforcement ratio and bar diameter. This is followed by a detailed study on bond between concrete and GFRP which results in the development of a strain distribution function to represent bond between cracks. This formed the basis for the development of a comprehensive model to analyse the tension stiffening behaviour of direct tension tests. After evaluating the tension stiffening test results against existing code-based formulations, the CEB-FIP model is recalibrated to represent the tension stiffening behaviour of GFRP RC, thereby providing a simplified means to evaluate tension stiffening behaviour of GFRP RC.

The successful implementation of the tension stiffening model is demonstrated through the prediction of deflection of flexural elements using a general nonlinear FE analysis package (ABAQUS) that uses the smeared crack approach to model the reinforced concrete behaviour.

Appropriate adjustments to the moment-curvature relationship of flexural elements to account for the effect of tension stiffening is also proposed, enabling better deflection predictions for the GFRP RC in flexure.

ACKNOWLEDGEMENTS

First and foremost I express my heartiest gratitude to my supervisors, the late Dr. Ewan Byars and Prof. Kypros Pilakoutas, for their untiring support during my study at the University of Sheffield. First it was Dr Byars who supported me in following my own research interest and in conducting my studies. Prof. Pilakoutas' enormous wealth of knowledge and experience in the field gave me a help into testing, shaping and publishing my research. I always relished opportunities Prof. Pilakoutas provided me to broaden my knowledge on FRP in construction and his kind friendly open door policy.

Special thanks are due to the all the technicians (Shane Smith, Paul Blackbourn, Chris Todd, and Jonathan Wood) in the heavy structures laboratory of the University of Sheffield for their continuous support during my experimental work. In particular, I gratefully acknowledge Paul Blackbourn and Shane Smith for their skills and support in developing the purpose built instrumentation and testing rig which required a high degree of precision.

My gratitude also extends to all the friends and colleagues of the concrete materials and structures research group especially Dr Maurizio Guadagnini, Dr Kyriacos Neocleous, Bruce Toroitich, Homayoon Sadeghi Pouya, Raed Al Sunna, Yanfei Che and Shahram Derogar.

Doug Gremel of Hughes Brothers Inc. is kindly acknowledged for providing the ASLAN 100 GFRP bars free of charge for the experimental work.

Grateful acknowledgements are also due to the ORS (Overseas Research Studentship) for their generosity in offering me the essential financial assistance for my study program at the University of Sheffield.

In addition, I would like to express my deepest gratitude and appreciation to all of my family members for their understanding and encouragement. Last, but not least, is my greatest gratitude to my wonderful wife for her unfailing support for the last three years in every aspect of life and for gifting us with our daughter.

TABLE OF CONTENT

LIST OF TABLES

LIST OF FIGURES

NOTATION

A_c - Area of concrete

A_{cr} - Area of cracked section

$A_{c,eff}$ - Equivalent direct tensile area of concrete in bending

A_e - Effective area of crack section

A_f - Area of FRP tensile reinforcement

A_g - Gross sectional area of concrete

a_0 -Initial crack length

b - Breadth of a tension or bending element

c - Concrete cover in flexural elements

$CTOD_c$ - Critical crack opening displacement

D, ϕ - Diameter of the bar

E_c - Modulus of elasticity of concrete

E_f - Modulus of elasticity of fibre reinforcement bar

E_s - Modulus of elasticity of steel

f'_c - Cylindrical compressive strength of concrete

f_{cu} - Cubic compressive strength of concrete

f_f - Stress of reinforcement bar at crack section used in the analysis of tension specimens according to the CEB-FIP model code

f_{fu} - Ultimate strength of the fibre reinforcement

f_{scr} - Tensile stress of the rebar at the first crack (CEB-FIP model code)

f_t - Tensile strength of concrete

f'_t - Tensile strength of concrete from direct tension test

f'_{tc} - Tensile strength of concrete from splitting cylinder test

f'_{td} - Dynamic tensile strength of concrete

f'_{tf} - Tensile strength of concrete in flexure

G - Shear Modulus

G_f - Fracture energy release rate

h - Height of a tension or bending element

I_{cr} - Second moment of area of a cracked section

I_e - Effective moment area of a section

I_g - Gross moment of area of a section

K_{IC} - Stress intensity factor at the crack tip

L_{cs} - Crack spacing

l_b - Bonded length

l_c - Composite length

l_d - De-bonded length

l_{di} - Damage length

l_t - Bond development length

M_{cr} - Bending moment at concrete cracking

M - Applied bending moment

n - Modular ratio

P - Applied normal load in tensile test or pull-out test

P_{cr} - Applied normal load at the occurrence of first crack

R - Fracture resistance

s - Slip

s_{end} - Slip at the loaded end of a pull out specimen

s_{free} - Slip at the free end of a pull out specimen

w - Crack width

$\bar{x}$ - Neutral axis depth

α_b - Bond dependent coefficient used for the calculation of deflection in ACI 440.1R-03

β_d - Reduction coefficient used in calculation of deflection in ACI 440.1R-03

Δ - Deflection

ΔE - Incremental energy

ΔU - Incremental displacement of the tension specimen

Δ_c - Elastic deflations calculated with $E_c I_c$

Δ_1 - Un-cracked state deflection of a bending element

Δ_2 - Cracked state deflection of a bending element

Σ - Circumference of the bar

ε_c - Concrete strain

ε_{cr} - Strain at the concrete cracking

ε_{cs} - Average strain of conventional steel reinforced concrete element in tension

ε_{cf} - Average strain of the fibre reinforced concrete element in tension

ε_f - Strain of fibre reinforcement

$\varepsilon_{f,cr}$ - Strain of the bar at the crack section

$\varepsilon_{f,t}$ - Strain of the bar at the end of the transfer length

$\varepsilon_{f,m}$ - Strain of the bar in the middle between cracks

ε_s - Strain of steel reinforcement

ε_1 - Strain in the first principal direction

ε_2 - Strain in the second principal direction

ε_3 - Shear strain

ρ - Reinforcement ratio

$\sigma_{ct,ave}$ - Average tensile stress of concrete between cracks

$\sigma_{ct,max}$ - Maximum tensile stress of concrete between cracks

σ_{cx} - Stress in the matrix

σ_{sx} - Stress in the bar

σ_1 - Stress in the first principal direction

σ_2 - Stress in the second principal direction

σ_3 - Shear stress

τ - Bond stress

$\bar{\tau}$ - Average bond stress

τ_{max} - Maximum bond stress

υ - Poison ratio

ψ_1 - Curvature of an un-cracked section

ψ_2 - Curvature of a fully cracked section

ψ_m - Intermediate curvature of a cracked section

CHAPTER 1

INTRODUCTION

1.1 Background

From the inception of Reinforced Concrete (RC), steel has been the main reinforcement material and it still is. However, corrosion of steel reinforcement, especially in aggressive environments, has been a considerable problem to the infrastructure. In Europe alone, the annual cost of repair and maintenance of the infrastructure is estimated to be over €30 billion, and in the United States, the overall costs associated with damage due to reinforcing steel corrosion were estimated at about $80 billion (Federal Highway Administrator 1997). Fig. 1-1 is an example of corrosion of steel reinforcement in RC structures exposed to aggressive environments.

Fig. 1-1 Example of reinforcement corrosion under aggressive environments (Federal Highway Administrator 1997)

Fibre Reinforced Polymer (FRP) reinforcements are now increasingly being used as alternative reinforcement for buildings and bridges, especially in corrosive environments (Pilakoutas, in Gdoutos et al. 2000). The use of FRP reinforcements is also inevitable for some special applications where the possibility of interference of

magnetic field prohibits the use of steel reinforcements, like the infrastructure for magnetic levitation trains and MRI scanning facilities.

Some of the FRP types like Carbon Fibre Reinforced Polymer (CFRP) cost several times more than conventional steel reinforcements. Glass Fibre Reinforced Polymer (GFRP) reinforcing bars are the cheapest alternative available today and are the most popular in construction. Fig. 1-2 below shows the use of GFRP in bridge deck construction.

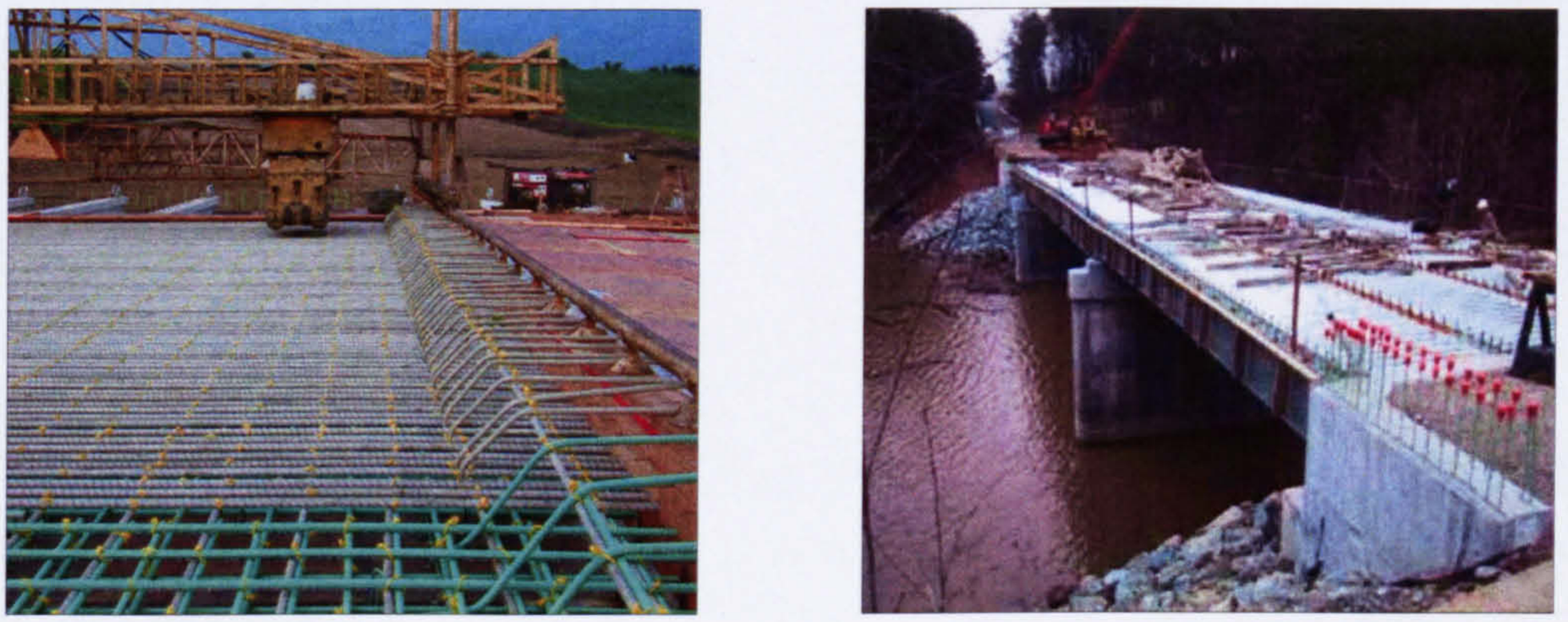

(a) (b)

Fig. 1-2 Use of GFRP in bridge deck construction ((a) 53rd Avenue Bridge- Bettendorf, IA, (b) Franklin county bridge Virginia) (Courtesy www.hughesbros.com)

GFRP bars come in different forms and are made by different manufacturers. They differ from each other in physical appearance, the type of glass fibres used and the type of resin used. Fig.1-3(a) shows the physical appearance of the GFRP used in this research and Fig.1-3(b) shows the tensile behaviour of the GFRP compared with steel reinforcement. The GFRP used in this study was supplied by Hughes Brothers Inc., and is of type 1 (commercial name ASLAN 100). Currently, it is one of the most widely used GFRP bars in construction.

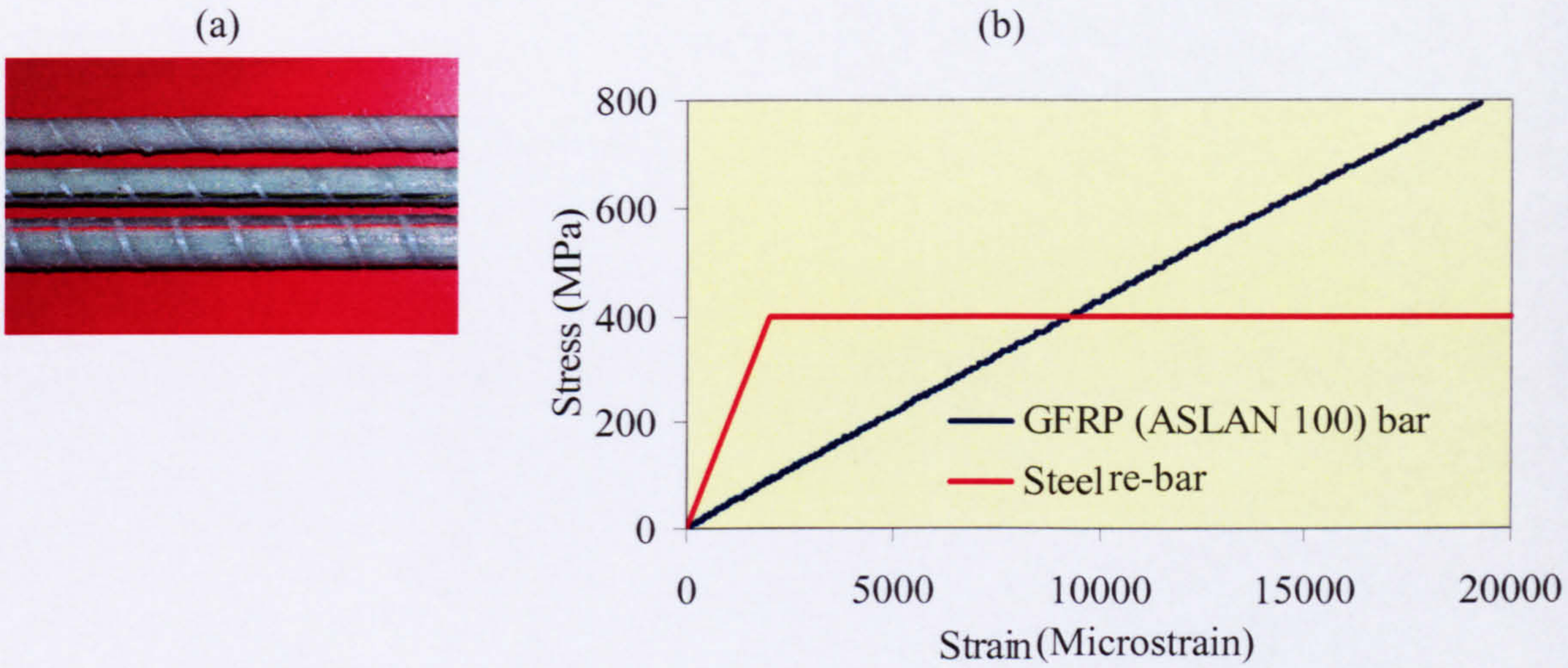

Fig. 1-3 Physical appearance of GFRP and tensile behaviour of GFRP compared to steel reinforcement.

From Fig.1-3 (b) it is clear that GFRP reinforcement has lower stiffness and higher strength compared to conventional steel reinforcement. This can make deflections and crack widths at service loads the governing criteria for design, making prediction of deflections, particularly at service loads, more important for GFRP RC than for steel reinforced concrete. In these instances, the contribution of concrete in the tension zone can be a controlling factor in determining both deflections and crack widths.

Despite concrete being a weak and brittle material in tension, concrete when reinforced seems to carry tension and provide additional stiffness to the overall behaviour even after cracking. This apparent ability of concrete to carry stresses in the tensile strain region is referred to as the "Tension Stiffening Effect" and its contribution to the overall structural behaviour is significant, especially at service loads. The tension stiffening effect of steel reinforced concrete is well researched and implemented in design and analysis of structural behaviour (Vecchio et al. 1985, Okamura et al. 1991, Gupta et al. 1990, Hsu et al. 1988). To account for the tension stiffening effect in the calculation of deflections of flexural elements, ACI 318-05, the code for steel reinforced concrete members, adopts a gradual reduction in stiffness of the reinforced concrete section from un-cracked state (I_g) to cracked state (I_{cr}). Fig. 1-4 below shows the proposed gradual reduction of stiffness for a section with a reinforcement ratio of 0.46%. In ACI 318-05, this gradual reduction of the stiffness in the section is accounted based on Branson's formulae (Branson D.E, 1977); detailed equations are given later in chapter 2.

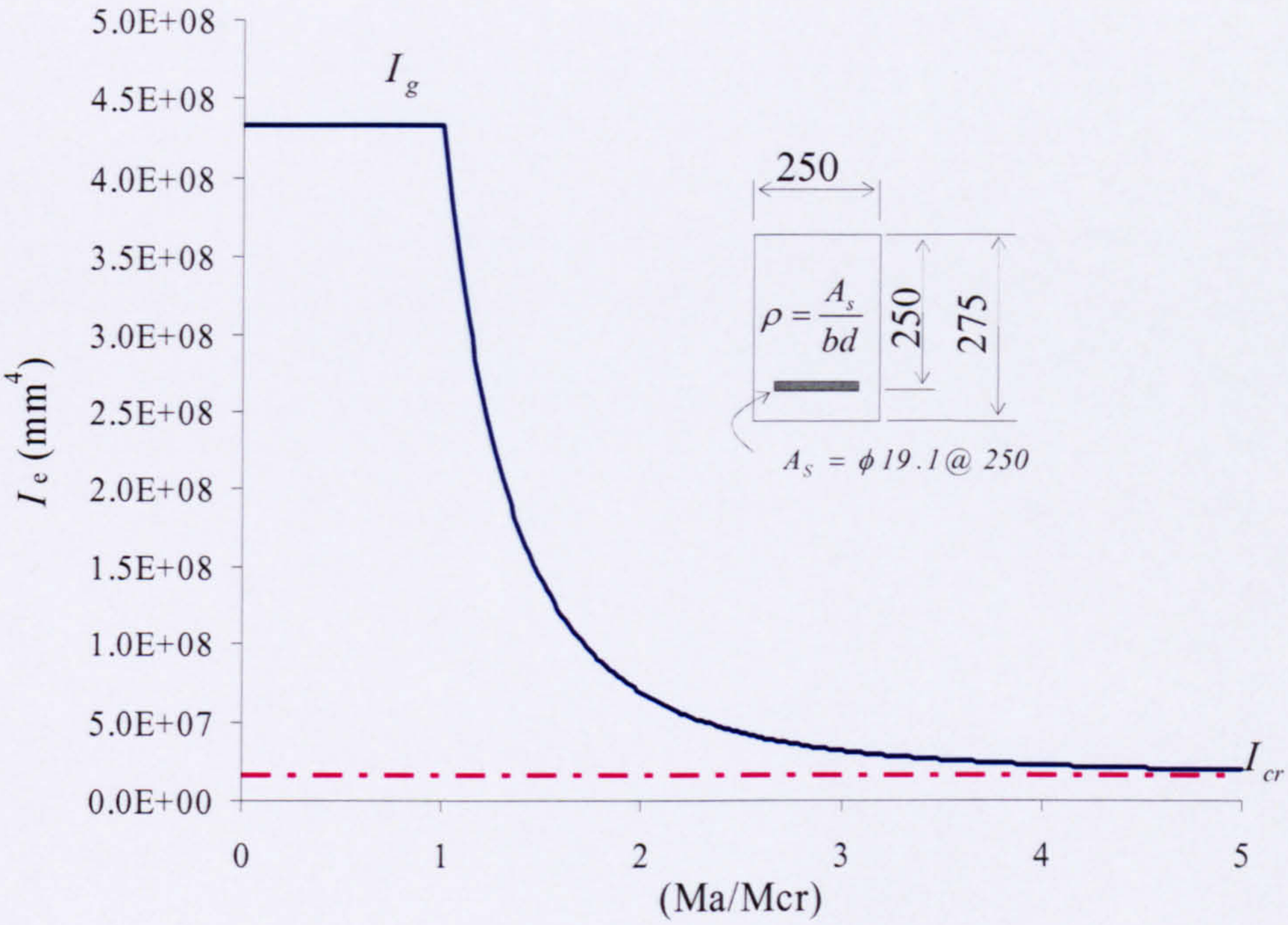

Fig. 1-4 Gradual reduction of stiffness adopted to account for tension stiffening effect

There are several design recommendations and guidelines for designing FRP reinforced concrete members including the JSCE (1997), ISIS (2001) and ACI (2003) (ACI 440.1R-03). The ACI design equations are based on the ACI 318-05 code for design of steel RC which currently is the most authoritative set of recommendations available. However, predictions of serviceability limit state performance of FRP RC members with these equations have been found to be un-conservative, and therefore deflections at service loads are underestimated, especially at low reinforcement ratios. Toutanji et al. (2003), summarised the works of Yost (1983), Masmoudi et al. (1998) and Benmokarane et al. (1995) as depicted in Fig. 1-5. The results showed that, as the reinforcement ratio decreases, the inaccuracy of deflection increases between the measured and predicted deflections (based on the Branson's formulae) of the FRP beams at service loads (50% maximum load).

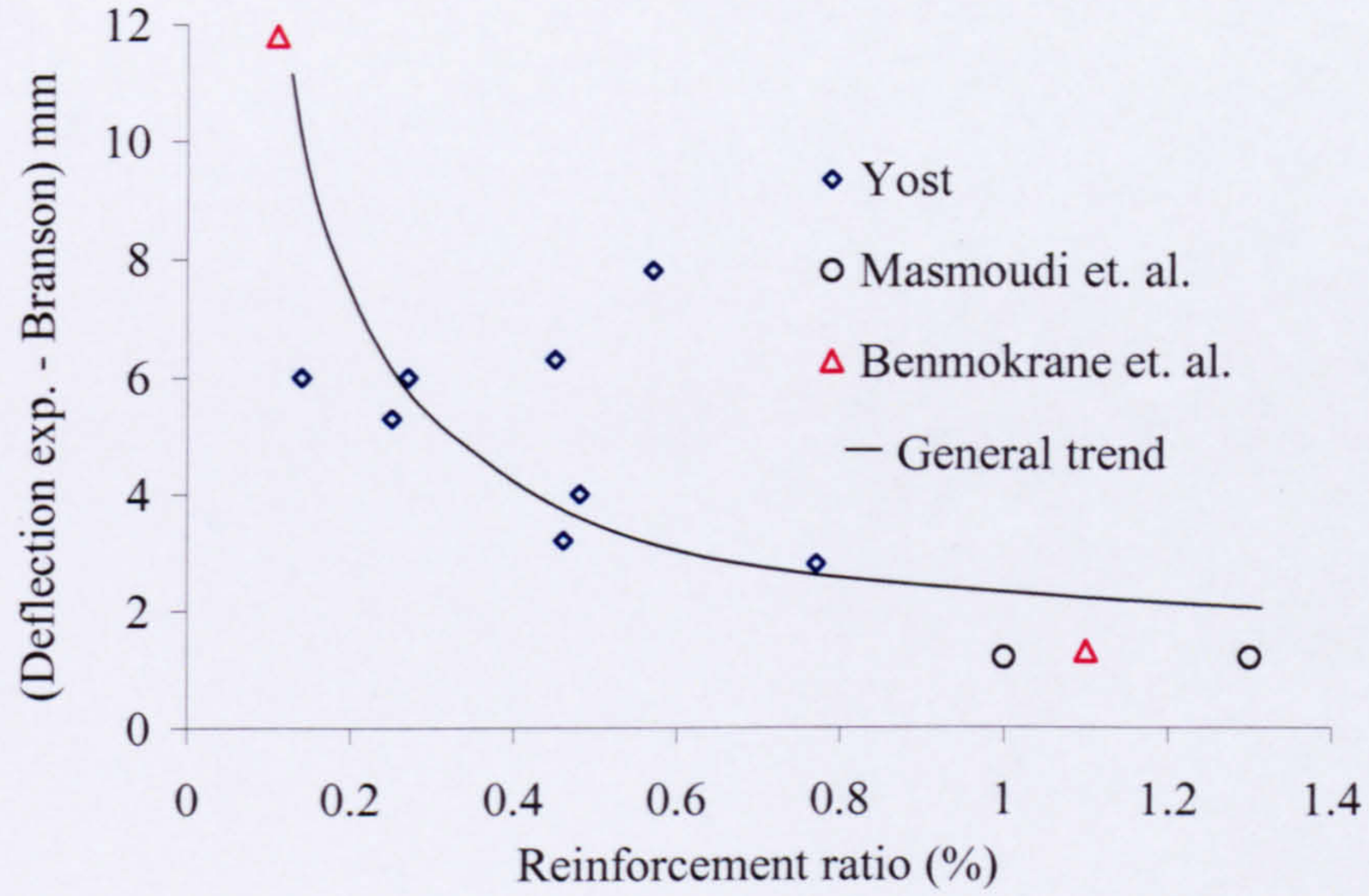

Fig. 1-5 Deflection inaccuracy versus reinforcement ratio (Reproduced from Toutanji et. al. 2003)

Abdalla (2002) illustrated even the ACI 440.1R-03 modification to Branson's equation is not adequate to predict deflections at low reinforcement ratios. As shown in Fig. 1-6 predictions of deflection based on the ACI 440.1R-03 equation did not compare well with the experimental results of Abdalla (2002): (a) slabs reinforced with GFRP "ISORODS" with 0.5% reinforcement ratio (b) beams reinforced with GFRP "ISORODS" with 0.6% reinforcement ratio.

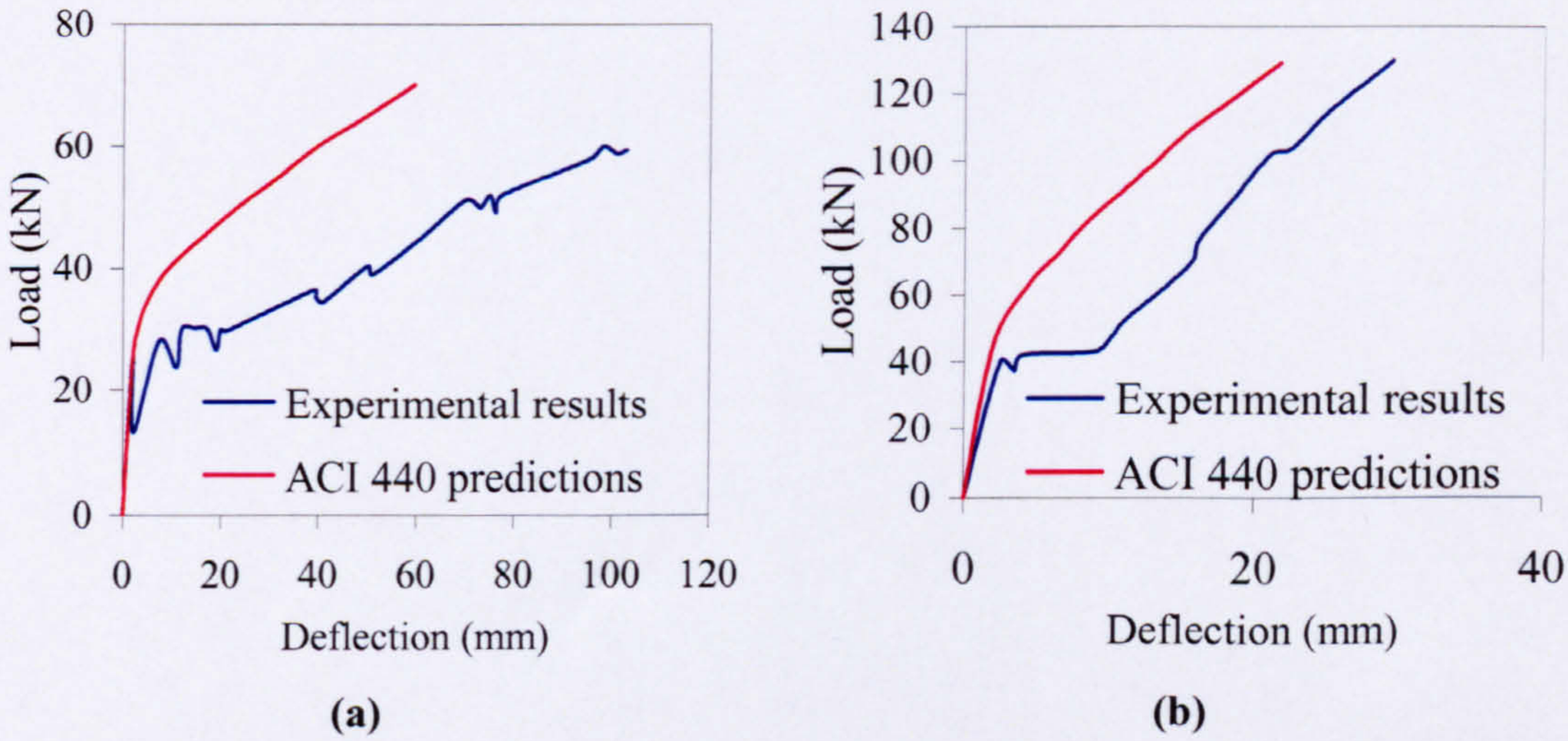

Fig. 1-6 Experimental results compared with ACI predictions (Abdalla 2002)

The accuracy of the ACI 440.1R-03 predictions largely depends on how well the effective moment of inertia (I_e) of partially cracked section (transitional stage between uncracked and fully cracked section) is accounted for in the equation. Due to the limitations of the ACI equation in estimating deflection of FRP RC flexural elements, various researchers (Faza et al. 1992, Alsayed et al. 2000, and Abdalla et al. 2002) proposed different approaches of treating the effective moment of inertia (I_e) of partially cracked sections. Fig. 1-7 shows the variation in opinion for a GFRP RC flexural member with 0.46% reinforcement ratio (equations are given in Chapter 2, Table 2.1). It is clear that there is still no agreement on how to account for the tension stiffening effect.

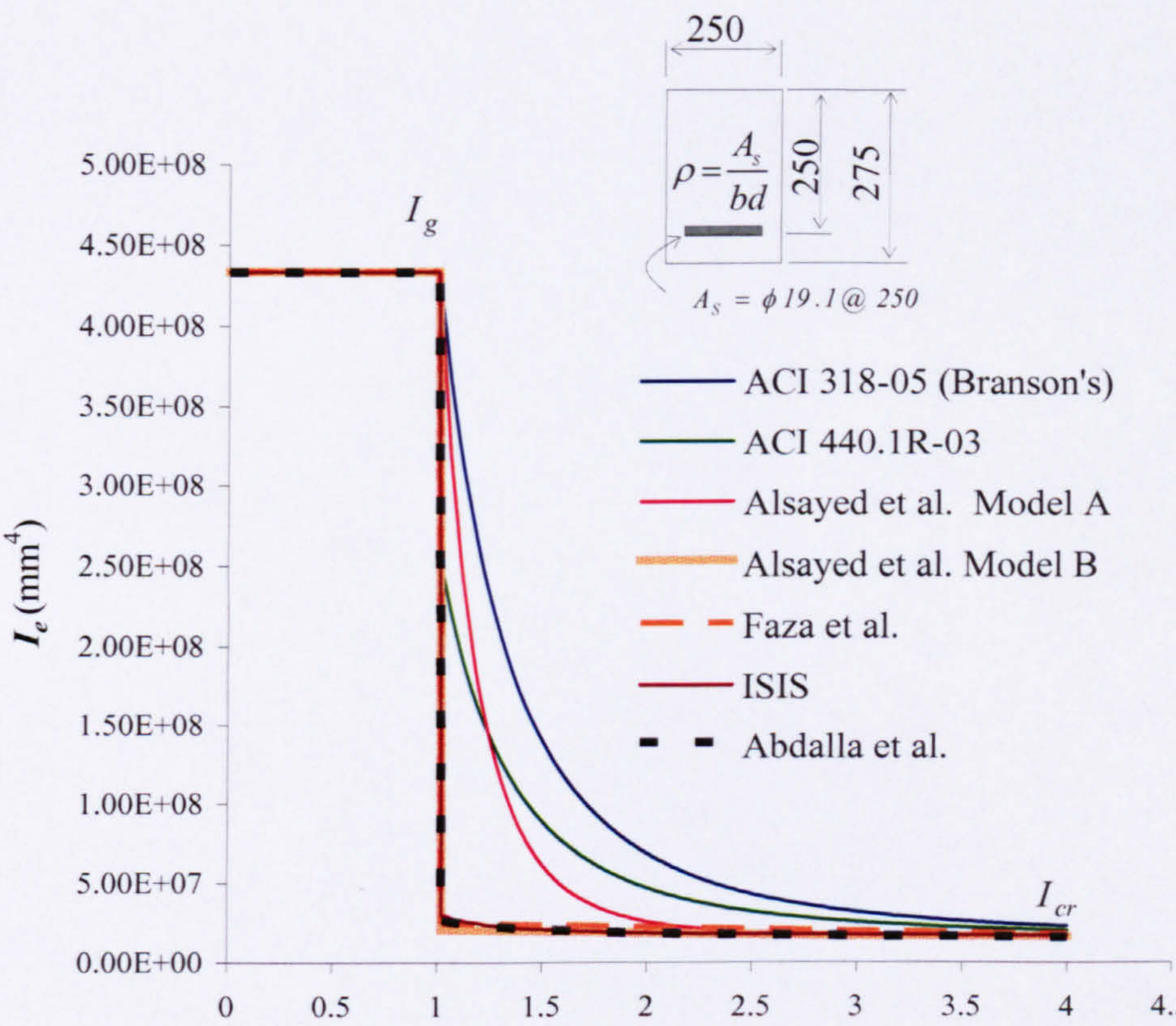

Fig. 1-7 Proposed different methods to account effective moment of inertia

So far, no research has been attempted to study the tension stiffening behaviour of FRP RC at a fundamental level. The ability of concrete to carry stress in the tensile strain region following tensile cracking depends primarily on the bond between concrete and reinforcement, as well as the relative stiffness of concrete and reinforcements. Hence,

this needs further investigation since the properties of FRP and its interaction with concrete are very different to conventional steel reinforcement. This research will, therefore, focus on the tension behaviour of GFRP RC, aiming to develop an understanding of tension stiffening and bond interaction between GFRP reinforcement and concrete, and to develop and implement a tension stiffening model to improve analytical predictions for deformation of GFRP RC.

1.2 Objectives of the Research

The main objectives of this study are:

- to study the tension stiffening effect of GFRP RC based on tension tests
- to evaluate the influence of reinforcement ratio, concrete strength and bar diameter on the tension stiffening behaviour of concrete
- to study the bond behaviour of GFRP as a building block for analysing the tension stiffening behaviour of GFRP RC
- to model tension stiffening behaviour of GFRP RC by modelling the interaction between reinforcement and concrete
- to incorporate the tension stiffening effect in an FE procedure based on the smeared crack approach and estimate deflections
- to provide theoretically sound and simplified analytical techniques to predict deflection, especially at service loads for design purposes.

1.3 Layout of the thesis

After this introduction, the second chapter of this thesis presents a state-of-the-art literature review on the tension stiffening effect of concrete and its effects on deformations. The tension stiffening effect is introduced and detailed account presented of all existing research approaches to incorporate tension stiffening in calculating deflection of FRP reinforced concrete flexural elements. In absence of substantial research on GFRP RC tension stiffening behaviour, a detailed account is given of both numerical and experimental studies on the tension stiffening behaviour of conventional steel RC and its modeling in FE analysis is discussed.

Chapter 3 presents the experimental procedure adopted to investigate the tension stiffening effect of GFRP RC. All experimental results are then presented and analysed to find the influence of the different parameters examined, namely concrete strength, reinforcement ratio and bar diameter. A discussion is included on the accuracy of

modified existing concrete codes, in particular ACI 224 and CEB-FIP model code, by comparing their predictions with experimental results of GFRP RC especially at low reinforcement ratios. Chapter 3 ends by introducing a modification to the CEB-FIP model code for predicting the tension stiffening effect of GFRP RC.

Chapters 4 and 5 examine the bond behaviour of GFRP reinforcement which is used as the fundamental building block for developing models for the tension stiffening effect of concrete. Chapter 4 deals with the bond behaviour of GFRP prisms in tension, whilst chapter 5 deals with the pull-out tests. In chapter 4, with the help of strain measurements, local bond stress slip relationships are rigorously examined, resulting in formulations of bond stress-slip-strain $(\tau - s - \varepsilon)$ relationship, which can be used to explain the local bond stress-slip behaviour with a greater degree of accuracy. The results of the pull-out tests are used in chapter 5 to investigate the bond development length. The chapter ends with a method for estimating the strain distribution between cracks, which forms the basis for a tension stiffening model examined in chapter 6.

Chapter 6 presents a new numerical model for tension stiffening based on a strain distribution function, equilibrium of forces at a section and principles of conservation of energy. Experimental results are then compared with the predictions of the model.

Chapter 7 demonstrates the use of the tension stiffening model in FE analysis for accurate predictions of deflections of GFRP RC flexural members. ABAQUS FE programme is used in this analysis. This chapter further provides a theoretically sound analytical technique to predict deflections for design purposes.

The thesis ends with chapter 8 providing a summary of the important findings, conclusions and recommendations for future research.

CHAPTER 2

LITERATURE REVIEW ON TENSION STIFFENING EFFECT OF CONCRETE

2.1 General

In reinforced concrete, concrete is often assumed to carry only compressive stress. The tensile capacity of plain concrete is usually less than one tenth of its compressive capacity and large differences of recorded tensile strength exist between tensile testing methods such as direct tensile test, splitting test and flexural toughness test (Neville A.M 1996). Moreover concrete being a brittle material exhibits little softening behaviour after cracking and experimental investigation of the softening behaviour requires extremely stiff testing machines to give any useful results. Fig. 2-1 below shows the plain concrete response in tension showing the limited softening behaviour after cracking (Hillerborg 1982).

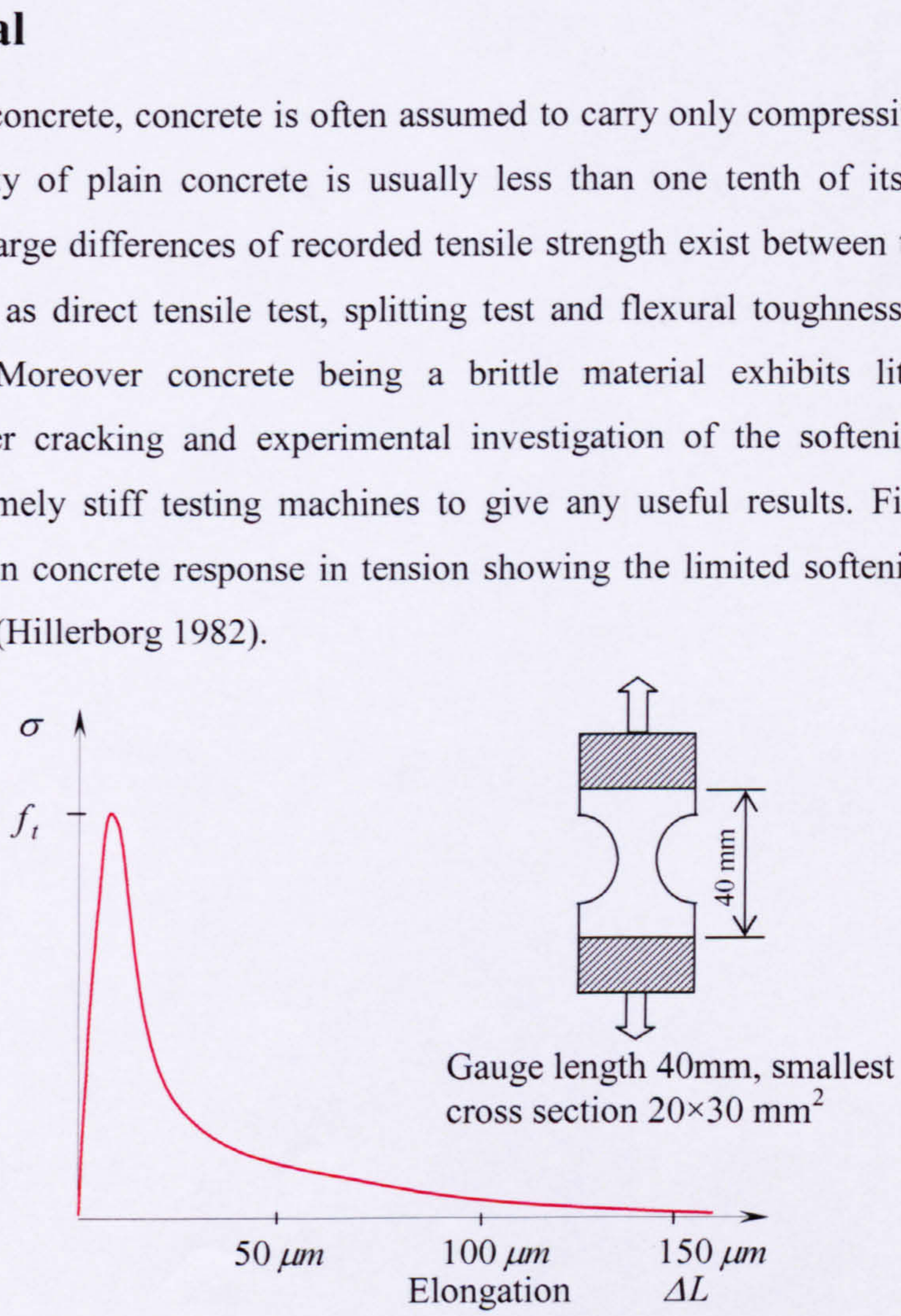

Fig. 2-1 Typical stress-elongation curve for concrete in tension (after Hillerborg 1982)

However, in the case of reinforced concrete, due to the interaction between the concrete and the reinforcement, concrete continues to carry tension between cracks, exhibiting an extended overall softening behaviour of concrete. This interaction provides additional stiffness to the overall structural response of the RC members and can be expected, for example, in the tension zone of a reinforced concrete element subjected to bending (Fig. 2-2), or in a RC tie in pure tension (Fig. 2-3).

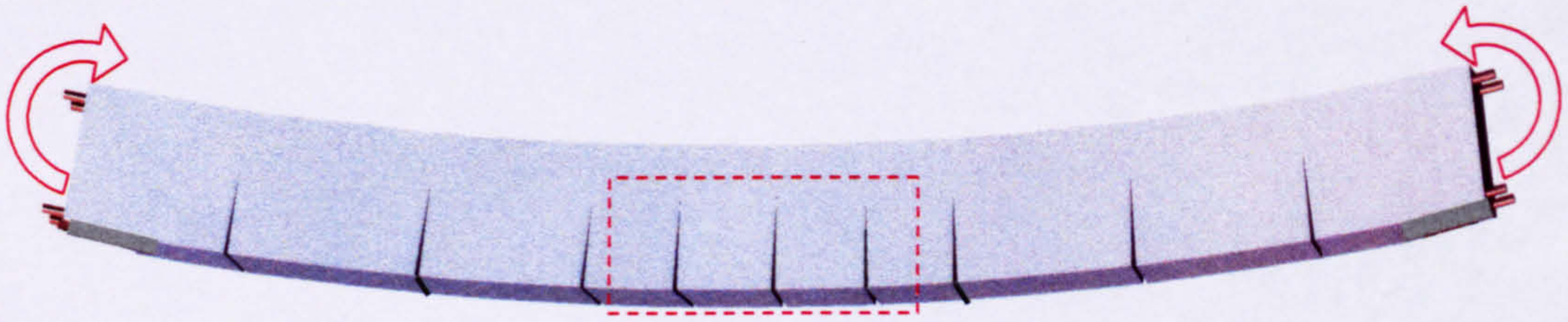

Fig. 2-2 Reinforced concrete in flexure

The ability of concrete to stiffen the reinforcing bar in tension can be best described through tests on RC in direct tension. Fig 2-3 compares the typical response of an RC element in tension, to that of the bare reinforcement bar. Although the presence of concrete makes no difference to the ultimate strength of the member, concrete can reduce the strain of the bar between cracks thereby reducing the overall strain of the RC element. For example, for the applied load P, whilst a bare bar would record a strain of ε_f (according to the stress-strain behaviour of the bar) the overall response of the bar encased in concrete is equal only to ε_{cf}, which is less than ε_f (see Fig. 2-3). In other words, at the applied load P, it is only at crack sections that the bar stretches to the strain ε_f, and in all other sections the bar stretches less than ε_f as it shares forces with the concrete, making the overall response of the RC element less than ε_f.

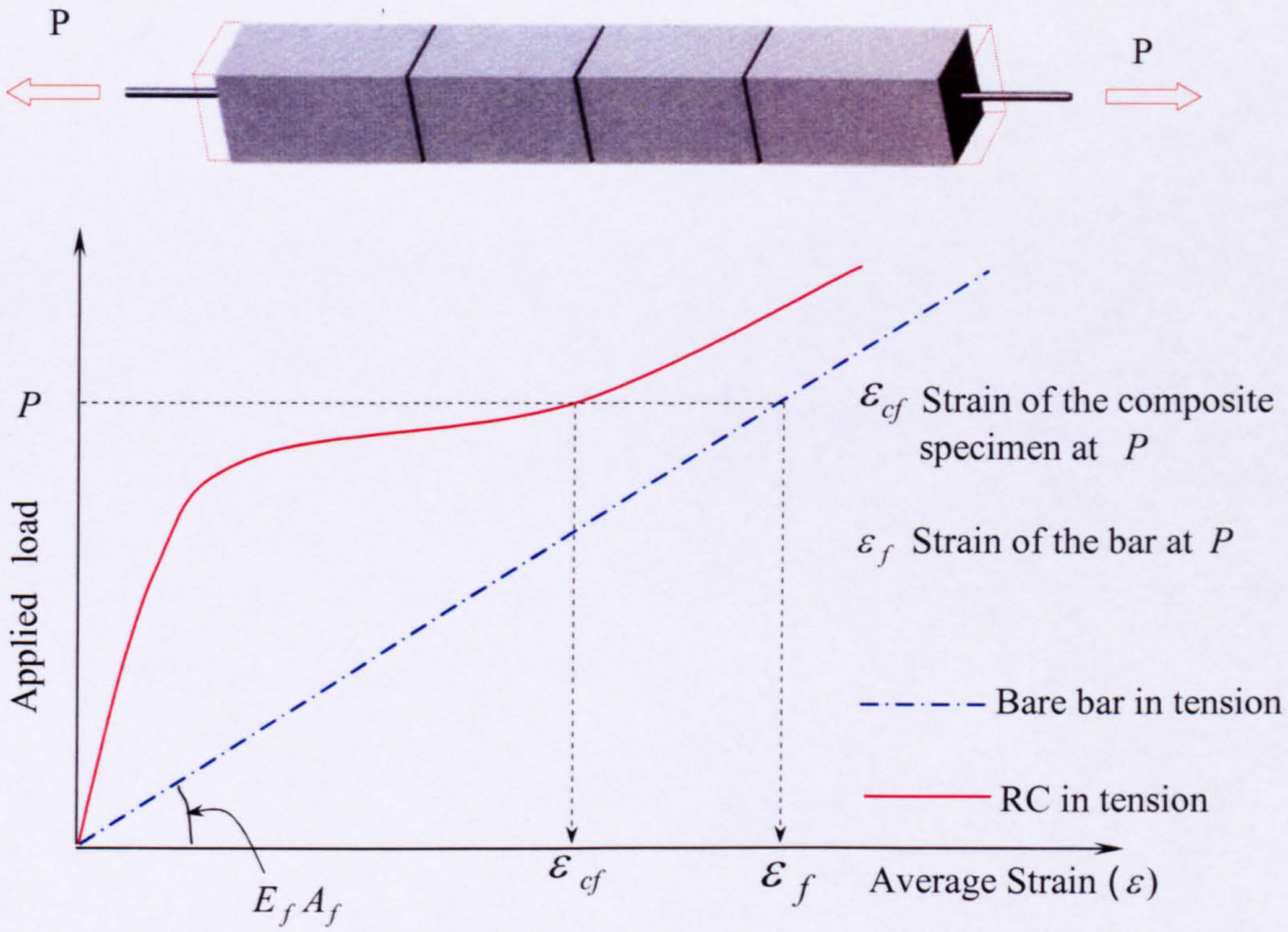

Fig. 2-3 Applied tensile force versus strain of reinforcing bar and reinforced concrete

The ability of a brittle material like concrete to enhance the tensile response of reinforcement was observed as early as 1899. As reported in Mitchell et al. (1996), Considere (1899) observed that the tensile load deformation response of small mortar prisms reinforced with steel wires was almost parallel to the response of the bare steel bar, but remained well above it. In 1908, Morsch explained that cracked concrete has the ability to decrease the strain in reinforcement due to tensile stresses in the concrete between cracks. This phenomenon of stiffening the reinforcement between cracks was later called "Tension Stiffening". After crack separation there is little or no tension carrying capacity for concrete at the crack. However, there are tensile stresses in the concrete between cracks. On formation of the first crack, the average tensile stress in the concrete between the cracks reduces. Further cracking reduces the average tensile stresses in concrete even further. ACI 224.2R-92 (1992) defines tension stiffening effect as the contribution of concrete between cracks to the net stiffness of a member and strain softening behaviour as the gradual reduction in stiffness due to progressive cracking (see Fig 2-3).

It is now important to distinguish the term tension stiffening and strain softening from tension softening. Tension softening is a property of plain concrete whilst tension stiffening and strain softening are properties of reinforced concrete. Tension softening refers to the post cracking tensile stresses in plain concrete and this phenomenon is attributed to the fact that concrete is not a perfect brittle material. From the fracture mechanics point of view, the formation of cracks requires a certain amount of energy which is spent on creating fractured surfaces. As cracks widen, stresses in the vicinity of widened cracks tend to be relieved and the released energy propagates the crack tip. Unlike metals, concrete does not have a clear crack boundary, but a fracture process zone. Hilleborg (1982) explained concrete fracture using the "Fictitious Crack Model" with crack separation width ,w_o, and energy released during cracking as the area under the stress and fictitious crack width diagram (see Fig 2-4).

The Influence of tension softening on the overall response of the RC is insignificant in most cases. However it may be important in modelling the stress redistribution and localised damage of lightly reinforced concrete exhibiting brittle failure modes. Tension stiffening, however, is significant in analysing the structural response of reinforced concrete.

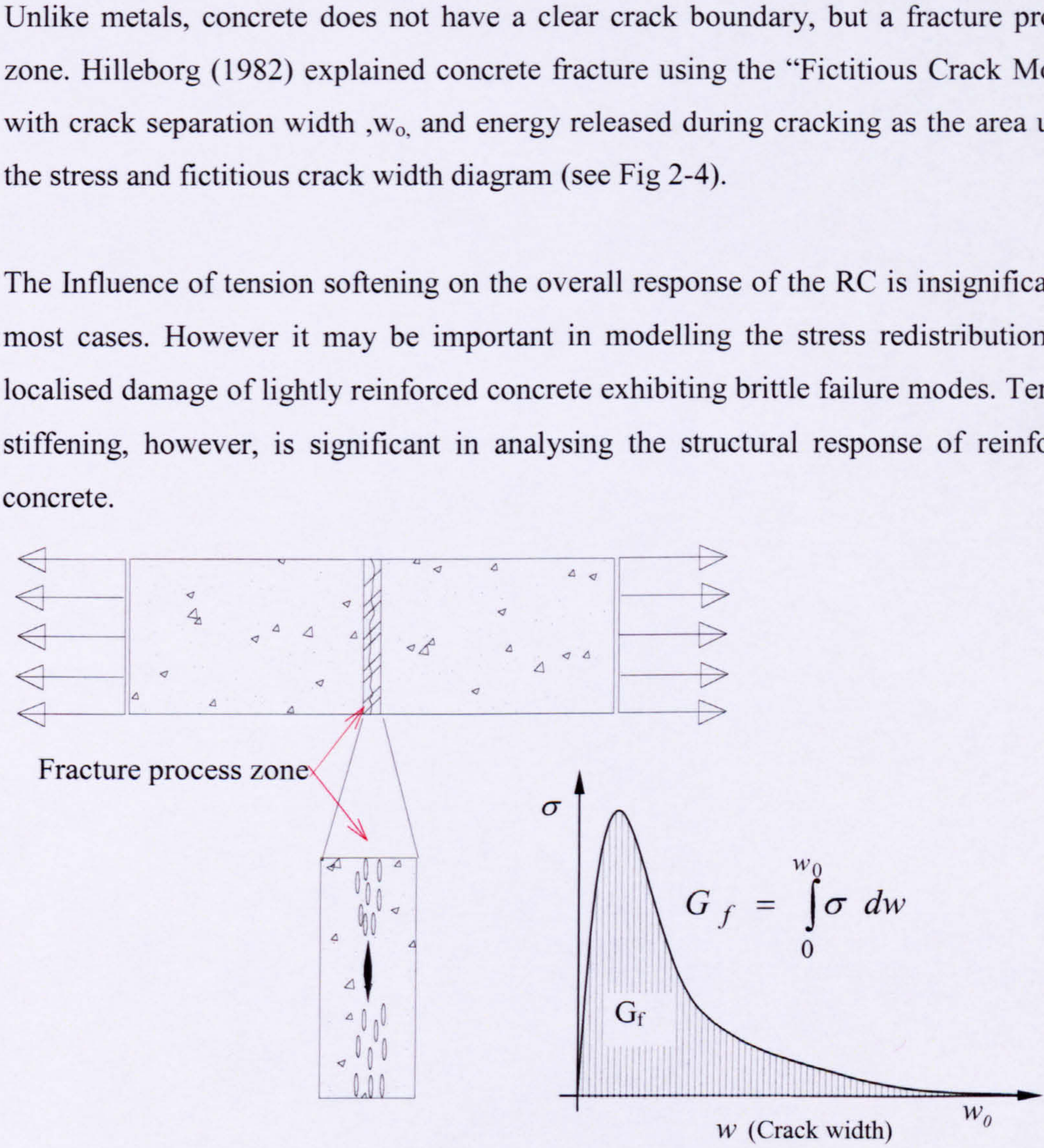

Fig. 2-4 Stress transfer mechanism at a crack

Accounting for the tension stiffening effect is important for the overall structural performance of reinforced concrete and is essential for predicting the deformation

characteristics at service loads. In the design of GFRP RC flexural elements, proper accounting of tension stiffening effect is even more important as design is often governed by serviceability limit state of deflections (Abdalla H.A. 2003) (Craig et al., 1998). Before discussing the models for tension stiffening effect, it is important to understand how tension stiffening effect is accounted for in design equations and how this affects the prediction of deflections of RC elements.

2.2 Accounting for tension stiffening effect in deflection calculations: code based formulations

This section looks at how the tension stiffening effect is considered in code-based formulations in relation to the prediction of deflections of GFRP RC flexural members. The ACI 440.1R-03 design equations are based on the ACI 318-05 code for design of steel RC and are the most widely used set of recommendations. Basically, the ACI 318-05 recommends the use of elastic deflection formulae, in the form shown in equation 2-1, and account for the tension stiffening effect and the nonlinear material behaviour by modifying the second moment of area, I_e. Branson's formulae (equation 2-2) (Branson D.E 1977) is used to modify the stiffness of the member between the un-cracked state I_g (second moment of area of the gross section) and cracked state I_{cr} (second moment of area of the cracked section). ACI 440.1R-03 introduces a factor β to account for the lower bond and relatively low stiffness of the FRP bars as shown in equation (2-3).

$$\Delta = \frac{KL^2}{E_c}\frac{M_a}{I_e} \tag{2-1}$$

$$I_e = \left[\frac{M_{cr}}{M_a}\right]^3 I_g + \left[1-\left(\frac{M_{cr}}{M_a}\right)^3\right] I_{cr} \tag{2-2}$$

$$I_e = \left[\frac{M_{cr}}{M_a}\right]^3 \beta_d I_g + \left[1-\left(\frac{M_{cr}}{M_a}\right)^3\right] I_{cr} \tag{2-3}$$

Where

K = Depend on the end conditions and loading in the elastic calculation of deflections

$$\beta_d = \alpha_b\left[\frac{E_f}{E_s}+1\right]$$

$\alpha_b = 0.5$ for FRP bars, bond-dependent coefficient

However, predictions of serviceability limit state performance of FRP-RC members with these equations have been found to be un-conservative (as described in section 1.1)

and therefore maximum deflections at service loads are underestimated, especially at low reinforcement ratios, as shown in Fig 1-5.

Table 2-1 summarises most of the notable attempts to modify Branson's equation including the ACI 440.1R-03 (2003) modification for FRP RC. Fig. 1-7 (see section 1-1) gives a comparison of the different models shown in table 2-1 for a GFRP RC beam calculated at an assumed nominal reinforcement ratio of 0.46%.

Table 2-1 Summary of different recommendations for I_e

Model	Expression	Reference & Remarks
ACI-318	$I_e = \left[\frac{M_{cr}}{M_a}\right]^3 I_g + \left[1-\left(\frac{M_{cr}}{M_a}\right)^3\right] I_{cr}$ (2-4)	ACI 318-05 (2005)
ACI- 440	$I_e = \left[\frac{M_{cr}}{M_a}\right]^3 \beta_d I_g + \left[1-\left(\frac{M_{cr}}{M_a}\right)^3\right] I_{cr}$ (2-5)	ACI 440-1R-01 (2003)
Ganga Rao and Faza	$I_m = \frac{23 I_{cr} I_e}{8 I_{cr} + 15 I_e}$ (2-6)	Faza et. Al.(1993) Only valid for four point bending test
Alsayed model A	$I_e = \left[\frac{M_{cr}}{M_a}\right]^{5.5} I_g + \left[1-\left(\frac{M_{cr}}{M_a}\right)^{5.5}\right] I_{cr}$ (2-7)	Alsayed et. al. (2000)
Alsayed model B	$I_e = \left[1.40 - \frac{2}{15}\left(\frac{M_a}{M_{cr}}\right)\right] I_{cr}$ (2-8) $for \quad 1 < \frac{M_a}{M_{cr}} < 3$ $I_e = I_{cr} \quad for \frac{M_a}{M_{cr}} > 3$	Alsayed et. al. (2000)
ISIS	$I_e = \frac{I_g I_{cr}}{I_{cr} + \left[1 - .5\left(\frac{M_{cr}}{M_a}\right)^2\right]\left(I_g - I_{cr}\right)}$ (2-9)	ISIS (2001)
Abdalla	$I_e = \frac{I_g I_{cr}}{I_{cr}\varsigma + 1.15 I_g (1-\varsigma)}$ (2-10) $\varsigma = M_{cr} / M_a$	Abdalla et. al. (2002) Based on the CEB-FIP formulae given below-modified for FRP
Eurocode 2	$\Delta = \Delta_2 - (\Delta_2 - \Delta_1)\beta' . \frac{M_{cr}}{M_a}$ (2-11)	CEN (2004), The term $(\Delta_2 - \Delta_1)\beta' . \frac{M_{cr}}{M_a}$ accounts for tension stiffening effect.

$$M_{cr} = \frac{f_{cr} I_g}{y_b} \quad (kN.m)$$

M_a = Service moment $kN.m$

I_e = Effective moment of inertia

$I_g = \frac{bh^3}{12}$ - The moment of inertia of the un-cracked transformed section.

I_m =Modified moment of inertia valid for concentrated point loads applied at the third point on the beam (Faza et al. 1993)

$I_{cr} = \frac{bd^3}{3}.k^3 + n_f.A_f.d^2.(1-k^2)$ Cracked moment of inertia

$$k = \sqrt{2.n_f \rho_f + (\rho_f.n_f)^2} - \rho_f.n_f$$

$$n_f = \frac{E_f}{E_c}$$

E_f = Modulus of elasticity of FRP

$E_c = 4560\sqrt{f_c'}$ (MPa)

$f_{cr} = 0.6\sqrt{f_c'}$ (MPa)

y_b = Distance from neutral axis to extreme tension fibre of concrete beam.

d = The effective depth of the concrete beam

$$\beta_d = \alpha_b \left[\frac{E_f}{E_s} + 1 \right]$$

$\alpha_b = 0.5$, Bond-dependent coefficient

$$\varsigma = 0.5 \left(\frac{M_{cr}}{M_a} \right)$$

Δ_1 =Deflection in un-cracked state, transformed moment of inertia is used for the calculation

Δ_2 =Deflection in cracked state, cracked moment of inertia is used for the calculation

β' =Bond related coefficient

It is clear from Fig. 1-7 that there is no universal agreement on how tension stiffening of GFRP RC should be accounted for in deflection calculations. Most of these proposals are derived to match the deflections of one set of tests without much attention to all variables and all practical design limits. To date, there has not been any fundamental research attempt to understand the tension stiffening behaviour of these new reinforcing materials.

2.3 Modelling tension stiffening in FEM based analysis

2.3.1 General

There are two different approaches for simulating reinforced concrete behaviour using the FE method: 1) Discrete crack model, 2) Smeared crack model. In the discrete crack model, cracks are modelled as discontinuities and reinforcement and concrete are modelled separately with a bond link element to model the interaction between them (see Fig. 2-5). In this way of modelling, the tension stiffening effect is automatically accounted for. However, the correct modelling of bond and a prior knowledge of the locations of the cracks are the main challenges in this method. During the early stages of this research, Ngo and Scordelis (1967) used linear elastic behaviour for the materials and bond, together with predetermined crack sections. Later on nonlinear properties were employed for material characterisation along with adoptive meshing and incremental loading to achieve better solutions (Nilson, 1967 & 1968).

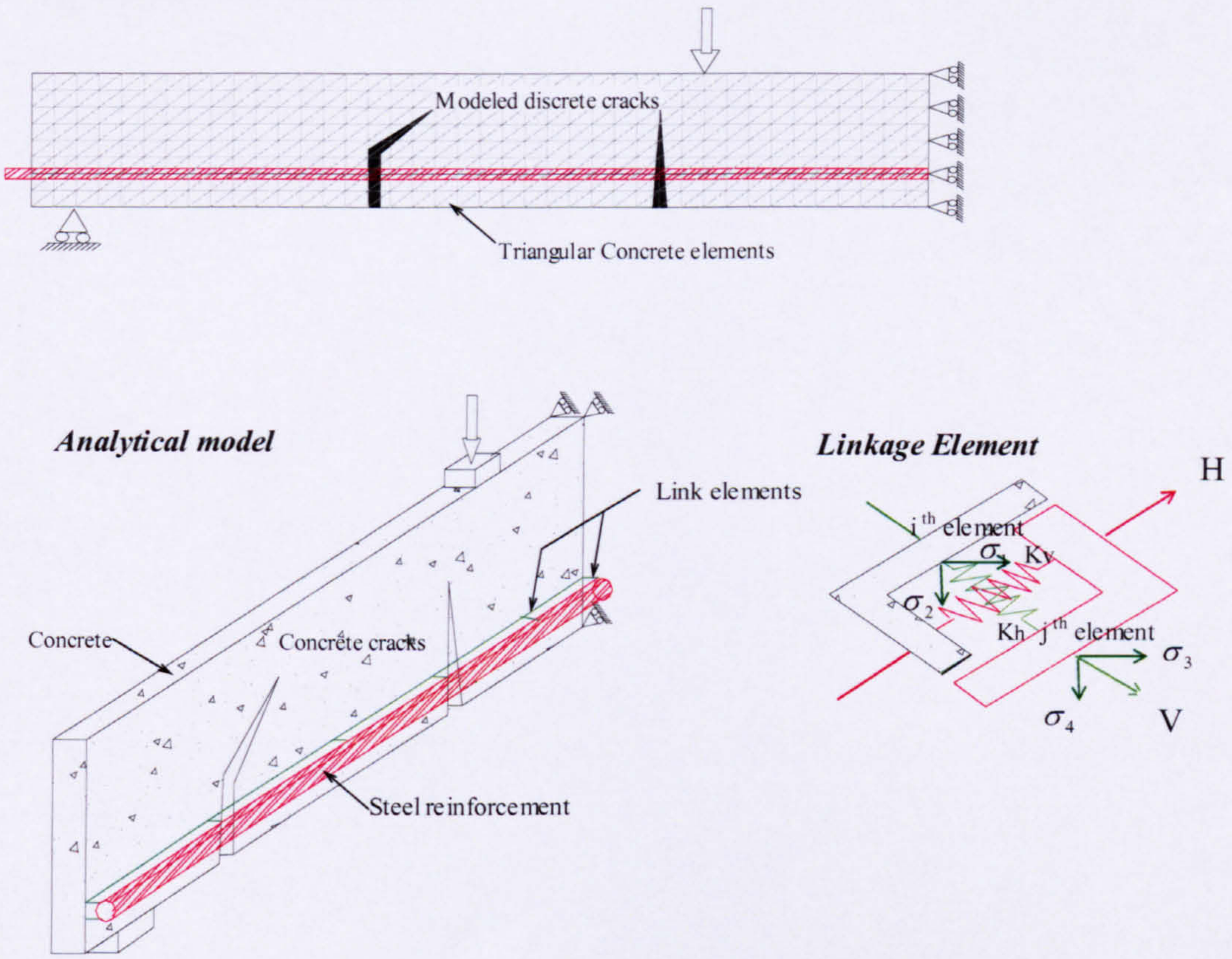

Fig. 2-5 Discrete crack concept (After Ngo and Scordelis 1967)

The smeared crack approach was first introduced by Rashid (1968) to overcome the problem of redefinition of the mesh during the course of the analysis. In the smeared

crack approach, cracks are assumed to be smeared over the element. After cracking, isotropic material properties are replaced by orthotropic ones in the direction perpendicular to the crack and cracked reinforced concrete is modelled using average material properties. In the smeared crack method the complication of analysing bond was avoided by considering the tension stiffening behaviour of concrete at the global level considering the average concrete contribution in tension.

In 2D stress state one can write the elastic isotropic stress strain relations for concrete as shown below (equation 2-12). Cracking essentially makes the material interaction orthotropic. Equation 2-13 shows the cracked orthotropic stress strain relations for concrete in the early attempts without considering the interactions of the bar and concrete (Rashid, 1968). The stiffness matrix of concrete in the principal directions with tension stiffening and interaction of cracked concrete due to aggregate interlocking considered are shown in equation 2-14.

$$\begin{bmatrix}\sigma_1\\ \sigma_2\\ \sigma_3\end{bmatrix}=\frac{E_c}{1-\nu^2}\begin{bmatrix}1 & \nu & 0\\ \nu & 1 & 0\\ 0 & 0 & \frac{1-\nu}{2}\end{bmatrix}\begin{bmatrix}\varepsilon_1\\ \varepsilon_2\\ \varepsilon_3\end{bmatrix} \tag{2-12}$$

$$\begin{bmatrix}\sigma_1\\ \sigma_2\\ \sigma_3\end{bmatrix}=\begin{bmatrix}0 & 0 & 0\\ 0 & E_c & 0\\ 0 & 0 & 0\end{bmatrix}\begin{bmatrix}\varepsilon_1\\ \varepsilon_2\\ \varepsilon_3\end{bmatrix} \tag{2-13}$$

$$\begin{bmatrix}\sigma_1\\ \sigma_2\\ \sigma_3\end{bmatrix}=\begin{bmatrix}\mu E_c & 0 & 0\\ 0 & E_c & 0\\ 0 & 0 & \beta G\end{bmatrix}\begin{bmatrix}\varepsilon_1\\ \varepsilon_2\\ \varepsilon_3\end{bmatrix} \tag{2-14}$$

Post cracking behaviour (mainly tension stiffening behaviour) of RC structures depends on many influencing factors which are deeply related to the bond characteristics between concrete and reinforcement. In early studies (Gilbert and Warner, 1978) (Lin and Scordelis, 1975) characterising the non negligible effects of concrete in tension was the main objective. Today, there are many numerical models that can implement the tension stiffening effect into a stress stain relation of concrete based on advanced theories such as non linear fracture mechanics (Ouyang et al. 1997) (Gerstle et al. 1978).

The Modified Compression Field theory MCFT (Vecchio et al. 1985) and the Softening Truss Model Theory STMT (Hsu, 1988) made a significant contribution in providing nonlinear material properties for the smeared crack approach (average properties of cracked reinforced concrete) using reinforced concrete material characteristics. The popularity of these approaches to material modelling led many researchers to adopt the smeared crack approach for modelling reinforced concrete.

As FRP has different mechanical properties and different bond properties to steel reinforcement, characterising the average stress-strain behaviour of FRP RC is essential for the analysis using the smeared crack concepts. The tension behaviour of concrete reinforced with FRP has not been studied before in a comprehensive manner. The purpose of this work is to develop an understanding of the tension stiffening behaviour of these new materials as internal reinforcements. As there is no significant body of research into the tension stiffening behaviour of concrete reinforced with FRP, it is useful to consider instead research into conventional steel bars as reinforcement.

2.4 Empirical and theoretical modelling of tension stiffening behaviour

2.4.1 Empirical methods

2.4.1.1 Introduction

The first notable attempts to characterise the tension stiffening behaviour using average stress-strain relationships include the stepped response by Scanlon and Murray (1974), gradual unloading by Lin and Scordelis (1975) and discontinuous unloading by Gilbert and Warner (1978). Fig. 2-6 depicts schematically the different average concrete stress-strain characteristics proposed by the above methods. These models aimed to provide an idealistic behaviour of reinforced concrete based on simple experiments for rationalising the post cracking response and are not universal in their nature. After these initial attempts various researchers developed more sophisticated models based on specially devised experiments.

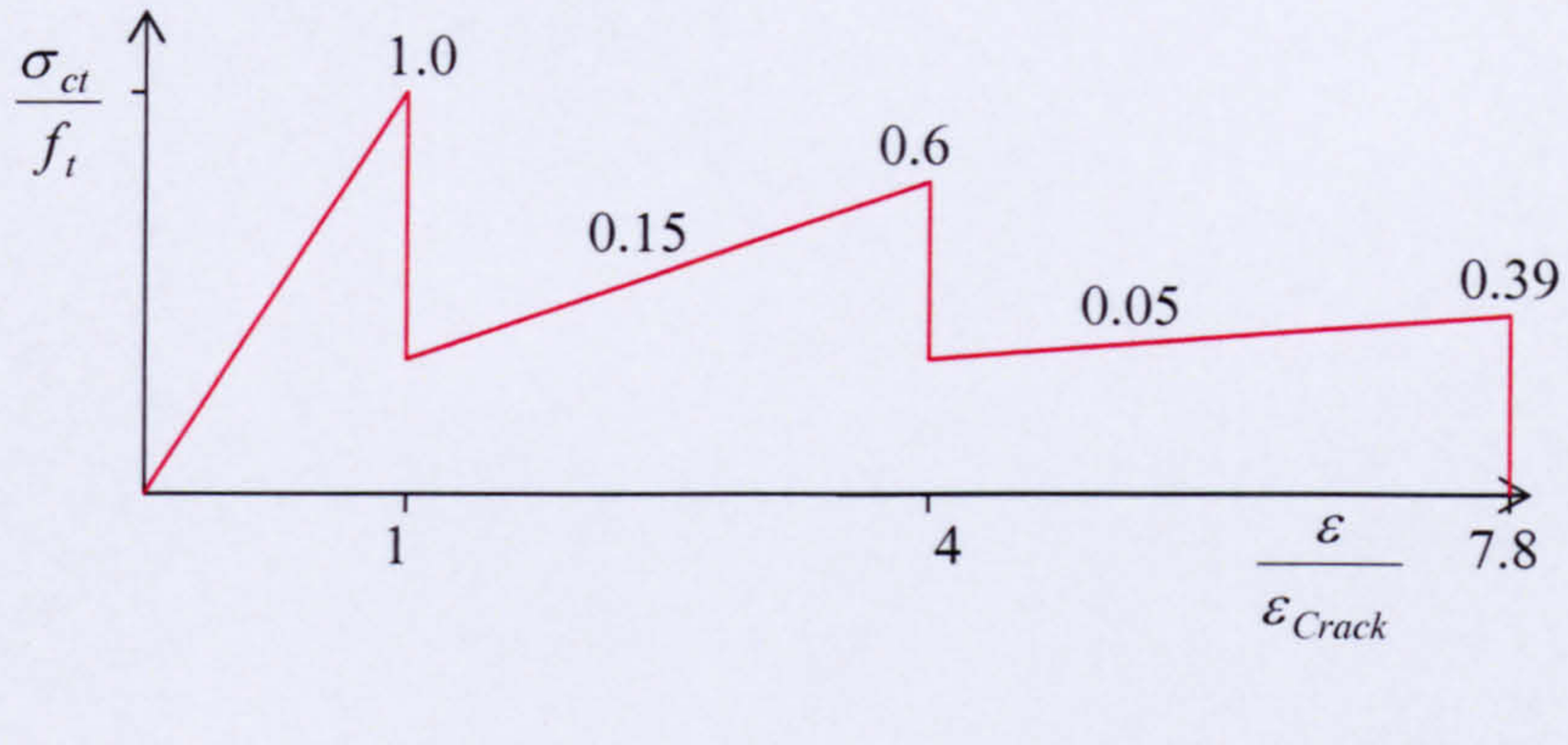

(a) Stepped response after cracking (Scanlon and Murray 1974)

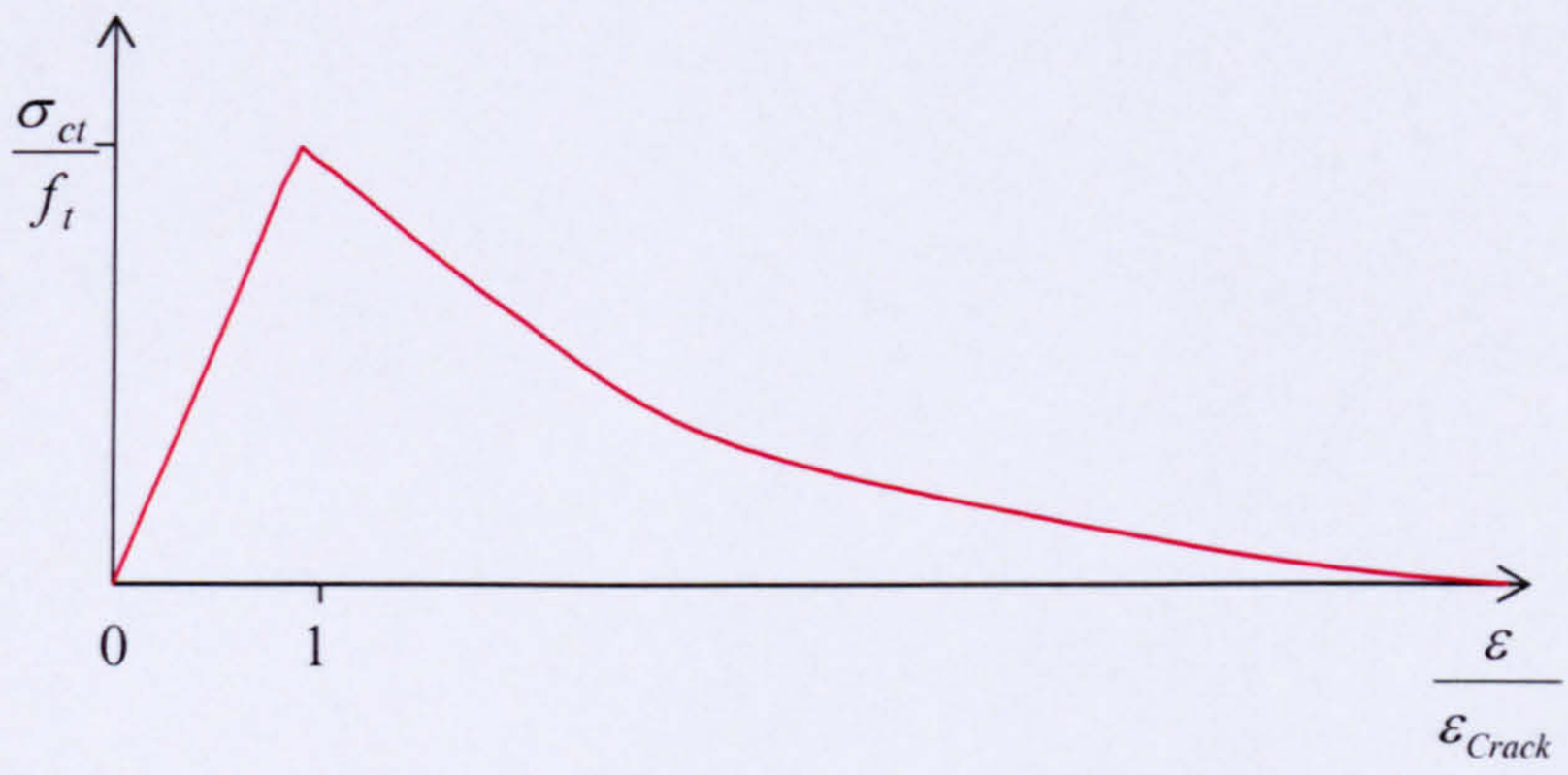

(b) Gradual unloading after cracking (Lin and Scordelis 1975)

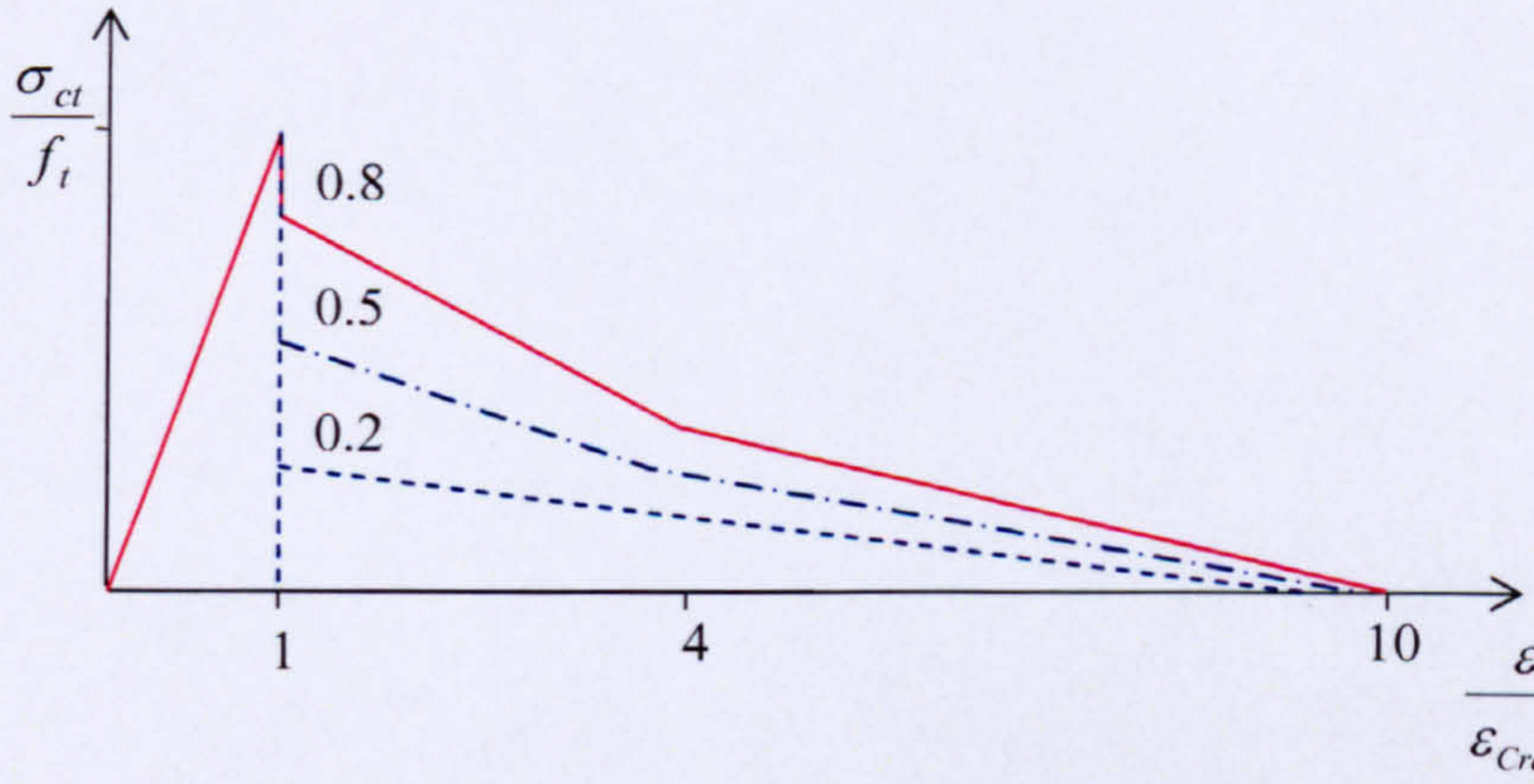

(c) Discontinuous unloading after cracking (Gilbert and Warner 1978)

Fig. 2-6 Early modelling of concrete tensile stress-strain curves

2.4.1.2 Shear panel experiments

Vecchio and Collins (1986) in their paper on modified compression field theory (MCFT) for reinforced concrete elements subjected to shear, (apart from their principal finding of reduced compressive behaviour of cracked concrete) derived an expression for the average tensile behaviour for concrete after cracking. Their experimental approach was unique at the time and used RC shear panels subjected to different combinations of loadings using the set-up shown in Fig. 2-7.

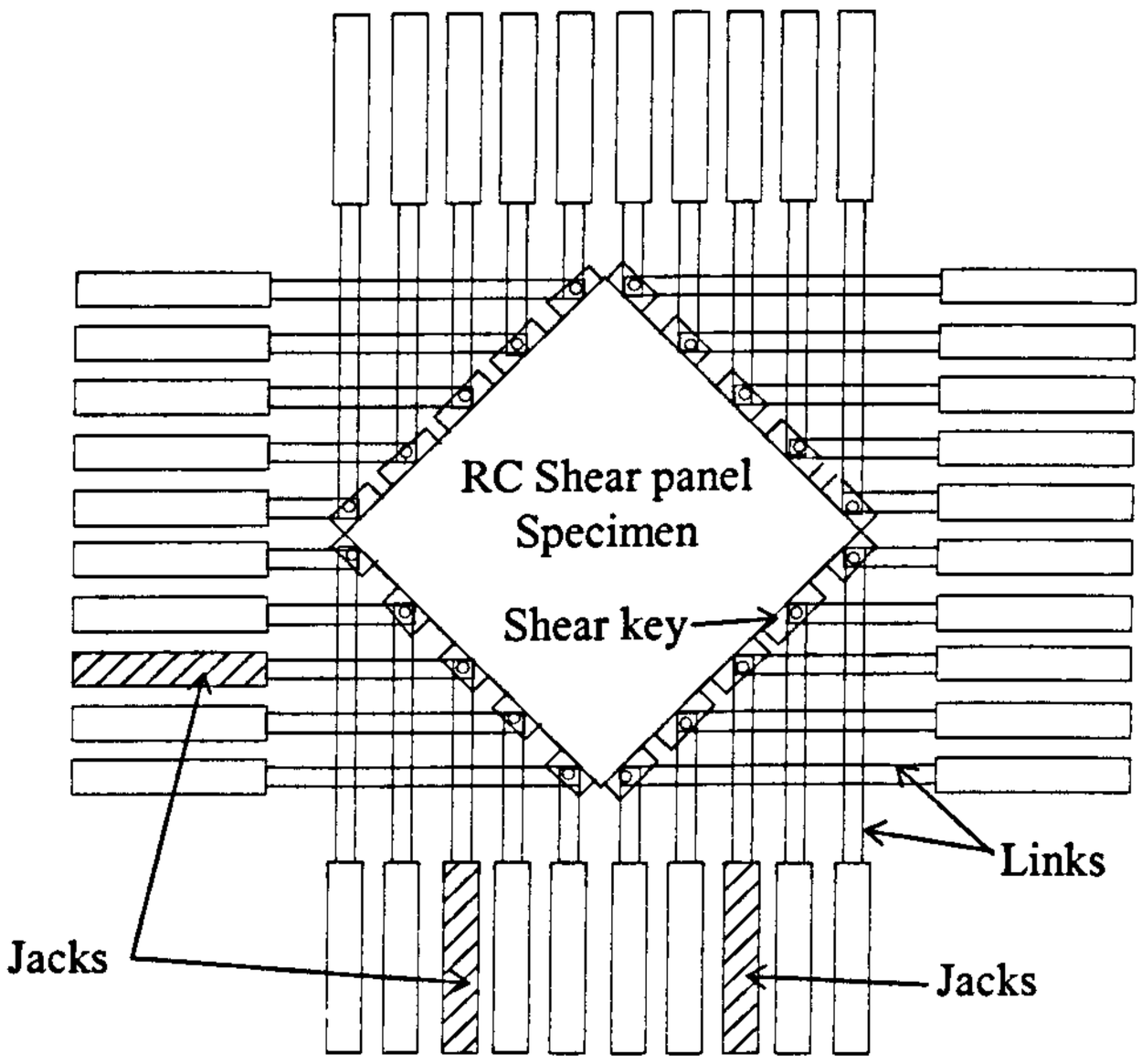

Fig. 2-7 Experimental set-up for testing shear panels (after Vecchio et al. 1986)

Fig. 2-8 represents a free body diagram showing forces acting on a part of the shear panel. Based on the free body diagram the following equilibrium equation can be derived.

$$f_x = f_{cx} + \rho_{sx} f_{sz} \tag{2-15}$$

$$f_y = f_{cy} + \rho_{sy} f_{sy} \tag{2-16}$$

Assuming no shear contribution from the reinforcement and that shear is only resisted by concrete, the following equation was written.

$$v_{xy} = v_{cx} = v_{cy} = v_{cxy} \tag{2-17}$$

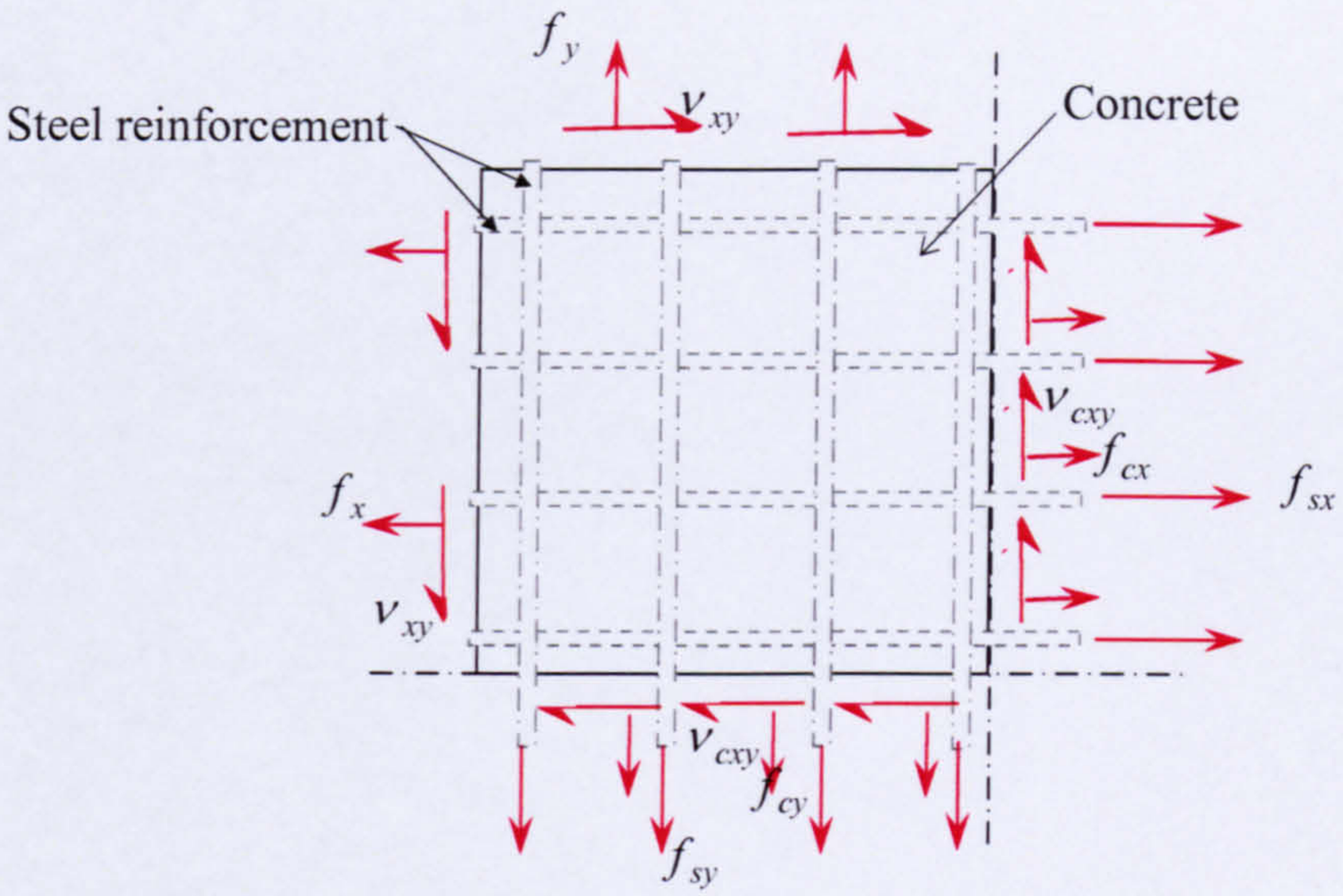

Fig. 2-8 Free body diagram of the shear panels tested with forces marked to identify the components for force equilibrium.

With these equilibrium equations, authors derived the stress state of concrete. Fig. 2-9 shows the stress state of concrete and the resolved principal stresses by applying Mohr's circle to represent the stress state. As the principal strains of the reinforced concrete panel is assumed to coincide with the principal stresses of the concrete, the authors managed to find average stress-stain relationship for concrete in tension and compression for different load combinations.

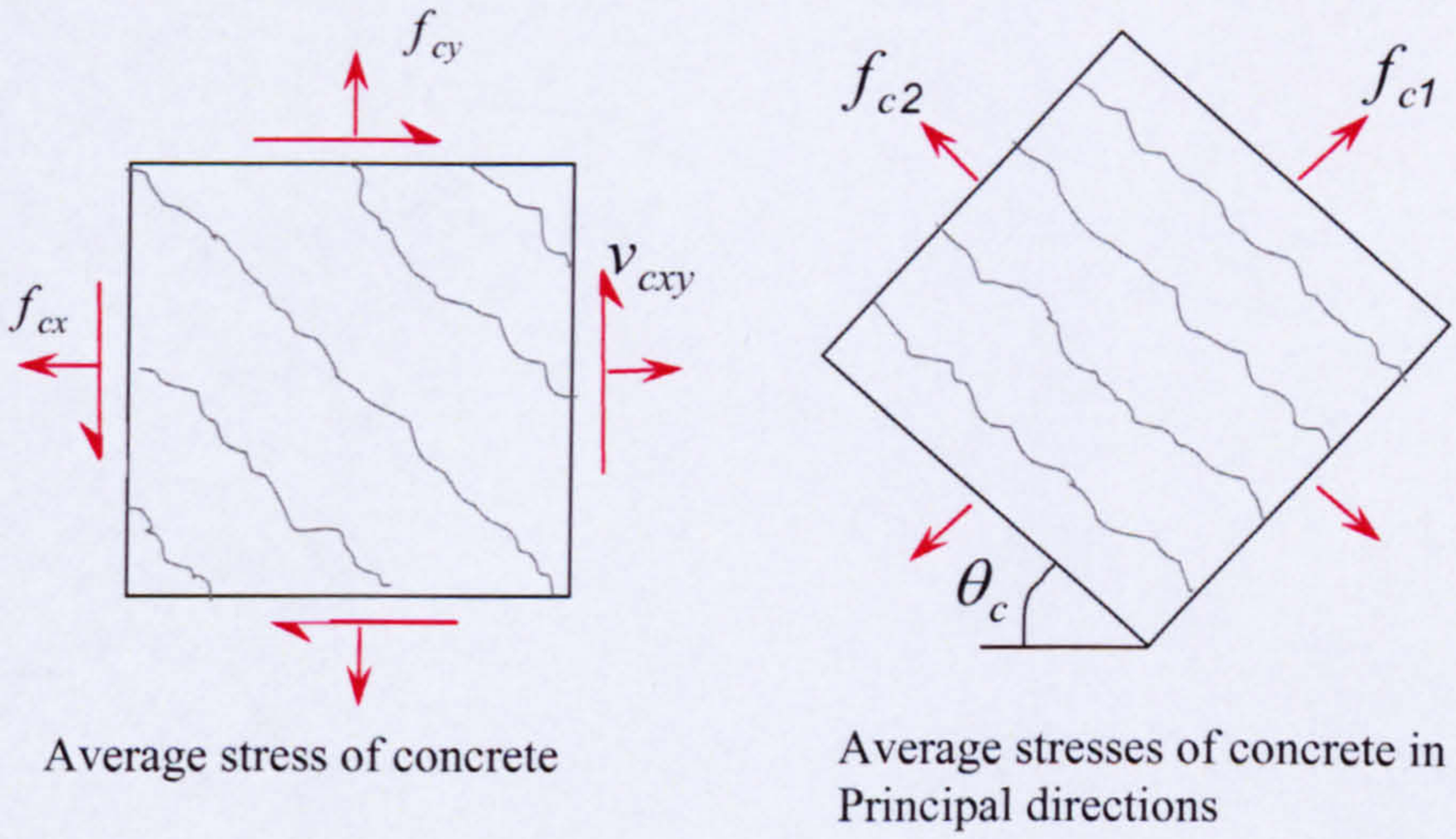

Fig. 2-9 Stress blocks representing the average stress state of concrete in representative coordinate directions and in principal directions.

The proposed relationship between the average principal tensile stress, f_{c1}, and strain, ε_1, from their experimental work (shown in Fig. 2-10) is nearly linear prior to cracking and then the stresses decreases with increasing values of ε_1 (equation 2-18 & 2-19).

The relationship prior to cracking (i.e., $\varepsilon_1 \leq \varepsilon_{cr}$ (strain in concrete at cracking)) is

$$f_{c1} = E_c . \varepsilon_1 \qquad (2\text{-}18)$$

where E_c is the modulus of elasticity of the concrete which can be taken as $2 f_c' / \varepsilon_c'$ (f_c'-Maximum compressive stress observed in cylinder test, ε_c'-Strain in concrete cylinder at peak stress f_c').

The relationship suggested after cracking (i.e., $\varepsilon_1 \geq \varepsilon_{cr}$) is

$$f_{c1} = \frac{f_{cr}}{1 + \sqrt{200 \varepsilon_1}} \qquad (2\text{-}19)$$

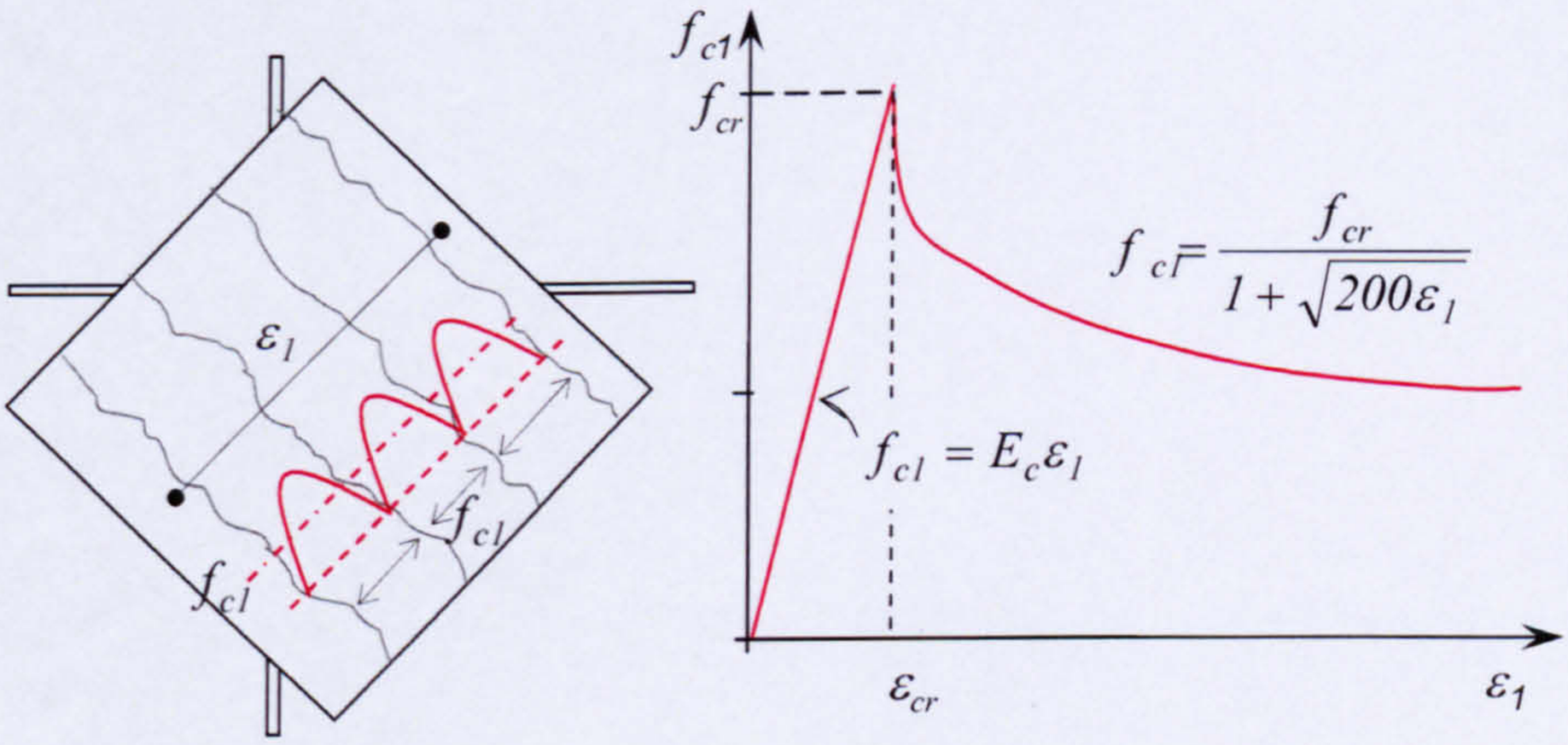

Fig. 2-10 Average stress strain relationship for cracked concrete in tension (after Vecchio et al. 1986)

2.4.1.3 Tension experiments

Okamura and Maekawa (1991) adopted a different approach using direct tension tests on RC elements as shown in Fig. 2-11. In their experimental study they connected a thin wire on the bar at opposite ends of the concrete section to measure the overall elongation of the RC specimen. The wires were then connected to the transducers held firmly on the testing floor using a pulley arrangement, as shown in Fig. 2.11. They studied various factors influencing the tension stiffening effect like concrete strength, bar diameter, yield point of the bar, reinforcement ratio and drying shrinkage. Based on

the experimental findings the average stress-strain characteristics of concrete in tension were derived.

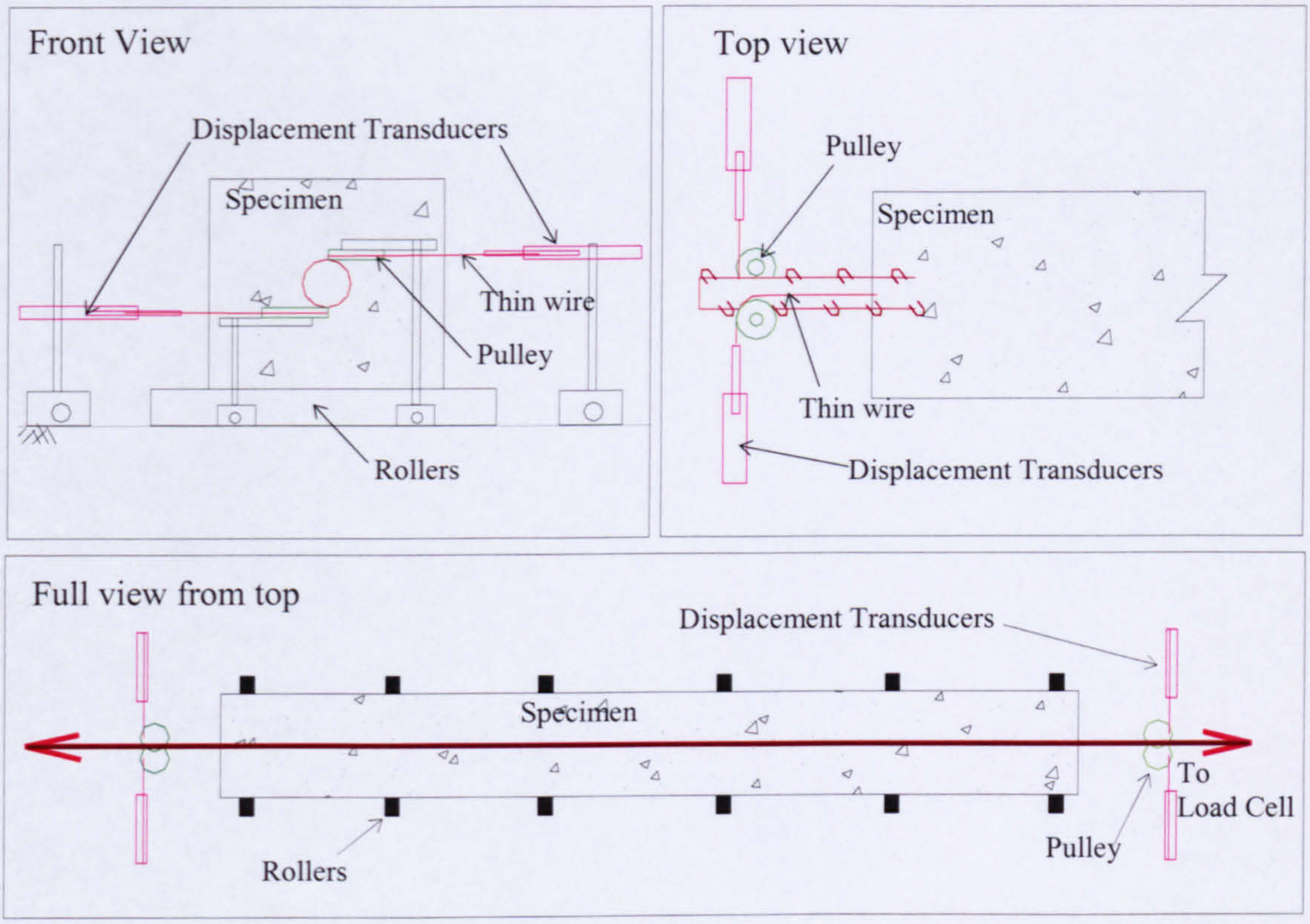

Fig. 2-11 Apparatus for the direct tension test (after Maekawa et al. 2001)

Their proposed average stress-strain curve, shown in Fig. 2-12, has an ascending path, a plateau and a descending branch. These are established using the test results and modified to account for the non-brittle fracture of concrete or plasticity of concrete in the fracture process zone. Equation 2-20 below shows the descending branch of the curve which includes a coefficient, c, to account for different bond properties of the reinforcement bar. The values of c =0.4 for normal ribbed bars and c =0.2 for welded mesh were found appropriate to fit the experimental results. Furthermore, this equation is claimed to be valid for the full domain including the post yield conditions.

$$\sigma_{ct} = f_t(\varepsilon_{tu} / \varepsilon_t)^c \qquad (2\text{-}20)$$

Where

σ_t = Average tensile stress

f_t = Uni-axial tensile strength

ε_{tu} = Cracking strain

ε_t = Average strain

Although the model was originally developed from uni-axial stress conditions, it is said to have been verified for two-dimensional RC elements containing two-way reinforcement with ratios between 0.1-2 percent. Moreover, the model is considered to be independent of crack spacing, element size and orientation of reinforcement in the element. The plateau represents the actual crack development strain which is around two times the actual strain based on the tensile fracture criterion ($\approx 0.03\%$). Cracks do not appear as soon as the stress reaches the cracking criterion, but when the principal strain reaches the limit strain to account for a certain degree of plastic deformation.

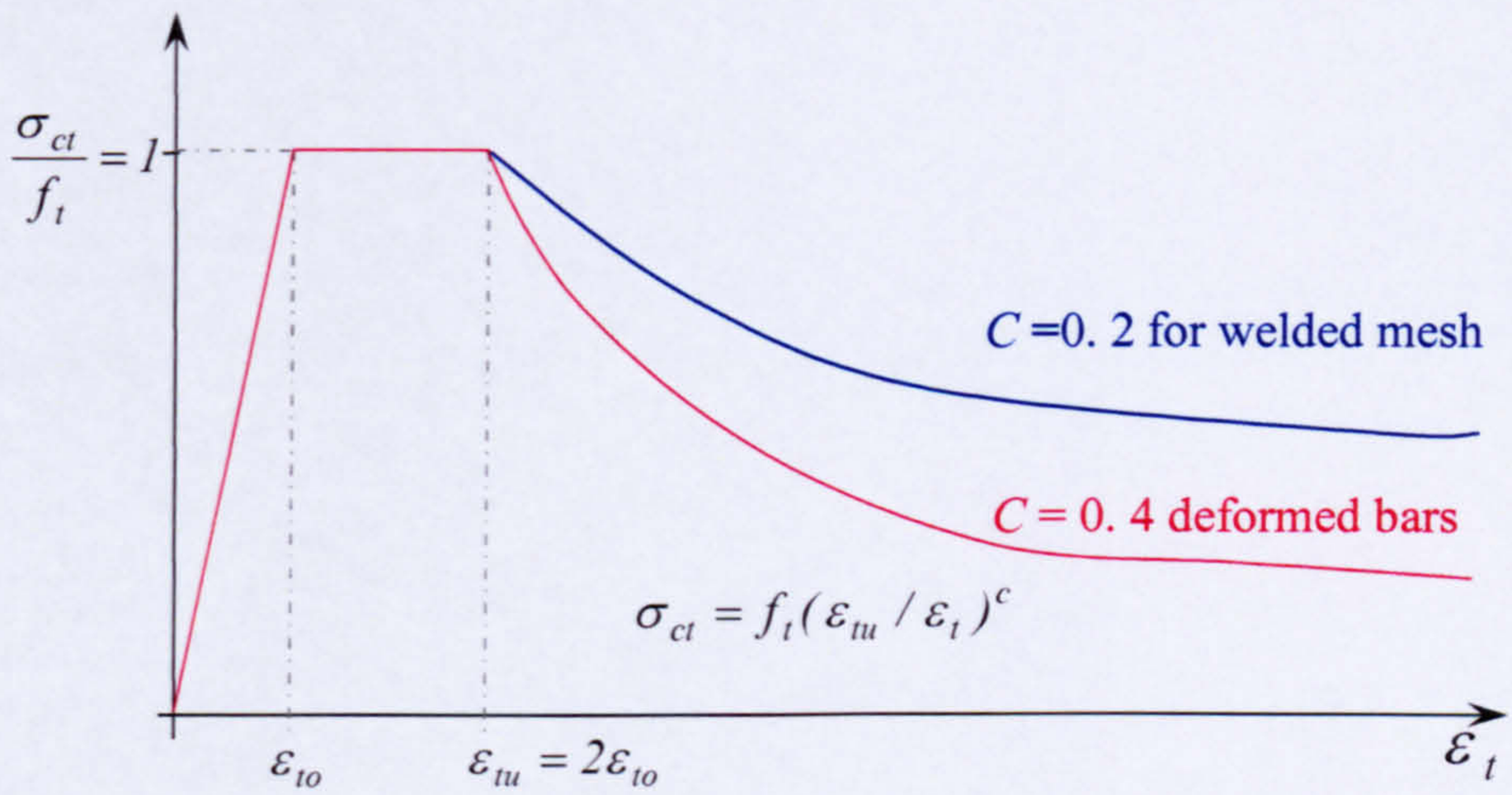

Fig. 2-12 Average stress-strain behaviour of reinforced concrete (Okamura H. et al. 1991)

Further to equation 2-20, which is only dependent on the bond properties and concrete tensile strength, the authors emphasised the importance of introducing the reinforcement ratio as a parameter when dealing with lower reinforcement ratios. Maekawa et al. (2002) provided a numerical model to deal with reinforcement ratios less than 1%, where the reinforcement ratio becomes an important parameter in determining the average stress-strain relationships. This model will be discussed in section 2.4.2.1.

In the smeared crack approach it is essential that both constituent materials (concrete and reinforcement) are modelled in spatial terms. Okamura and Maekawa (1991) demonstrated that the overall performance of direct tension tests is overestimated by analysis when the bare bar stress-strain behaviour of reinforcement is modelled together with the average stress-strain behaviour of concrete. The error is more pronounced

when using low reinforcement ratios or reinforcements with low yield strain. However, the requirement to use average stress-strain behaviour for the bar arises only when the reinforcing material undergoes strain hardening after yielding.

Fig. 2-13 shows a schematic representation of the average response of steel reinforcement calculated based on the overall response of a reinforced concrete direct tension test.

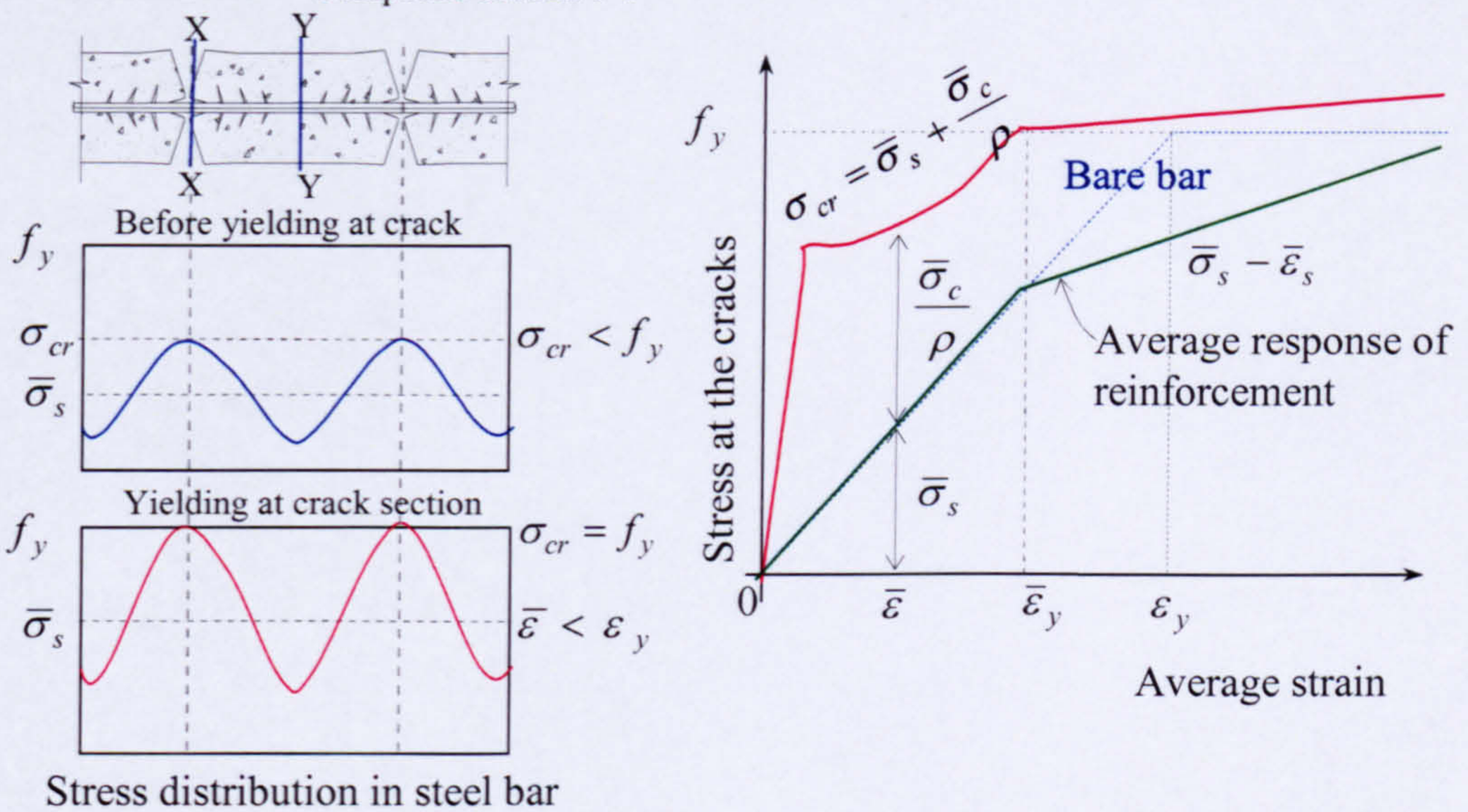

Fig. 2-13 Average stress and average strain of a steel bar when yielding starts

After cracking, equation 2-21 can be derived by considering force equilibrium at the crack section (X-X) and composite section (Y-Y).

$$\sigma_{cr} = \bar{\sigma}_s + \frac{\bar{\sigma}_c}{\rho} \qquad (2\text{-}21)$$

Where, σ_{cr} is the bar stress at crack, $\bar{\sigma}_s$ is the average stress of steel and $\bar{\sigma}_c$ is the average stress of concrete and ρ is the reinforcement ratio.

When σ_{cr} reaches the yield strength of the bar, f_y, the steel starts to yield at the crack section and this occurs at an average strain of the bar ($\bar{\varepsilon}_y$) less than the yield strain of the bare bar (ε_y) (see Fig 2-13). As yielding is associated with large increase in strain, the average stress-strain relationship of the reinforcement ($\bar{\sigma}_s - \bar{\varepsilon}_s$) will deviate from

the bare bar response at $\bar{\varepsilon}_y$, as shown in Fig. 2-13. The apparent yield point depends on many factors including the yield point of the bar and the reinforcement ratio.

Belarbi and Hsu (1994), after conducting tests on 17 reinforced concrete panels in tension, endorsed the Okamura and Maekawa (1991) formulae derived using direct tension tests (equation 2-20 with c=0.4). Belarbi and Hsu also pointed out the importance of modelling average steel stress- strain relationships and the importance of using different yield stresses which they named "apparent yield stress (f_y^*)" since reinforcement yielding at the crack takes place before the average stress reaches the material yield stress (f_y) (see Fig. 2-14).

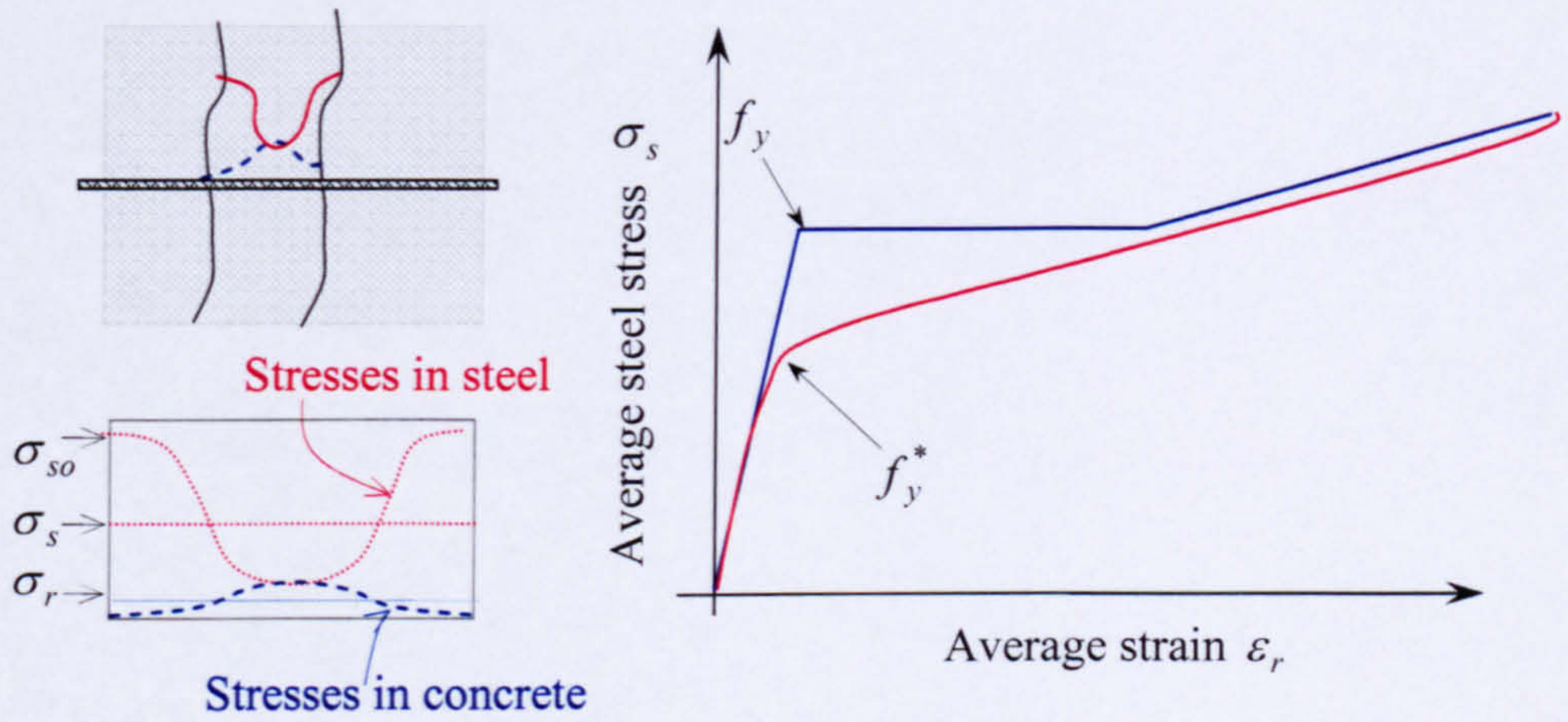

Fig. 2-14 Average stress strain behaviour of reinforcement with yield point followed by strain hardening

Equation 2-22 is derived by considering the equilibrium between the cracked and composite sections (see Fig 2-14).

$$\sigma_{so} = \sigma_s + \frac{1}{\rho}\sigma_r \qquad (2\text{-}22)$$

where, σ_s and σ_r are the average stresses of steel and concrete respectively and σ_{so} is the steel stress at the crack.

By substituting the average concrete stress from equation 2-20 (which is valid before and after yielding of the reinforcement) into equation 2-22 the above equation can be further modified as follows, equation 2-23.

$$\sigma_{so} = \sigma_s + \frac{f_{cr}}{\rho}\left(\frac{E_s \varepsilon_{cr}}{\sigma_s}\right)^{0.4} \qquad (2\text{-}23)$$

According to the above equation, the apparent yielding, f_y^* , is reached when the stress in the reinforcement at the crack, σ_{so}, reaches the yield stress of the bar, f_y. By substituting f_y^*, f_y, $f_{cr} = E_C \varepsilon_{cr}$ and $n = E_s / E_c$ in equation 2-23 and rearranging it, a close-form solution for the apparent yield point can be found (see equation 2-24). A simplified version of equation 2-24 is also given in equation 2-25.

$$\left[\frac{f_y^*}{f_y}\right]^{0.4} - \left[\frac{f_y^*}{f_y}\right]^{1.4} = \frac{n^{0.4}}{\rho}\left[\frac{f_{cr}}{f_y}\right]^{1.4} \tag{2-24}$$

$$\frac{f_y^*}{f_y} = 1 - \frac{4}{\rho}\left(\frac{f_{cr}}{f_y}\right)^{1.5} \tag{2-25}$$

As GFRP has linear elastic response until failure, the need to consider a different model for the average stress strain response of the bar does not arise and the linear elastic material response can be applied without any modification.

Until now the discussion concentrated on empirical formulae accounting for the tension stiffening effect and other associated average stress strain behaviours. From this point, discussion will deal mainly with the principles of theoretical modelling of tension stiffening behaviour. As tension stiffening effect depends on many factors, including tensile strength of concrete, bond development length of embedded reinforcing bar, reinforcement ratio and reinforcement spacing, fundamental theoretical understanding of its behaviour is very important. In particular, as GFRP has very different mechanical properties and bond properties from steel, understanding the various mechanisms attributed to the tension stiffening effect at a more fundamental level is very important for building up tension stiffening models for GFRP RC.

2.4.2 Theoretical models for tension stiffening

2.4.2.1 Models based on solution to bond-slip equation

Early attempts of theoretical modelling of the tension stiffening behaviour were based on solving differential equations representing bond-slip relationships (Characteristic equation for bond). The derivation of the bond-slip relationship is presented next with the help of typical concrete section diagram between cracks, as shown in Fig. 2-15.

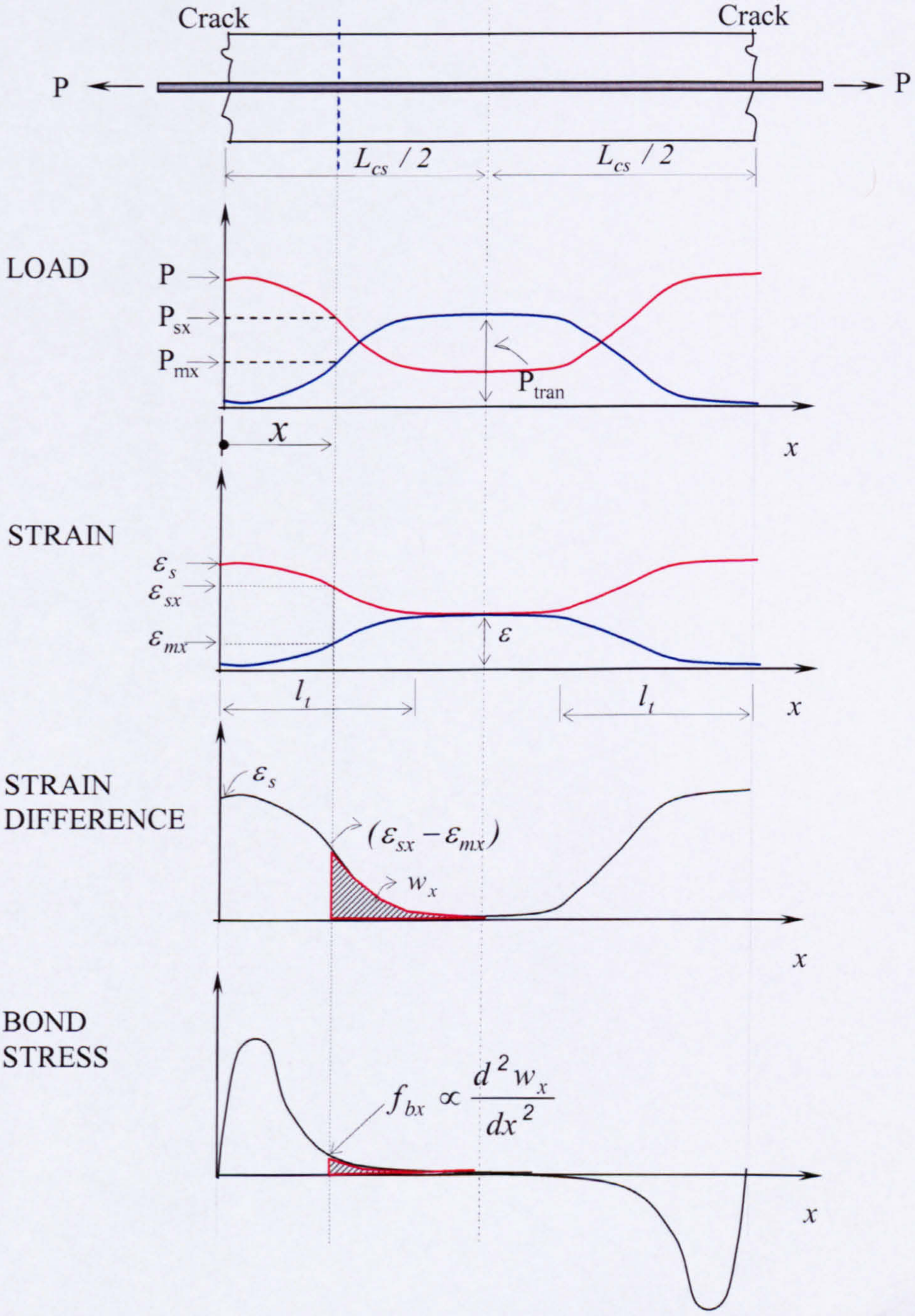

Fig. 2- 15 Load, strain, slip and bond stress distribution (Somayaji and Shah 1981)

By considering the equilibrium of horizontal forces between the cracked section ($x = 0$) and a distance x away from the cracked section (see Fig 2-15 Load and equation 2-26) the total force P is the sum of the force in concrete, P_{mx}, plus the force in the reinforcement, P_{sx}.

$$P = P_{mx} + P_{sx} \tag{2-26}$$

Assuming both concrete and steel behave elastically, equation 2-26 can be modified to arrive at equation 2-27, as shown below (see also Fig 2-15 strain).

$$P = A_m E_c(\varepsilon_{mx} + \varepsilon_{sx} n\rho) \tag{2-27}$$

Where n is the modular ratio of steel to concrete, ρ is the reinforcement ratio, A_m is the area of concrete, E_c is the Young's modulus of concrete, ε_{mx} is the strain of concrete and ε_{sx} is the strain of the steel bar.

Local slip s_x is derived by integrating the strain difference between the reinforcement and concrete over half the element as shown in equation 2-28 below (see Fig 2-15 Strain difference).

$$s_x = -\int_{x}^{L_{cs}/2}(\varepsilon_{sx} - \varepsilon_{mx})dx \tag{2-28}$$

Equation 2-29 is derived by differentiating equation 2-28 with respect to x

$$\frac{ds_x}{dx} = -(\varepsilon_{sx} - \varepsilon_{mx}) \tag{2-29}$$

Substituting the value of ε_{mx} derived from 2-27 into 2-29 leads to equation 2-30

$$\frac{ds_x}{dx} = [\varepsilon_s n\rho - \varepsilon_{sx}(1 + n\rho)] \tag{2-30}$$

Where ε_s is the strain of the bar at the cracked section.

Equation 2-30 when further differentiated with respect to x results in equation 2-31

$$\frac{d^2 s_x}{dx^2} = -(1 + n\rho)\frac{d\varepsilon_{sx}}{dx} \tag{2-31}$$

Local bond stress f_{bx} can be defined as the decrease in force carried by the reinforcement over a differential length dx at x, per unit surface area ($\sum_o$) of the bar which can be written below as equation 2-32.

$$f_{bx} = -\frac{dP_{sx}/dx}{\Sigma_o} = -\frac{A_s E_s(d\varepsilon_{sx}/dx)}{\sum_o} \tag{2-32}$$

Substituting $d\varepsilon_{sx}/dx$ from equation 2-32 into equation 2-31 the governing differential equation for bond is obtained, equation 2-33.

$$\frac{d^2 s_x}{dx^2} - \frac{(1+\eta\rho)\sum_o}{A_s E_s} f_{bx} = 0 \qquad (2\text{-}33)$$

The above equation represents the basic relationship between the second derivative of local slip s_x and local bond stress f_{bx} and any solution to this equation must satisfy the boundary conditions. Slip at the centre of the segment should be zero, if for example the control volume between two cracks is chosen; $ds_x/dx = -\varepsilon_s$ at $x = 0$, $ds_x/dx = 0$ at $x = l_t$ and at $x = 0$, where l_t is the end of transfer length (see Fig 2-15 strain), and at $x = 0$ and $x = L_{cs}/2$; $d^2 s_x/d^2 x = 0$ as the bond stresses are zero at the crack faces and at the centre of the crack.

Equation 2-33 shows that the local bond stress is a function of local slip. Substituting a local bond stress-slip relationship into equation 2-33 is one way to solve the equation. However there is no bond stress slip relationship that uniquely represent local bond stress-slip at all points along the section.

Somayaji and Shah (1981) solved the equation 2-33 by assuming an exponential bond stress distribution function along the crack section as shown below.

$$\frac{d^2 s_x}{dx^2} = Ae^x + Be^x + c \qquad (2\text{-}34)$$

By twice integrating, equation 2-34 becomes equation 2-35 as shown below.

$$w_x = Ae^x + Be^x + Cx^2/2 + Dx + E \qquad (2\text{-}35)$$

A solution to the above equation can be found by applying the boundary conditions discussed above. Once a solution to local slip, s_x , is found, the steel strain, the concrete strain, and the contribution of steel and concrete at various sections to carry the applied load can be found using equations 2-27~2-29. With the above procedure the concrete contribution in tension (tension stiffening effect of concrete) can be derived by integrating the contribution at various sections along the length of the specimen.

Instead of using an exponential bond distribution function shaped by the boundary conditions, Chan et al. (1993) used an idealised bond distribution function based on

experimental investigations to model the bond between cracks. In order to conform to the experimentally derived bond stress distributions, different bond distributions functions were considered before and after bond stress reaching the ultimate bond stress value, see Fig. 2-16. In the model they employed a transfer length (l_t), which is determined by equation 2-35 (see Fig 2-16 b). When the transfer length (l_t) reaches half the distance between cracks (l), the peak bond stress is assumed to reach an ultimate value (see Fig 2-16(c)). After that point, the ultimate stress propagates inwards (see Fig 2-16(d)) and three functions need to be defined to describe the bond distribution at this stage.

The transfer length is given by equation 2-35 below.

$$l_t = k_p \frac{P}{(1+n\rho)\pi D} \tag{2-35}$$

Where l_t is the transfer length and k_p is a constant determined by pull out tests.

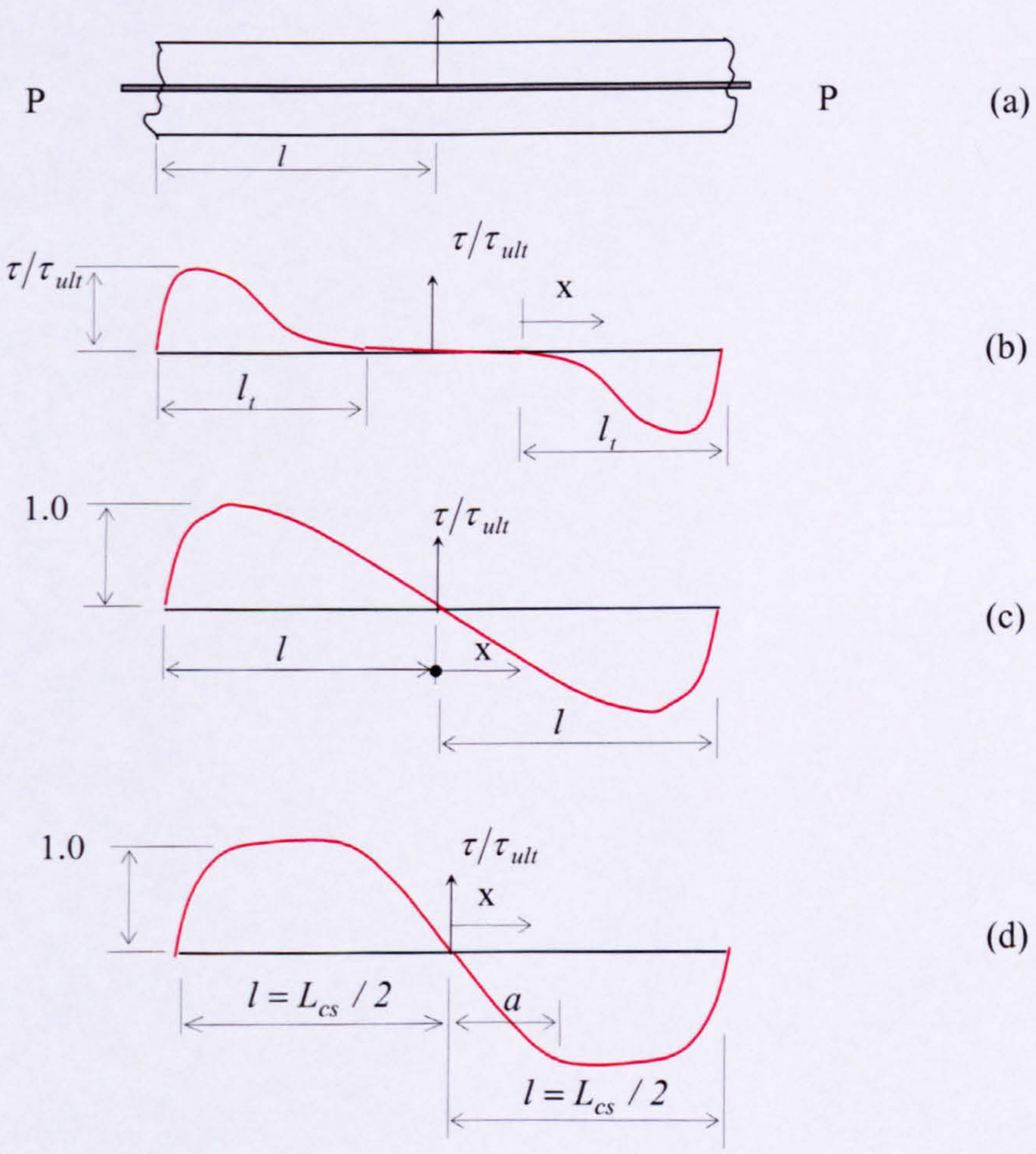

Fig. 2- 16 Bond stress distribution model (after Chan et al. 1993)

Equation 2-36 is the bond stress distribution function for small loads where the bond stress does not reach the peak bond stress value at any section. This is determined by the condition $l_t \leq L_{cs}/2$, see Fig. 2-16(b).

$$\tau(x) = k_u \tau_m \left(\frac{x}{l_t}\right)^2 sin\left(\frac{\pi x}{l_t}\right) \qquad (2\text{-}36)$$

Where, k_u is a constant that needs to be derived from the boundary conditions and τ_m is the peak bond stress. From boundary condition $d\tau/dx = 0$ at $\tau = \tau_m$, k_u was found to be 2.5016 and the peak value to be located at $x = 0.7286\ l_t$.

When $l_t > s/2$ the peak bond stress reaches the ultimate value and the bond stress distribution function considered consists of three parts, see Fig 2-16(d).

$0.728 \times L/2 \leq x \leq L_{cs}/2$

$$\tau_1 = 2.501 \tau_{ult} \left(\frac{x}{l_t}\right)^2 sin\left(\frac{\pi x}{l_t}\right) \qquad (2\text{-}37)$$

$a \leq x \leq 0.7286 \times L_{cs}/2$

$$\tau_2 = \tau_{ult} \qquad (2\text{-}38)$$

$0 \leq x \leq a$

$$\tau_3 = 1.3280 \tau_{ult} \left(\frac{x}{l_t}\right)^2 sin\left(\frac{\pi x}{l_t}\right) \qquad (2\text{-}39)$$

Since the bond stress distribution is now fully defined, from equilibrium conditions the concrete and steel stress (σ_{cx} and σ_{sx}) can be found at any section for any given load level by using equations 2-40 & 2-41.

$$\sigma_{cx} = \frac{\pi D}{A_c} \int_x^{l=L_{cs}/2} \tau(x)\, dx \qquad (2\text{-}40)$$

$$\sigma_{sx} = \frac{P}{A_s} - \frac{\pi D}{A_s} \int_x^{L_{cs}/2} \tau(x)\, dx \qquad (2\text{-}41)$$

Where D is the diameter of the reinforcing bar and A_s and A_c are the steel and concrete cross sectional areas respectively. Once the stress components of any section are known, the average stress strain distribution of concrete for different loadings can be calculated. For example, the average concrete contribution between cracks can be calculated by integrating and then averaging the equation 2-40 along half the crack spacing.

$$\bar{\sigma}_{cx} = \frac{2}{L_{cs}} \frac{\pi D}{A_c} \int_0^{L_{cs}/2} \int_x^{L_{cs}/2} \tau(x)\, dx dx \qquad (2\text{-}42)$$

With concrete cracking criteria as shown below, equation 2-43, they extended their model to predict the test results for a tension member of any given length.

$$f_t' = \alpha f_t \left(\frac{\sigma_{c,max}}{\sigma_{c,ave}} \right)^{\beta} \qquad (2\text{-}43)$$

Where, α and β are experimental constants, f_t is the tensile strength of concrete, $\sigma_{c,ave}$ is the average concrete tensile stress between cracks, $\sigma_{c,mac}$ is the maximum concrete tensile stress and f_t' is the dynamic tensile strength of concrete.

Gupta et al. (1990) showed a solution procedure to the characteristic equation of bond, equation (2-33), by way of substituting a bond stress-slip ($\tau - s$) relation. They used both a linear and bilinear bond stress slip relationship to solve the differential equation. Firstly, they found the solution of the characteristic equation based on the linear elastic bond stress-slip relationship, equation 2-44, and found the average stress-strain relationship for concrete based on the equilibrium conditions and compatibility conditions similar to a procedure above.

$$f_b = A\, s \qquad (2\text{-}44)$$

Where A = the slope of the $\tau - s$ curve and is termed slip modulus and s is the slip.

Then they used a bilinear $\tau - s$ relationship that approximated the bond stress slip curves of Nilson (1971) as shown in Fig. 2-17, deriving equation 2-45 to solve the characteristic equation for bond.

$$f_b = A\, s \qquad f_b \le f_m \qquad s \le s_m; \qquad f_b = f_m \qquad s \ge s_m \qquad (2\text{-}45)$$

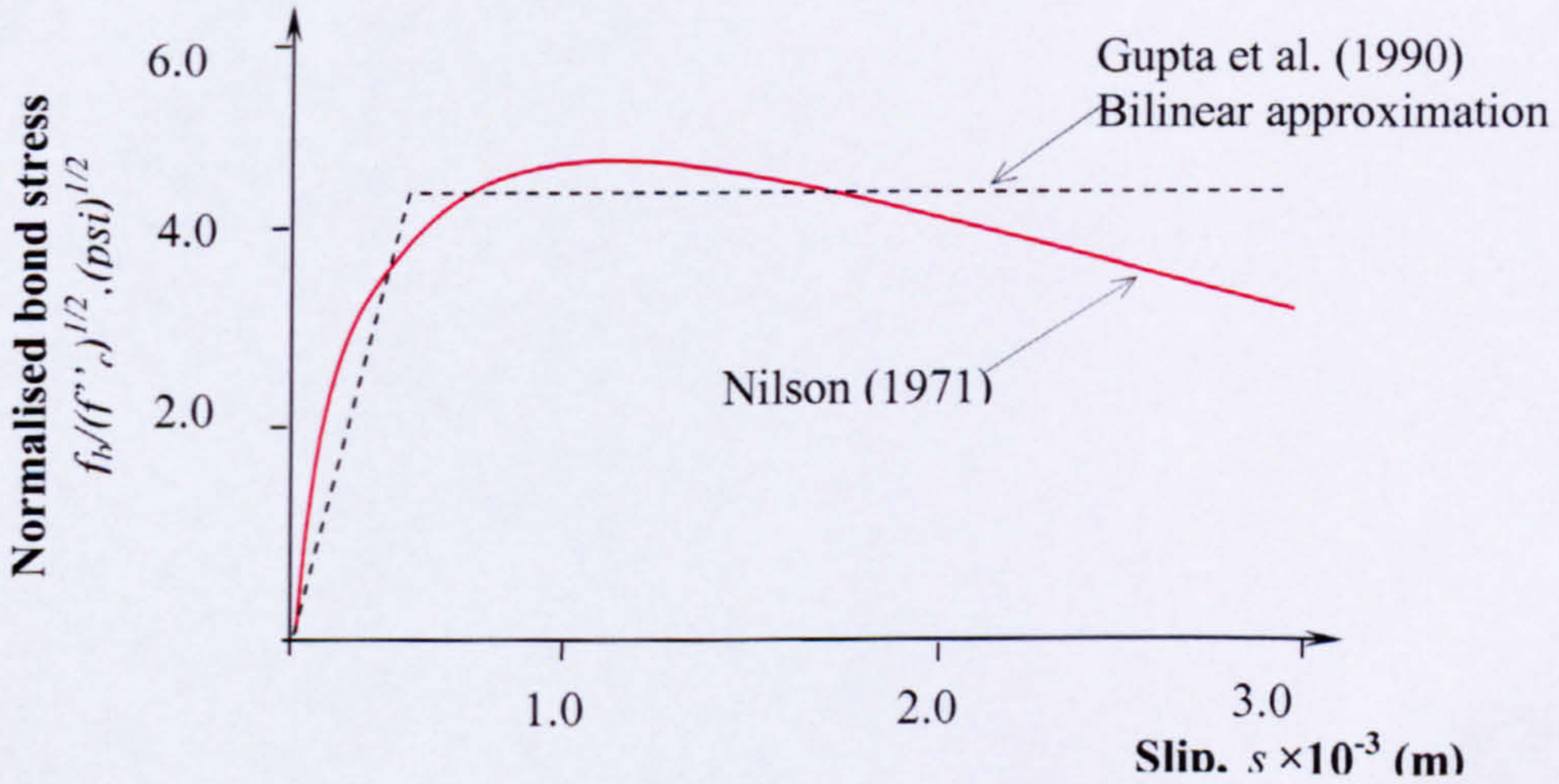

Fig. 2- 17 Bilinear approximation for the bond-slip relationship

Once the solution to equation 2-33 is found, this is used to calculate the average stress-strain relationship of concrete in tension. Based on their solution procedure they performed various parametric studies to assess the influence of various parameters like reinforcement ratio and different ultimate bond stress values on the concrete contribution in tension.

The above mentioned methods are representative of numerous attempts to solve the characteristic equation of bond, selected on the basis of their significance and differences to each other. The use of local bond slip relationship by Gupta et al. (1990) has many weaknesses as there is no unique bond stress slip relationship. Moreover, it is inadequate to assume linear or bilinear relationship for slip (Nilson 1972), (Maekawa et al. 2002). Deriving the bond distribution by conforming to the boundary conditions (Somayaji and Shah 1981) does not necessarily yield the correct bond distribution between cracks. Fig. 2-18 compares the bond stress distribution functions used in the first two studies: the exponential function shaped by boundary conditions as proposed by Somayaji and Shah (1981) and the empirical bond distribution function of Chan et al. (1993). It is clear that the exponential function does not agree well with the empirically derived equation.

However, the variations of different models on the calculation of tension stiffening effect may still be insignificant as tension stiffening deals with the overall average stress strain behaviour.

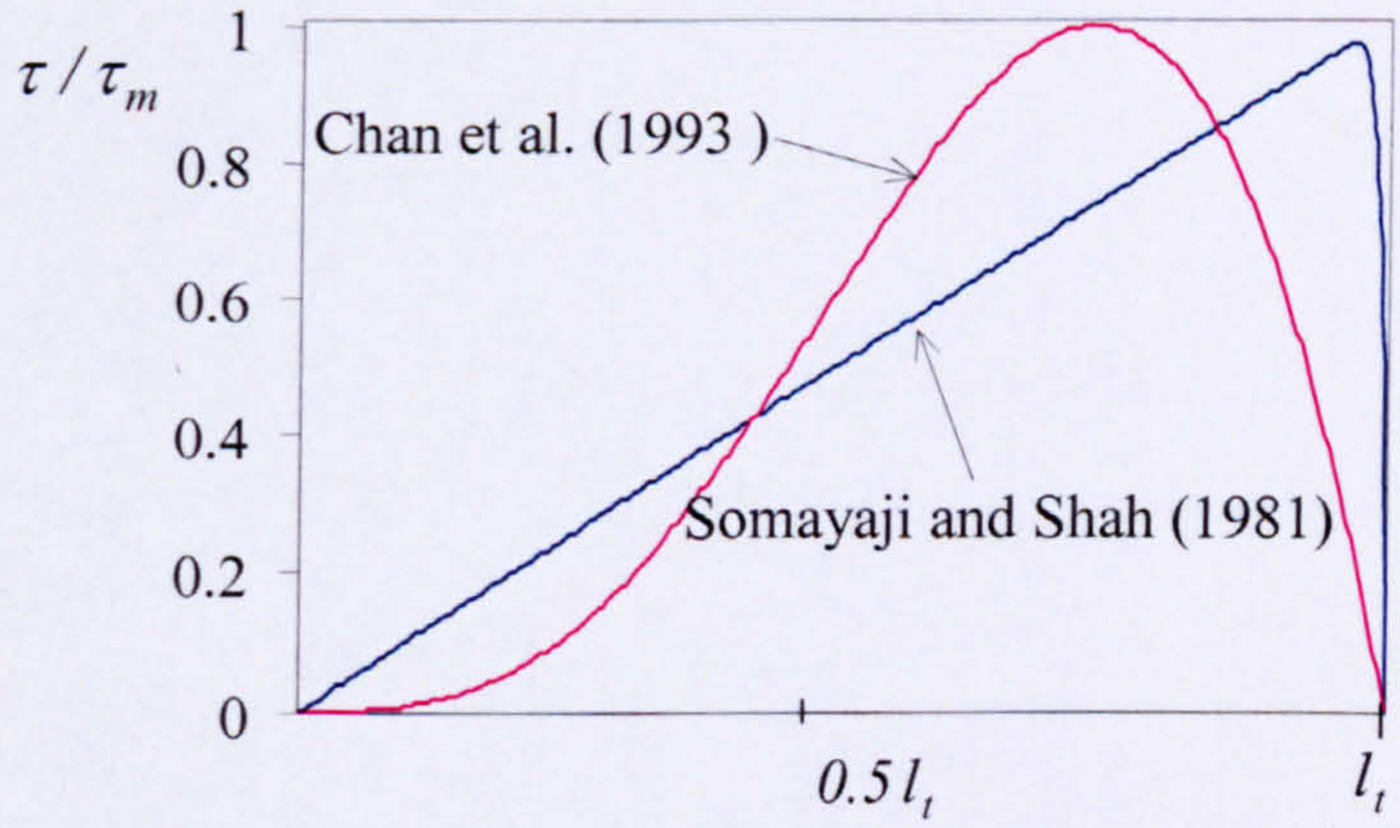

Fig. 2-18 Comparison of different bond stress distribution functions

The main draw back of the earlier models based on bond-slip equation is the lack of consideration given to stress transfer mechanism at the cracked section (tension softening behaviour of concrete). Maekawa et al. (2002) proposed a solution procedure for tension behaviour of reinforced concrete that can still be categorised as a model based on the bond-slip equation. The main difference is that this model uses the concrete tension softening and bond induced tension stiffening together to introduce a generalized model for the tension behaviour of RC.

The bond distribution used in the models is constructed first by using an assumed bar stress as shown in equation 2-46.

$$\tau(x) = \frac{d\sigma_s(x)}{dx}\frac{A_s}{\pi D} \tag{2-46}$$

Based on experimental evidence, the initial bond distribution is then revised to represent bond degradation adjacent to the cracked section. Linear bond degradation which results in zero bond at the cracked section is first used over a length of 5D (D is the diameter of the bar). Within this length, a length of 2.5D next to the crack section is further modified to represent a de-bonded length. A Schematic representation of the idealised bond distribution is shown in Fig.2-19.

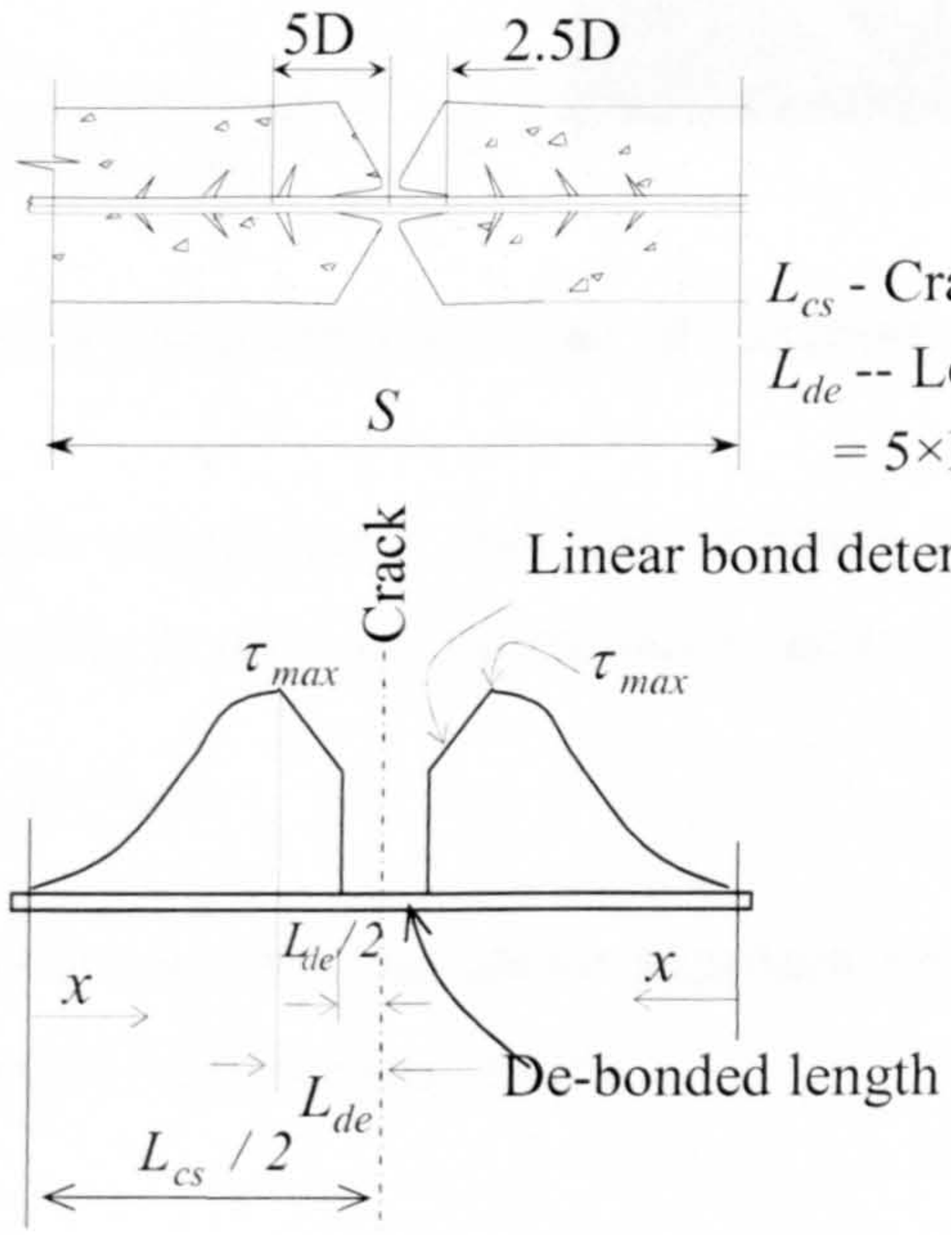

Fig. 2-19 Bond model used for the analysis (Maekawa et al. 2002)

By having a new bond distribution between cracks now fully defined, concrete and reinforcement stresses ($\sigma_s(x),\sigma_c(x)$) and strain profiles ($\varepsilon_s(x),\varepsilon_c(x)$) can be derived using the compatibility and equilibrium conditions similarly to any of the models discussed previously. However, unlike the models discussed previously this model goes one step further to account for the contribution of tension softening effect on the average concrete behaviour in tension. The authors used an empirical formulae (equation 2-47) to account for the additional bridging stress (σ_{br}) due to interaction between the crack faces (see also Fig 2-20).

$$\sigma_{br} = f_t\left[1+0.5\left(\frac{f_t}{G_f}\right)w\right]^{-3} \qquad (2\text{-}47)$$

$$w = c(2\,s) \qquad \textit{Where} \qquad s = \int_0^{L_{cs}/2}\varepsilon_s(x)dx \quad , \quad c = 1/1.3$$

The factor c is used as an attempt to determine the average crack width from a measured crack at the concrete surface, w.

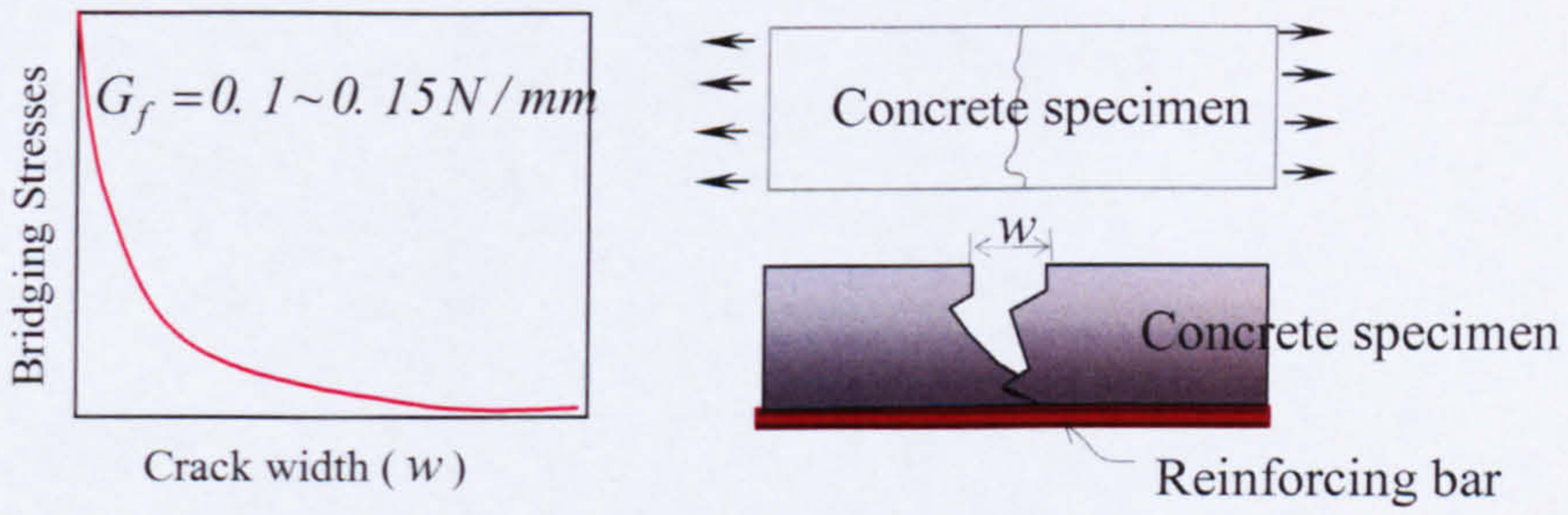

Fig. 2- 20 Tension softening behaviour of concrete considered in the model

With bridging stresses incorporated into the concrete contribution, a new average concrete stress (according to the usual notations) is shown in equation 2-48.

$$\bar{\sigma}_c = \sigma_{br} + \frac{2}{L_{cs}}\int_0^{L_{cs}/2}\sigma_c(x)\,dx \qquad (2\text{-}48)$$

The authors here concluded that the above approach provides better predictions for specimens with even low reinforcement ratios.

2.4.2.2 Fracture mechanics approach

Fracture mechanics can also be used for modelling average stress-strain behaviour of concrete. Many non-linear fracture mechanics models have been proposed to predict cracking of concrete (Shah et al. 1989). Concrete can be looked as a quasi-brittle material with inherent defects, which can propagate and crack the concrete under applied load. In fracture mechanics, fracture progresses when the energy release rate, G, is equal to the fracture resistance, R. G is the rate of strain energy released per unit crack length. R is the rate of change of consumed energy at the crack tip per unit crack length.

$$R = G \tag{2-49}$$

G depends on the geometry of specimens, boundary conditions and nature of applied loading. G-curves can be derived from linear elastic fracture mechanics (LEFM) considerations (Ouyang and Shah 1990). R-Curves depend on material properties and geometry of the specimen. For brittle materials, R is a material constant and propagation of the flaw may mean catastrophic failure of the structure. However, due to crack arresting mechanisms in concrete, like aggregate bridging, cracks steadily propagate until a second condition is also satisfied, equation 2-50 (see Fig. 2-21):

$$\frac{\partial G}{\partial a} = \frac{\partial R}{\partial a} \tag{2-50}$$

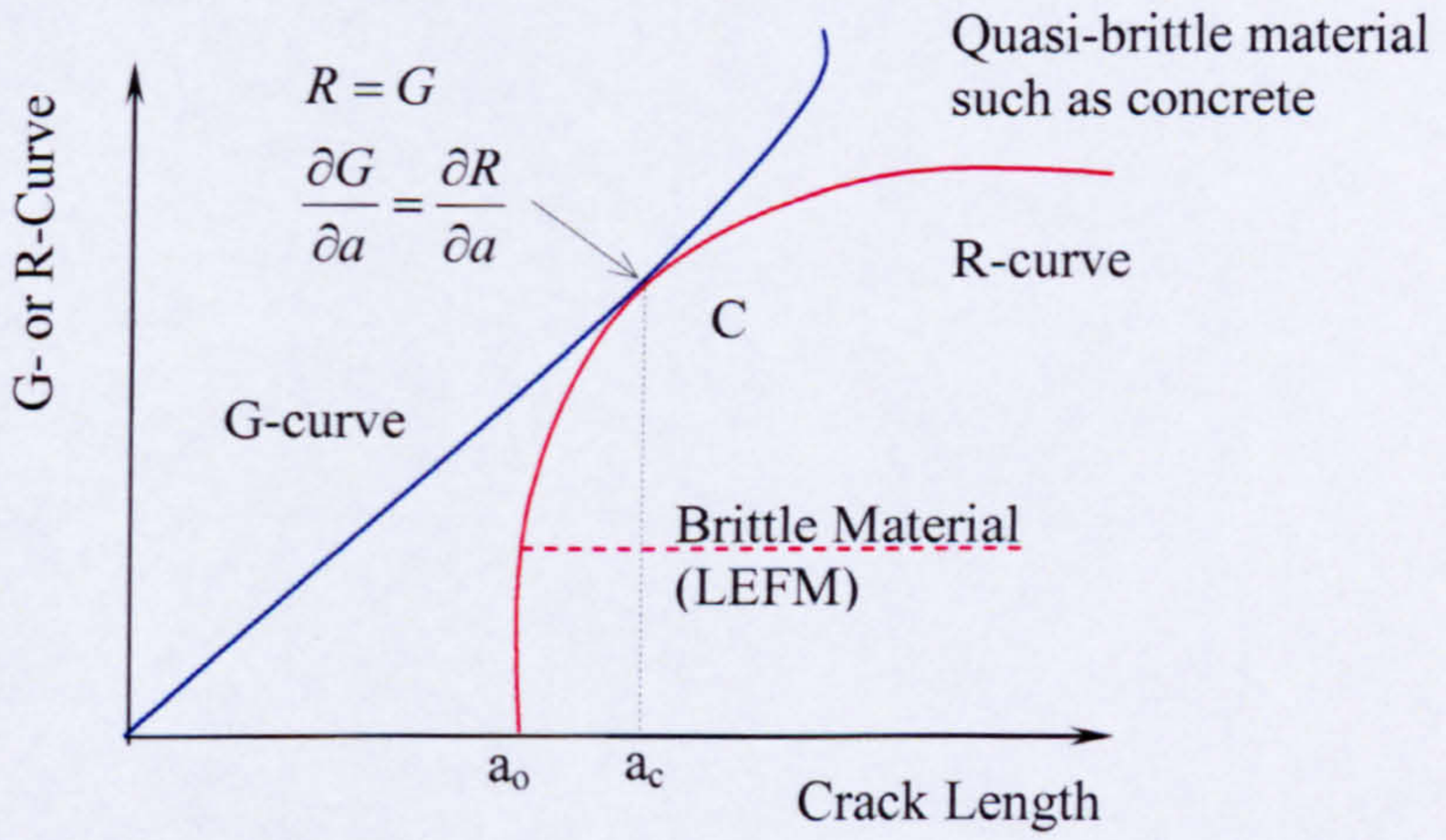

Fig. 2- 21 R- curves for Quasi-brittle materials such as concrete (after Ouyang et al. 1994)

In order to use fracture mechanics based models for the analysis of concrete cracking (tensile behaviour of concrete) both R and G curves should be known. Ouyang et al.

(1990) attempted to model the cracking behaviour of plain concrete by considering a rising fracture resistance curve to account for the existence of a fracture process zone and non-linearity of concrete fracture. They used the equivalent crack approach to calculate the geometry dependent R curves. In their study rising R curves for concrete are considered as a series of G curves (see Fig 2-22). With the equivalent crack approach, they showed how to establish geometry dependent R curves based on material properties, $E, K_{IC}, CTOD_c$ and a_o .where E is the Young's modulus, K_{IC} is the critical stress intensity factor and $CTOD_c$ is the critical crack tip opening displacement which can be easily found from the notched beam test RILEM (1990). The initial crack length, a_o, depends on the flaw size, and for concrete it is typically equal to the aggregate size.

Detailed derivation of R curves can be found in Ouyang and Shah(1990). R curves derived for finite size (R_{ICf}) followed the same curves of infinite size specimen (R_{IC}) until the maximum strength for the given section is reached (illustrated in fig 2-22).

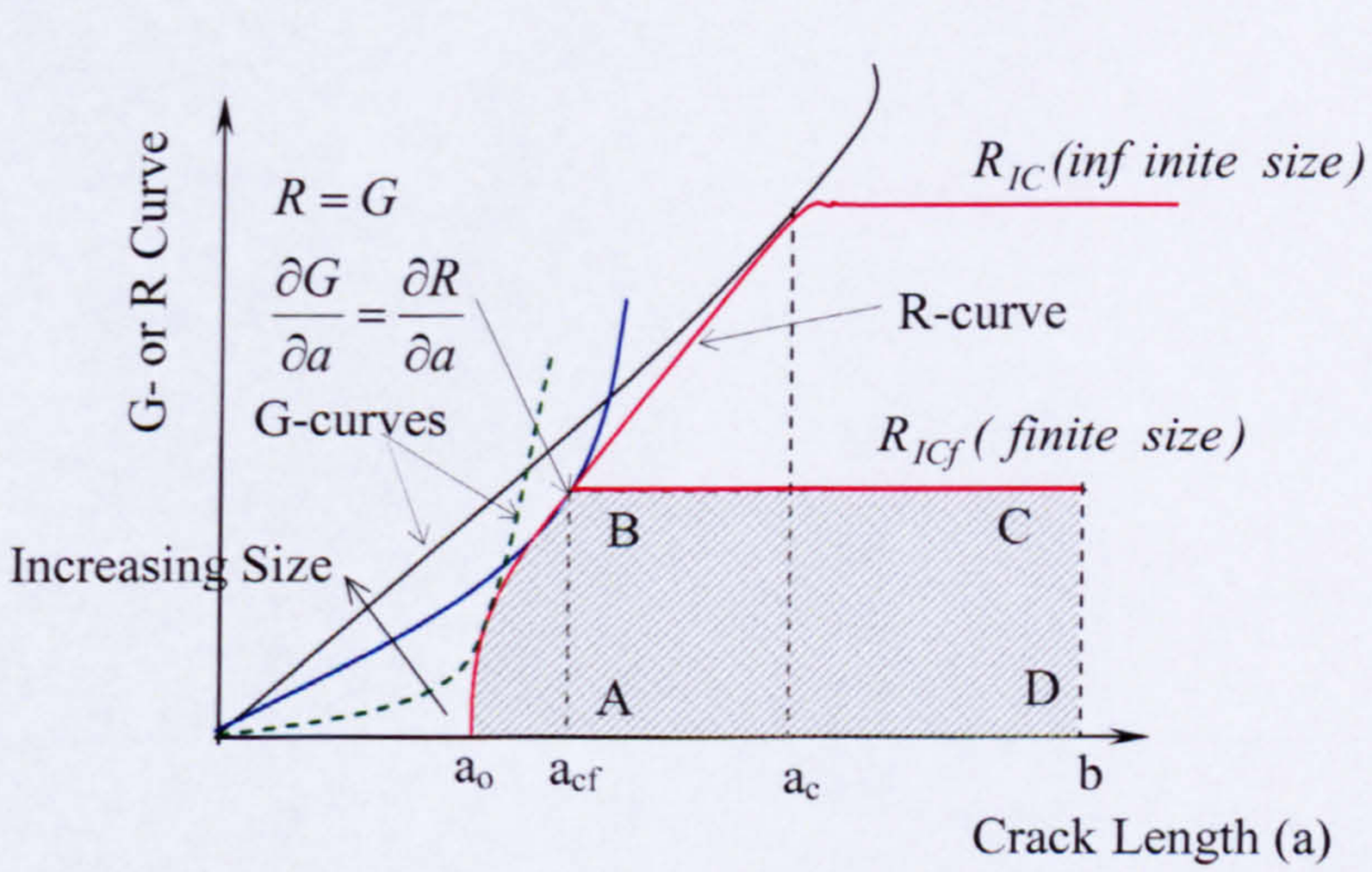

Fig. 2-22 Illustration of G and R curves for description of fracture of concrete

The propagation of a crack requires energy to be absorbed, W, to create new surfaces and during crack propagation this is in equilibrium with the strain energy release rate due to crack propagation, U. This condition in relation to crack length is given in equation 2-51.

$$\frac{\partial U}{\partial a} = \frac{\partial W}{\partial a} \tag{2-51}$$

In terms of fracture mechanics, the two terms $\partial U / \partial a$ and $\partial W / \partial a$ are the energy release rate G and fracture resistance of concrete R.

The same concepts can be applied for reinforced concrete in uni-axial tension. However, the propagation of transverse cracks in reinforced concrete requires additional considerations as it involves de-bonding and slip at the interface of reinforcing bar and concrete. Therefore Equation 2-50 needs to be modified as shown below (equation 2-52) to account for the de-bonding and slip energy at the interface between steel and concrete.

$$\frac{\partial U}{\partial a} = \frac{\partial W}{\partial a} + \frac{\partial W^*}{\partial a} \Rightarrow \frac{\partial U}{\partial a} = R + \frac{\partial W^*}{\partial a} \tag{2-52}$$

where W* = additional energy consumed due to de-bonding and slip at concrete-steel interface.

In order to apply the above equation, energy equilibrium during cracking and the strain distribution in reinforcing bars and concrete should be known. Ouyang and Shah (1997) used the above equation as the basis for modelling tension stiffening behaviour of reinforced concrete. Fig. 2-23 shows idealised strain distribution of the bar and concrete used in their calculation. In their formulation, the authors considered the de-bonding and slip to take place only at a distance 'd' (diameter of the reinforcement) from the crack, and composite reinforced concrete behaviour to occur elsewhere between cracks. In Fig. 2-23, the idealised strain of concrete and steel at the crack section are denoted $\varepsilon_{co}, \varepsilon_{so}$ while $\varepsilon_{cl}, \varepsilon_{sl}$ $(\varepsilon_{cl} = \varepsilon_{sl})$ are the composite strain of concrete and reinforcement at the middle of the section. Average strain of concrete and reinforcement are denoted by ε_s and ε_c, respectively.

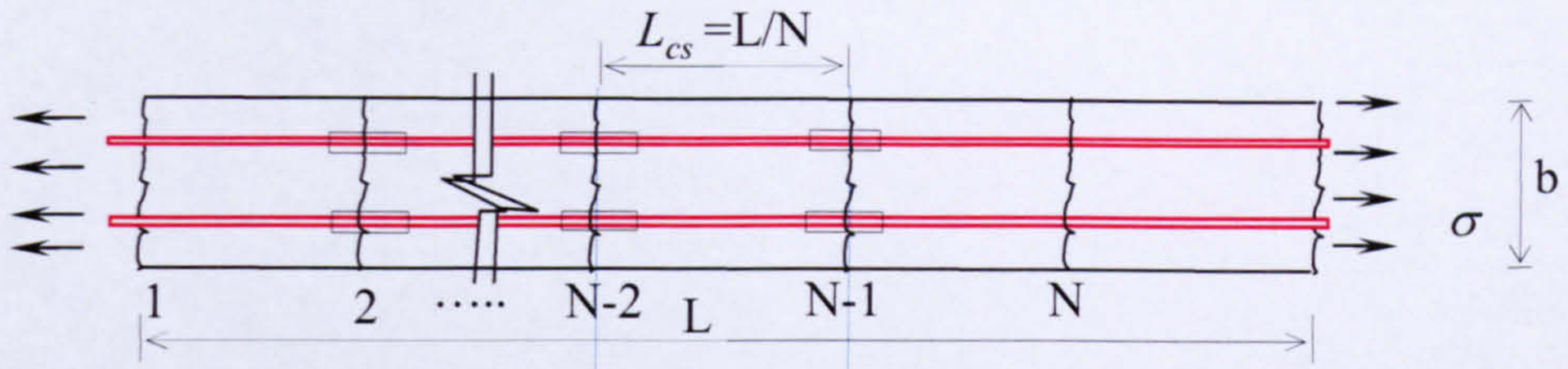

(a) Fracture of reinforced concrete member

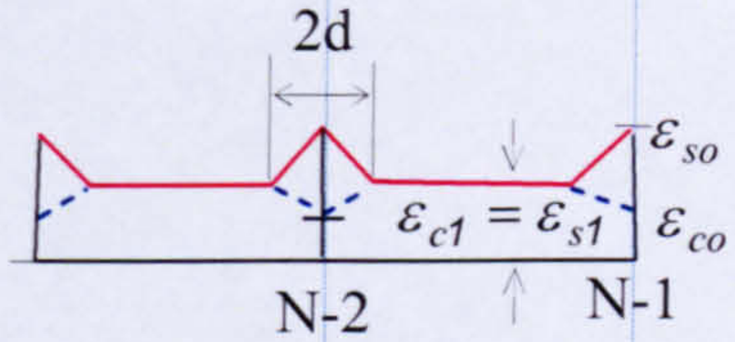

(b) Strain distribution in steel bar and concrete

Average Stresses

$\sigma_c = \varepsilon_c / E_c^*$

$\sigma_s = E_s \varepsilon_s$

$= E_s(\varepsilon_c + Nw_o / L)$

$\sigma = (1-\rho)\sigma_c + \rho\sigma_s$

Stresses at crack section

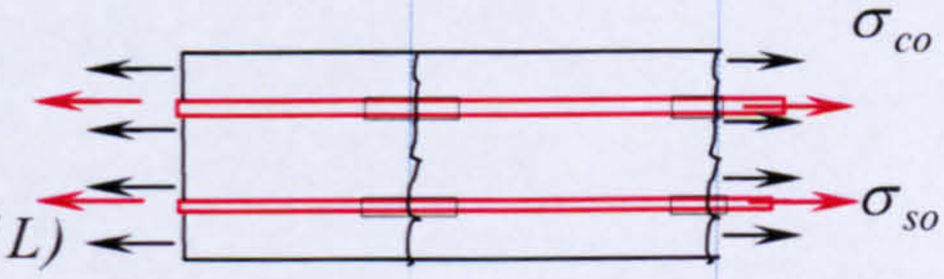

$\sigma = (1-\rho)\sigma_{co} + \rho\sigma_{so}$

(c) Stresses in steel bar and concrete at crack section

Fig. 2-23 Idealized fracture approach for reinforced concrete in tension (Ouyang and Shah 1997)

Considering energy equilibrium during cracking of RC in pure tension with multiple cracks (N number of cracks), equation 2-52 can be written for a number of crack increments as shown bellow:

$$-\frac{1}{bt}\frac{\partial \varphi_c}{\partial N} = R_{ICf} + \frac{1}{bt}\frac{\partial(\varphi_d - \varphi_s)}{\partial N} \qquad (2\text{-}53)$$

where b and t are the section dimensions (breadth and width of the concrete specimen), φ_c is the strain energy of concrete containing N cracks, φ_d is the total de-bonding energy associated with N cracks, φ_s is the total slip energy on all de-bonded surfaces. R_{ICf} is the fracture resistance of a finite dimension as shown in equations 2-54 to 2-56 (see Fig. 2-20 shaded area showing the energy spent in extending an initial defect of a_o to the full section width, b).

$$R_{ICf} = t\int_0^{a_{cf}} \frac{K_I^2(a)}{E}da + \frac{K_I^2(a_{cf})(b-a)}{E_c} \tag{2-54}$$

Substituting $K_I(a) = \sigma_c\sqrt{a}F(a)$ (2-55)

$$R_{ICf} = t\int_0^{a_{cf}} \frac{\sigma_c^2 aF^2(a)}{E}da + \frac{\sigma_c^2 aF^2(a_{cf})(b-a)}{E_c} \tag{2-56}$$

where $F(a)$ for side notched tensile beam is given as below (Tada et al. 1985)

$$F(a) = \frac{1.122 - 0.561(a/b) - 0.205(a/b)^2 + 0.471(a/b)^3 - 0.19(a/b)^4}{\sqrt{1-(a/b)}}$$

Equations 2-57 and 2-58 show the energy of concrete, expressed in terms of average strain of concrete and the de-bonding energy, respectively. With R_{ICf} known, the average strain of concrete can be found by substituting equations 2-57 and 2-58 into equation 2-53.

$$\varphi_c = \frac{Lbt(1-\rho)\varepsilon_c^2}{2M_N} \tag{2-57}$$

$$\varphi_d = \frac{4N\rho d\gamma_d bt}{r} \tag{2-58}$$

Where γ_d is de-bonded energy per unit area of interface between steel and concrete, r is the radius of the steel bar, d is the de-bonded length, ρ is the reinforcement ratio and M_N is the compliance of concrete with N number of cracks (literary meaning reduced Young's modulus of concrete (see the derivation in Oyang and Shah 1997).

In the above formulations, the average strain of concrete only includes the concrete strain between cracks. Therefore the relationship of the average strain of reinforcement and concrete with N number of cracks is given below.

$$\varepsilon_s = \varepsilon_c + \frac{Nw_o}{L} \tag{2-59}$$

Where L = length of member; N= number of cracks and w_0 is the crack width.

Using equation 2-58, the average steel strain (ε_s) for a member with N cracks, the authors managed to establish the average stress-strain relationship of concrete based on fracture mechanics considerations.

The model, however, can be applied only up to the service loads. In addition, the basic assumption of de-bonded length of only one bar diameter also has little theoretical or experimental proof. The linear strain distribution assumed along the de-bonded length is a highly idealistic view of true behaviour. However, this model laid the foundation for the use of fracture mechanics approach for the analysis of tension stiffening behaviour and it was found to be capable of predicting experimental results with a reasonable degree of accuracy.

The simplistic approach used for the bond stress transfer mechanism at the cracked section is the main drawback of this fracture mechanics based model for modelling the behaviour of reinforced concrete in tension. The problem can become worse when using GFRP bars with relatively low bond stiffness compared to deformed steel bars.

2.4.3 Code based modelling of tension stiffening behaviour

In code based equations, there are two basically different approaches used to implement the stiffening effect of concrete between cracks:

(1) An approach adopted in CEB-FIP model code (1978) based on modifying the bar strains at the crack section to arrive at an average strain of the tensile member.

(2) An approach adopted in ACI 224.2R-92 based on the effective area of concrete to model the stiffness of the cracked section, which is similar to the effective second moment of area (I_e) adopted in the deflection calculation of the ACI 318-05.

These two approaches are presented and discussed in the following section.

2.4.3.1 CEB-FIP Approach

According to the CEB-FIP model code, concrete contribution in tension is modelled by expressing an average strain of the reinforced concrete element in terms of the strain of the bar at the cracked section. For example, for the applied load P ($>P_{cr}$) when the strain of the bar at the crack section is ε_s, the average strain of the specimen is ε_{cs} (see Fig. 2-24).

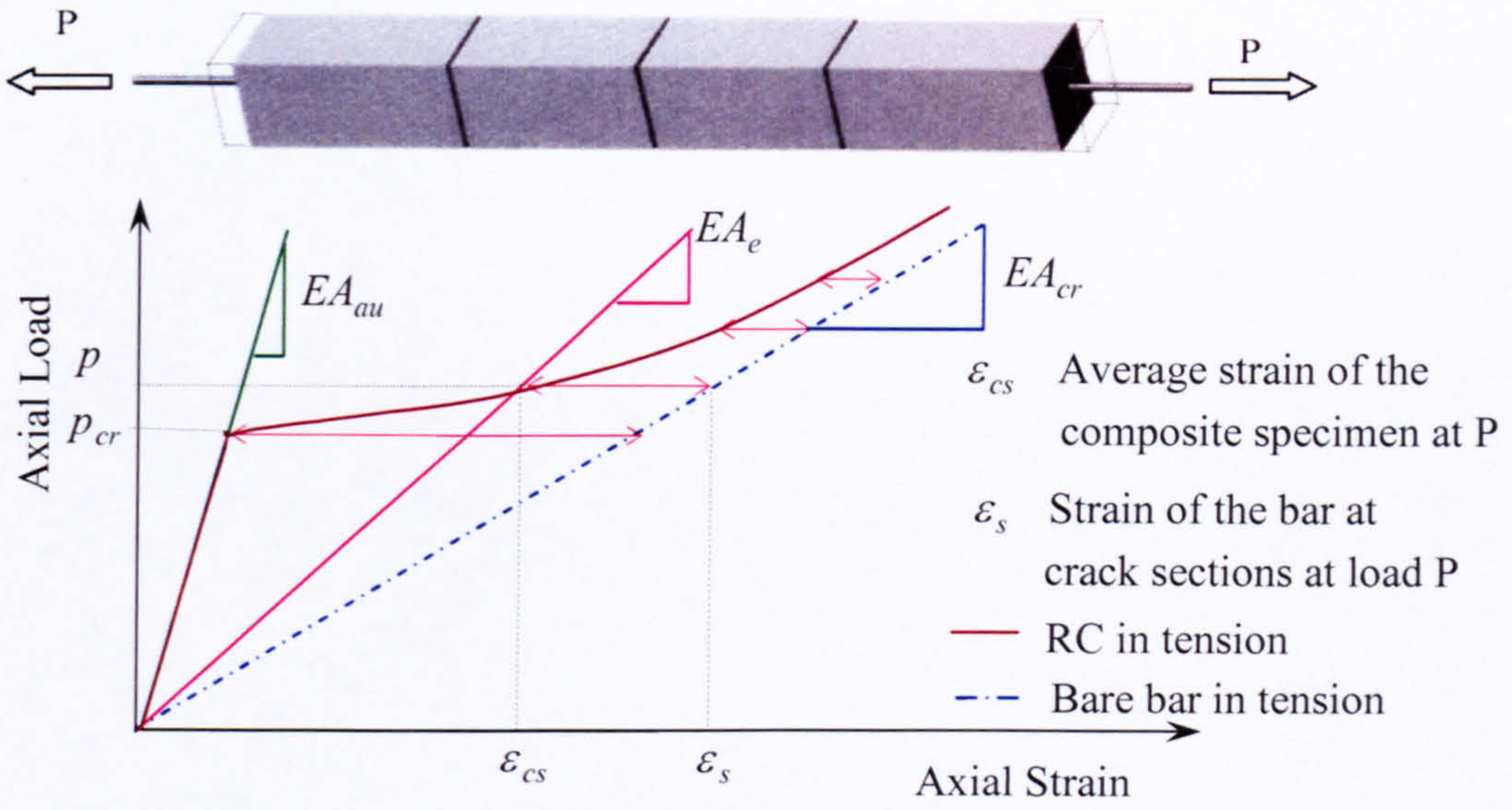

Fig. 2- 24 Tensile load versus strain diagram showing decreasing tension stiffening behaviour with increasing strain

When a symmetrical un-cracked element is loaded in tension, tensile forces are shared between concrete and reinforcement in proportion to their respective stiffness. Considering composite behaviour, equation 2-60 shows the force contribution of reinforcement and concrete at a total applied load, P.

$$P = P_c + P_s = (E_c A_c + nE_c A_s)\varepsilon = E_c A_g (1 - \rho_f + n\rho_f)\varepsilon \qquad (2\text{-}60)$$

Cracking occurs when the strain, ε, corresponds to the strength of concrete. If linear elastic behaviour is assumed in the ascending branch up to cracking and the elastic modulus of concrete in tension is equal to the modulus in compression, cracking can be assumed to be happening when $\varepsilon_{cr} = f_t / E_c$, where f_t is the tensile strength of concrete measured from direct tension test. When a crack occurs, the total load applied at the crack is carried by the reinforcement alone and the stress of reinforcement at the first crack is given by equation 2-61.

$$f_{scr} = \frac{P_{cr}}{A_f} = f_t \left(\frac{1}{\rho} - 1 + n \right) \qquad (2\text{-}61)$$

As more and more cracks occur the contribution of concrete to the overall stiffness of the member tends to diminish. Equation 2-62 is given by the CEB-FIP model to estimate the average strain of the specimen ε_{cs} for the given strain of the bar at the crack section ε_s.

$$\varepsilon_{cs} = \varepsilon_s \left(1 - k \left(\frac{f_{scr}}{f_s} \right)^2 \right) \qquad (2\text{-}62)$$

where $\varepsilon_s = f_s / E_s$, $f_s = P / A_s$ and k is a factor that accounts for the bond between reinforcement and concrete.

2.4.3.2 ACI Approach

This approach is analogous to the effective moment of inertia concept for the evaluation of deflections developed by Branson and incorporated in ACI 318-05 (see section 2.2). Using the same form of the equation used for the effective moment of inertia, the effective cross sectional area for a member in tension is written as shown below.

$$A_e = A_g \left(\frac{P_{cr}}{P} \right)^3 + A_{cr} \left(1 - \left(\frac{P_{cr}}{P} \right)^3 \right) \qquad (2\text{-}63)$$

Where A_g gross cross is section area and A_{cr} is the cracked cross section and is equal to nA_s. The term A_g here could be replaced by the transformed area, A_t, which can be calculated as follows.

$$A_t = A_c + nA_s = A_g + (1 - n)A_s \qquad (2\text{-}64)$$

Using the effective concrete area defined in equation 2-63, the overall behaviour of a reinforced concrete member can be expressed as shown in equation 2-65.

$$P = E_c A_e \varepsilon_{cs} \qquad (2\text{-}65)$$

Both codes provide empirical equations to account for the tension stiffening effect of concrete. Unlike the choice of effective area in the ACI method, use of strain of the bar at the crack section to estimate the average strain of the specimen adopted in CEB-FIP methods seems to provide a direct relationship to account for the tension stiffening effect. Although the results of both methods converge at higher reinforcement ratios (ACI 224.2R-92), at low reinforcement ratios, the ACI approach tends to over estimate the tension stiffening effect (see section 3.3.6).

This chapter presented a state-of-the-art experimental and theoretical investigation on tension stiffening effect. It summarised all the notable experimental and analytical approaches for modelling tension stiffening effects of reinforced concrete. However,

due to the obvious limitation of tension stiffening studies on FRP, the discussion was limited to the conventional steel reinforcements. The chapter also looked at how tension stiffening is accounted in the deflection calculations of flexural elements.

GFRP is altogether a different material and it is difficult to extend the understanding of tension stiffening behaviour of conventional steel reinforcement into the behaviour of GFRP reinforcement. However, this chapter laid the foundation for understanding and studying the tension stiffening behaviour. It also highlighted the need to do an independent study on tension stiffening behaviour of GFRP RC to shed light to the problems identified at the beginning of this thesis on deflections of FRP RC and the impact of tension stiffening effect on deflection. Next chapter will look into the experimental investigation carried out in this study on the GFRP reinforced concrete tension ties to understand and model tension stiffening effect of GFRP RC.

CHAPTER 3

EXPERIMENTS AND ANALYSIS OF TENSION BEHAVIOUR OF GFRP RC

3.1 General

This chapter presents the experimental work on tension stiffening effect of GFRP reinforced concrete. The chapter starts with tension tests of bare GFRP bars and goes on to present experimental investigations of GFRP RC in tension. The results are used to identify the contribution of concrete to the overall element behaviour. Finally, the test results are compared with code-based approaches (ACI and CEB-FIP), modified to account for the different elastic modulus and interaction of GFRP with concrete.

3.2 Tension tests on bare bars

Before the tension stiffening effect of concrete can be established, it is essential to establish the stress-strain behaviour of the GFRP bar in tension. As different bar diameters contain slightly different fibre fractions (ratio between cross sectional area of fibre filaments crossing a given cross section to the cross section of the bar), bars with different diameters tend to have slightly different stress-strain behaviour to each other. Therefore, both the 19.1 mm and 12.7 mm diameter bars used in the tension stiffening study were tested in tension. Testing FRP bars in tension is not trivial, as conventional gripping arrangements to hold the bars are not appropriate for GFRP bars. Conventional holding mechanisms rely on the wedging action of two interlocking jaws as seen schematically in Fig. 3-1.

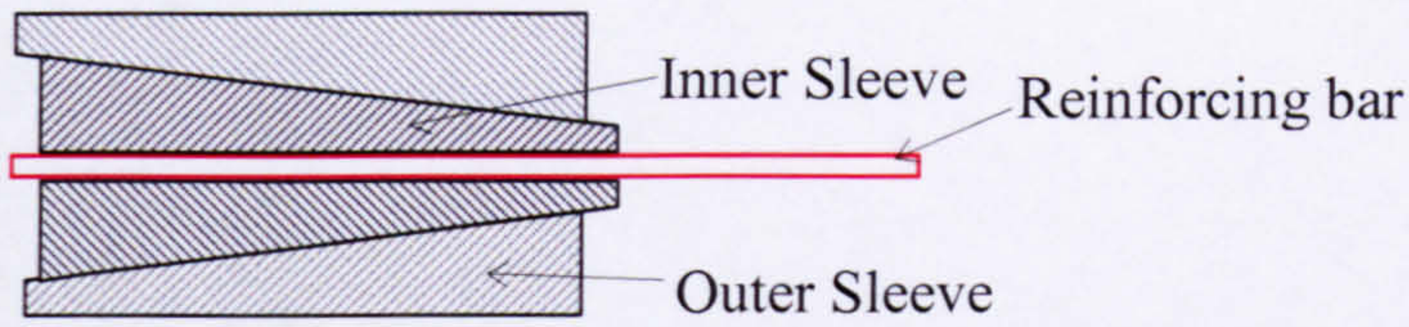

Fig. 3-1 Interlocking sleeve system normally used for tension tests

This system is very effective for testing conventional steel reinforcement as it puts increasing lateral pressure onto the bar being pulled with increasing longitudinal load. However, this is not suitable for testing FRP bars, as the high lateral pressure can crush the FRP bar at the jaws thereby reducing its strength. Therefore, in this experimental work, drilled-through threaded-bars were used to house the bar and a Thixotropic Anchor Grout (Weber sbd Ltd. 2003) was used to bond the bar to the housing.

To give extra grip, the steel screws that houses bars were drilled at two different diameters, one slightly bigger than the other, so that step inside the housing was formed (see Fig. 3-2). While in the vertical position, resin was poured into the housing and the bar was inserted gently from the top with a screw action. The bonded ends were cured under standard laboratory conditions for at least 24 hours before being tested. For the two diameters, 12.7 mm and 19.1 mm, bonded lengths of 200mm and 300 mm were used respectively. Fig 3-2 shows the details of the gripping system used for the two bar diameters.

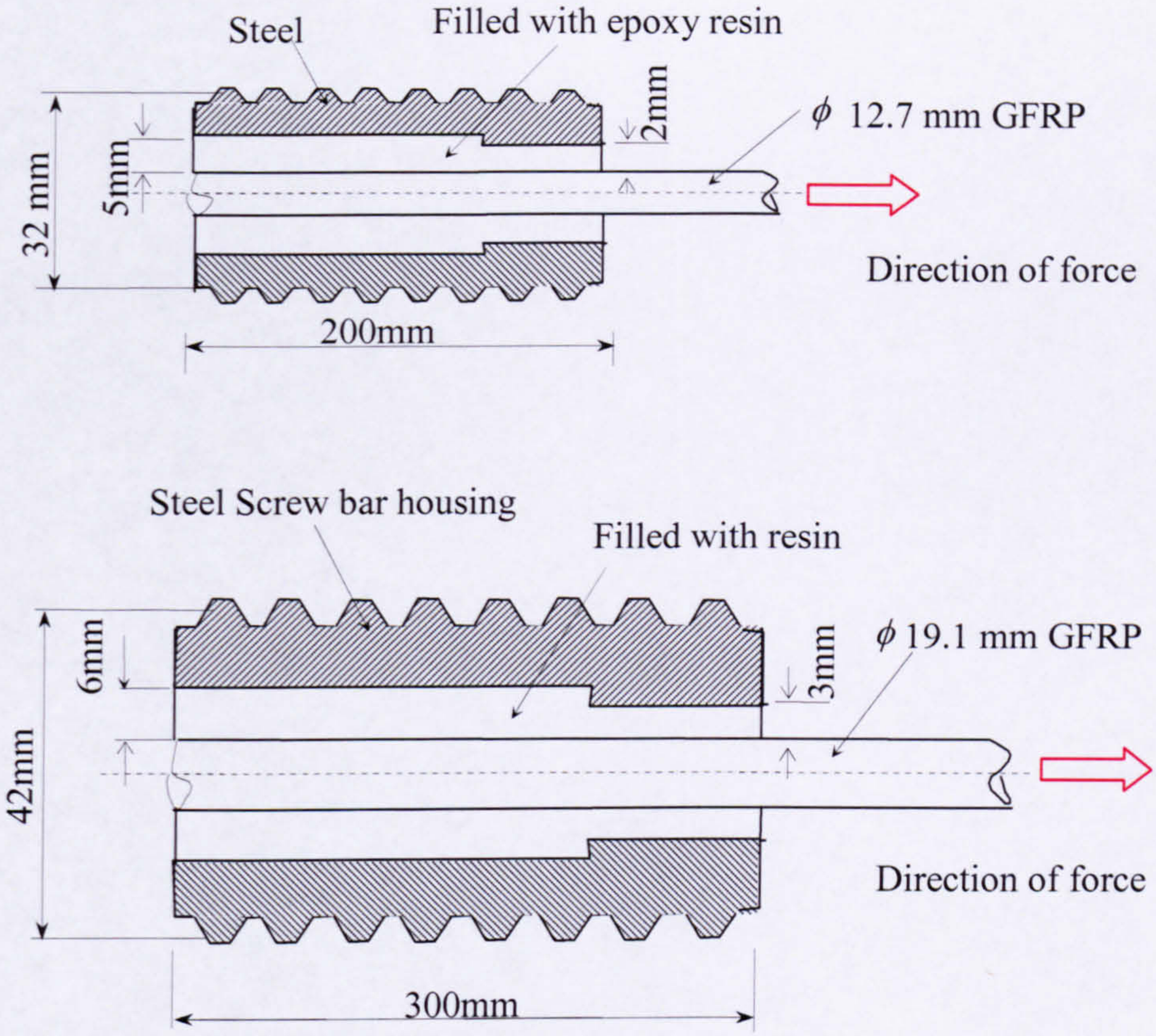

Fig. 3-2 Details of the gripping system for the GFRP bar used for both tension test and tension stiffening studies

The rebar tests were carried out on rigid frame with connectors to hold the threaded bar to the frame at one end and actuator at the other end (see Fig 3-3). Strain gauges were attached to the bar surface at a number of sections. Two strain gauges at each section were glued at 180° apart. Measurement of load and strain gauge readings were recorded at regular intervals using a computerised data logging system. Loading was applied to the bar at a constant rate until failure, using displacement control. Figure 3-4 shows a typical bar failure.

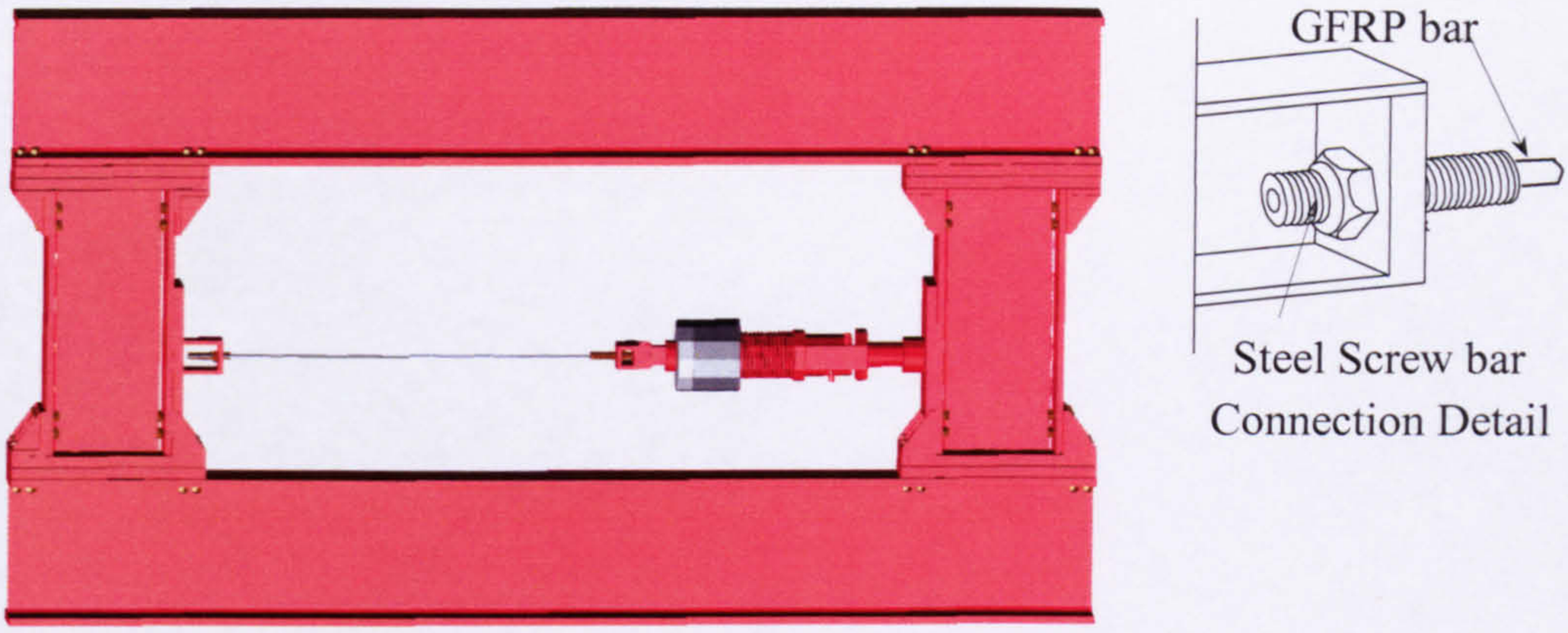

Fig. 3-3 Schematic view of the experiment set up for the tension test and connecting detail

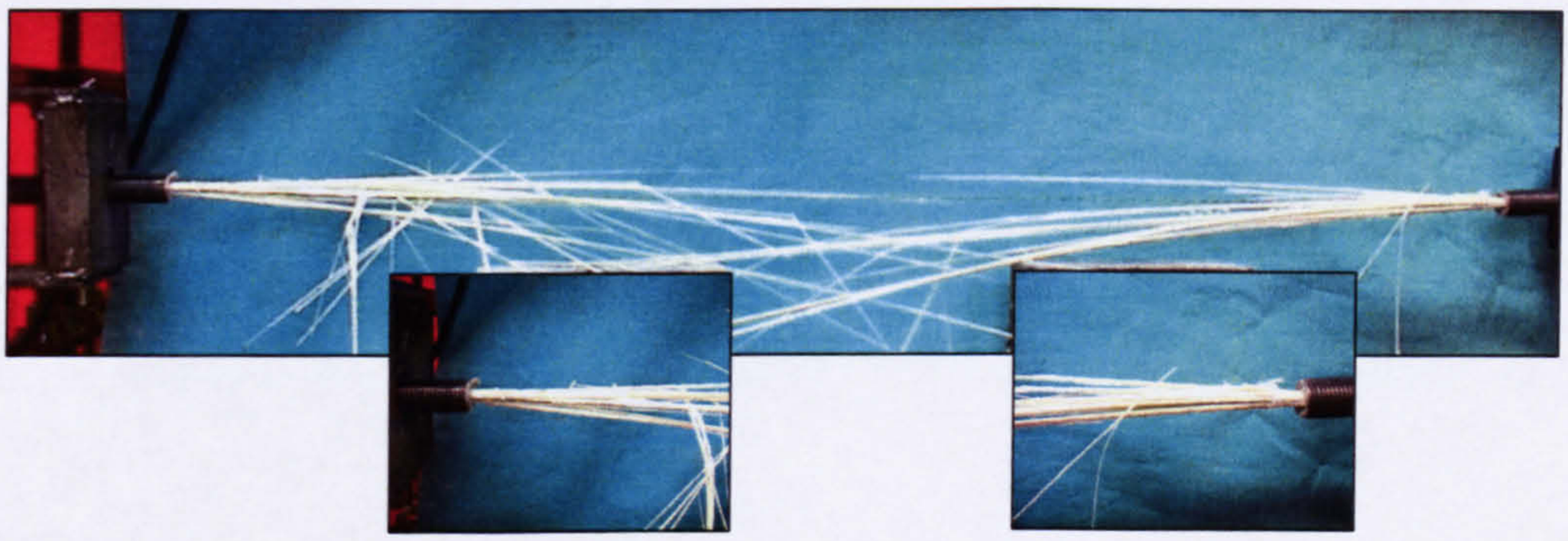

Fig. 3-4 Photograph of bar failure in direct tension: close ups at either end show no damage due to grip forces

The gripping arrangement described above was found to be very effective in achieving the failure of the bar without crushing fibres at the jaws. Three 12.7 mm bars were tested to failure. However, for the 19.1 mm bar, only one bar was tested to failure, whilst the other two were unloaded after 95% of the expected failure load, to avoid the sudden impact at failure. This was necessary since the sudden shock and release of energy can damage the actuator load cell. In calculating strain, strain of the bar is considered to be the average strain of the two opposite strain gauges. Fig. 3-5 shows the stress-strain behaviour of the two bar diameters.

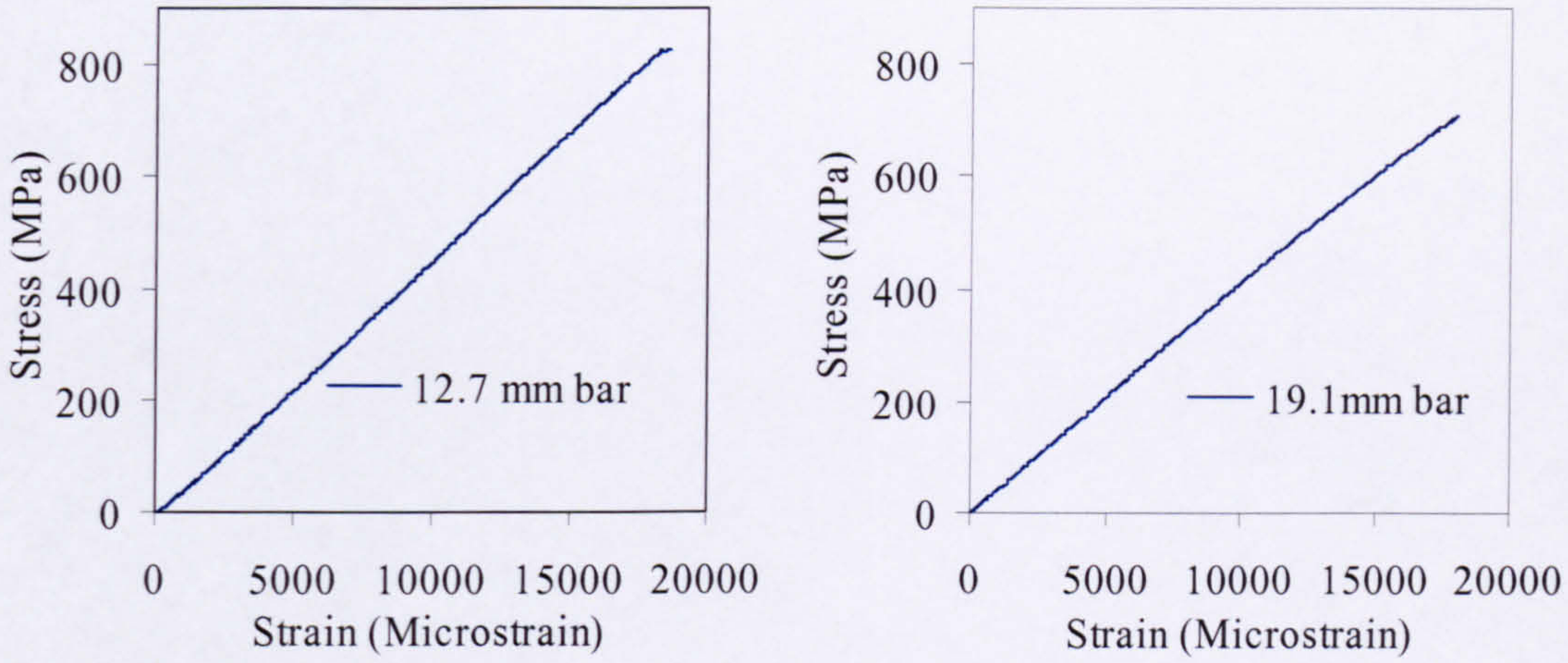

Fig. 3-5 Stress strain relationship of the two bar diameters tested

Table 3.1 shows the average test results compared with the manufacturer specified strength for this batch of bars (data supplied by Hughes Brothers, Inc.). A close agreement of the results and manufacturer data is noted.

Table 3-1 Tested results compared with manufacturer specified values for this batch

	12.7 mm Diameter bar		19.1 mm Diameter bar	
	Manufacturer	**Tested at Sheffield**	**Manufacturer**	**Tested at Sheffield**
Strength (MPa)	836	792	713	715
Stiffness (GPa)	43.2	42.9	41.4	41.9

3.3 Tension tests on Reinforced concrete elements

3.3.1 Experimental setup

A direct tension test on reinforced concrete elements was the main experimental focus of this research study. The purpose of these tests was to establish the average stress-strain relationship for the GFRP reinforced concrete. Experiments were carried out to find out the influence of reinforcement ratio, concrete strength and bar diameter on the tension behaviour of reinforced concrete. The test set-up used for testing reinforced concrete elements in tension is similar to the arrangement used for the tension tests on the bare bars described in the previous section. However, the measuring arrangement used is much more complex and was designed to obtain the overall displacement of the

reinforced concrete element. Fig 3-6 gives a schematic representation of the arrangement used to measure the overall displacement of the reinforced concrete element, while Fig. 3-7 shows a close up view of the measuring arrangement at one end of the specimen. As seen in Fig 3-6 and Fig 3-7, two types of measurements were used for determining the overall displacement of the tension specimen; one measures displacement of the concrete and the other measures the bar slip at each end. Figs. 3-8 (a) and (b) show photographs of the specimen and measuring arrangements during testing.

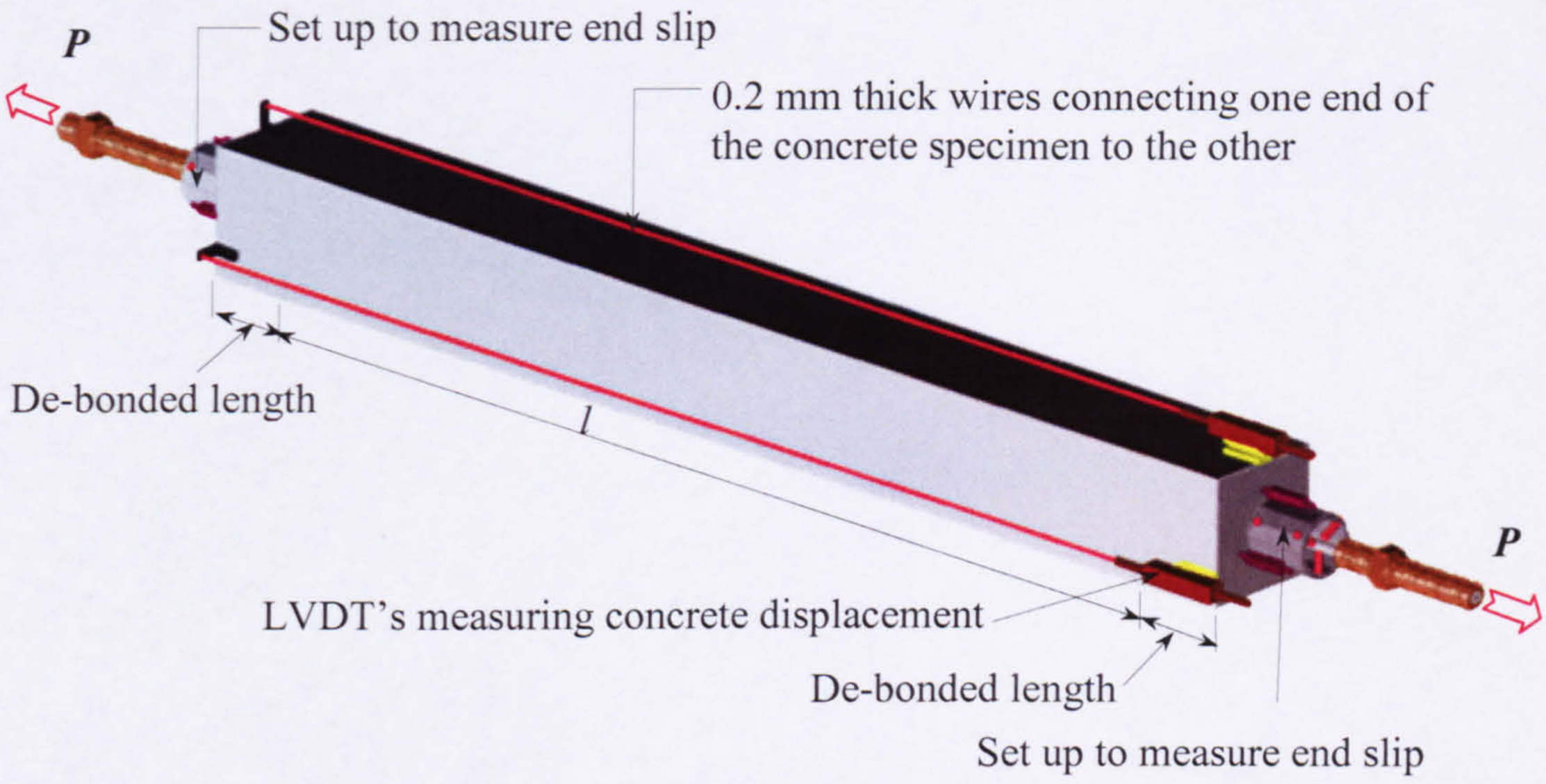

Fig. 3-6 Schematic representation of the instrumentation used to measure the overall displacement of the reinforced concrete element in tension

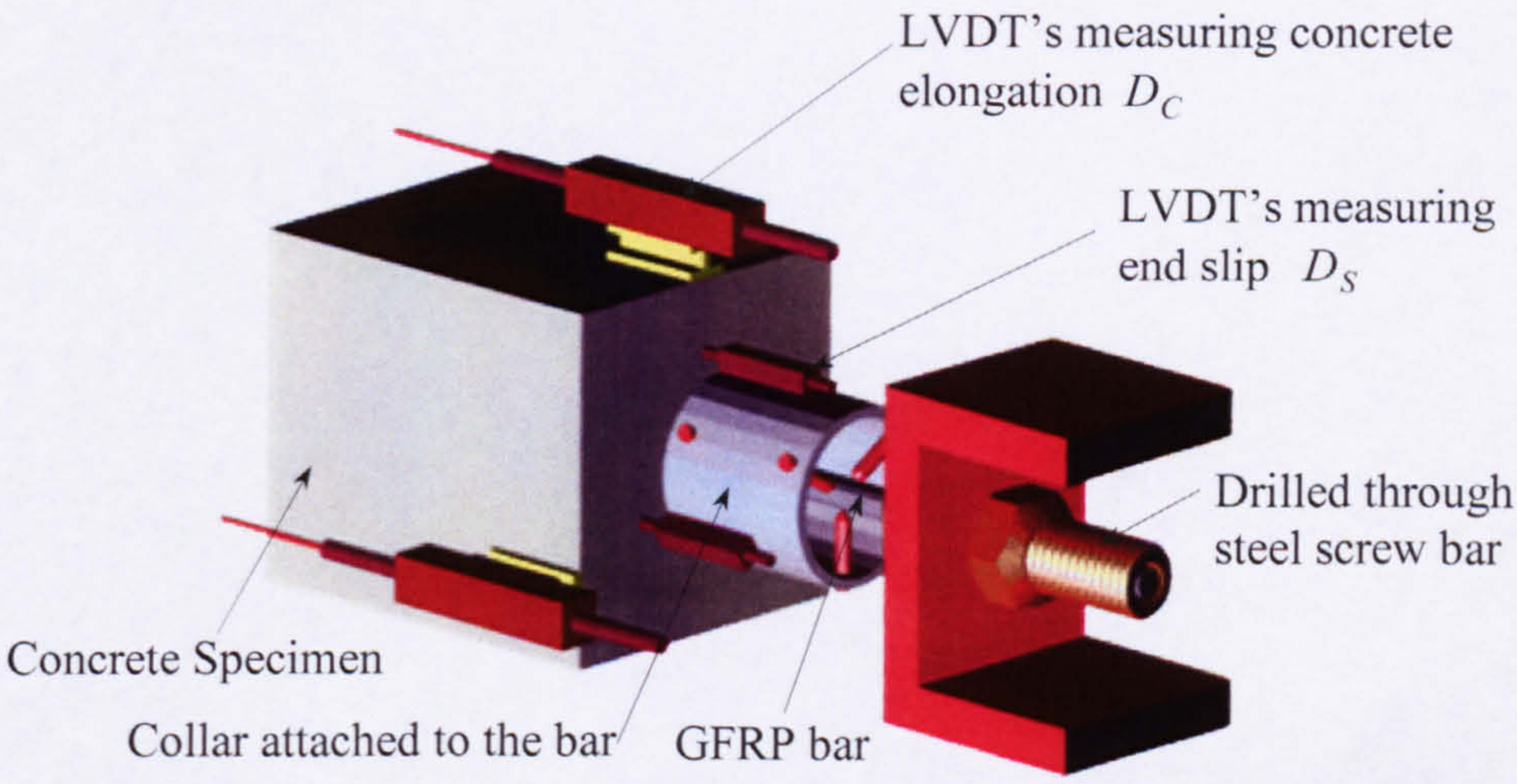

Fig. 3-7 Close up of the measuring arrangement at one end

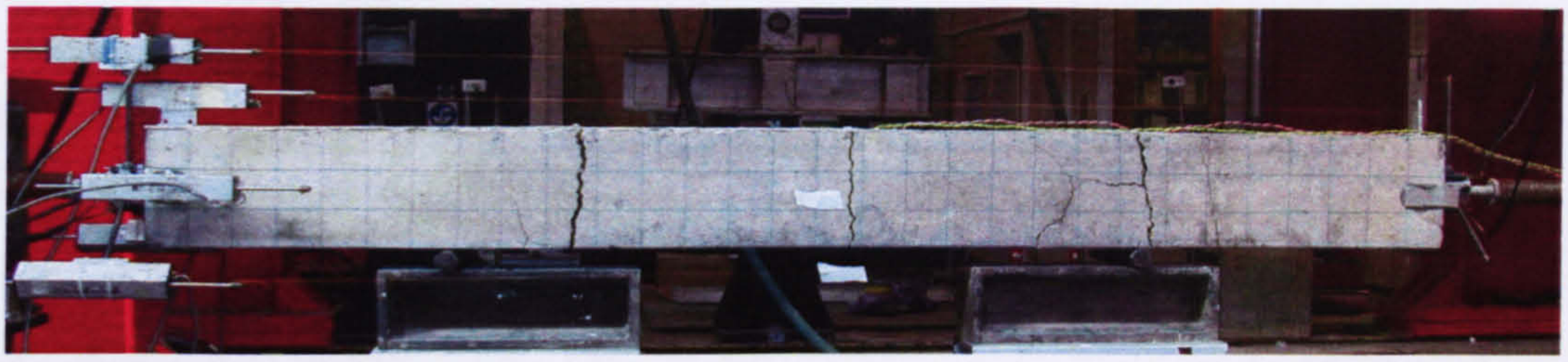

(a) View from the front

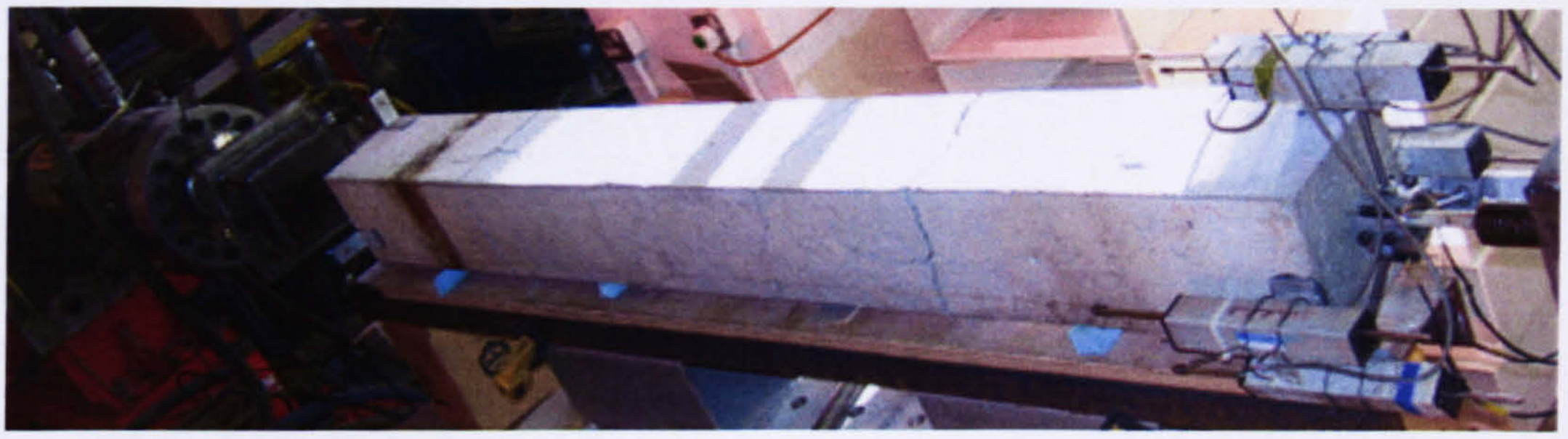

(b) Close up of the measuring arrangement at the end.

Fig. 3-8 Views of the measuring arrangement for direct tension

Measurements of concrete displacement (predominantly due to cracking of concrete) were done using three LVDT's equally spaced at 120° around the centre line of the concrete specimen. The LVDT's were attached to one end of the concrete specimen and connected to fixed points on the other end using a 0.2 mm diameter special light-weight wire (see Fig. 3-6). Bond slip at each end was measured by using a collar, having three small LVDT's equally spaced at 120°, attached to the bar as shown in Fig. 3-7. A fifty millimetre de-bonded length was maintained on either side of all tensile specimens to avoid local concrete tensile failure at the ends.

In establishing the average stress-strain behaviour of the RC element in tension, it is necessary that displacements are measured with reference to the movement of the bar from one end of the specimen to the other end. Considering the measuring arrangement used in this experimental work, the total elongation of the test specimen is considered to be equal to the sum of the end slips D_S plus the total concrete displacement D_C. Therefore, the composite strain (ε_{com}) of the reinforced concrete element with bonded length, *l*, at a given applied load, *P*, can be determined as shown below, equation (3-1).

$$\varepsilon_{composite} = \frac{D_S + D_C - P/(A_f E_f) \times L_{L\&R}}{l} \qquad (3\text{-}1)$$

where $L_{L\&R}$ refers to the sum of de-bonded length at both ends (see Fig 3-7) and any additional length requirements to fix transducers measuring slip D_S to the reinforcement bar. A distinct advantage of this measuring arrangement is that it minimizes any errors due to global movements of the specimen during loading, as measurements are done locally. All specimens were loaded in displacement control to avoid sudden movements during concrete cracking. Fig 3-9 gives a schematic representation of the final testing set up, while Fig 3-10 shows a photograph taken during testing.

For some of the specimens, In addition to the above measuring arrangements, independent measurements were taken from a reference point on the bar from one end of the specimen to the other end. Fig 3-10 shows the additional independent measuring arrangement in place. In this arrangement three independent transducers are placed around a collar at 120^{o} apart on one end and were connected to collars on the opposite end. The measurement taken with the two systems were always found to be in good agreement. This confirms that the total elongation is the sum of D_S and D_C.

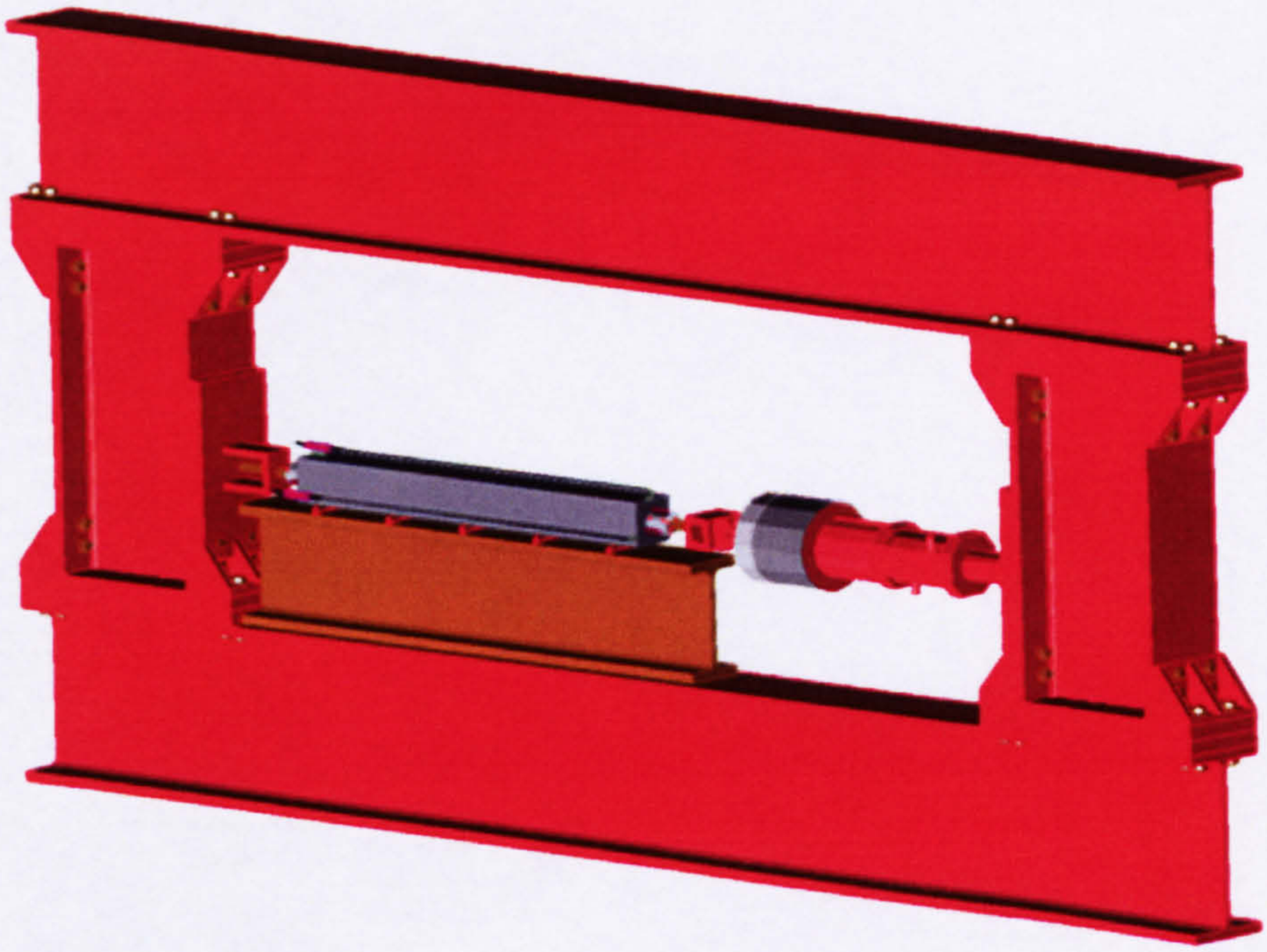

Fig. 3-9 Schematic representation of the final experimental set-up

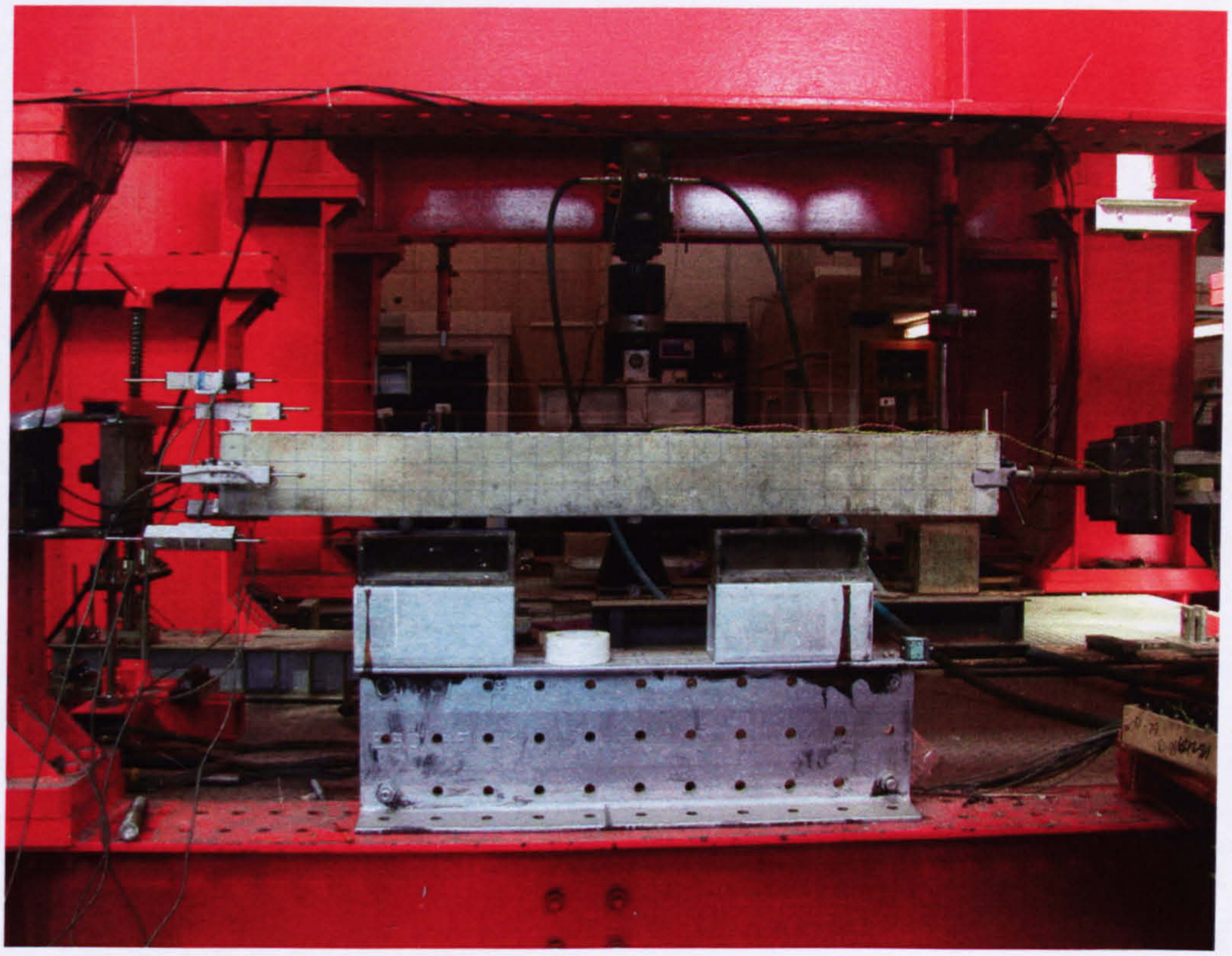

Fig. 3-10 Experiment in progress

3.3.2 Specimen details

In this experimental work two concrete grades and two GFRP bar diameters were used in specimens with square concrete cross-sections of 100, 150, and 200 mm. After casting, all the tensile specimens were cured at 20°C and 100% relative humidity. The curing was done carefully and consistently for all the specimens to control the effects of drying shrinkage on the tension stiffening behaviour. Table 3-2 gives details of all the test specimens, whilst Table 3-3 summarises the material properties of concrete and GFRP bar.

Table 3- 2 Specimen details for the direct tension tests

Specimen	Concrete Cube Strength (MPa)	Bar Diameter D *(mm)*	Dimensions *b×d×l (mm)*	Reinforcement Ratio ρ %
C50/13/100	46	12.7	100×100×1500	1.26
C90/13/100	91	12.7	100×100×1500	1.26
C50/13/150	46	12.7	150×150×1500	0.56
C90/13/150	91	12.7	150×150×1500	0.56
C50/13/200	46	12.7	200×200×1500	0.32
C50/13/200	91	12.7	200×200×1500	0.32
C50/19/150	46	19.1	150×150×1300	1.27
C90/19/150	91	19.1	150×150×1300	1.27
C50/19/200	46	19.1	200×200×1300	0.72
C90/19/200	91	19.1	200×200×1300	0.72
C50/19/200N	46	19.1	200×200×1300	0.72

Table 3- 3 Summary of material properties

Property	GFRP Bar		Concrete Strength	
	13 mm bar	19 mm bar	Grade 50	Grade 90
Strength (MPa) f_{fu}	792	715	46	91
Stiffness (GPa) E_f	42.9	41.9	32.2	48.3

3.3.3 Specimen preparation

Although the casting was done over a period of time, identical mix proportions and materials were used for the two concrete grades every time. In addition, two concrete cubes were cast with every batch to ensure the quality. The consistent quality of the mix is reflected in the small standard deviation across the various batches (3 MPa). The stiffness of the concrete in Table 3-3 is the average stiffness derived from testing three cylindrical specimens 100mm in diameter and 200 mm in length. The strain was monitored by means of 50mm electrical foil type strain gauges. Testing and interpretation of results were carried out according to BS1881: Part 121:1983 method for determination of static modulus of elasticity in compression.

All tension specimens were cast with the bar held horizontal with enough measures to make sure that the bar remained horizontal along the specimen length. Concrete was cast in two layers, with each layer sufficiently vibrated using a poker vibrator. Immediately after casting, the specimens were placed inside a temporary built chamber and were covered with wet Hessian and wrapped in polythene sheets to make sure that the concrete was kept in saturated humidity conditions while hardening. De-moulding was done 24hours after casting. After de-moulding, specimens were wrapped with two to three layers of wet Hessian and a layer of polythene to avoid loss of moisture and were regularly wetted (almost daily) to keep the concrete surface moist until the day of testing. The specimens were normally tested after 28 days from the date of casting.

3.3.4 Test results

Fig 3-11(a) shows the test results for the two specimens C90/13/150 and C50/13/150 compared with the bare bar response. On the Y axis the applied load is converted to the equivalent bar stresses (force/ rebar cross sectional area) and is plotted against the composite strain. From Fig. 3-11(a) one can deduct the bare bar response and filter out the concrete contribution. Fig. 3-11(b) shows the filtered out tension softening behaviour of concrete for the two test specimens shown in Fig. 3-11(a). The Y-axis represents the average stress of concrete calculated by averaging the force contribution of concrete over the concrete cross section.

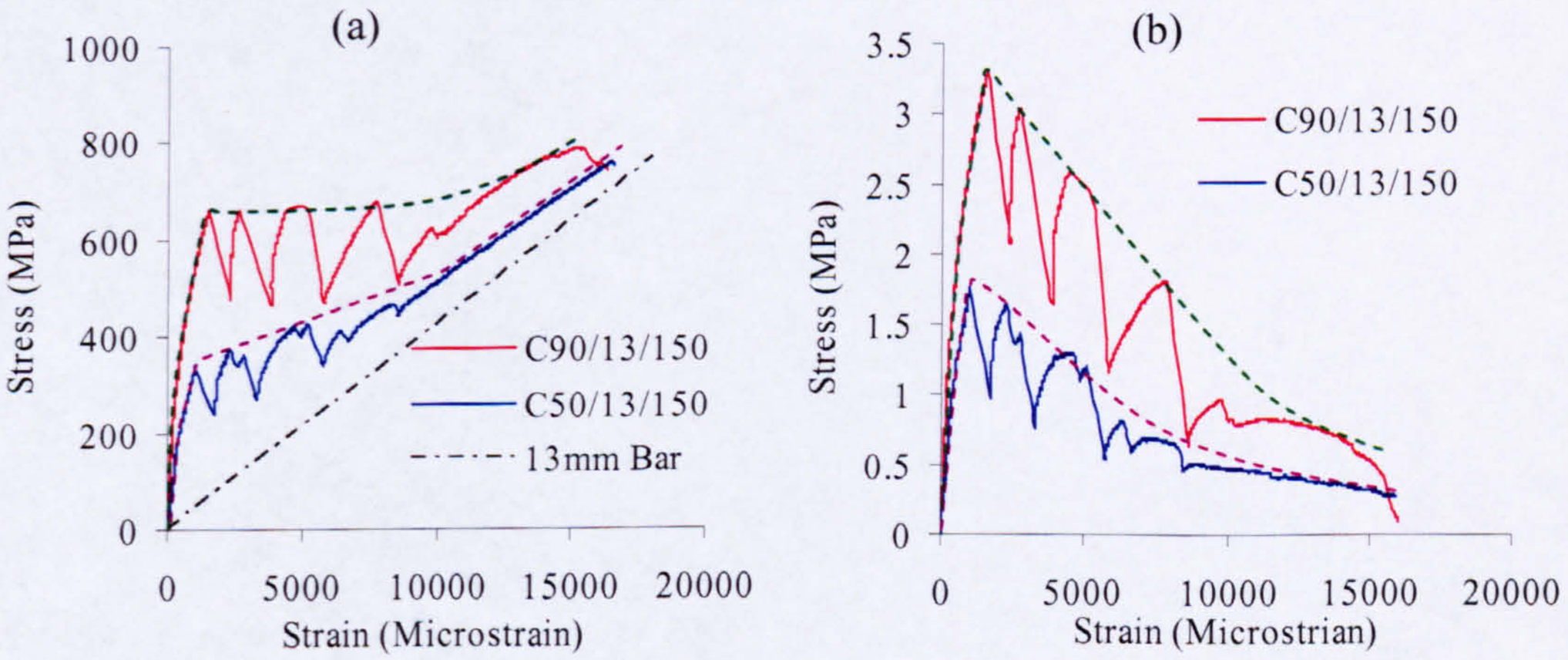

Fig. 3-11 Tension response of reinforced concrete specimens and derived average stress-strain relationship of concrete

Appendix I contains the experimental results for all specimens shown in the table 3-2 including photographs of the actual specimens. Each page presents experimental results of one specimen including: (1) Applied load (P) vs. composite displacement, compared with the bare bar response, (2) Stress-strain response of the composite section compared with bare bar response (3) Derived average stress-strain response of concrete, and (4) Final crack pattern at the time of bar failure.

3.3.5 Discussion on experimental results

3.3.5.1 Typical response of tension members

Based on the stiffness characteristics, the tension response of GFRP-RC can be generalised into three distinct regions (see Fig 3-11): (a) Pre crack stage: response of the specimen before the first crack, (b) Cracking stage: response of the reinforced concrete specimen while cracking is taking place, and (c) Post cracking stage: steady state response of the reinforced concrete specimen after cracking with overall response lying above the bare bar response. The typical tensile response of GFRP-RC can therefore be schematically represented as in Fig 3-12.

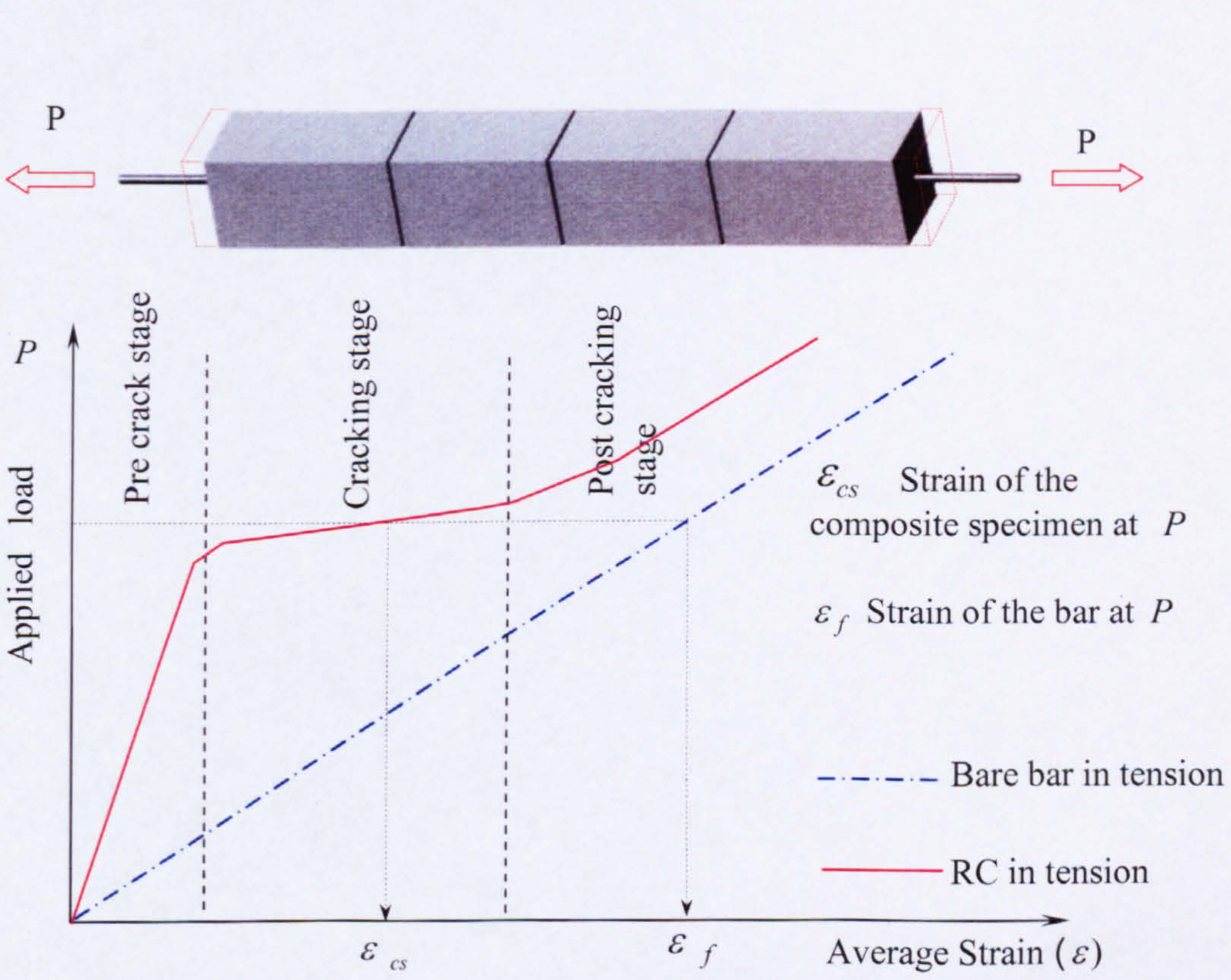

Fig. 3-12 Typical response of a specimen subjected to direct tension tests

In the pre-cracked stage one can assume that the reinforcement and concrete are acting compositely and, therefore, the stiffness is equal to the combined stiffness of the two materials. Experimentally, this can only be achieved by testing a specimen of infinite length. For finite length specimen, slip at the ends contributes significantly to the strain at first crack. Given the relatively weak bond of GFRP compared to conventional ribbed steel reinforcement, the average strain at first crack can be relatively high (see Fig 3-11). In this experimental work, high average strain at first crack was observed in the test specimens with low reinforcement ratios or high concrete strengths, as both factors increase the tensile force required to develop the first crack (see tension tests of C90/19/200, C50/19/200, C90/13/150, C50/13/150 and C90/19/150).

In terms of load strain characteristics, the cracking stage is very turbulent. As the testing was conducted in displacement control, after each crack the load carrying capacity dropped sharply, producing a saw teeth effect response in the stress-strain characteristics. However, it is the line connecting the peaks that constitutes the response of concrete in tension (see Fig 3-11). As each addition of crack increases the overall strain of the tension specimen substantially, the stiffness during cracking reduces progressively.

The post cracking stiffness always lies higher than the bare bar stiffness, but the two curves are mostly parallel due to the steady contribution of the concrete between cracks after crack maturity. However, stiffness reduction is inevitable if bond deterioration is encountered either due to reduced bond at higher loads or when occurrence or propagation of splitting cracks causes de-bonding of the bar from the concrete. In the next section, the global tensile response will be further explained with the help of strain distribution.

3.3.5.2 Discussion on global response using strain distribution

The objective of this section is to explain the characteristic global behaviour of the tensile response and to develop an understanding of the composite behaviour of concrete with reinforcement. This is done using strain profiles obtained from tests on specimen C50/19/200N, a specially designed notched specimen with a specially manufactured internally strain gauged bar (see Fig 3-13).

For the purpose of measuring the strain profile along the bar, strain gauges are normally attached on the surface at close centres in the vicinity of the cracked regions. The problem with a series of strain gauges on the surface is that their presence interferes with the bond development, and, hence, can adversely influence the test results. To avoid such problems in this specimen C50/19/200N, strain gauges were placed at 50mm centres in the centre of the bar. Conventional wire foil strain gauges were used and were glued on a bar cut longitudinally in half. On the other half, a groove 6 mm wide and 3mm deep was cut to accommodate the gauges and wiring of the strain gauged side. After that, the two halves were glued together to form a single round bar Fig 3-13. Because of the limitations associated with the volume required to accommodate the instrumentation, this technique was possible only on the 19.1 mm bar.

(a)

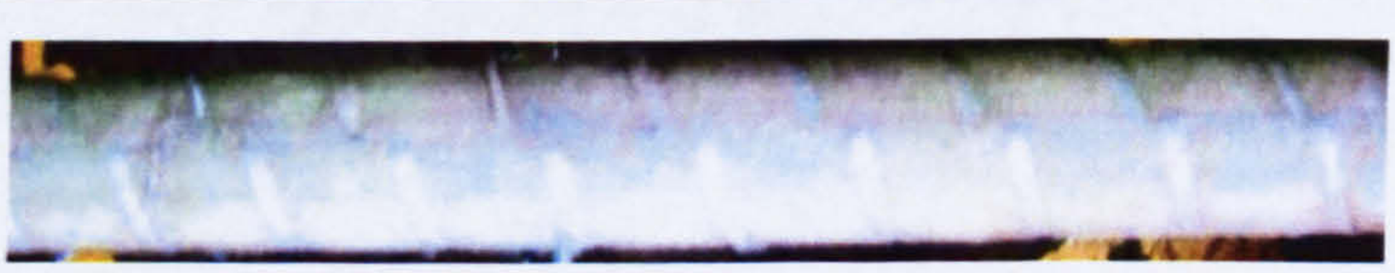

(b)

Fig. 3- 13 (a) Two halves of the bar before gluing them together and (b) the glued bar

Three 25 mm deep notches were induced right around the perimeters of the C50/19/200N concrete specimen dividing the length into four equal direct tension specimens once all cracks were formed. In this section, results of C50/19/200N are explained only in relation to the global response of the tensile member deferring the more detailed analysis of these experimental results to Chapter 4. Fig 3-14 shows the test specimen before the loading and Fig. 3-15 show the final bar failure in the middle section.

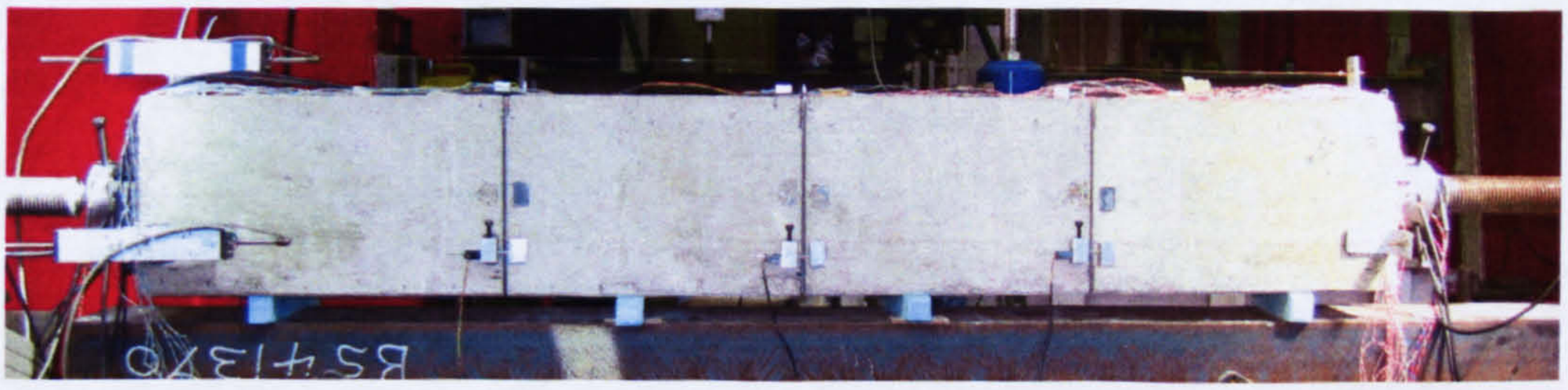

Fig. 3- 14 Notched tension specimen used in the experiment

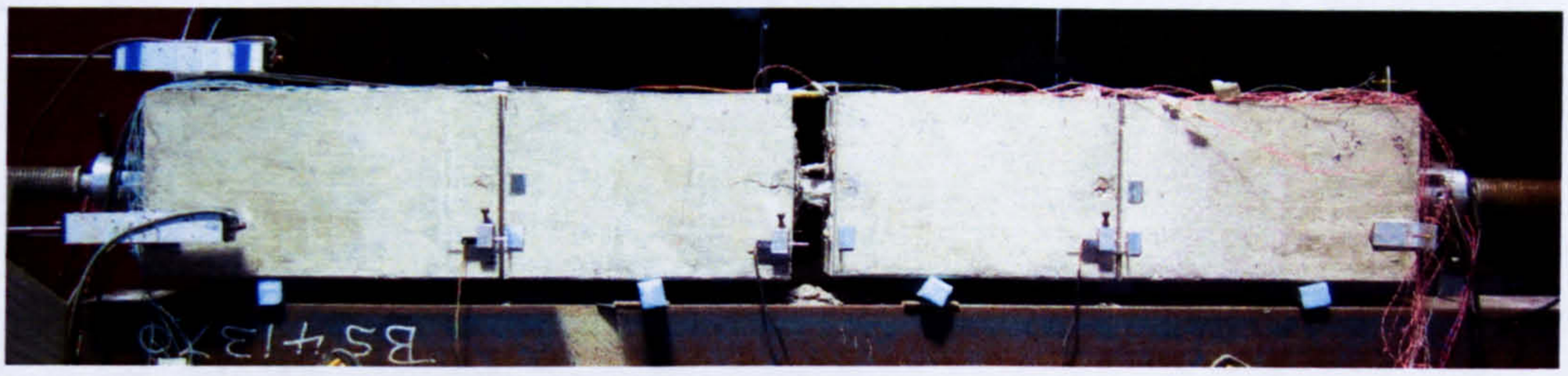

Fig. 3- 15 View of the notched specimen after bar failure in the middle crack

Fig 3-16 shows the strain distribution during crack propagation. Fig 3-16 (a) depicts the strain distribution in the specimen just before the occurrence of the first crack. Fig. 3-16(b) depicts the strain distribution of the bar just before and after the first crack whilst Fig 3-16(c) depicts the strain distribution of the bar at the onset of the 3rd crack. As intended, all cracks happened at notched sections and no other transverse cracks occurred. Final failure of the bar took place at the middle notch as seen in Fig. 3-15. Fig 3-16(a) shows the strain distribution during the pre crack stage. From Fig 3-16(a), it is clear that composite action is present along the length of the specimen except in the vicinity of the ends and that strain in the composite section is on average around the limits of maximum concrete strain prior to cracking (80~150 $\mu\varepsilon$). It is this composite action that contributes to the very high initial stiffness of the reinforced concrete element in tension. During the cracking stage, as seen in Fig 3-16 (b) and (c), each addition of a crack contributes to a large increase in overall tensile strain and this is the reason for the stiffness reduction in the cracking stage of the tension test. Fig 3-17 shows the strain distribution before and after each crack when the specimen is loaded back to the same load.

Finally, Fig. 3-18 shows the strain distribution between cracks after the cracking stage. It is clear that the strain at the middle of the crack section continues to increase after crack maturity. Strain at the middle between cracks even exceeded 10000 $\mu\varepsilon$. However, parallel strain lines at increasing loading (see Fig 3-18) suggest that the concrete contribution has not deteriorated substantially in the post cracking stage. This constant contribution of concrete, often found in tension experiments during the post cracking stage, is idealised in the overall tension response of reinforced concrete by a parallel line lying above the bare bar response (see Fig 3-12).

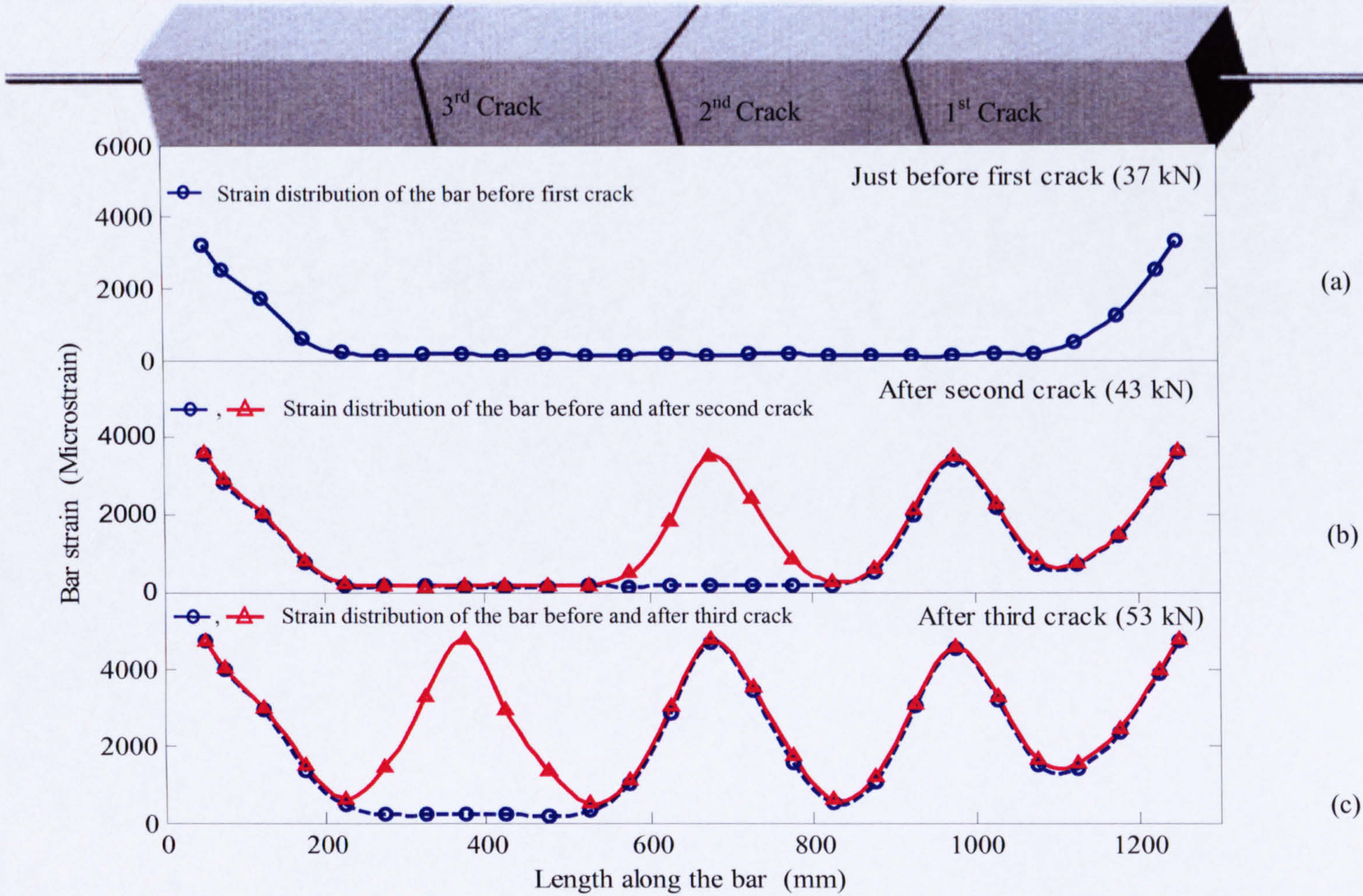

(a)

(b)

(c)

Fig. 3- 16 Strain distribution of the bar during pre crack and cracking stage

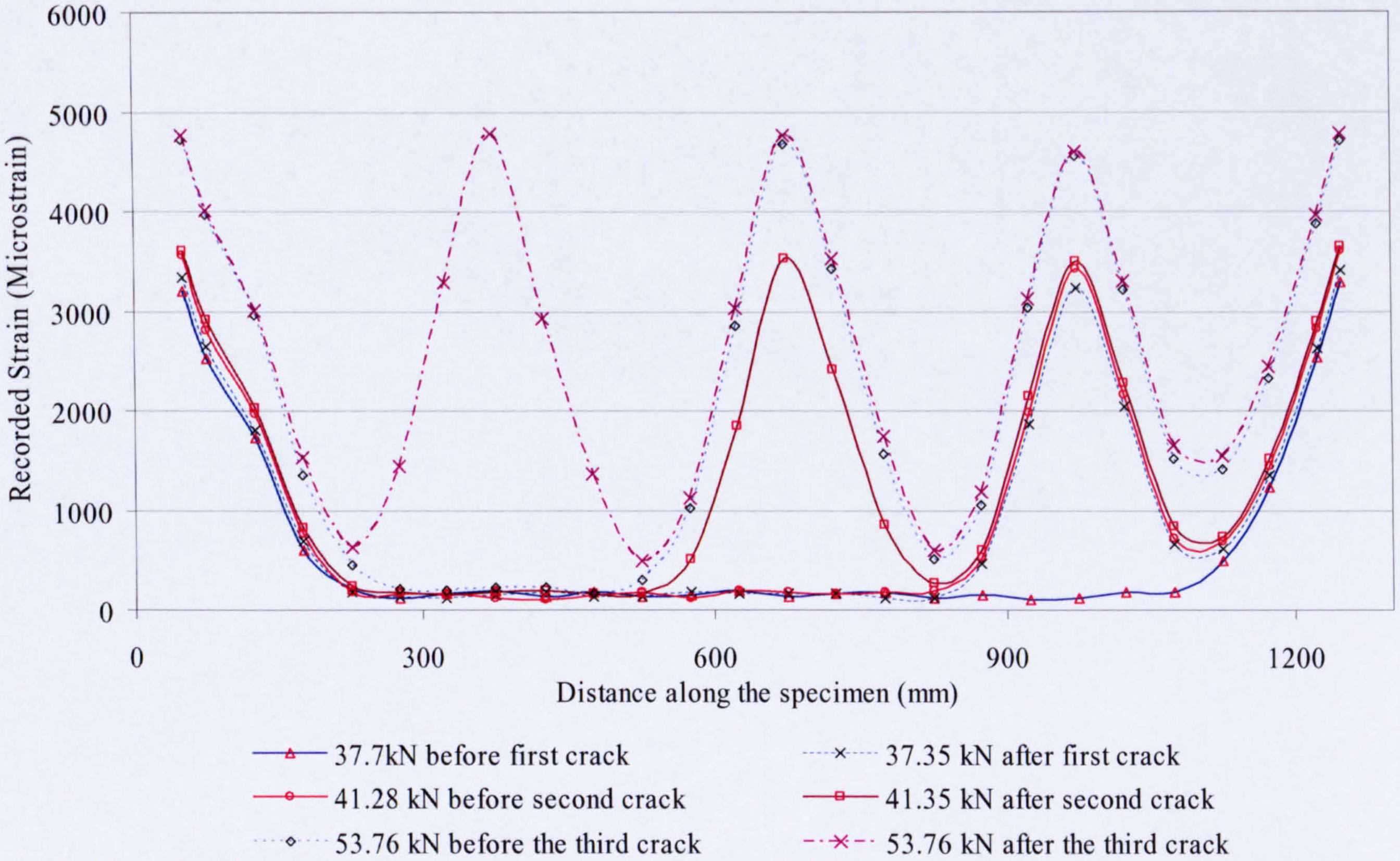

Fig. 3- 17 Strain profile before and after cracking when the specimen is loaded back to the same loading

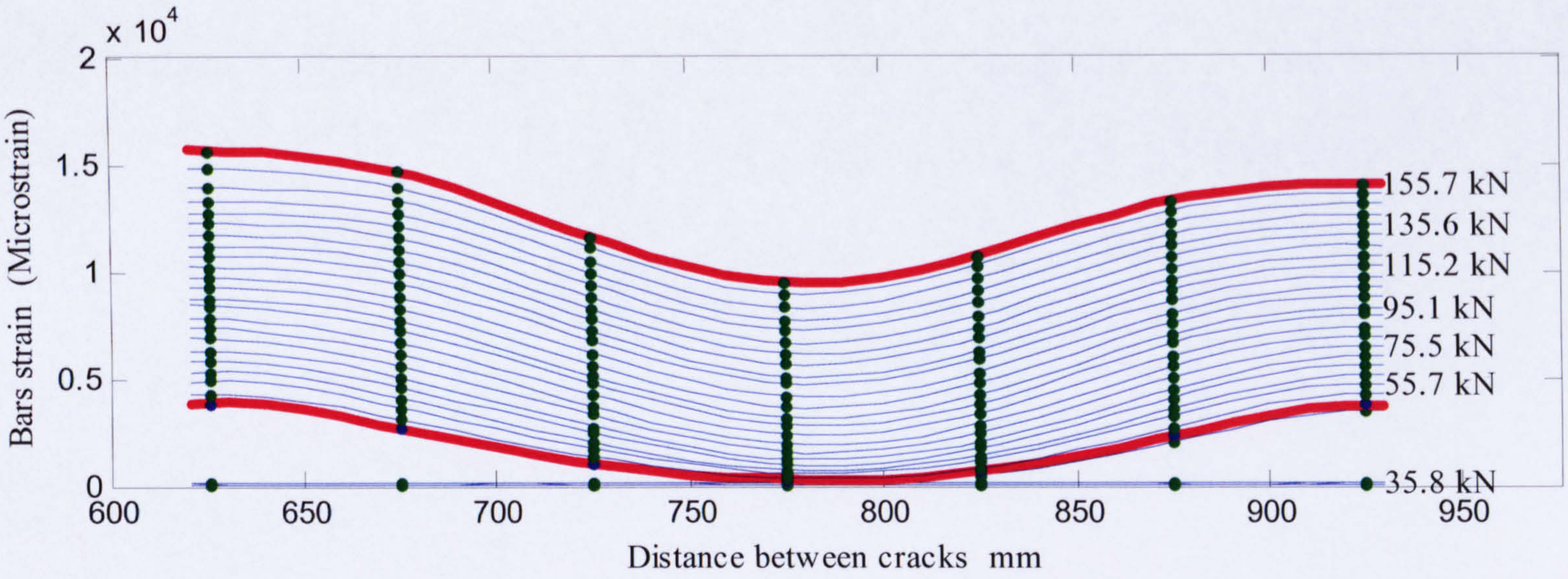

Fig. 3- 18 Post cracking strain pattern between cracks

3.3.5.3 Tensile strength and cracking

Estimating tensile strength and location of the first crack in a tensile specimen are both difficult tasks especially given the fact that concrete is not a homogeneous material. Theoretically, the first crack can occur through the weakest section anywhere between the bond development lengths (length required to anchor the bar to concrete at the two ends) through the weakest section. Due to the length of the specimen, the tensile strength of concrete obtained from these direct tensile tests is expected to be less than that derived from tensile tests, on smaller volumes of concrete. Many researchers have experienced lower tensile strengths for concrete in direct tension tests (Vecchio and Collins 1986), (Maekawa et al. 2002) and (ACI 224 1997). Tensile test results obtained in this experimental work agree well with the tabled values and formulae (equation 3-2) of ACI 224(1997), and the formulae $0.33\sqrt{f_c'}$ used by Vecchio and Collins (1986), as shown in table 3-4.

$$f_t' = g_t[W_c(f_c')]^{1/2} \quad \text{(MPa)} \qquad (3\text{-}2)$$

Where

g_t=0.0069

W_c=Unit weight of concrete (kg/m^3)

f_c'= Compressive strength of concrete (Cylinder strength) (MPa)

As the compressive strength of concrete in this experimental study was determined mainly by using cube tests, values of cylinder strength are computed by multiplying the cubic strengths, 46MPa and 91MPa, by 0.8 and 0.89 respectively according to CEB-FIP model code 90 (1993).

Table 3-4 Tensile strength from direct tension tests

f_{cu}	f_c'	This study f_t' (SD)	ACI 224 ($f_{cu}=42$) f_t' (SD)	$f_t'=0.33\sqrt{f_c'}$	Equ. (3-2) f_t'
46	36.8	1.9 (0.18)	1.9 (0.13)	2.00	1.98
91	81.0	3.4 (0.21)		2.98	3.24

Note: All values in MPa. SD is standard deviation

3.3.5.4 Parametric study on tension stiffening effect of GFRP RC

This section examines how concrete strength, reinforcement ratio and bar diameter influence the tensile stiffening behaviour of GFRP-RC.

Influence of reinforcement ratio

It is important to understand how the area of concrete around the bar contributes to the tension stiffening effect. Fig. 3-19 compares the tension stiffening effect of different reinforcement ratios tested in this study. As the experimental work involved testing two grades of concrete, the results are plotted in separate graphs: Fig. 3-19(a) shows grade 50 concrete whilst Fig.3-19(b) shows grade 90 concrete. It is clear from the figures that tension stiffening increases with a decrease in reinforcement ratio. However, it is not clear whether the effect is directly proportional to the decrease in reinforcement ratio.

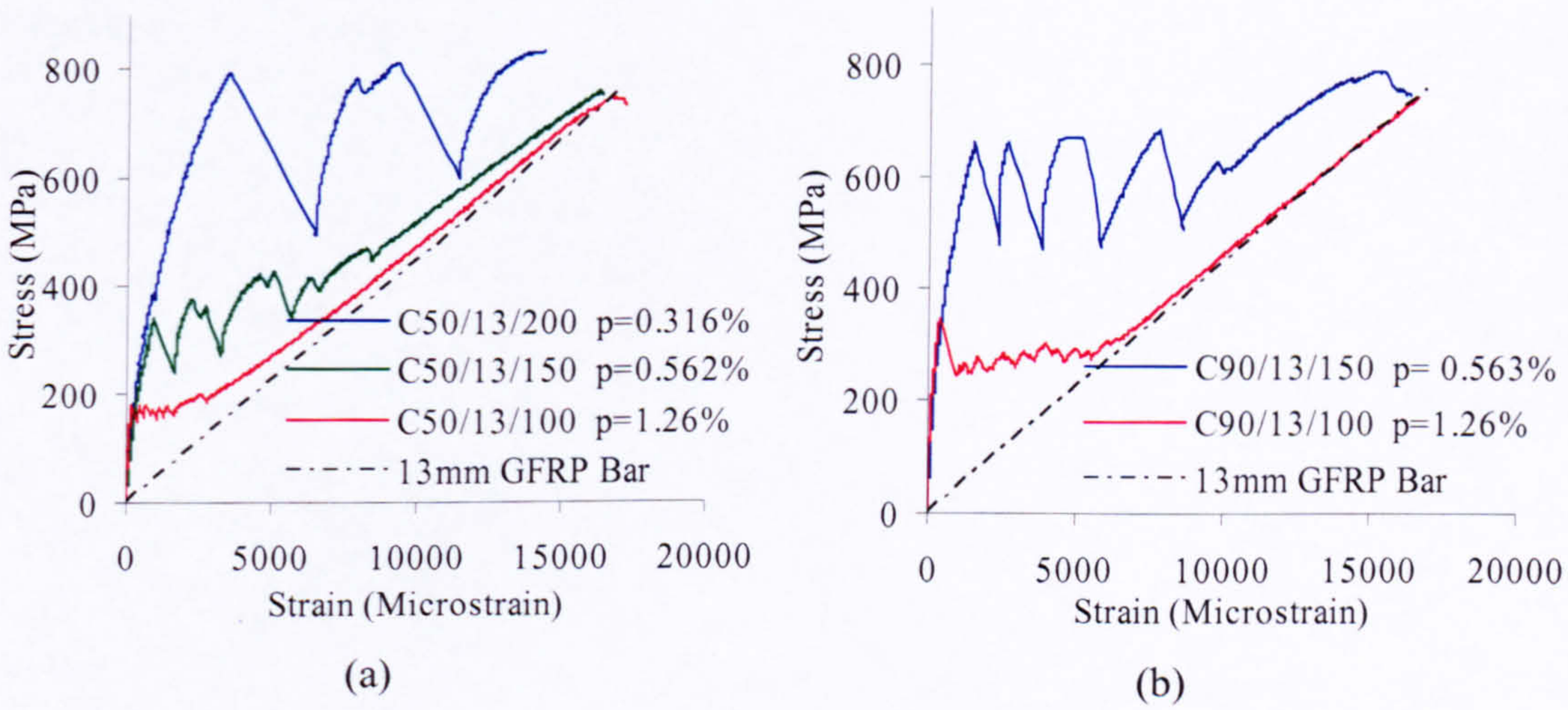

Fig. 3-19 Influence of reinforcement ratio on the tension stiffening (a) C 50 (b) C90

Influence of concrete strength

Concrete strength can influence the tension stiffening behaviour in two different ways. Firstly, high strength concrete requires higher loads to crack the specimens. In addition, better bond between concrete and reinforcement allows stresses to be transferred more effectively between the bar and concrete making the average stress contribution of concrete higher. Fig. 3-20 illustrates this effect by comparing different concrete strengths at constant reinforcement ratio.

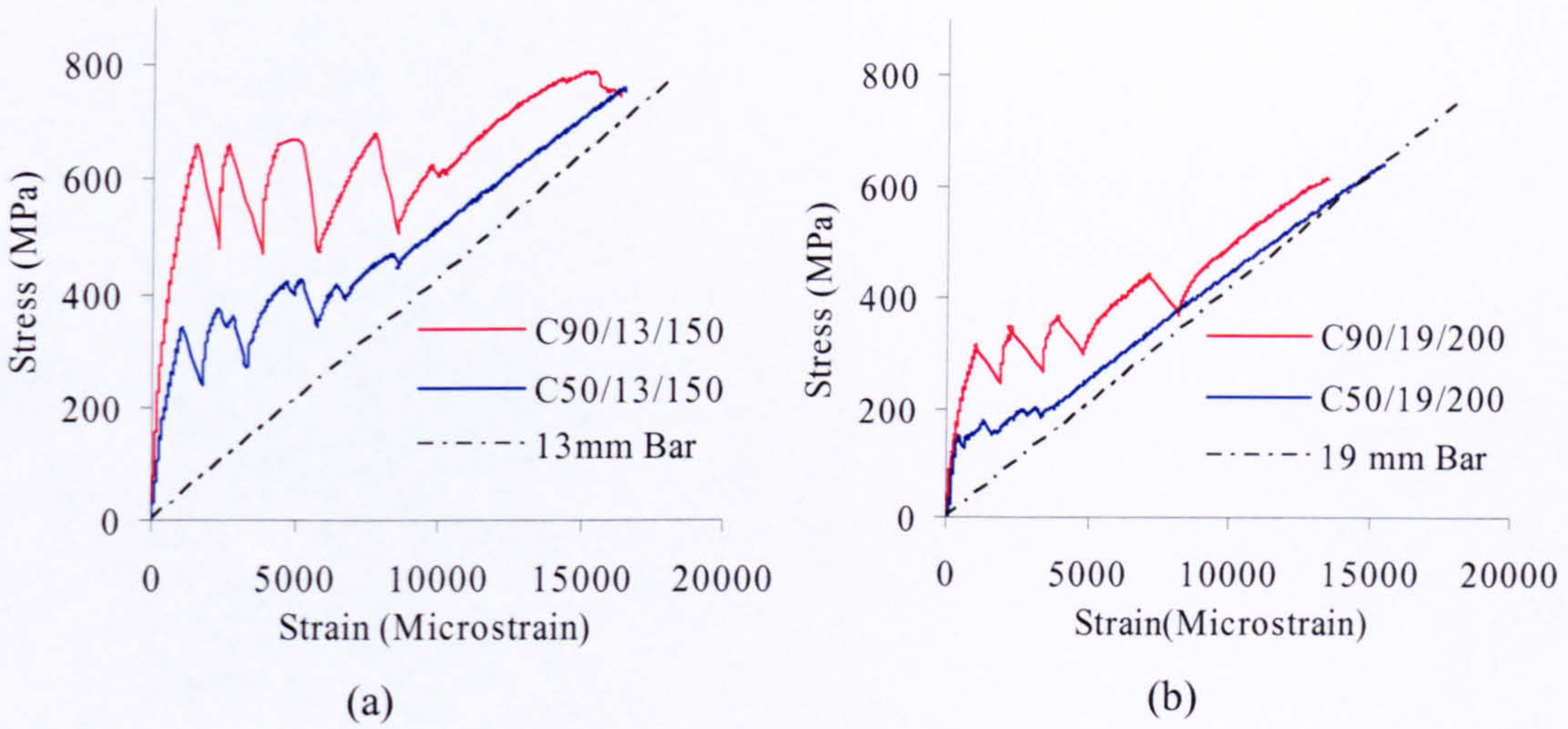

Fig. 3-20 Influence of concrete strength on tension stiffening (a) 13 mm (b) 19 mm bar

Influence of bar size on tension stiffening behaviour

Bar size is another factor that might influence tension stiffening. However, in this experimental study no significant influence on tension stiffening is recorded for different bar sizes when specimen having same reinforcement ratio are compared as shown in Fig. 3-21.

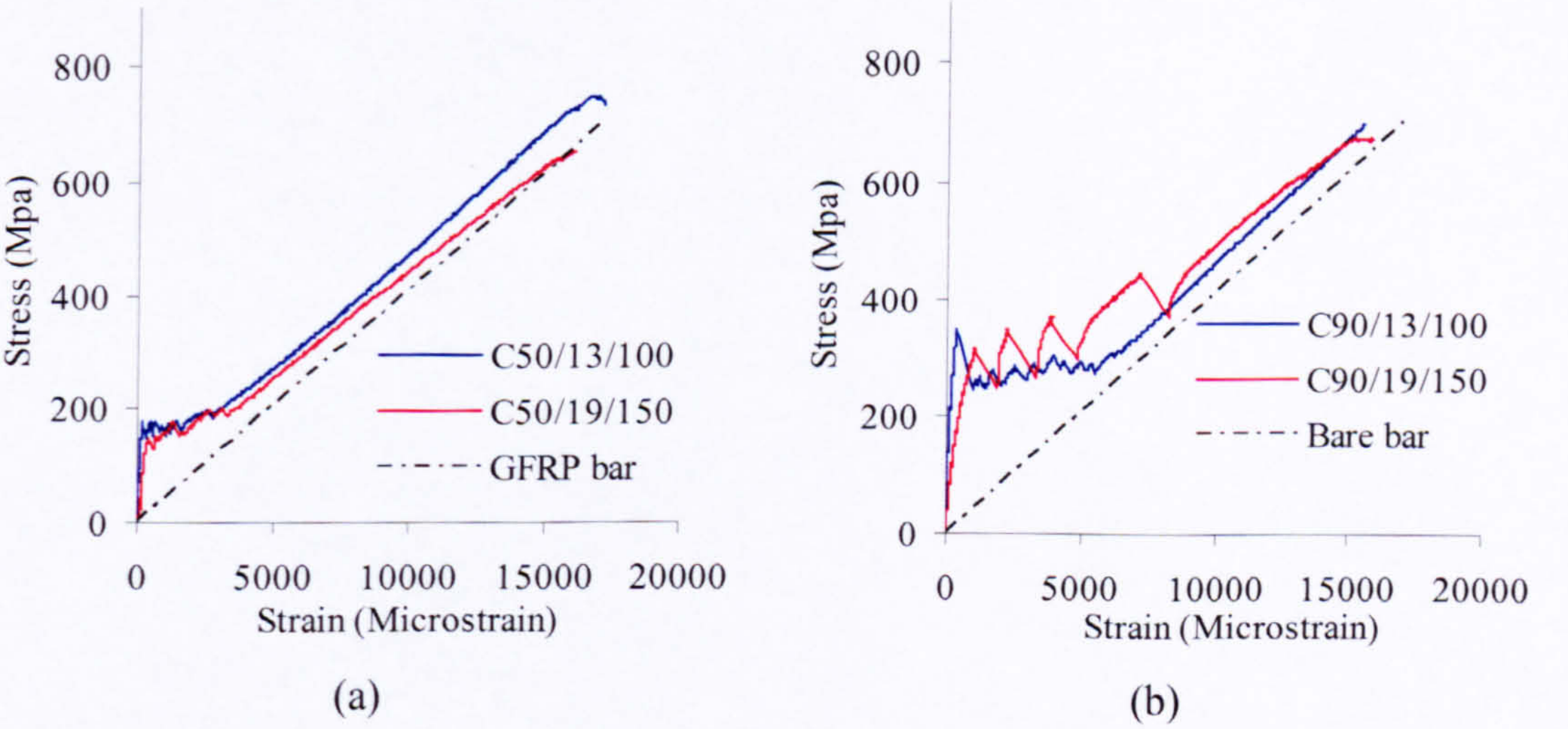

Fig. 3-21 Influence of bar diameter on tension stiffening (a) C50 (b) C90 concrete ($\rho = 1.26\%$)

3.3.6 Prediction of Tension stiffening effect of GFRP RC

As presented in chapter 2, both CEB-FIP and ACI in their respective publications Concrete Model Code 78, 90 (1978)(1993) and ACI 224 (ACI Committee 224 1997) provide guidelines to predict tension stiffening behaviour of concrete or the general response of reinforced concrete in tension. The Model code 78 introduces a method to calculate the average strain of concrete by decreasing the difference between the strain in the crack section and the average strain of the specimen with increasing load. ACI, on the other hand, use a reduced tensile cross sectional area to model the overall stiffness of the member, which is along the lines of their modelling deflections through the use of effective moment of inertia.

The above code formulations were developed for steel reinforced concrete and may require more than changing the stiffness to apply for FRP, as bond between concrete and reinforcement also is vital for the overall behaviour of the element. Many researchers and design guidelines for deflection adopt 'bond' factors to account for the difference in bond between steel and FRP reinforcement. In this section, the validity of such modifications in predicting the tension stiffening behaviour of GFRP RC is evaluated and appropriate values and adjustments are recommended.

The bond factor k in the CEB-FIP model, Equation 3-3, is a modification for bond degradation due to repeated loading and can also be used to model the differences in bond behaviour of GFRP reinforcement.

$$\varepsilon_{cs} = \varepsilon_s \left[1 - k \left(\frac{f_{scr}}{f_f} \right)^2 \right] \qquad (3\text{-}3)$$

The ACI 224 equation for predicting the tension stiffening behaviour of steel reinforced concrete, equation 3-4, can also be modified to account for the different bond of FRP reinforcement. A bond factor, β_d, of 0.5 can be used since the same value has been used by ACI 440.1R-03 to modify Branson's formulae for effective moment of inertia in deflection calculations.

$$A_e = \left[\frac{P_{cr}}{P} \right]^3 A_g + \left[1 - \left(\frac{P_{cr}}{P} \right)^3 \right] A_{cr} \qquad \text{for} \qquad \frac{P_{cr}}{P} < 1.0 \qquad (3\text{-}4)$$

Equation 3-5 shows the modified equation for calculating the effective concrete area.

$$A_e = \left[\frac{P_{cr}}{P}\right]^3 \beta_d A_g + \left[1 - \left(\frac{P_{cr}}{P}\right)^3\right] A_{cr} \qquad (3\text{-}5)$$

Figs. 3-22 and 3-23 show two examples of how the existing CEB-FIP model code and modified existing ACI equations simulate tension stiffening behaviour. It is clear from these results that even the modified ACI 224 is not capable of estimating accurately the tension stiffening effect. It is also seen that the error in estimating is much more pronounced at low reinforcement ratios where the concrete contribution is dominant. The CEB-FIP model on the other hand, though still overestimates the tension stiffening effect, provides a closer and more realistic approximation.

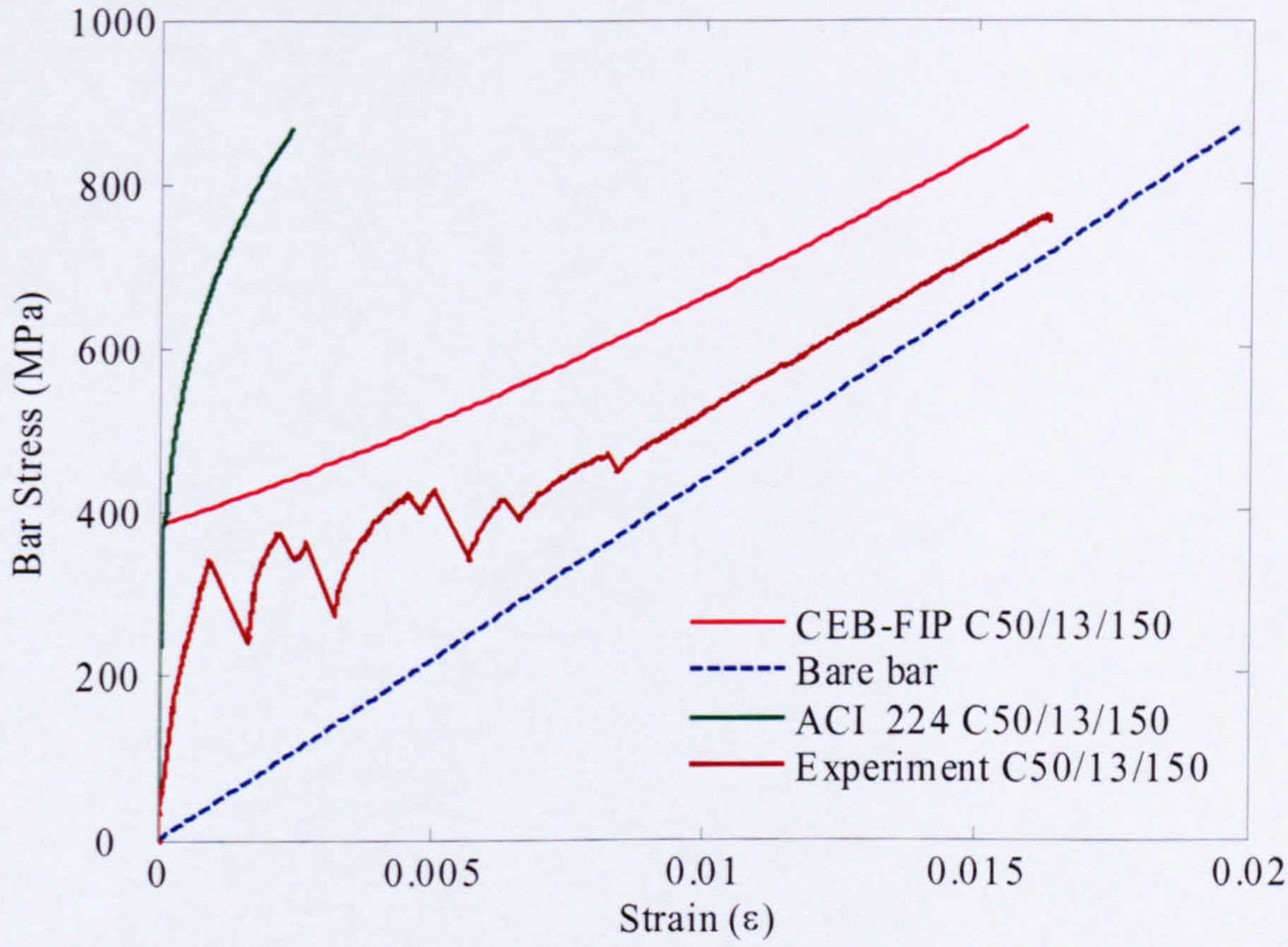

Fig. 3-22 Experimental results of C50/13/150 compared with CEB-FIP and modified ACI code predictions

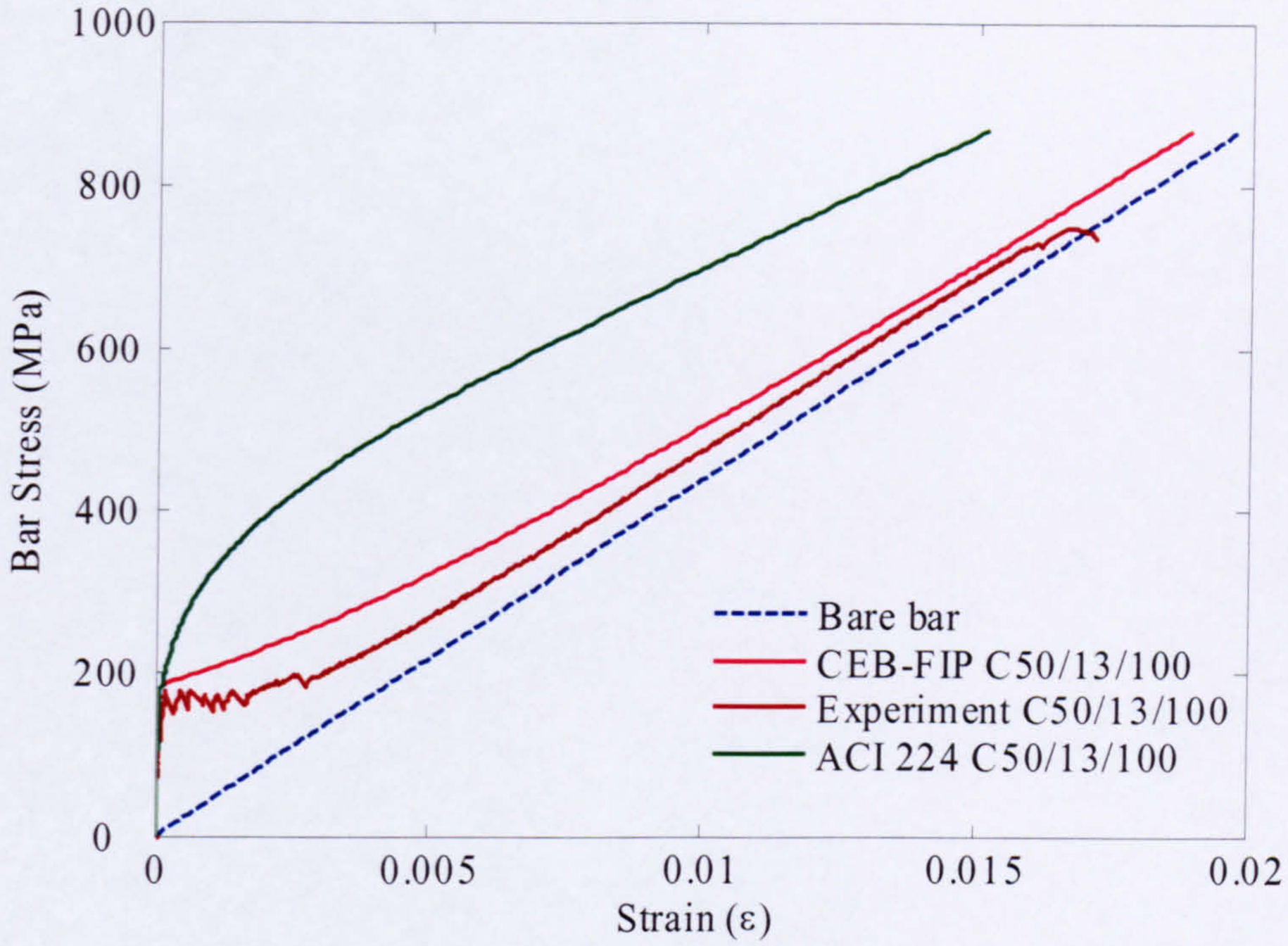

Fig. 3-23 Experimental results of C50/13/100 compared with CEB-FIP and modified ACI code predictions

Fig 3-24 shows the results of equation 3-3 modified with k=0.5 (see equation 3-6) against the test results of 12.7 mm bars in 46 MPa concrete with reinforcement ratios of 0.56% and 1.26%.

$$\varepsilon_{cf} = \varepsilon_f \left[1 - 0.5 \left(\frac{f_{scr}}{f_f} \right)^2 \right] \tag{3-6}$$

The modifications show good agreement with the test results and equation 3-6 appears to be a good contender for representing the tension stiffening effect of GFRP reinforced concrete for all the tests.

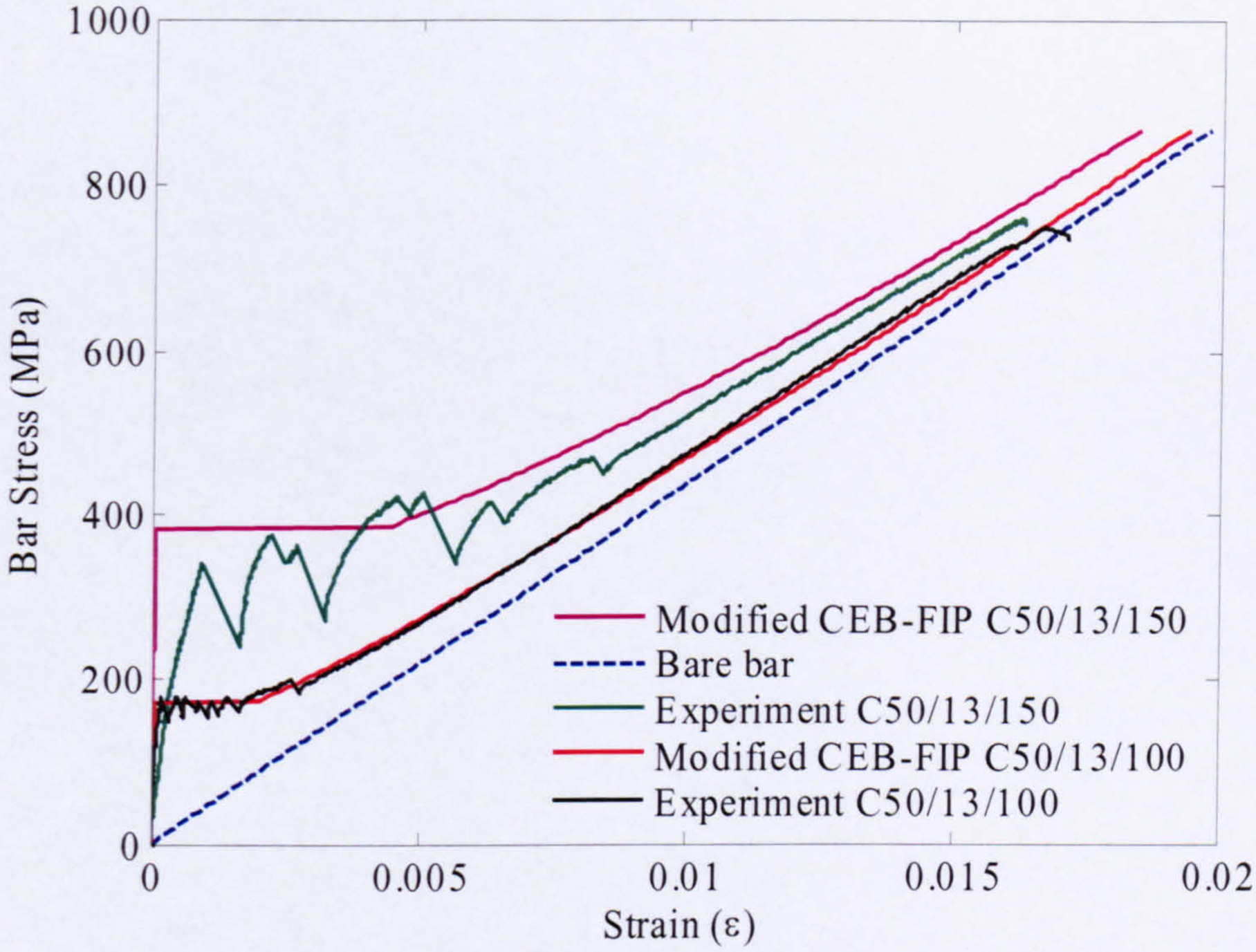

Fig. 3-24 Experimental results of C50/13/200, C50/13/150, and C50/13/100 compared with the CEB-FIP model with the proposed modification

From Fig 3-24 it is clear that the model does not follow the experimental stiffness at the pre-crack stage. This is due to the finite length of test specimen which includes end slip which is equivalent to one crack. The code equations are based on an infinite length with no initial crack. The force required for the first crack increases with the decrease in reinforcement ratio, making the contribution of end slip towards the average strain very significant, especially, at short specimen lengths.

Fig. 3-25 shows the normalised post cracking strain softening behaviour of concrete in the presence of GFRP. These results are obtained using the difference between the overall response and the response of the bare bar averaged over the area of concrete (explained in section 3.3.4) and then normalising. Normalisation is achieved by dividing the concrete contribution by the maximum recorded tensile strength for that experiment. The figure shows that the modified CEB-FIP model agrees well with the normalised experimental results of the two concrete grades (46MPa and 91MPa) at different reinforcement ratios (Fig. 3-24(a) 1.26% and (b) 0.56%). Similar agreement between the experimental results and the predictions obtain according to the modified CEB-FIP model was also found for the other experimental results, which means this model can

provide a convenient and accurate method for representing the tension stiffening effect of GFRP reinforced concrete.

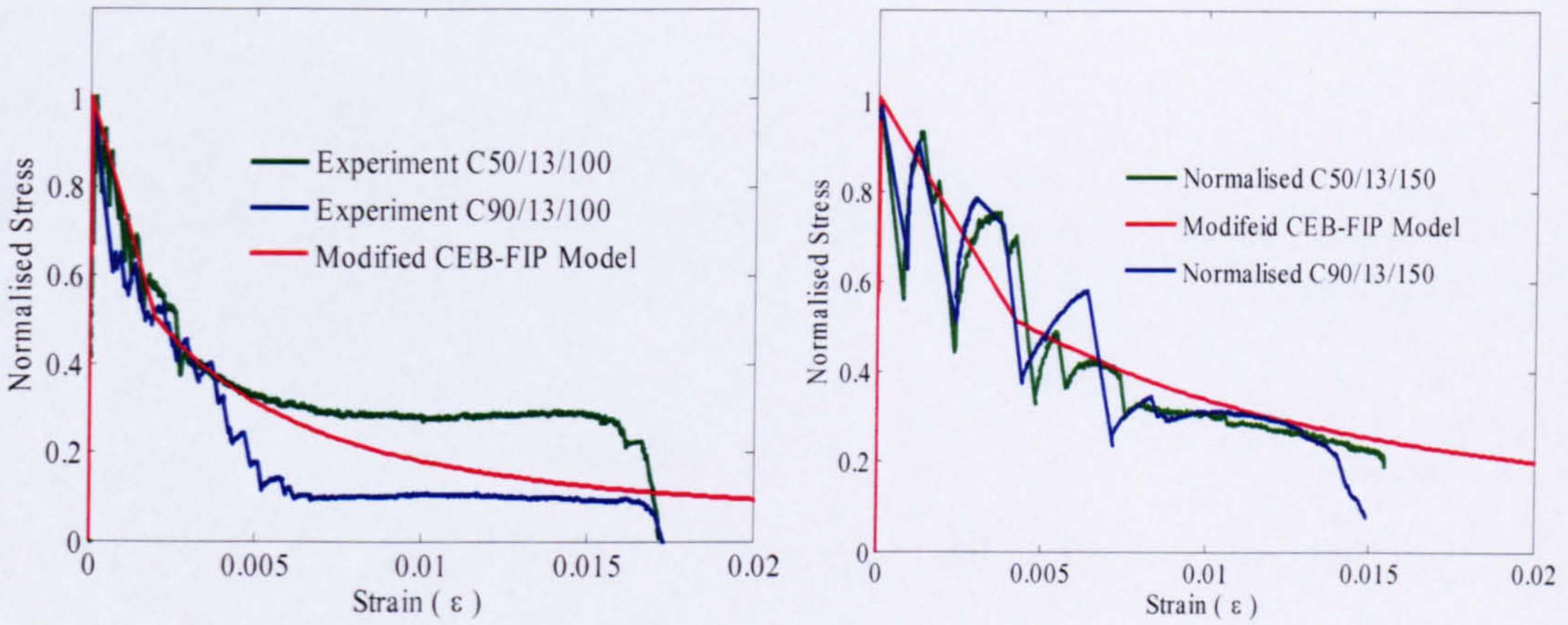

(a) (b)

Fig. 3-25 Normalised concrete strain softening behaviour for two reinforcement ratios equal to (a) 1.26% and (b) 0.56% compared with the predictions of modified CEB-FIP model code equation

However, further considerations are required before a model for reinforced concrete in tension can be completed. The initial stiffness of concrete before cracking can be considered equal to the concrete stiffness in compression. After cracking, concrete tends to continue to transfer stress across the crack due to aggregate interlocking. Okamura et al. (1991) proposed the use of a plateau at peak tensile strength over a strain equal to two times the concrete strain at peak strength to reflect the fracture process zone in the average stress-strain relationship. Fig. 3-26 shows a schematic representation of the average stress-strain behaviour for the GFRP reinforced concrete in tension when combining the modified CEB-FIP model and the earlier suggestion by Okamura.

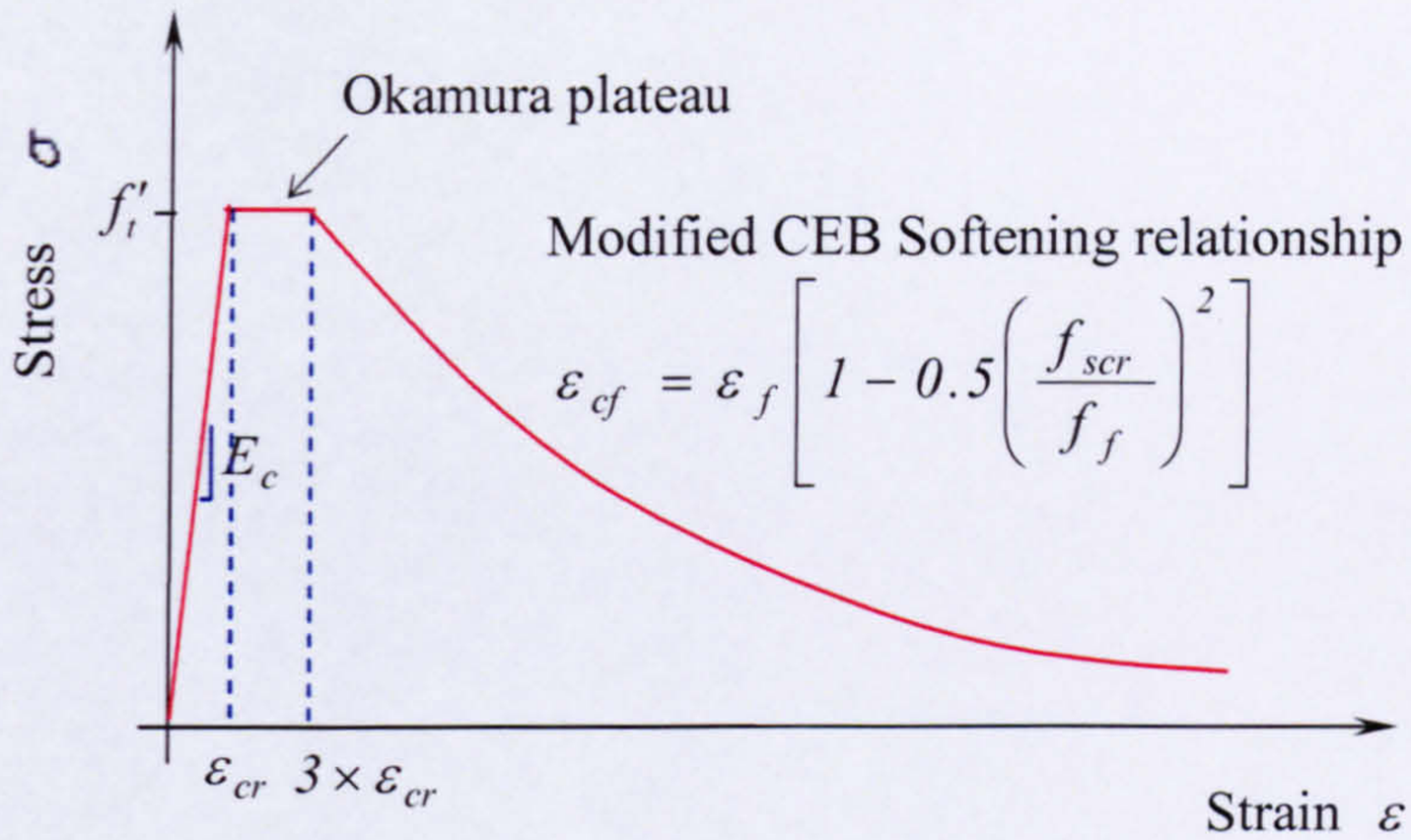

Fig. 3- 26 Schematic representation of the complete model for the tension stiffening behaviour of FRP reinforced concrete

CHAPTER 4

BOND CHARACTERISTICS OF GFRP-RC

4.1 Introduction

Bond is a very important property in developing the composite behaviour of reinforced concrete. Constitutive models for bond mechanics can be grouped into two types: micro models and macro models. This categorization is mainly done depending on the size of the control volume. If the behaviour of different segments of the interface geometry is considered, taking into account the mechanism by which individual bar lugs transfer stresses to concrete, this is classed as micro level analysis of bond. On the other hand, if the member response is considered on a global scale, averaging between several cracks, like in the case of tension stiffening effect, this is classed as macro modelling. Models developed directly from pull-out tests fall in between these two extremes, as the control length in this case is neither short enough to be considered as a micro model nor long enough to be considered as a macro model. Therefore, bond modelling using tests like the pullout test is generally classed as meso-level modelling. A diagrammatic representation of bond modelling schemes is shown below, Fig 4-1.

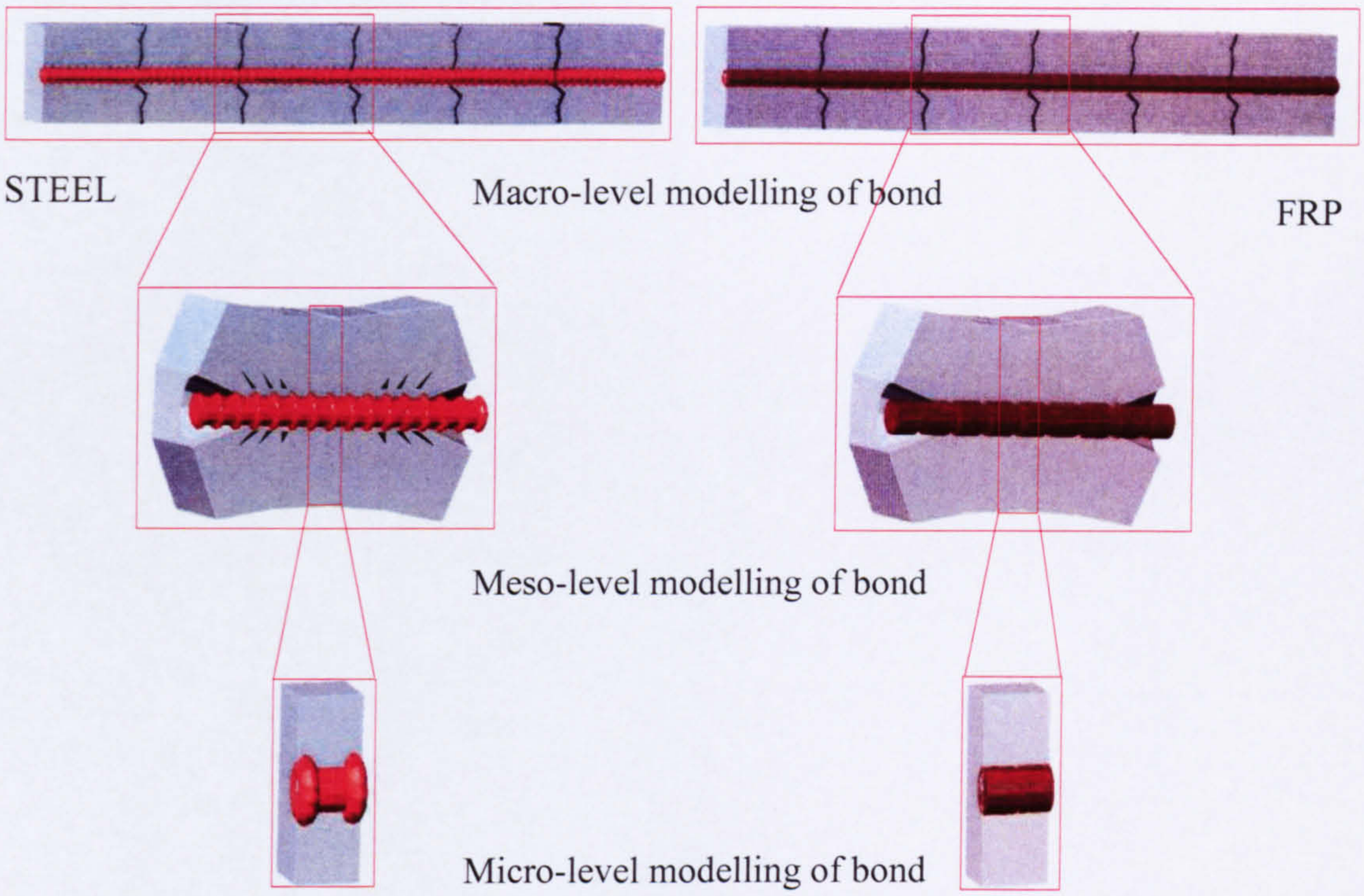

Fig. 4-1 Hierarchy of bond modelling.

Bond interaction of deformed steel bars is different from that of GFRP bars in many ways. In the case of the deformed steel bars the interaction arises primarily from the mechanical action of the bar lugs against concrete. In steel reinforced concrete, in addition to primary cracks, multiple secondary cracks can develop from the lugs along the length of the bar in between the primary cracks as shown in Fig. 4-2(a). These secondary cracks get trapped inside the concrete matrix without surfacing. In the case of FRP bars, with lower elastic modulus and lower surface undulations, bond interaction has more of a frictional character and occurrence of secondary cracks is very much limited. Bond failure in steel bars is by crushing of concrete in the vicinity of the lugs and opening of the secondary cracks, whereas in FRP it is largely caused by partial failure in the concrete and some surface damage on the FRP as shown in Figs. 4-2(b) & (c).

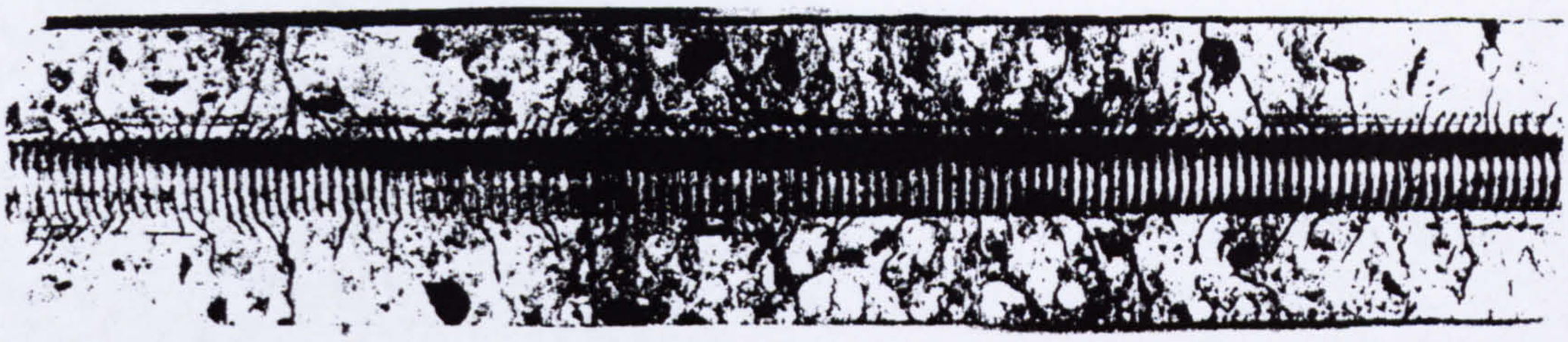

(a)

(b)

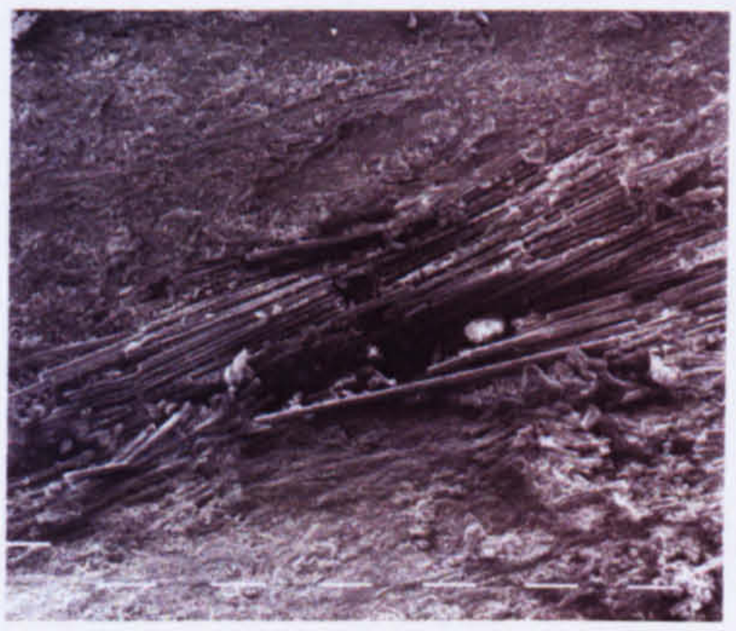

(c)

Fig. 4-2 (a) Close up of bond failure reported for steel (Goto et al. 1971); (b) Close up from a GFRP-RC bond failure from tensile test; (c) Microscopic view of the FRP interface failure after a pull out test showing residues of fibre still attached to the concrete (Achillides 1998)

Micro level analysis of bond is very useful for the overall understanding of bond mechanics, however, it is not practical for analyzing real structures. Microscopic analysis of bond has been attempted for steel reinforcement by using a very fine three dimensional finite element mesh to model each lug and the surrounding concrete matrix (Maekawa et al. 2002). However, this is of very little use to improve the understanding of the bond mechanics of FRP since the bars are relatively smooth and bond failure is largely caused by damage to the interface between concrete and rebar. Therefore microscopic analysis is not attempted in the current study.

Discussion on macro level analysis of bond, i.e. tension stiffening effect of GFRP-RC, will be attempted in chapter 6. The main objective of this and the next chapter is to develop an understanding of bond between GFRP bar and concrete and to provide the essential ingredients to model the tension behaviour starting from bond interaction.

This chapter discusses the results of tension tests on specimen with crack inducers. With the help of strain distribution between cracks, the chapter presents a systematically derived unique bond stress-slip-strain $(\tau - s - \varepsilon)$ relation to explain the local bond stress-slip $(\tau - s)$.

4.2 Meso level Investigation of bond

4.2.1 Definition of local bond stress using strain distribution of the bar

Meso level analysis is really a building block for the understanding of the composite response of reinforced concrete. It is believed that by integrating meso level response between cracks and then along the specimen, the global response of the member can be established. Local bond stress (τ) is defined as the force transferred from the reinforcing bar to concrete per unit surface area and is proportional to the slope of the strain distribution curve of the bar in its elastic range (equation 4-1).

$$\tau = \frac{E_f D}{4} \frac{d\varepsilon_f}{dx} \tag{4-1}$$

Where

τ =Bond stress

E_f =Elastic modulus of reinforcement

D =Bar diameter

ε_f = Reinforcement strain

ε_c = concrete strain

Local slip is determined by integrating the difference in strain between the bar and the concrete as shown in equation 4-2. The concrete strain compared to the strain of the bar is very small and generally ignored in the calculation of slips (see equation 4-3).

$$s = \int_0^x (\varepsilon_f - \varepsilon_c) dx \tag{4-2}$$

$$s = \int_0^x \varepsilon_f \, dx \tag{4-3}$$

In the case of tension tests, equation 4-3 can be applied directly with limits of integration varying from the centre of the cracked block to the point where the slip is being calculated, see Fig. 4-3. However in the case of pull out tests, free end movement (S_{free}) needs to be taken into consideration as shown in equation 4-4, also see Fig.4-4.

$$s_{end} = \int_0^x \varepsilon_f dx + s_{free} \qquad (4\text{-}4)$$

Figs. 4-3 and 4-4 show typical strain distributions of the bar during axial tension and pull-out test. In the calculation of slip it is important to note that the relative movement at the bar and concrete interface has little physical meaning until bond failure or loss of composite action has occurred. However for FRP with low stiffness and high strain capacity it is likely that physical damage to the bond will initiate earlier on and resulting in an actual physical movement of the bar relative to the concrete. By assuming the FRP bar to be elastic up to failure, equations 4-1 to 4-3 can be used at all strain levels.

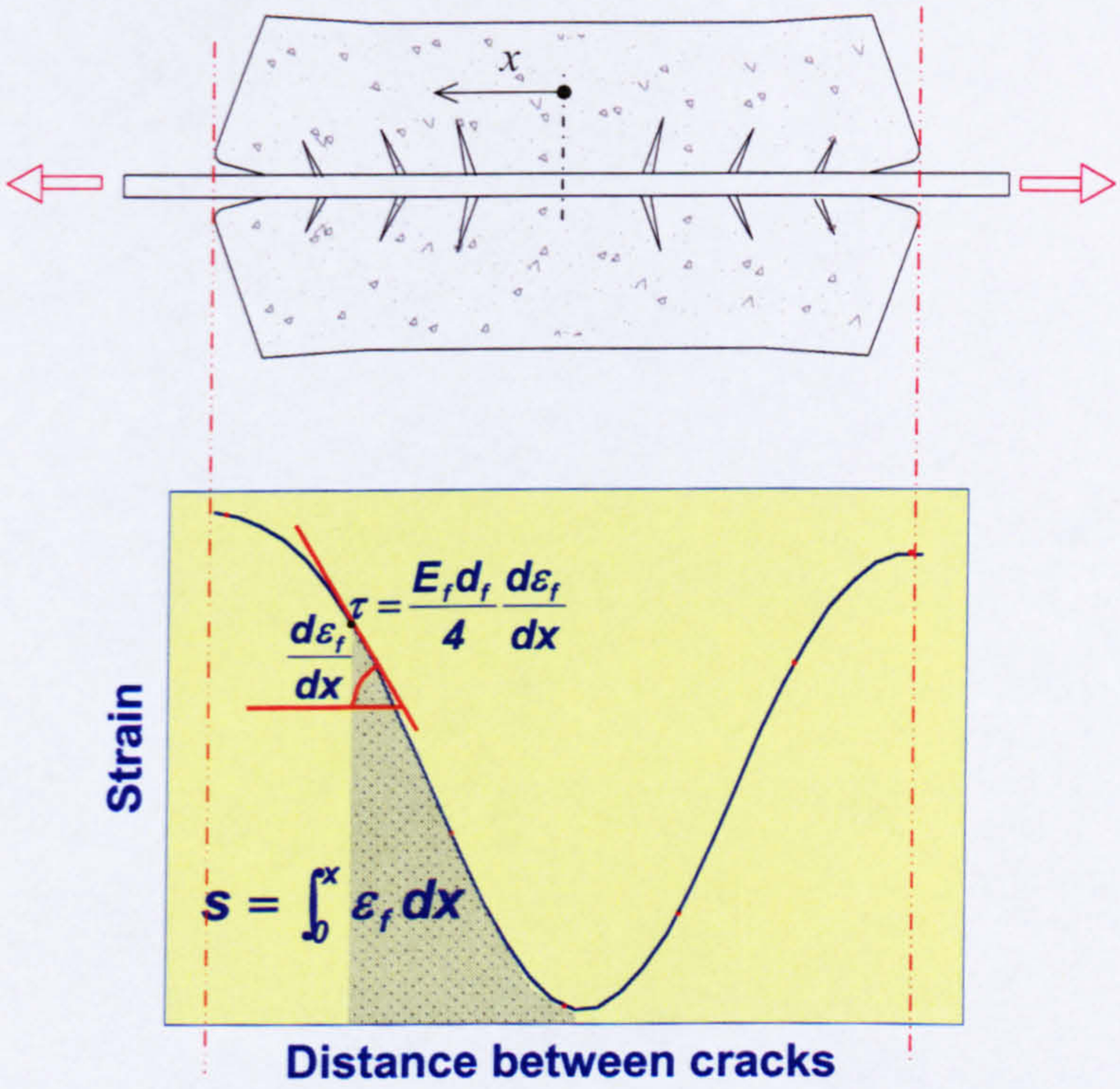

Fig. 4-3 Schematic representation of strain distribution of the bar between cracks during tension test

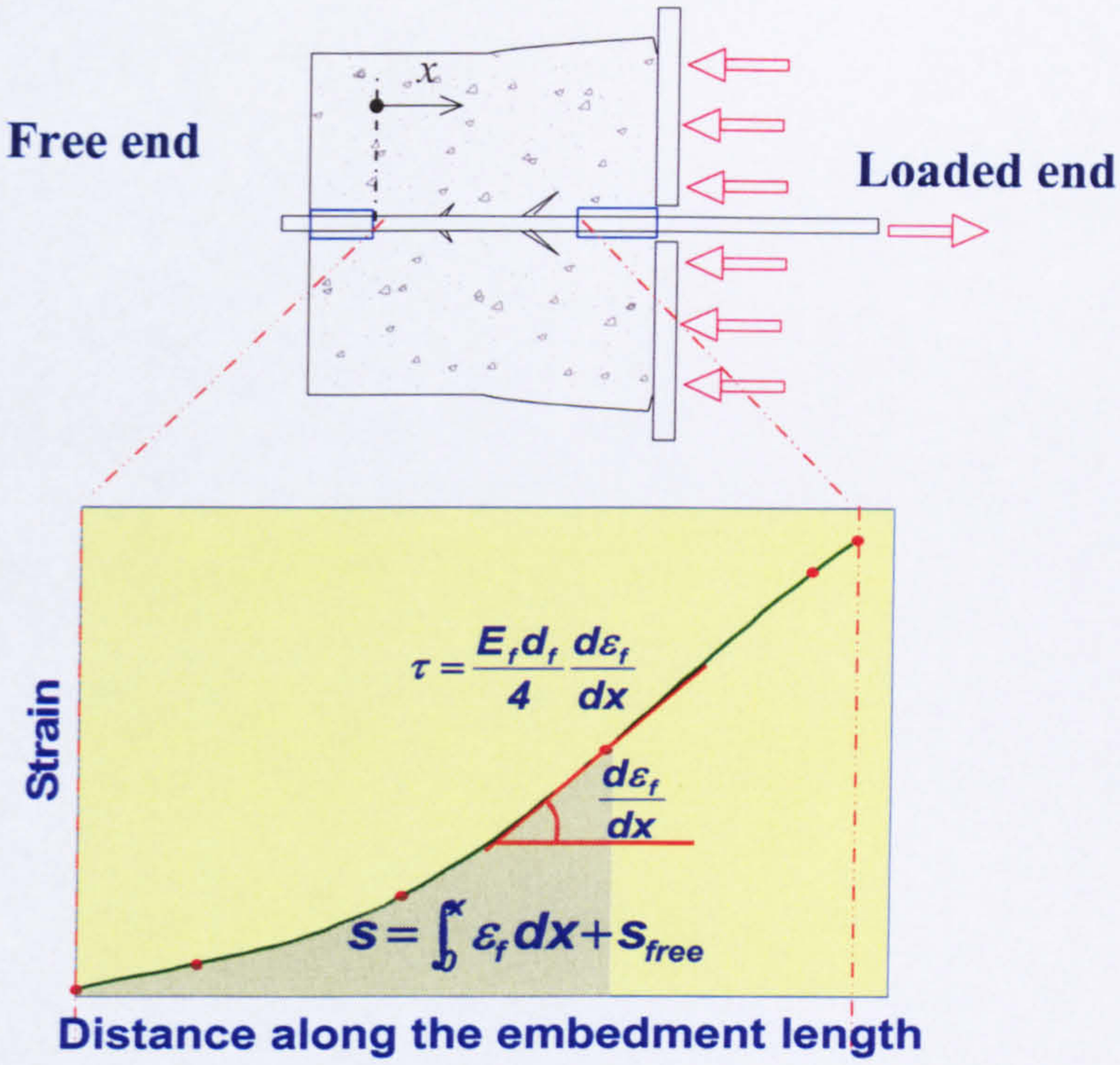

Fig. 4-4 Schematic representation of strain distribution of bar during pull out test

4.2.2 Direct tension test

4.2.2.1 Specimen preparation

The testing arrangement used for the direct tension test is similar to the testing arrangement used in the tension stiffening studies with the only exception being that the concrete specimen used for this study was notched at specific locations as shown in Fig 4-5(a) to induce cracks.

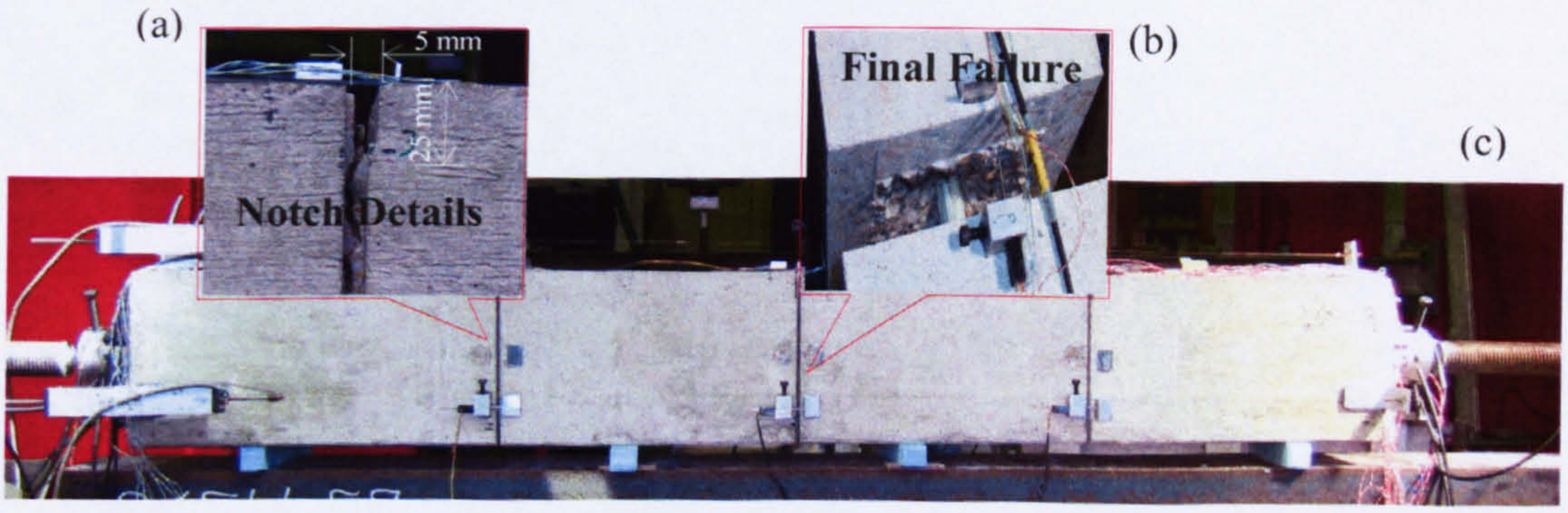

Fig. 4-5 Notched concrete specimen

4.2.2.2 Data analysis to evaluate the bond stress

Theoretically bond stress can be determined directly from successive strain gauges on elastic materials by using the strain to determine the difference in force between the two locations and assuming that the bond stress is linear between the two points. The problem with this method is that results can look erratic and irrational along the length with sudden changes in bond stresses. To achieve better results, a cubic spline is fitted between successive strain gauge reading providing a smooth strain distribution along the bar.

A cubic spline is a series of third order polynomials used concatenated to interpolate readings of two adjacent strain gauges. These two data points are also called breakpoints. Since a straight-line is uniquely defined by two points, an infinite number of cubic polynomials can be used to approximate a curve between two points. Therefore to make the results unique additional constrains are required. This is achieved by constraining the first and second derivatives of the cubic polynomials to match at the break points. However, this is still not enough to solve all the unknowns as the first and last break points do not have adjacent polynomials beyond the first and last breakpoints. By constraining the third derivative of the first and second and last and second to last polynomial to be equal, sufficient equations can be generated to solve the unknown set of cubic polynomials. With this method it is possible to interpolate all the data points and have a smooth curve joining all the test points. This was performed using MATLAB built-in functions for cubic splines (Hanselman 2001).

Derivatives of such function are also required for calculating the local bond stresses (based on equation 4-1) and were used to determine bond at any location and at any load. Calculation of slip for a given location can be done with piecewise integration between the point of zero relative movement, which is assumed to be the centre between cracks in the case of direct tension tests, to the coordinate for which slip is required.

Fig. 4-6 shows strain distribution along the bar of a typical direct tension specimen. Dots indicate the actual strain gauge measurements corresponding to the various locations along the bar at selected loading values. Lines drawn through are the results of cubic spline approximation for the given strain measurements. The figure also shows

the location of crack inducers. Fig. 4-7 shows the calculated slip along the length of the bar.

Fig. 4-8 (c) shows the calculated bond stress distribution between cracks 1 and 2 (shown in Fig. 4-8(a)) calculated using the strain distribution shown in Fig. 4-8(b).

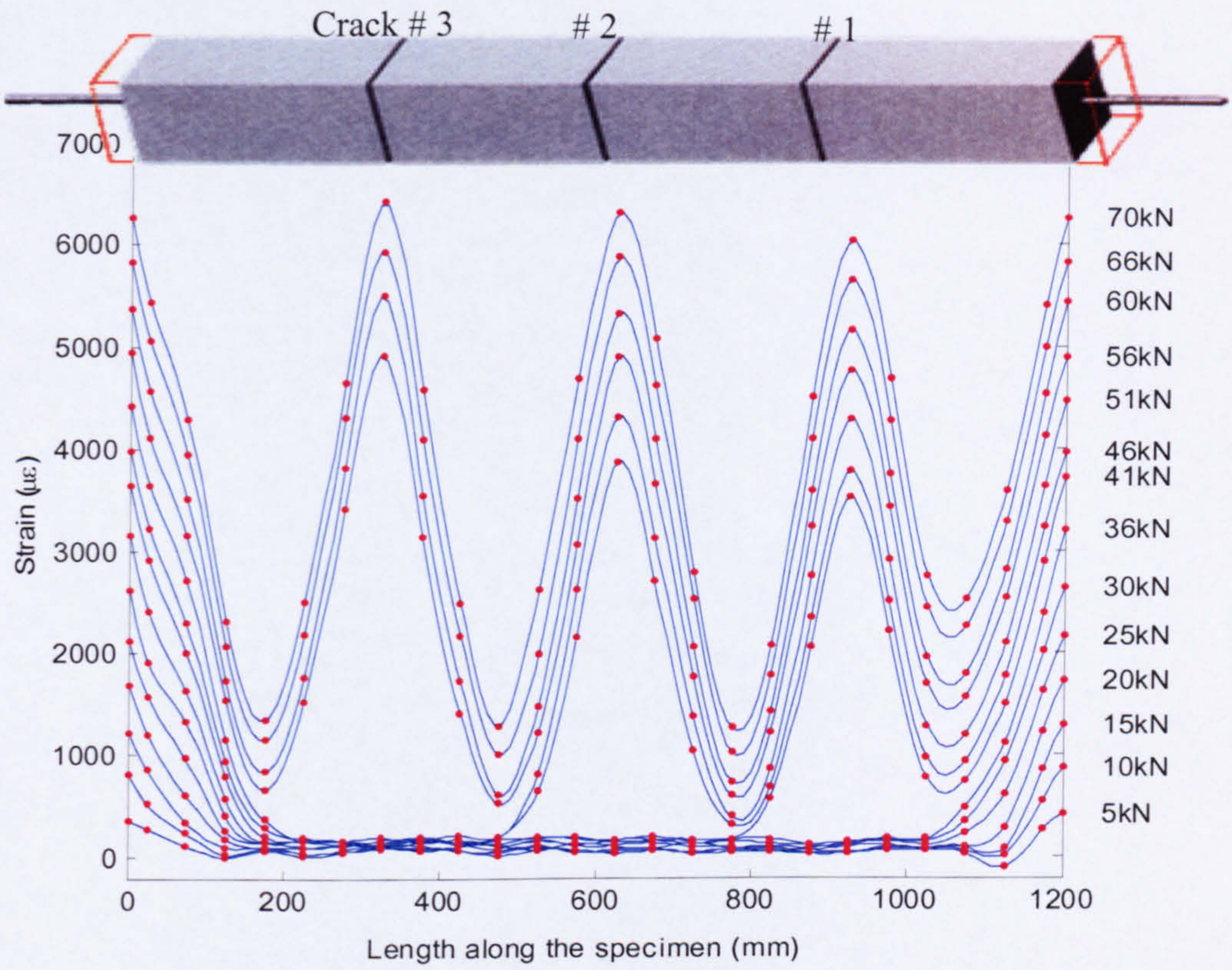

Fig. 4-6 Strain measurements and cubic spline approximation of strain distribution along full length of the tension specimen

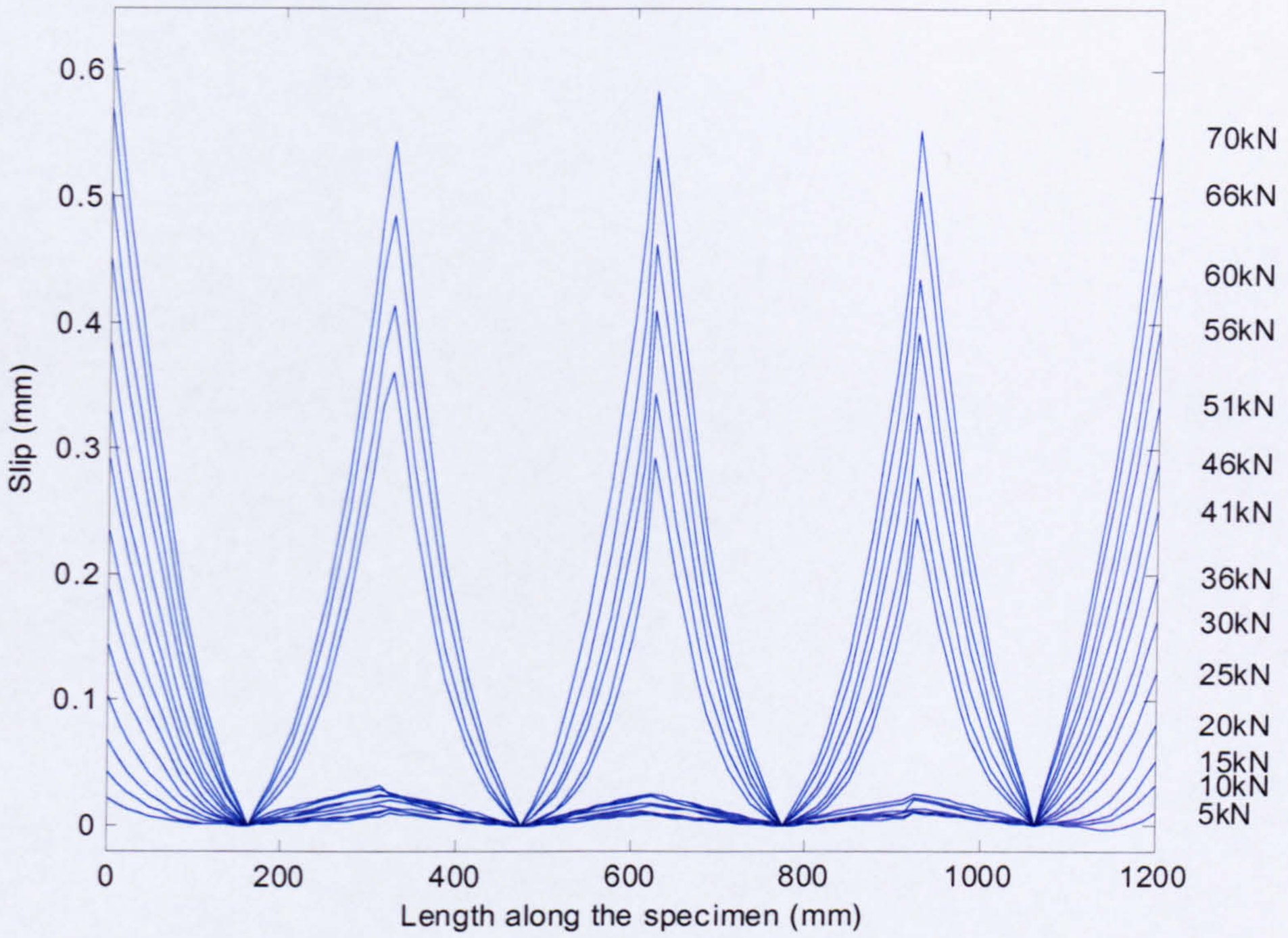

Fig. 4-7 Slip along the bar calculated using cubic spline according to equation (4-2)

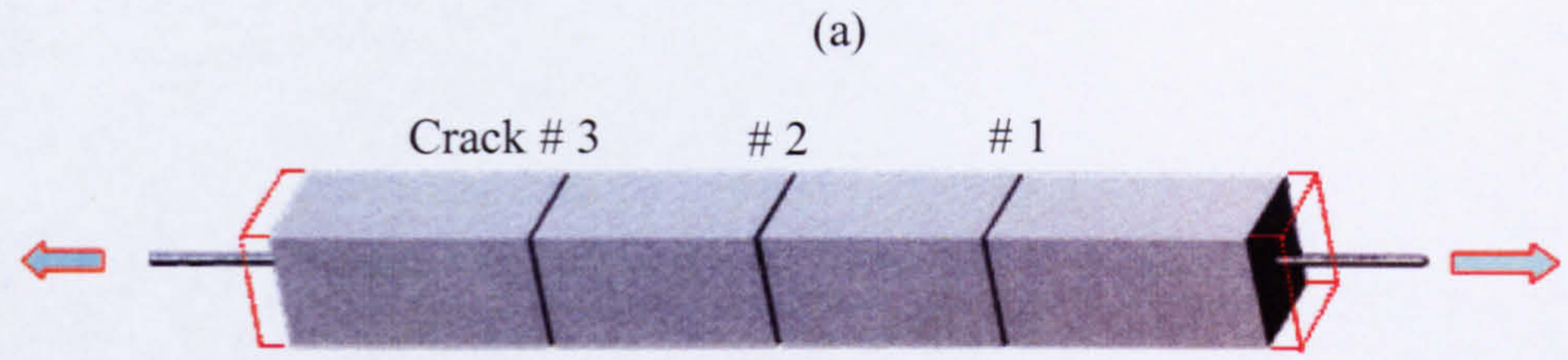

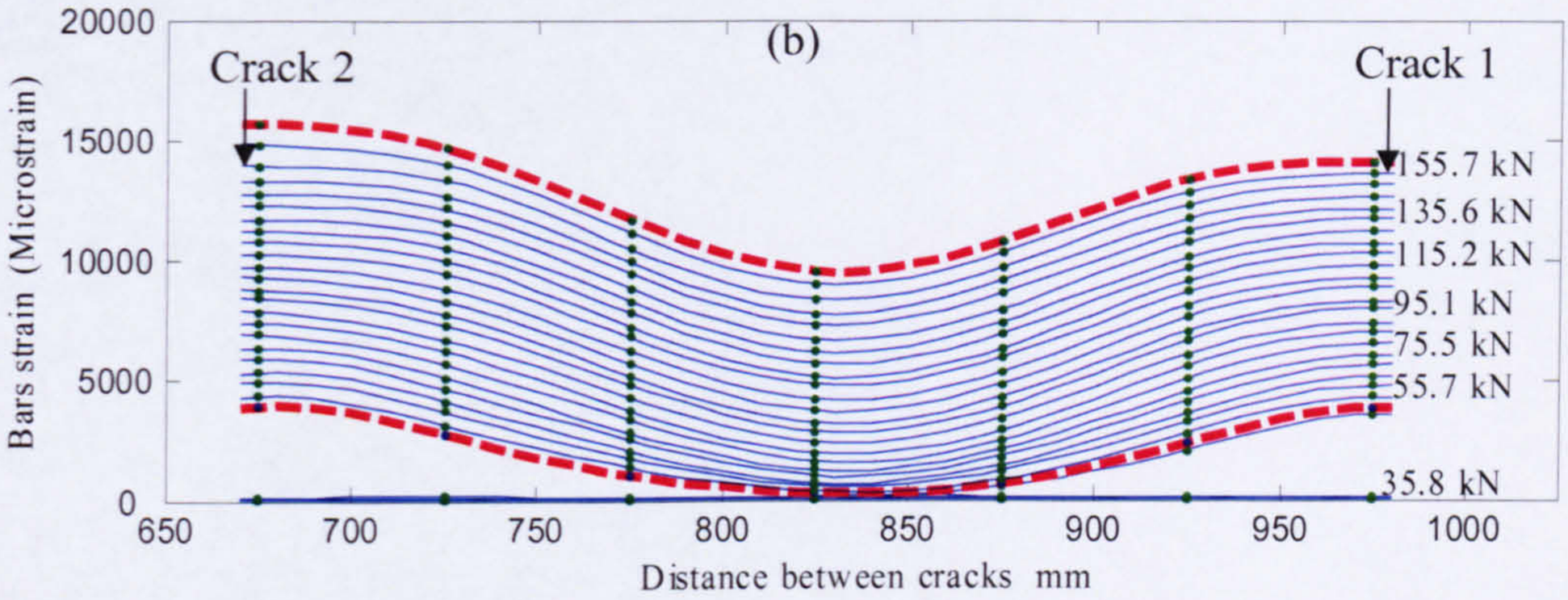

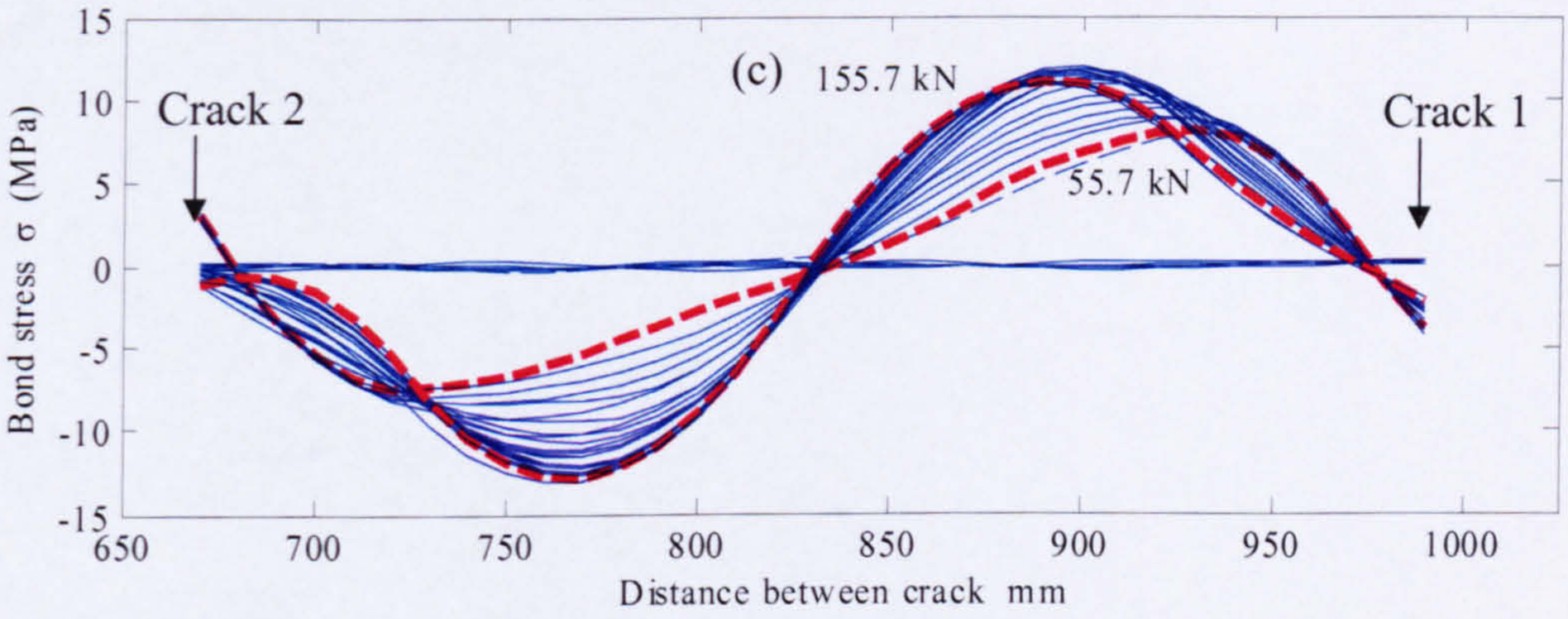

Fig. 4-8 Strain distribution between cracks 1 and 2 and corresponding bond stress distribution

4.2.2.3 Discussion on bond stress distribution

Fig. 4-9 shows the assumed bond stress distribution for steel reinforced concrete segments between adjacent cracks (Chan et al 1993). The experimentally determined bond stress distribution for GFRP, as shown in Fig 4-8 and diagrammatically in Fig.4-9, indicates that the bond stress distribution for FRP is different to that of steel reinforcement. The bond stress distribution for GFRP-RC is characterized by the loss of bond stresses close to the crack surface and a shift of the maximum bond stress away from the crack.

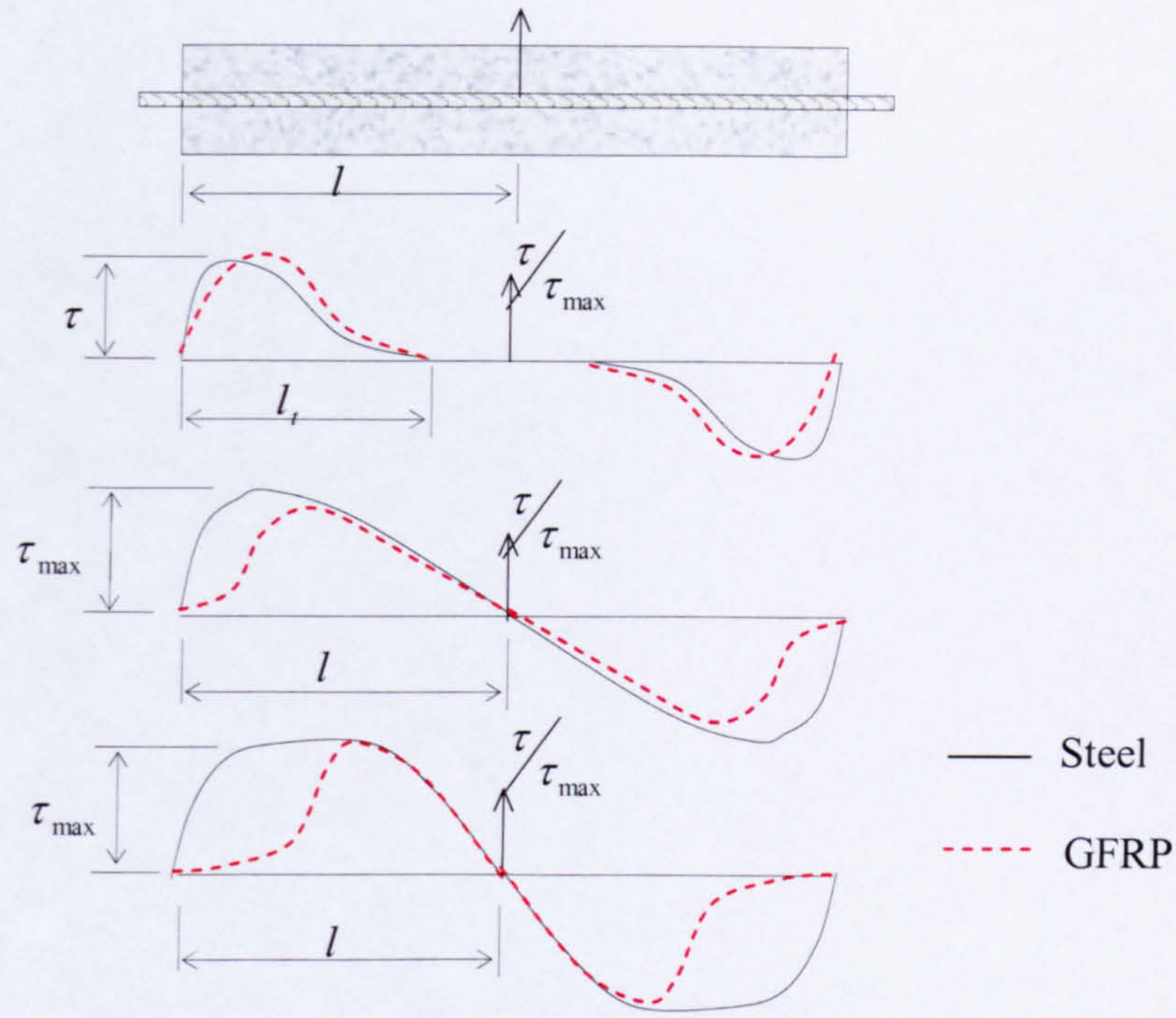

Fig. 4-9 Assumed bond stress distribution for steel and GFRP reinforcements

4 2.2.4 Average bond stress-slip $(\tau - s)$ relationship

Average bond stresses used in design are often mistaken for local bond stresses. However, when using direct tension tests it is difficult to quantify the average bond stress directly. Direct tension tests with 3 cracks and 4 segments, as used in this research, provide eight independent regions for calculating average bond stresses between points of maximum and minimum strains. Fig. 4-10 shows average bond stress-slip curves determined for four segments (a,b,c,d) of the tension test. The four curves are very similar in shape and show that there is a tendency towards a constant maximum average bond stress value of around 6 MPa. In this approach, the average bond stresses are derived by averaging the local bond stresses over the concrete block length considered. Slip at the crack section is calculated by integrating the strain profiles between the centre of a segment and the crack section, assuming zero relative displacement at the centre.

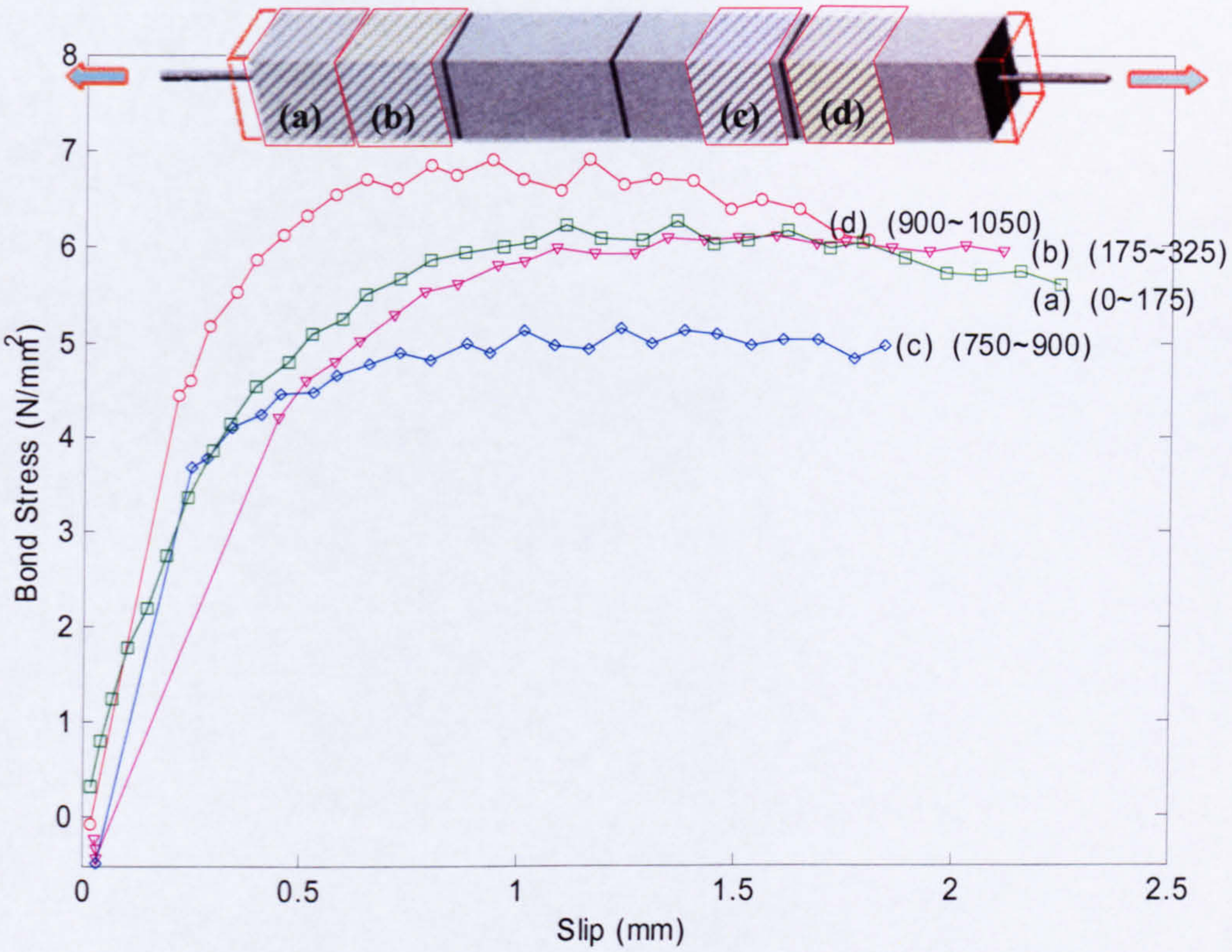

Fig. 4-10 Average bond stress-slip relationship at different locations of the tension test specimen

4.2.2.5 Local bond stress-slip relationship

Local bond stress-slip curves can provide more information on the peak bond stress and are more useful than average bond stress-slip relationships to model the bond between concrete and reinforcement. Figs. 4-11 & 12 show the local bond stress distribution calculated from strain measurements on two segments of the tension specimen (a) & (c). The left hand diagrams show the strain measurement at different load levels, whilst the right hand diagrams show the calculated bond stress and corresponding slips at various locations along the length, identified by the distances of the sections from the centre of the concrete block. It is clear that the local bond-slip relation changes at different locations away from the crack and the peak values are never reached in some of the sections close to the middle of the concrete block and towards the crack section. Hence, analytical models which are based on constant spring values based on average bond stress-slip relationships, often established by pull-out tests, can not realistically model the bond between concrete and GFRP. These results suggest that the use of a strain distribution model which considers the effects of bond deterioration closer to the crack

section is more realistic for modelling the bond stress than the use of an average bond stress-slip relationship.

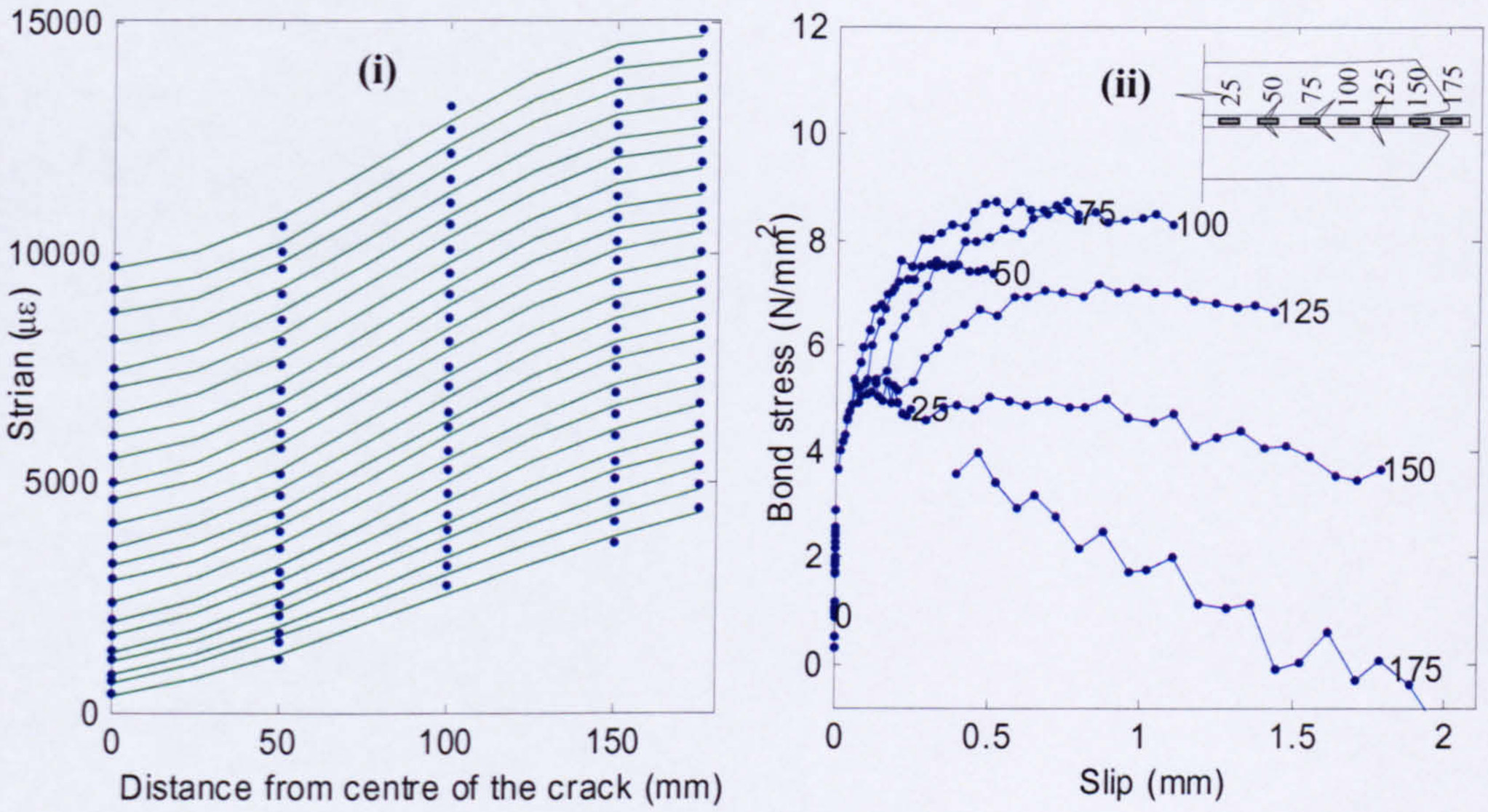

Fig. 4-11 Strain distribution and local bond stress distribution of segment (a)

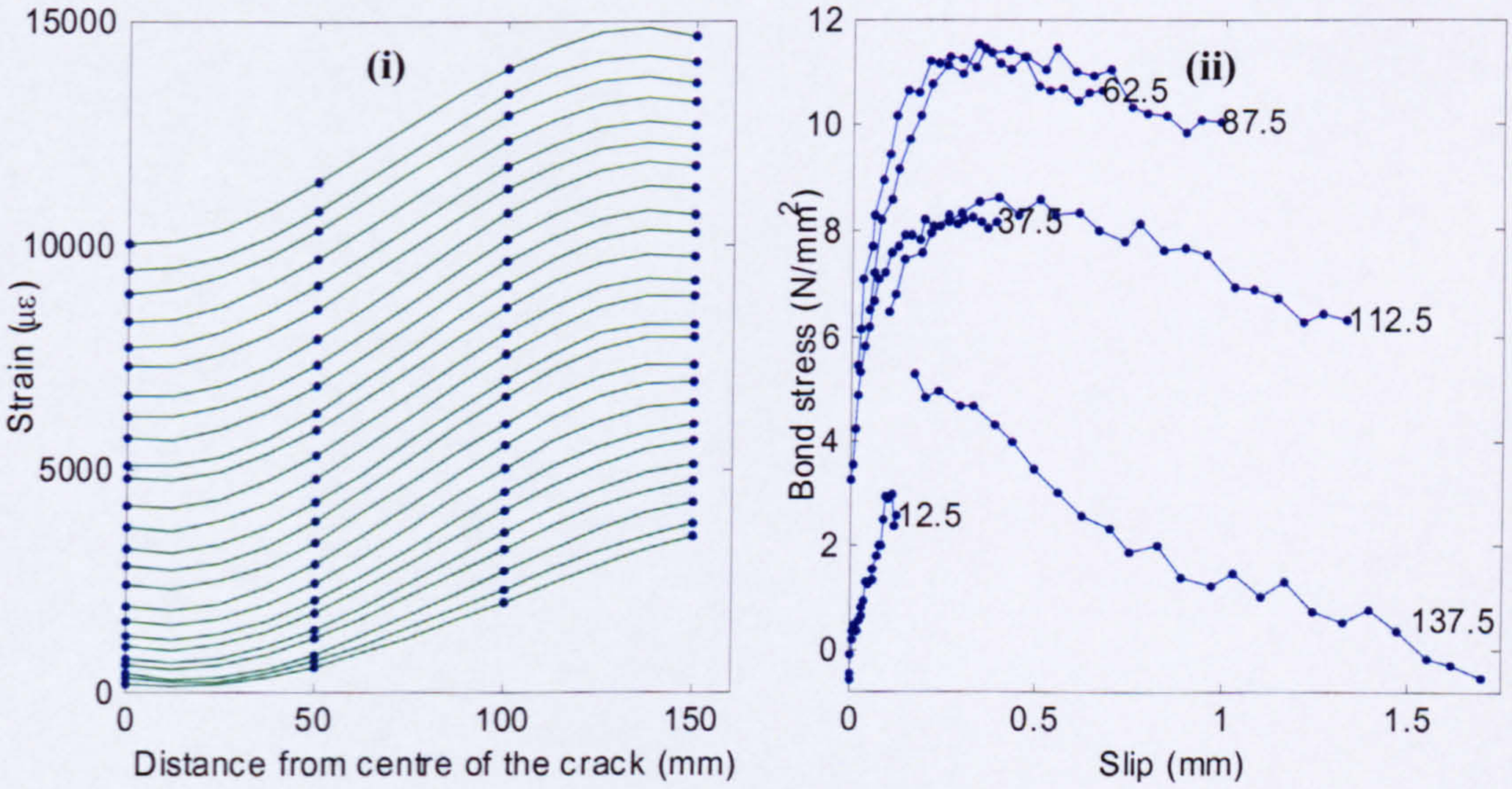

Fig. 4-12 Strain distribution and local bond stress distribution of segment (c)

4.3 Towards a unified constitutive bond stress-slip-strain relationship

4.3.1 General

There are several alternative hypotheses dealing with ways to arrive at constitutive relationships for bond between reinforcement and concrete. Initially, there were attempts to relate bond slips to bar stresses (reported in Mirza and Houde 1979). Now, bond between concrete and reinforcement is commonly characterized by using bond stress-slip relationships. However, it is seen from the above results that there is no unique bond stress-slip relationship to explain the local bond stress-slip behaviour. The bond stress between the reinforcement and the concrete is dependent on both the longitudinal strain of the reinforcement and slip. First acknowledgement of differences in local bond behaviour came from a study by Nilson (1972). Having found the local differences, Nilson coupled the bond stress-slip relationships with the distance from the crack section and suggested the following equation for the bond stress-slip relationship at different locations from the crack section.

$$\tau = 3100(1.43 \times C + 1.5)s\sqrt{f_c'} \quad \text{(inches and psi)} \qquad (4\text{-}5)$$

Where

τ = Bond stress $\tau < (1.43C + 1.5)\sqrt{f_c'}$

C = Distance from the loaded end (inches)

f_c' = Concrete strength (psi)

s = Slip (inches)

However, such models that couple distance are scarcely useful for numerical computations as it is quite implausible to keep track of the crack locations and to adjust the local bond stress-slip depending on the distance from a crack section. A constitutive equation for bond by coupling bond stress, slip and strain is the only pragmatic solution to this problem. Coupling bond stress, slip with strain has been attempted for bond behaviour of steel reinforcement and good agreement between test results and empirical formulations were reported by Maekawa et al (2001). This study was limited mostly to service loads and was for undamaged bond response. However, FRP with low stiffness and softer surfaces are more prone to surface damage and reach peak behaviour earlier, making post peak bond response an absolutely essential part of a constitutive relationship for FRP. Although there are several models dealing with average bond stress-slip relationship of FRP (Cosenza et al. 1995) (Tighiouart et al. 1998), the

variation of local bond stress-slip relationship is yet to be addressed. This section presents a systematic derivation of bond stress-slip-strain relationship for GFRP to explain local bond stress-slip behaviour of GFRP.

4.3.2 Relationship between bond stress, slip and strain

Before formulating the constitutive relationships for bond by coupling bond stress-slip with strain, it is necessary to investigate the relationships of bond stress-slip at different strain levels. By considering constant strain levels and constructing imaginary lines at those strains on the strain distribution diagrams, e.g. Fig. 4-11 or 4-12, the family of curves intersecting the given strain levels can be found. Then by considering the location of the intersection, bond stresses and slip for the given strain level can be found from equations 4-1 and 4-2. Fig 4-13 illustrates how a bond stress-slip relationship is established for a given strain level, ε^*, from a strain distribution diagram.

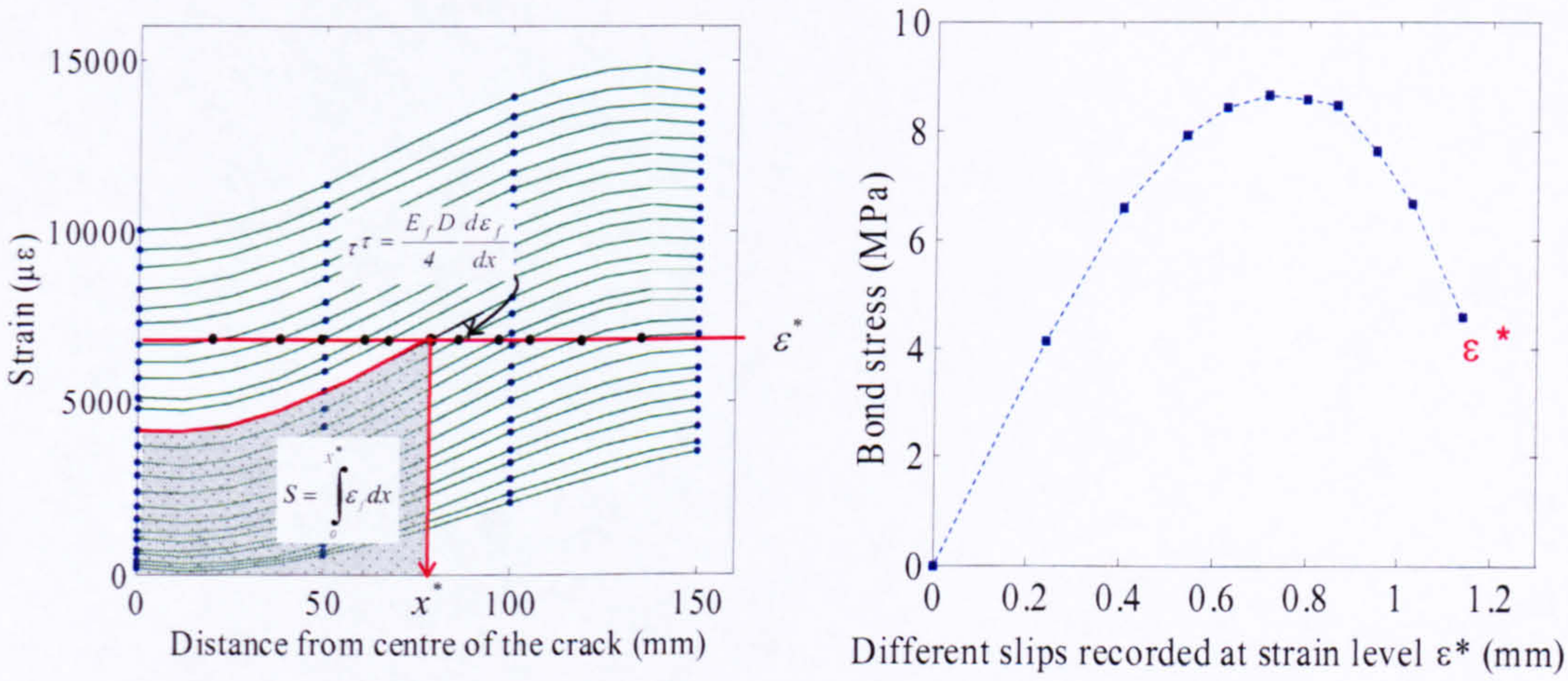

Fig. 4-13 Calculation of bond stress-slip relationship for an arbitrary strain ε^*

Fig. 4 –14 shows the bond stress versus slip relation found for different strain levels derived from Fig. 4-11 for segment (a). In the analysis it is assumed that the bond stress is equal to zero at zero slip for any bar strain and therefore all bond stress-slip curves are shown to go through the origin. From Fig. 4-14 it is clear that the peaks of the local bond stress-slip relations can be encapsulated by an envelope. Another important observation is that there is a decrease in the initial stiffness of the bond stress-slip curves with an increase of strain and that bond stress versus slip at any given strain level can easily be approximated by a second order polynomial.

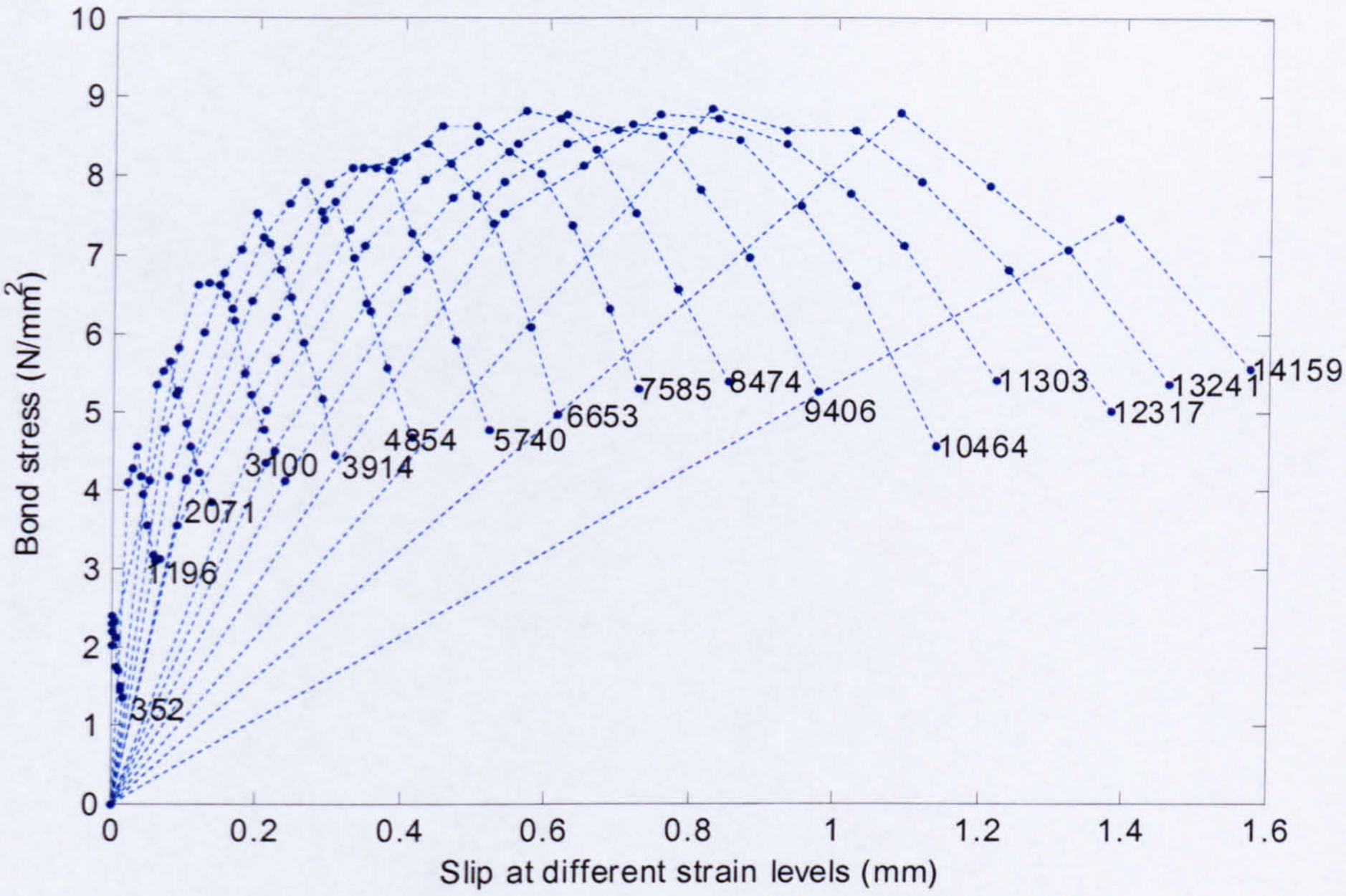

Fig. 4-14 Bond stress-slip at different strain levels

In the quest to find the unified bond stress-slip-strain relationship $(\tau - s - \varepsilon)$, data at different strains were approximated by a second order polynomial equation, as shown in equation 4-6. This equation is initially derived for a reference strain level (ε_{ref}) of the bar and is extended to other strain levels (ε_i) by a factor β, which can vary the shape of the polynomial for different strain levels, yet maintaining a constant peak value. Fig. 4-15 shows the approximated polynomials according to equation 4-6 compared with experimental results for different strain levels. It is clear from Fig. 4-15 that the peak stresses cannot be kept constant and should follow the envelope of results.

$$\tau = 4.\tau_{max}(\eta - \eta^2) \qquad (4\text{-}6)$$

where

$$\eta = \frac{1}{\beta} s$$

s = Slip at a given point

$$\beta = S_{ref}\left(\frac{\varepsilon_i}{\varepsilon_{ref}}\right)^{1.25}$$

S_{ref} = Slip at peak bond stress at calibrated strain

ε_i = Strain

ε_{ref} = Reference strain for calibration

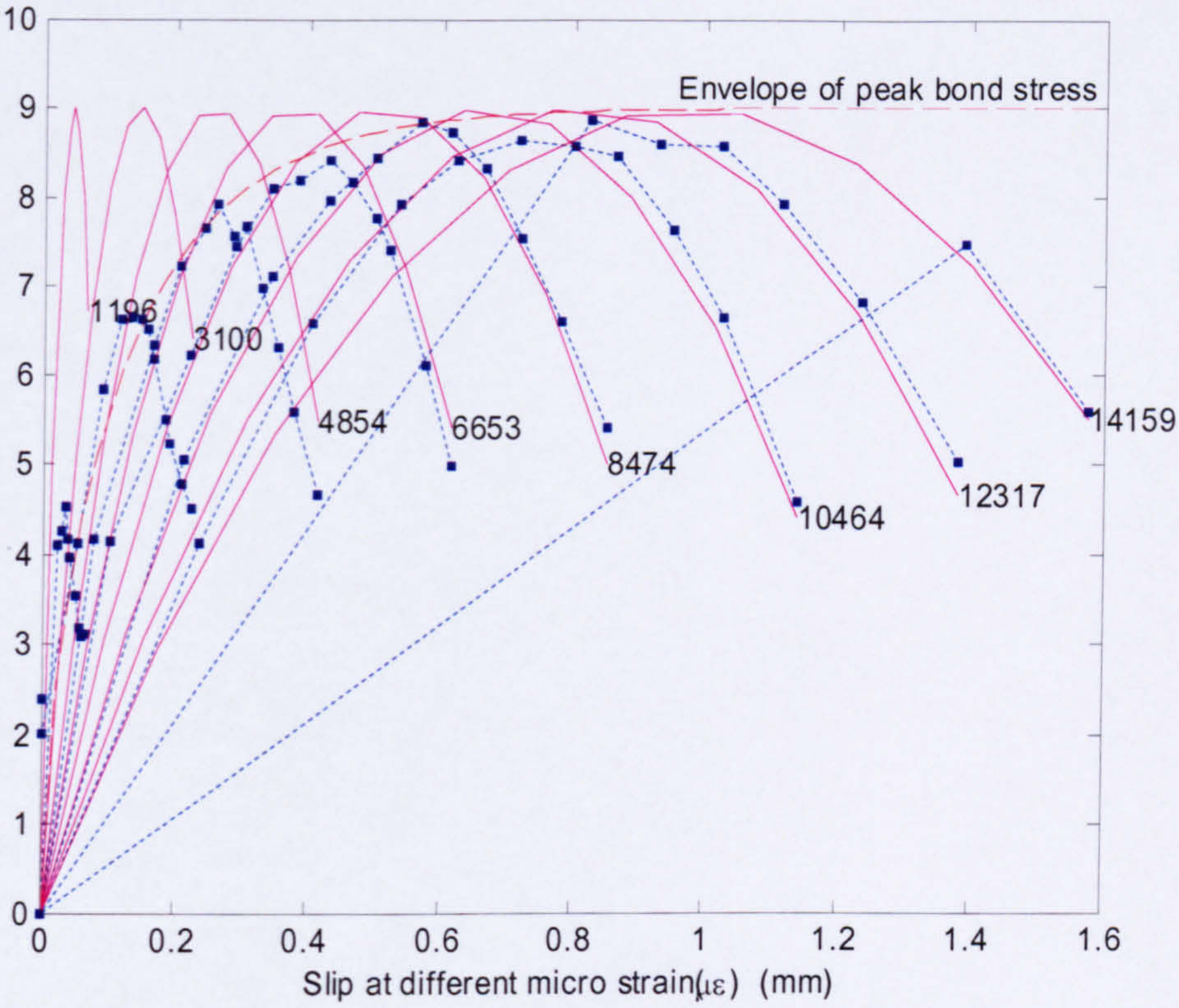

Fig. 4-15 First estimate of bond stress-slip at various strain according to equation 4-5 compared with the experimental values

This is achieved by multiplying Equation 4-6 by an exponential function resulting in equation (4-7). Predictions of the experimental results according to equation 4-7 are shown in Fig.4-16.

$$\tau = 4.\tau_{max}(1 - e^{-3.5\beta})^{0.5}(\eta - \eta^2) \qquad (4\text{-}7)$$
$$\tau \geq 0.0$$

τ_{max} = Maximum recorded local bond stress obtained from experiments

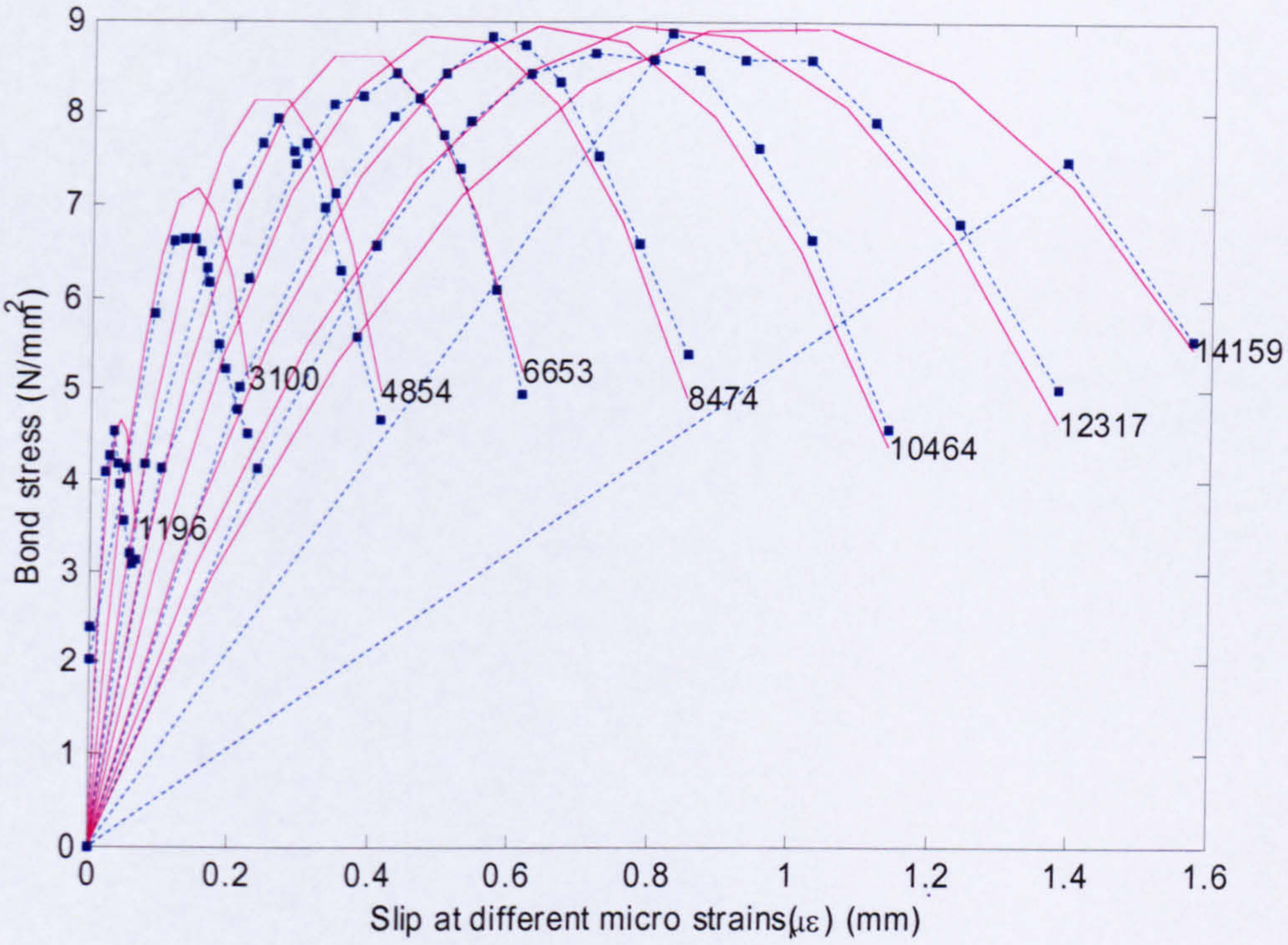

Fig. 4-16 Bonds stress slip at different strain levels according to Equation 4-6 compared with experimental results

Fig. 4-17 shows the accuracy by which this equation can predict the local bond stress-slip at different locations along the bar. In Fig. 4-17, blue lines with dots represent the experimental results and red continuous lines represent the estimates from equation 4-7.

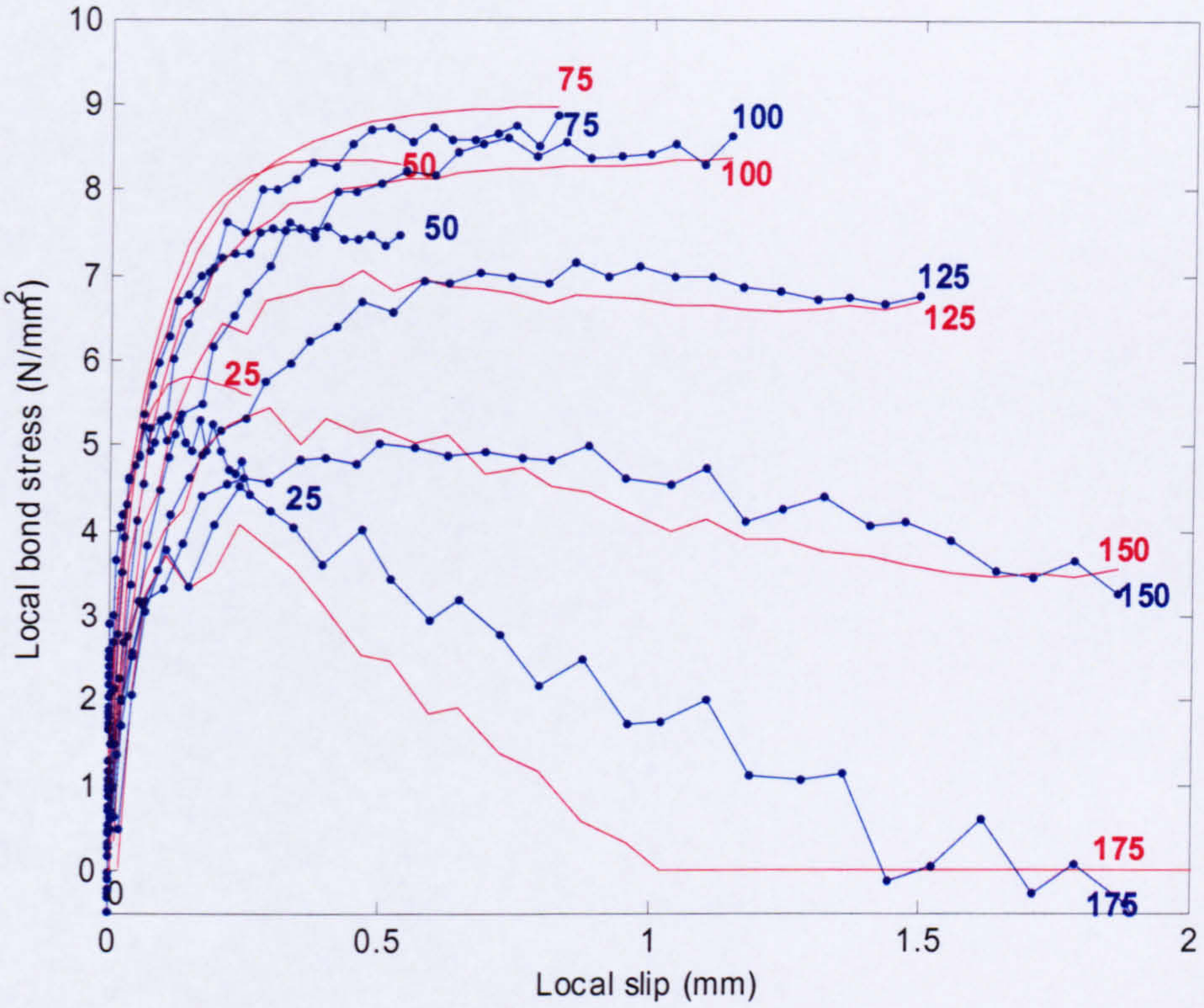

Fig. 4-17 Comparison of experimental results with results obtained using the proposed $\tau - s - \varepsilon$ relationship of equation 4-6.

From the above figure it is clear that the local bond stress-slip relationship is very different from the average bond stress-slip behaviour and that it is possible to explain the local bond stress behaviour by coupling bond stress-slip with strain $(\tau - s - \varepsilon)$. This formulation also underlines the importance of strain in determining the local bond stresses.

From this study, it is clear that the establishment of the strain profile between cracks is sufficient to model the interaction between concrete and reinforcement accurately and avoid difficulties of modelling bond locally. The next chapter examines the bond development length as an essential element of bond modelling.

CHAPTER 5

PULL-OUT TESTS AND DETERMINATION OF BOND DEVELOPMENT LENGTH

5 .1 General

The pull-out test is a relatively simple test to carry out and it is used extensively to provide a comparative insight into bond behaviour of FRP. Like the tension test, it can provide information at the meso-level and can help develop models for bond. It is frequently used to find the average bond stress slip behaviour of reinforcement and in predicting the splitting effects of bond stresses on reinforced concrete. However, bond modelling, based solely on pull-out test results is not the best way to understand the bond behaviour of reinforced concrete. This is due to the fact that, in pull-out tests, the concrete close to the reinforcement is mostly subjected to a compressive state of stress which is not entirely accurate representation of the state of stress in concrete between cracks in tension, eg : the tension zone of a bending element. Fig. 5-1 shows diagrammatically the difference of state of stress between the tension and pull-out tests. The diagrams show the approximate 2D principal stress fields and possible location of secondary tensile cracks.

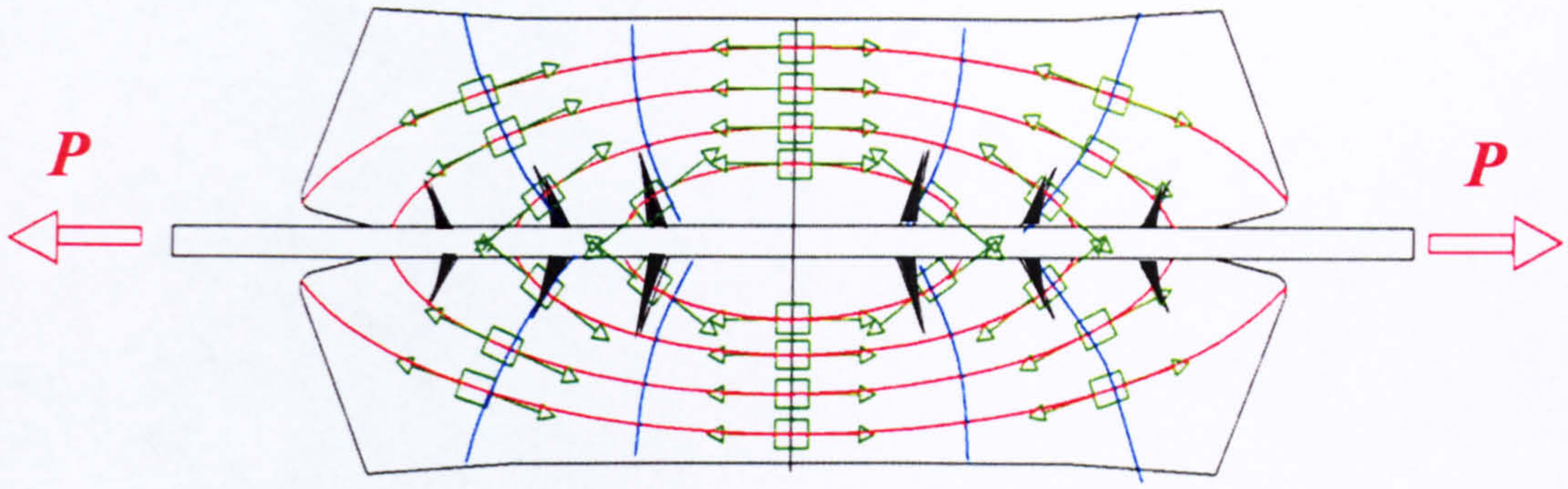

Principal stress direction in concrete in the tension test

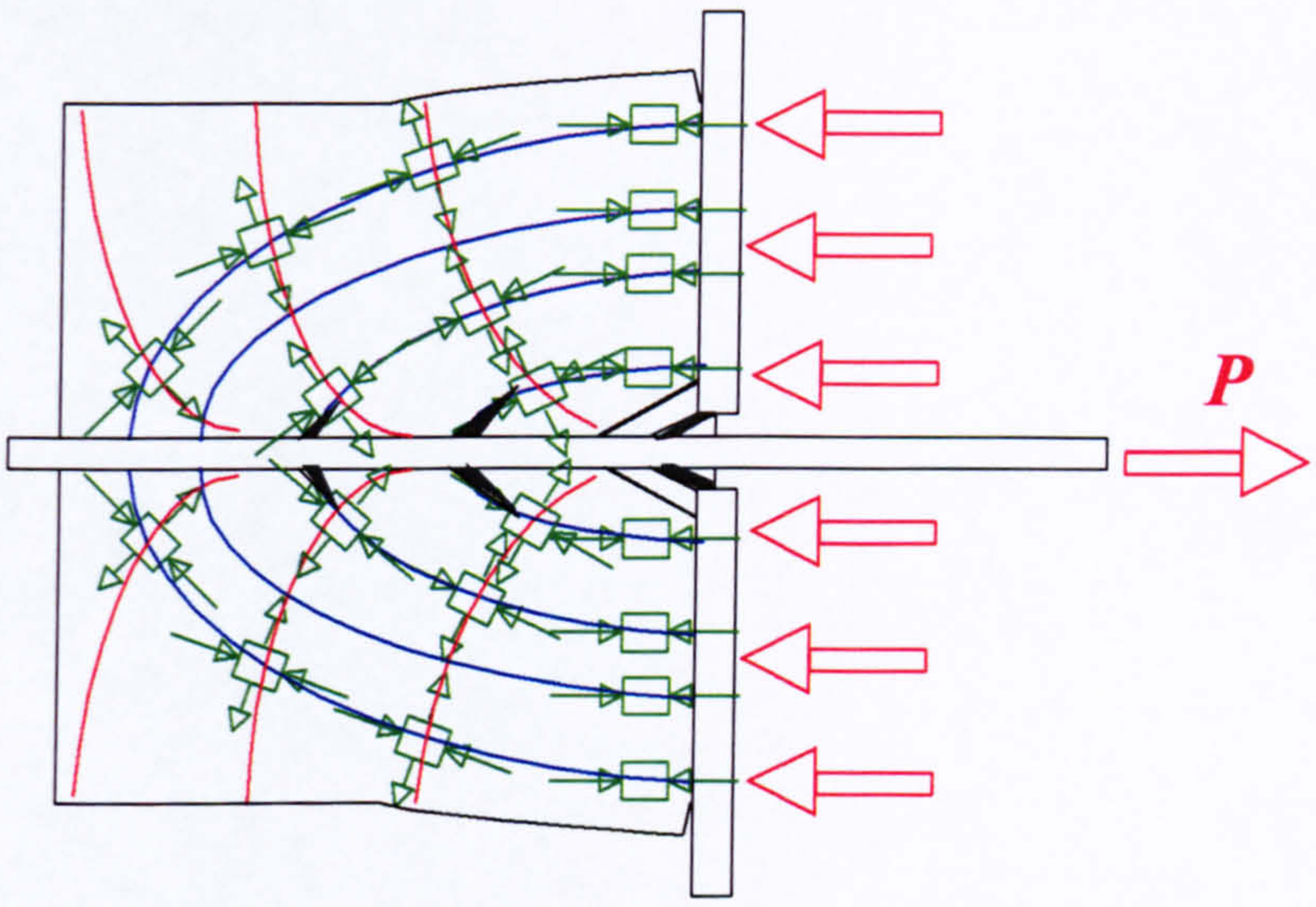

Principal stress direction in concrete in the pull-out test

Fig. 5-1 Diagrams of principal stress fields in tension and pull-out tests

In this study, pull-out experiments are primarily used to determine the bond development length of GFRP RC. Two bar diameters (D), two different concrete strengths (f_{cu}), and two different bonded lengths (l_b) are used in the experimental study to examine their influence on the bond behaviour of GFRP bars. The first part of this chapter presents details of the experimental procedure adopted. This is followed by a detailed analysis of the results. Results presented in this section include average bond stress-slip relations derived from the pull-out studies. This is followed by a discussion on factors influencing average bond stresses leading to the development of an empirical

equation for bond development length. The chapter ends by coupling a strain distribution function with the derived bond development length as a means to represent the strain distribution between cracks in the tension test.

5.2 Specimen preparation

Sufficiently large concrete cubes were used in this study to avoid splitting of concrete. Figs. 5-2(a) to (c) show three photographs of pull-out tests: (a) general view of the pull-out test rig, (b) free end slip measuring arrangement and (c) loaded end slip measuring arrangements. Fig. 5-3 provides a schematic representation of the pull-out test rig, measuring arrangements and embedment details. In all specimens, de-bonded lengths were provided both at the loaded end and the free end as shown in Fig 5-3. The de-bonded length at the loaded end is especially important to avoid diagonal concrete cracks reaching the concrete surface. The de-bonded length at the free end is maintained to a minimum, just long enough to avoid the boundary effect due to concrete quality.

The two diameters (D) of GFRP used in the study are12.7mm and 19.1mm, representing medium and large size bar diameters. The use of these different bar diameters resulted in two reinforcement ratios (two bars are cast in identical moulds) to study the influence of reinforcement ratio on bond performance. Two concrete grades (f_{cu}) 45MPa and 90 MPa are used representing typical normal concrete strength and high strength concrete to study the influence of concrete strength on bond behaviour. In addition, two bonded lengths; one length equivalent to $5D$ and the other equivalent to $10D$ are used. The length of 5 D was selected so that the test results of this study could be compared with the FRP pull-out tests conducted by international round robin test exercise on bond of FRP bars in concrete (Research network TMR "ConFibreCrete"). The length of $10D$ is included in the study with two objectives: to study the influence of bonded length on bond stress development and to enable the study of fully bonded response.

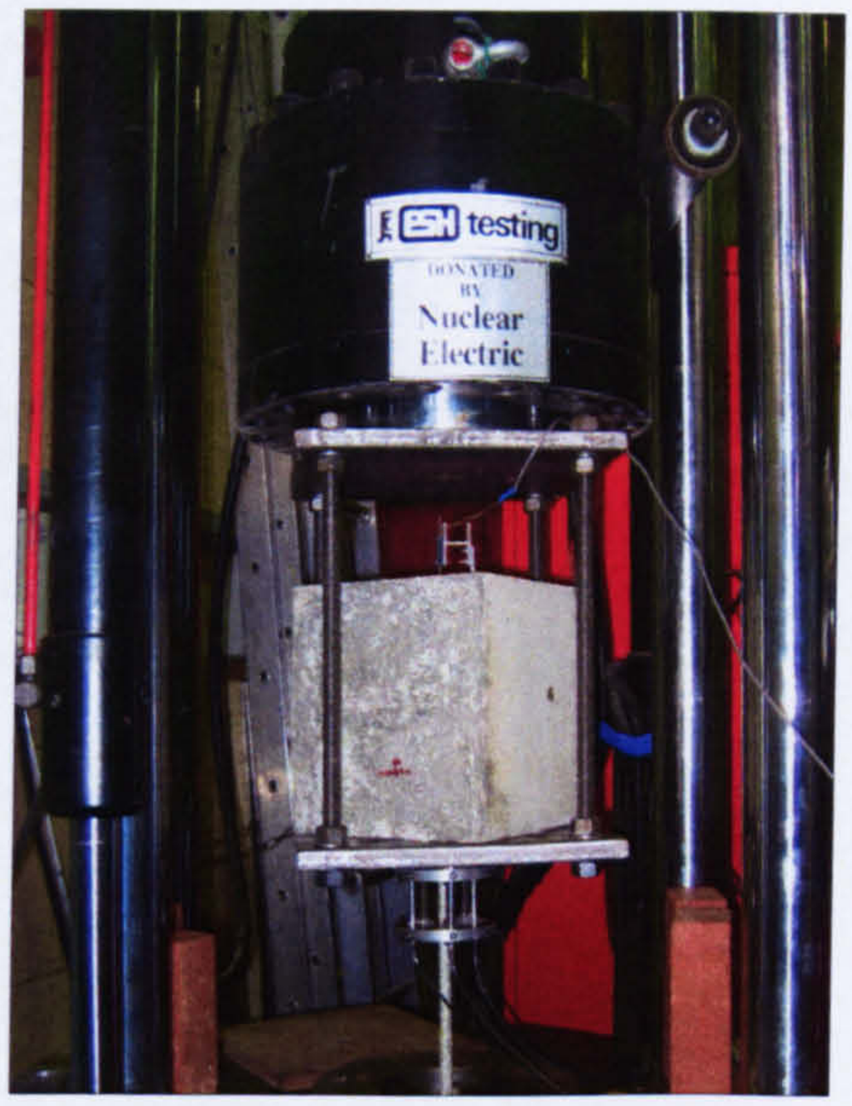

(a) General view

(b) Measuring arrangement at loaded end

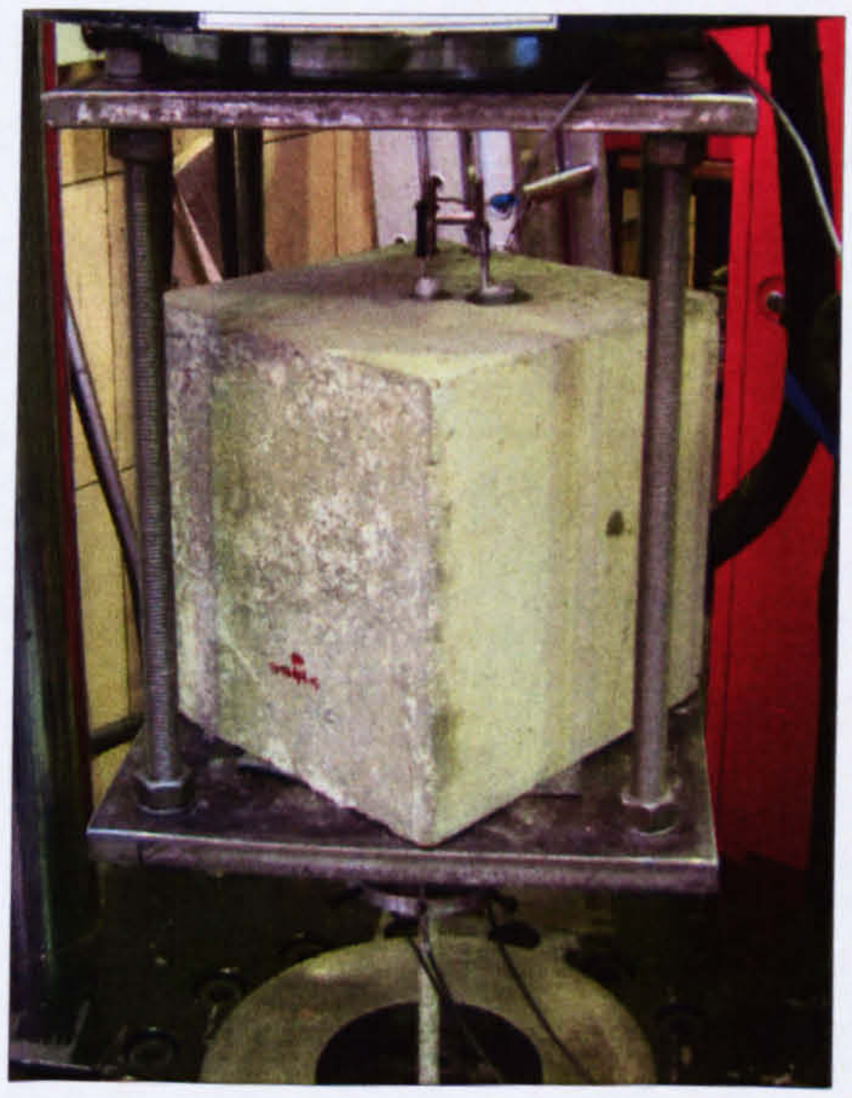

(c) Measuring arrangement at free end

Fig. 5-2 Photographs of pull-out test showing slip measuring arrangements at the two ends

TESTING RIG

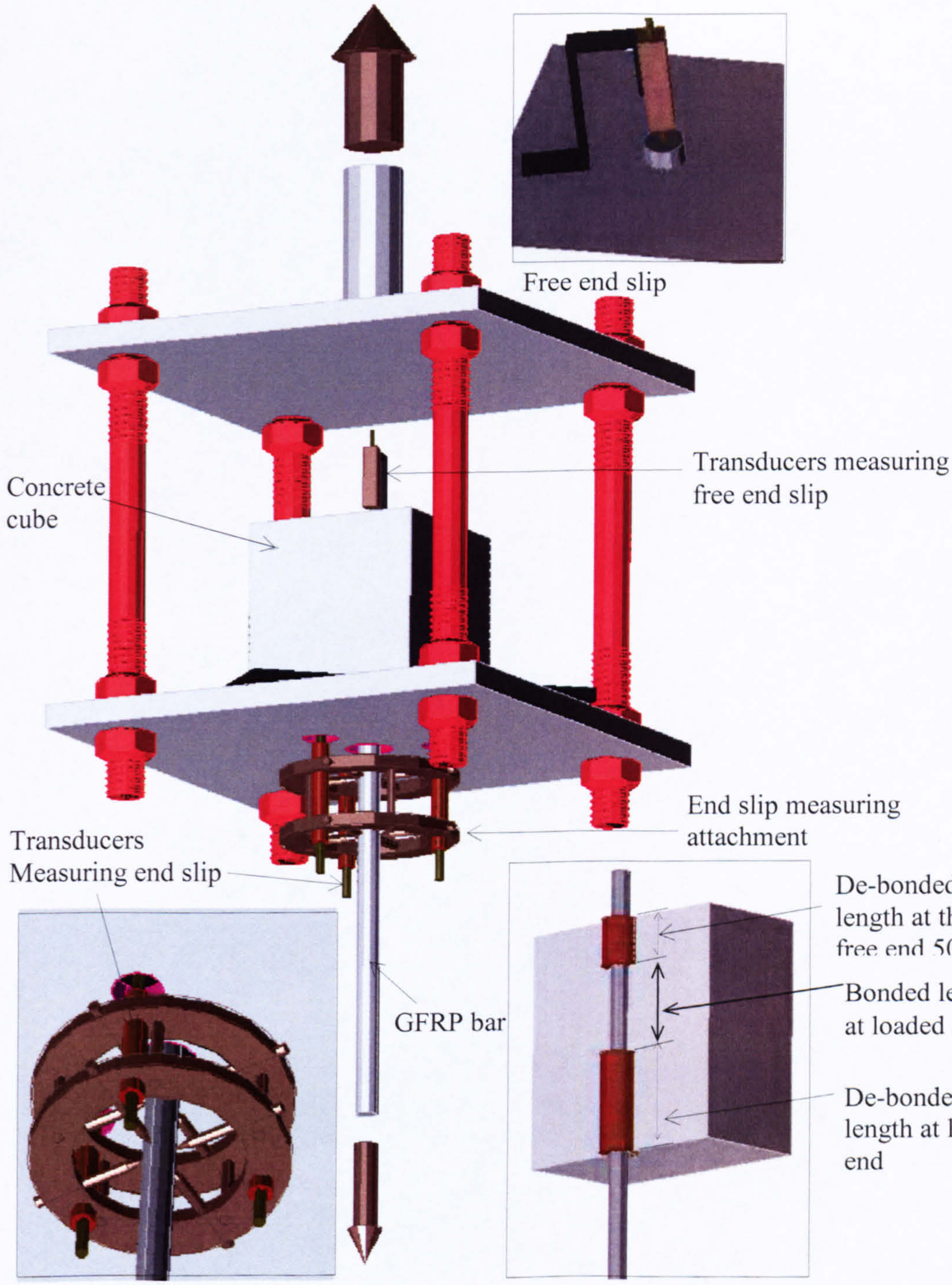

Fig. 5-3 Schematic representation of pull-out test rig and testing specimen

Table 1 shows the details of the specimen groups tested in the experimental study. Each group had multiple specimens. All 19.1 mm bars had one specimen with a bar strain gauged internally similar to the one described in section 3.3.5.2. Strain gauge readings of these experiment analysed for bond development and local bond stress-slip relationship are shown in Appendix II.

Table 5-1 Details of the pull-out specimens

Specimen Group	D (mm)	f_{cu} (MPa)	l_b (mm)	Specimen dimensions (mm)
13-45-5D	12.7	45.4	5 D	250×250×250
13-45-10D	12.7	45.4	10 D	250×250×250
13-90-5D	12.7	90.7	5 D	250×250×250
13-90-10D	12.7	90.7	10 D	250×250×250
19-45-5D	19.1	45.4	5 D	250×250×250
19-45-10D	19.1	45.4	10 D	250×250×300
19-90-5D	19.1	90.7	5 D	250×250×250
19-90-10D	19.1	90.7	10 D	250×250×300

During casting the FRP bars were positioned horizontally to simulate the bond of flexural elements in practice with horizontal bars. Bond strength in horizontally held bars during casting is found to be less compared to vertically held bars as bleeding water and air can get trapped on the under side of the bars thereby reducing the effective contact with concrete (Maekawa et al. 2002).

Fig. 5-4 shows the moulds for the pull-out test specimen just before casting of concrete. De-bonded lengths at either ends were first covered in a thick layer of paraffin and then wrapped by a steel tube to make sure full de-bonding is achieved. To measure the compressive strength, concrete cubes were also cast and cured alongside the pull-out specimens for all different concrete batches used in the experimental work. After de-moulding, specimens were cured for at least 28 days immersed in water at 20°C before carrying out the pull-out test.

Fig. 5-4 Prepared moulds for pull-out test just before casting of concrete

Testing was done whilst concrete was still moist. Compressive strength tests on concrete belonging to the same batch of concrete were carried out along with all the pull-out tests. The concrete mean strengths of the two grades used are shown in Table 5-1. Since the standard deviation of the different batches, calculated based on the average of all the tests results for an individual grade, was within the accepted level for each grade, the value of 45.6 MPa for normal concrete and 90.7 MPa for high strength concrete, are considered as the strength of the two grades.

5.3 Test procedure

In this experimental work free end slip was measured using a transducer attached to the concrete which measured free end slip with respect to concrete as shown in Fig. 5-2(b). The loaded end slip was measured using three transducers attached to the reinforcing bar as shown in Fig. 5-2(c) which measure slip with respect to a known point on the bar. Before the test specimens were loaded into the testing rig a reference point was decided to attach the slip measuring attachment at the loaded end. The distance between this marked point and the face of the concrete was also measured. This length added to the de-bonded length, l_d, at the loaded end gives length, l_{free}, the distance between the transducers connected to the bar and the point where the bond between the concrete and bar starts. The specimens were then positioned in the rig and the loaded end slip

measuring arrangement was attached to the marked point on the GFRP bar. The three transducers (LVDT's) in the loaded end measuring arrangement were then adjusted to go through the holes provided in the lower plate of the testing rig to touch the underside of the concrete specimen. The free end slip measuring transducer was connected to a fixed stand attached to the top face of the pull-out specimen which holds the transducer vertical with its measuring end touching the bar at the free end. All transducers were then connected to a computer controlled data logger and initialized.

For economy reasons, in the pull-out tests no special attachments were used to grip the bar to the loading machine during the pull-out tests. This worked in most of the pull-out tests as pull-out was achieved at a relatively low load. However, in the case of fully bonded specimens, bar failure was reached at a stress much lower than the expected strength of the FRP. An attempt was made to increase the load at failure by using a loading machine which has jaws that could apply a controlled amount of lateral pressure. This enabled the development of a stress up to 70% of the expected GFRP bar strength.

The pull-out tests were conducted using displacement control. Both cyclic and monotonic loading was applied to different specimens. Cyclic loading was applied to observe possible bond degradation due to repeated loading. Complete pull-out of the bar from concrete was achieved in all of the $5\,D$ and $10\,D$ bonded length specimens of the normal strength concrete and $5\,D$ bonded length specimens of the high strength concrete.

5.4 Data Analysis

For bars without internal strain gauges, only average bond stresses can be determined from the experimental data. Similarly, bond slip in the absence of internal strain measurements along the bar is only possible at the two ends, loaded and free end. Free end slip is measured directly and required no corrections. The loaded end slip is measured with respect to a fixed perimeter on the bar which extends with load. Hence, the bar movement between the reference perimeter and the bonded perimeter needed to be deducted from the measured average transducer extension, Δ_T. Equation 5-1 shows the adjustment to Δ_T in arriving at the estimated loaded end slip, s_{end}, for an applied

load, P. Equation 5-2 below shows the average bond stresses calculated from the pull-out test based on the pull-out load and the total bonded area of the bar.

$$s_{end} = \Delta_T - \frac{Pl_{free}}{E_f A_f} \tag{5-1}$$

$$\bar{\tau} = \frac{P}{\pi D l_b} \tag{5-2}$$

Where

$\bar{\tau}$ = Average bond stress over the bonded length

P = Applied load

D = Bar diameter

l_b = Bonded length

A_f = Area of FRP reinforcement

E_f = Young's modulus of FRP bar

Table 5-2 below is a summary of the average bond strengths recorded in this experimental investigation.

Table 5-2 Average bond strength and mode of failure for the pull-out tests

Specimen Group	Test results $\bar{\tau}$ (MPa)	Ave. bond strength ($\bar{\tau}$) (MPa)	Failure mode
13-45-5D	16.17, 15.18	15.67	Pull
13-45-10D	13.39, 13.60	13.50	Pull
13-90-5D	21.64, 18.14	19.89	Pull
19-45-5D	8.53, 11.34, 10.19	10.02	Pull
19-45-10D	10.48, 12.7, 12.05	11.74	Pull
19-90-5D	15.19, 18.05	16.62	Pull

5.5 Influence of different variables on the $\bar{\tau}-s$ relationship

5.5.1 Concrete strength

Fig. 5-5 shows typical results for the influence of concrete strength on the bond properties of GFRP. For clarity, the results of the two bar diameters used are shown separately. Although bond strength is not directly proportional to the concrete strength, the influence of concrete strength is evident for both bar diameters. The increase in bond strength with concrete strength is found to be proportional to $\sqrt{f_c'}$ as predicted by ACI 440.1R-03.

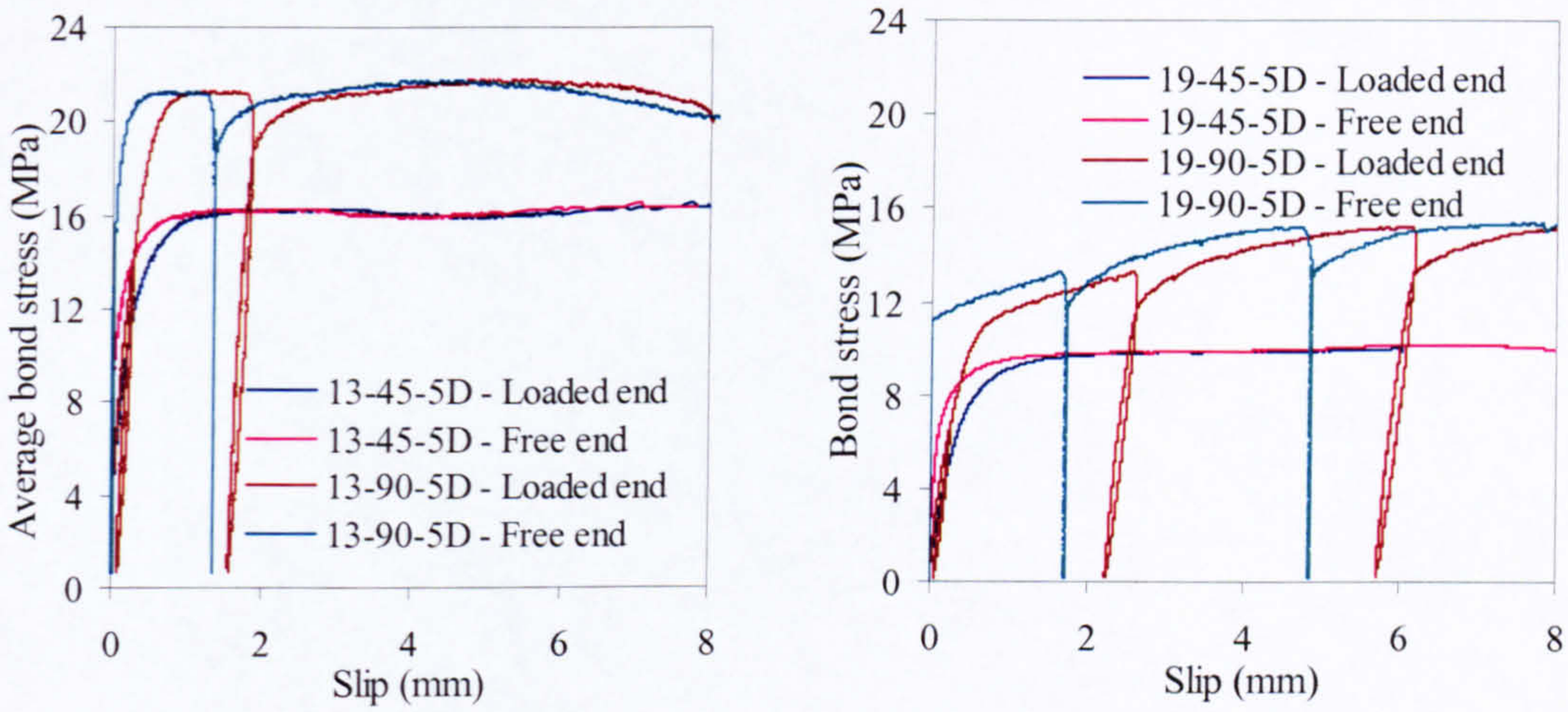

(a) 13 mm bar 5D embedment length (b) 19.1 mm bar 5D embedment length

Fig. 5-5 Influence of concrete strength on the bond

5.3.2 Embedment length

Fig. 5-6 shows typical results for the influence of embedment length on the bond properties of the GFRP bars. Here again the results of two bar diameters are separated for clarity. It is clear from the results that the embedment length to diameter ratio has little influence on the maximum average bond stress of the two bars. However, it is clear that the larger embedment lengths result in larger end slips at the maximum bond stress.

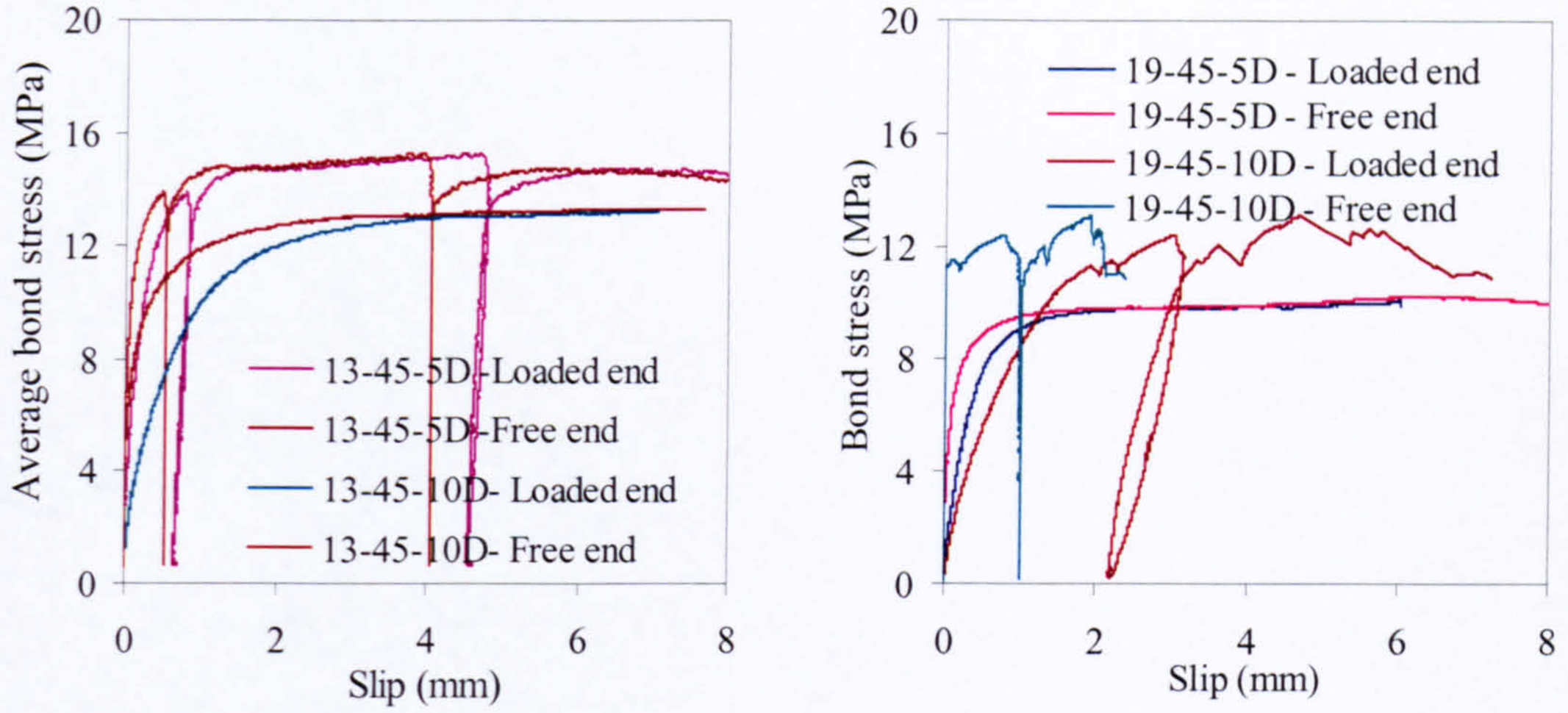

(a) 13 mm GFRP bar Grade 45 concrete (b) 19.1 mm GFRP bar Grade 45 concrete

Fig. 5-6 Influence of embedment length on the bond

5.3.3 Bar diameter

Fig. 5-7 compares the different pull-out responses at different bar diameter for the two grades of concrete. In this case results of two bar diameters (12.7mm & 19.1mm) in 250×250 mm concrete cross section are presented for the two concrete grades separately. As there are two reinforcement ratios involved, test results are not independent from the reinforcement ratio. From the tension stiffening studies it is clear that sections with different bar diameters but the same reinforcement ratio had similar overall tension stiffening responses. However this does not mean that bond characteristics of different bar diameters are the same. Due to the size of the specimen and different confinement and boundary conditions of the two tests, reinforcement ratio is presumed to have little influence on the bond properties of the pull out tests discussed here.

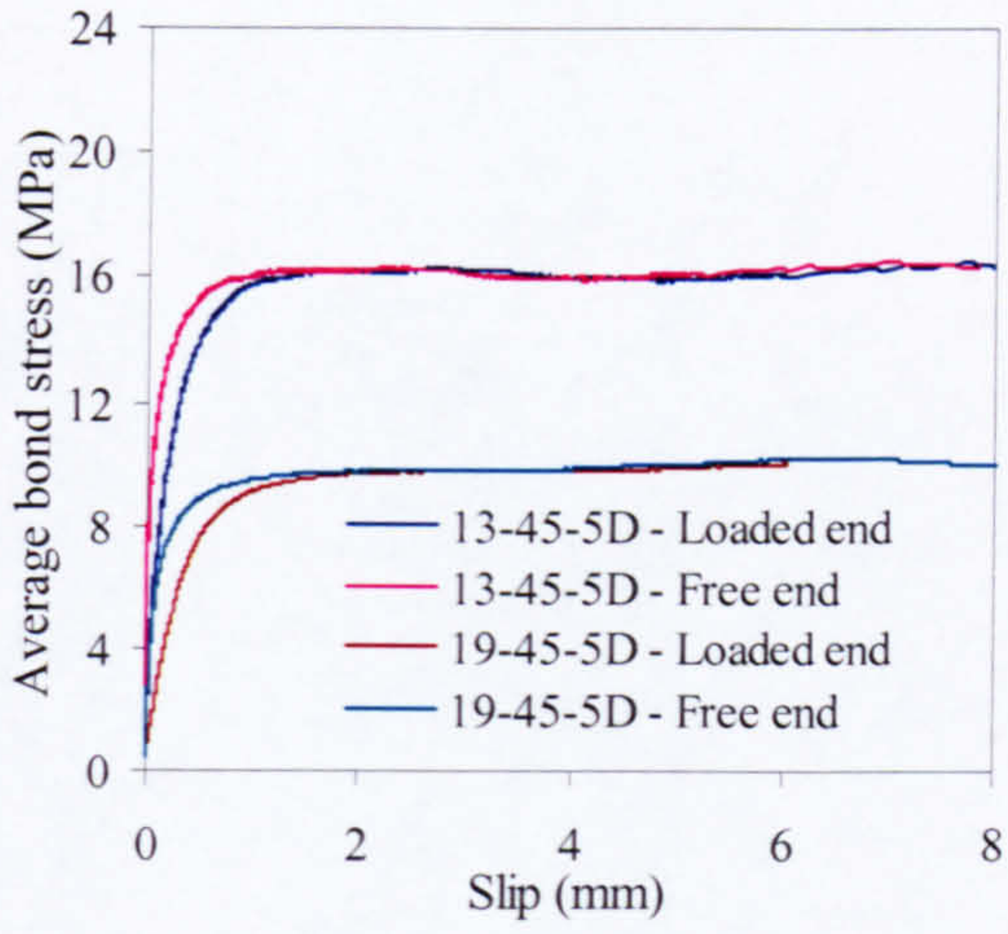

(a) G. 45 concrete 5D embedment length

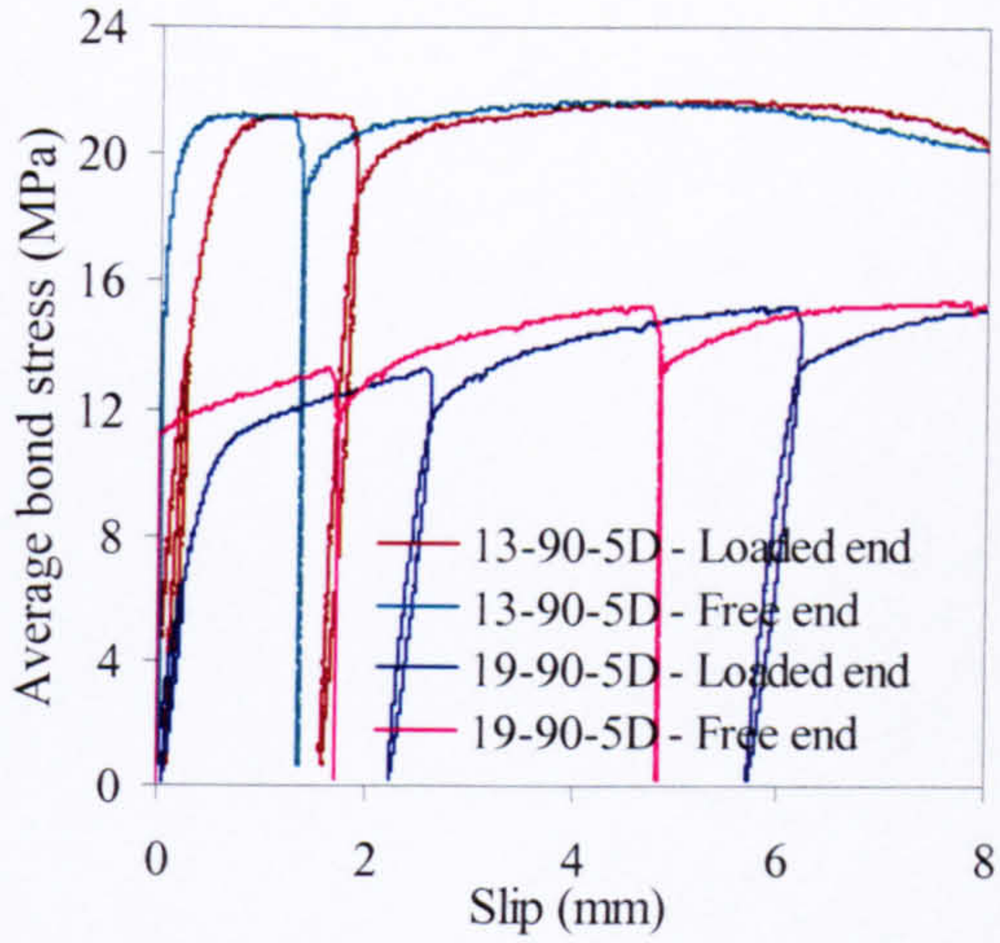

(b) G. 90 concrete 5D embedment length

Fig. 5-7 Influence of reinforcement ratio/bar diameter on the bond.

5.4 Bond development length

5.4.1 General

Bond development length is generally considered to be a linear function of bar stress, as typically shown in equation 5-3 (Somayaji and Shah 1981). Although there are many alternative formulations, the basic determination of the "bond constant", coefficient 'k', is done using the results of pull-out tests. It is also assumed that the development length varies linearly for the determination of bond development length at different load levels N_c. This assumption may be true for more or less elastic plastic bond-slip relationships as obtained for these experiments. However, this assumption is not valid for other bars with a softening bond-slip relationship after the peak value.

$$l_t = k\frac{P_c}{\sum} \qquad (5\text{-}3)$$

where

k = Coefficient determined by pullout test (mm^2/N)

$$P_c = A_c E_c \varepsilon_{cs} = \frac{P}{(1+n\rho)}$$

Σ = Circumference of the bar (mm)

P = Applied load (N)

n = Modular ratio

ρ = Reinforcement ratio

ε_{cs} = Composite strain

The ACI 440.1R-03 equation for the development length of FRP is shown below (equation 5-4). Since ACI uses a factor $\sqrt{f_c'}$ to account for the variation of bond strength with the concrete strength, this equation provides a more general equation compared to equation 5-3.

Equation 5-5 shows the basic development length calculated by equating the bond force over the surface of the rebar to the ultimate tensile strength of the rebar (f_{fu}).

$$l_t = k_p A_f f_{fu} / (f_c')^{0.5} \quad (5\text{-}4)$$

$$l_t = D f_{fu} / 4\bar{\tau} \quad (5\text{-}5)$$

where

A_f = Rebar area

l_t = Development length (mm)

f_{fu} =Ultimate tensile strength of bar (MPa)

$\bar{\tau}$ = Average bond strength from pull-out tests (MPa)

f_c' = Concrete cylinder compressive strength (MPa)

D = Bar diameter (mm)

By equating equations 5-4 and 5-5, the value for k_p can be found (equation 5-6).

$$k_p = (f_c')^{0.5} / \bar{\tau} \pi D \quad (5\text{-}6)$$

Values of k_p calculated for the GFRP bars used in this study are shown in table 5-3 along with the average maximum bond stress values used to calculate them. Bond values normally tend to have larger scatter than most other concrete properties like strength (Mirza and Houde, 1979). The derived values are similar to values recorded elsewhere and have a reasonable variability (Tighiourt et al. 1998).

Table 5-3 k_p values for the development length under different conditions

Specimen Group	Average maximum bond stress (N/mm^2)	k_p SI unit	Failure mode
13-45-5D	15.67	0.011	Pull
13-45-10D	13.50	0.012	Pull
13-90-5D	19.89	0.012	Pull
19-45-5D	10.02	0.011	Pull
19-45-10D	11.74	0.010	Pull
19-90-5D	16.62	0.010	Pull

5.4.2 Adjustments to the development length

The influence of concrete confinement around the bar can affect the bond strength and that needs to be taken into account for the determination of development lengths for the tension tests. Fig 5-8 shows the average bond stress slip relationship derived from the two tests, tension test and pullout test, for similar embedment lengths. The average bond stress slip values for the tension test are obtained from the notched tensile test specimen presented in chapter 4 and are calculated from the measured strain distribution between cracks. Slip in the tension test is the slip at the crack section, calculated by integrating the strain profile as explained in chapter 4.

Fig 5-8 shows that the average bond stress-slip response in pull-out test is higher than that of the tension test. Bond strength in the pull-out test is found to be around 50% higher than that recorded in the tension test. This means that the development length based on average bond stress values from the pull-out test needs to be modified to reflect the lower bond stress developed in the tension test. A multiplication factor of 1.5 is proposed for calculating the bond development length in direct tension when using results from the pull-out tests.

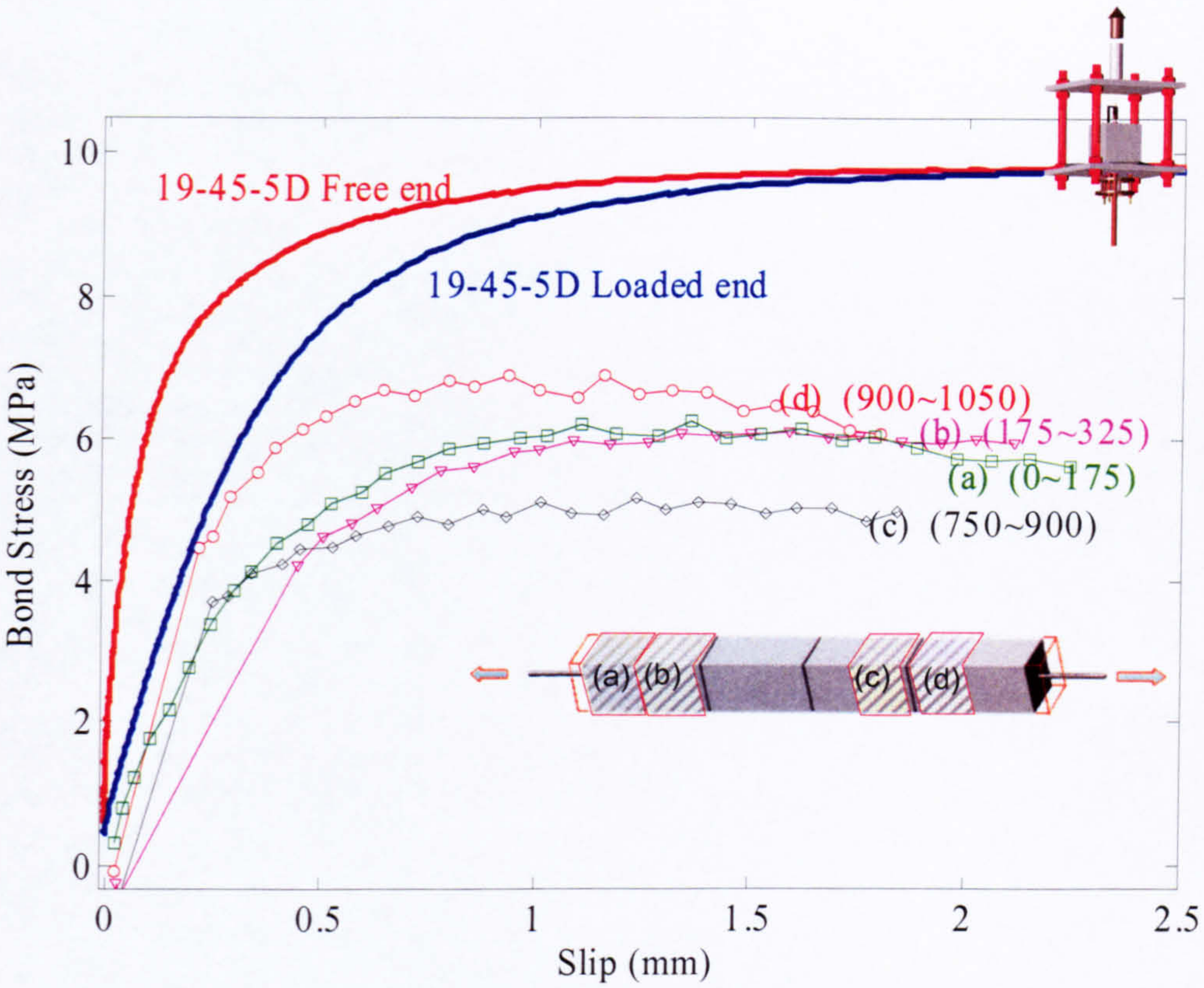

Fig. 5-8 Comparison of average bond stress slip values of the tension and pull-out test

The use of peak average bond stress at all load levels to arrive at the development length is far from accurate at low levels of applied loads, since the average bond stress is still in the ascending branch. This makes the development length at low load levels comparatively higher than the ones calculated assuming average bond strength. Experimental evidence of direct measurement of strain using internally strain gauged bars also provides evidence of this phenomenon, both for the tension and pull-out tests. However, the existing data are inadequate to enable the accurate determination of the development length for all loads. Therefore, a linear bond development length based on the bond strength is assumed in this calculation. The next section presents and evaluates the strain distribution function within the development length.

5.5 Estimation of strain distribution between cracks

There are different mathematical equations that can describe the bar strain within the embedment length. In this study a sinusoidal distribution function, as shown in equation 5-7, is used as an approximation. Fig. 5-9 shows the assumed strain distribution between cracks. This strain distribution can be used to determine the strain profile along the bar.

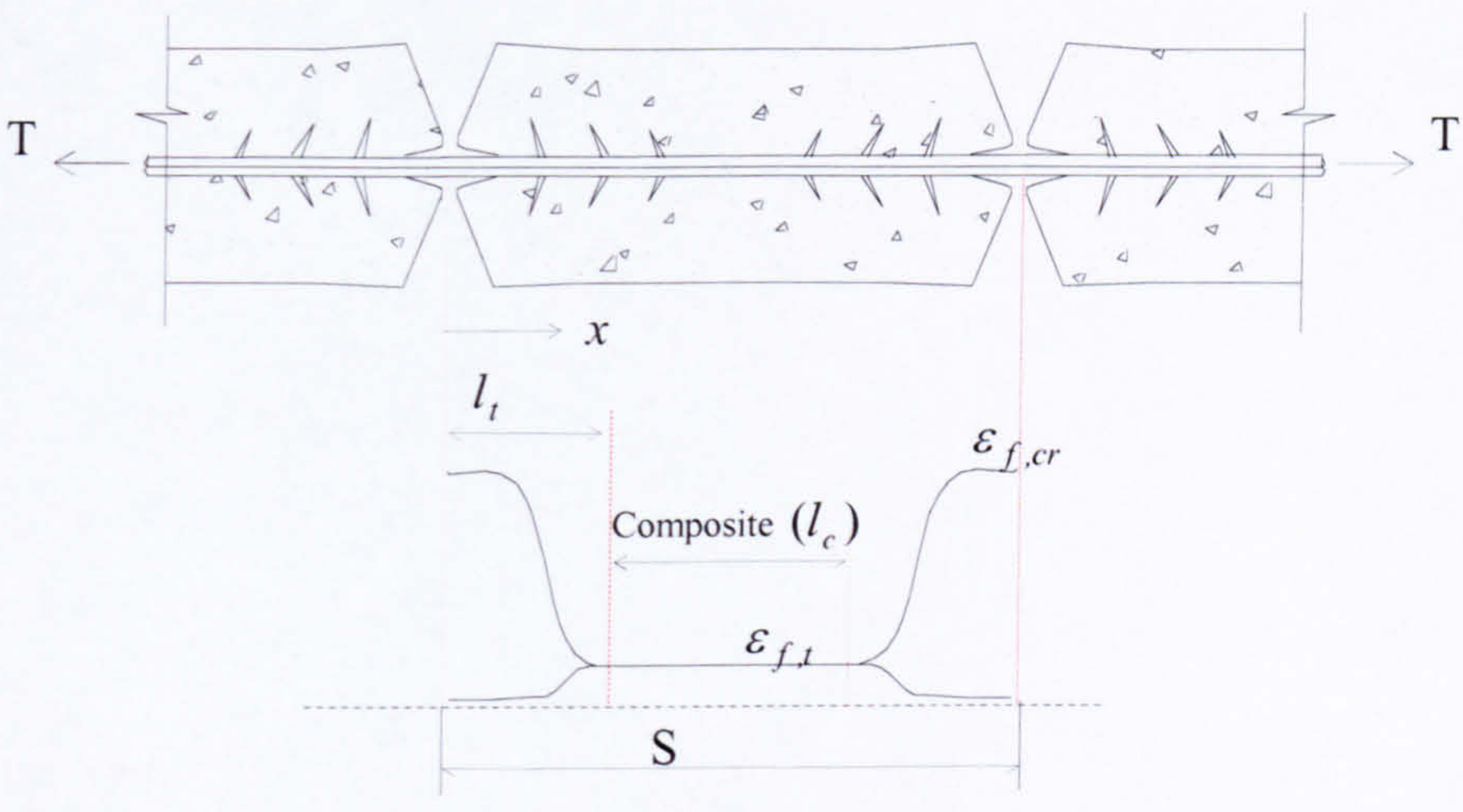

Fig. 5-9 Strain distribution between cracks

$$\varepsilon_f(x) = 0.5\left(\cos\left(\frac{\pi x}{l_t}\right)+1\right)\left(\varepsilon_{f,cr}-\varepsilon_{f,t}\right)+\varepsilon_{f,t} \qquad 0 \le x \le l_{bd} \qquad (5\text{-}7)$$

l_t = Bond development length (derived from equation 5-4)

$\varepsilon_{f,t}$ = Strain of the bar at the end of bond development length (Transfer length)

$\varepsilon_{f,cr}$ = Strain of the bar at crack section

Fig. 5-10 below compares the predicted strains along the bar versus experimental strain. Dots in Fig 5-10 indicate the strain gauge readings while the continuous lines show the predicted strains. The results show a reasonable agreement. However, it is clear that a better bond development length can certainly enhance the predictions, especially at low load levels where prediction with linear bond development length does not provide accurate estimates. The next chapter deals with modelling tension stiffening behaviour

based on the strain distribution function and the bond development length introduced in this chapter.

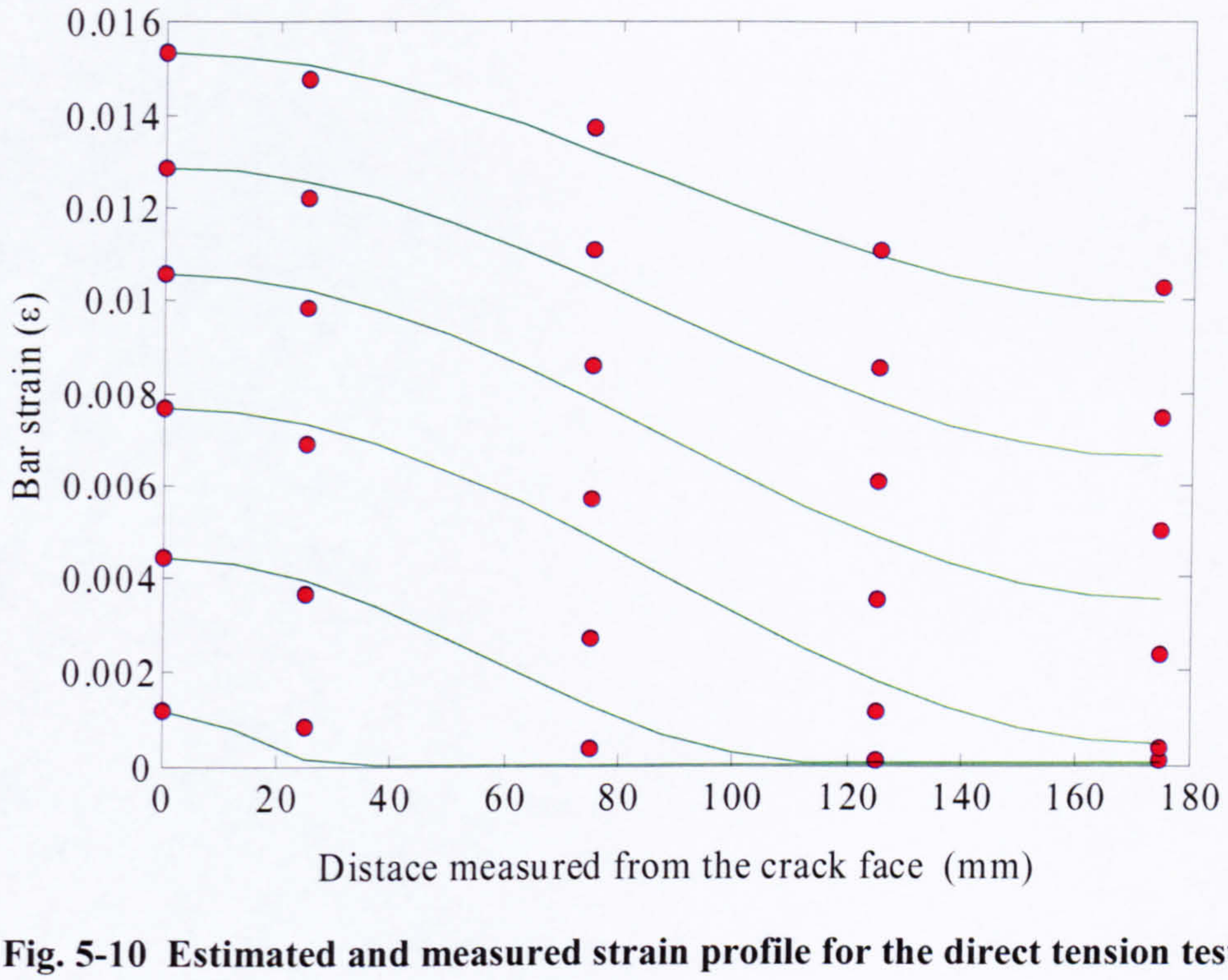

Fig. 5-10 Estimated and measured strain profile for the direct tension test

CHAPTER 6

MODELLING TENSION STIFFENING BEHAVIOUR

6.1 Introduction

In order to improve the deflection predictions for FRP RC structures, especially for low reinforcement ratios, a better understanding of the tension stiffening behaviour needs to be developed. This chapter attempts to model the tension stiffening behaviour by adopting a fundamental approach, based on the interaction of concrete and reinforcement.

There are two different basic approaches to define the tension stiffening effect of reinforced concrete in tension.

(1) Modified stiffness method: This approach is commonly used in formulating code equations for representing tension stiffening behaviour. Examples include: the reduction in effective cross sectional area adopted by ACI 224 (1997), and the continuous reduction of the difference between the composite strain and bar strain at first crack to define subsequent average strain of cracked concrete as adopted in CEB-FIP (1993).

(2) Bond stress slip approach: This is based on the strain compatibility and force equilibrium of RC with an assumed bond stress slip relationship to define the stress transfer from reinforcement to concrete. This method has more appeal to numerical approaches for representing the tension stiffening behaviour of concrete. As this is based on material constitutive relationships, it provides a better insight into how tension stiffening is built up starting from the interaction of the bar and concrete.

The first approach was examined earlier in chapter 3. Chapter 2 presented the fundamentals of the bond stress slip approach in finding a theoretical solution for modelling tension stiffening behaviour based on the solution to the characteristic equation for bond (equation 6-1). Chapter 2 also presented various approaches of finding a solution for the characteristic equation. Bond stress distribution functions, bond stress-slip relations and bar stress distribution functions have all been used with their relative advantages and disadvantages to solve the characteristic equation.

$$\frac{d^2 s(x)}{dx^2} = \frac{\Sigma f_b(x)}{A_f E_f}(1+n\rho) \quad n = \frac{E_f}{E_c} \quad \rho = \frac{A_f}{A_c} \tag{6-1}$$

As there is no significant research on FRP as internal reinforcement, all discussions in chapter 2 are based on conventional steel reinforcement. Chapter 4 highlighted the difficulty of finding a unique bond stress-slip relationship for GFRP reinforced concrete. It also highlighted that the GFRP bond stress distribution between cracks has no standard behaviour as assumed for steel reinforced concrete. The apparent loss of bond stress at the crack face and the migration of the peak bond stress away form the crack made it very difficult to introduce a bond stress distribution function to obtain a solution to its characteristic equation. Instead, it is shown in chapter 4 that "strain distribution" provides a realistic opportunity to model the tension stiffening behaviour of GFRP RC.

The model discussed in this chapter uses the strain distribution between cracks to represent the bond between cracks. For this end, the model uses a sinusoidal strain distribution function coupled with a damage mechanism for bond deterioration at the crack face to represent the strain distribution of the bar between cracks. The model uses the development length derived in Chapter 5 to determine the length over which the bond stress mechanism is active between cracks. After an initial description of the model, this chapter presents a comparison and discussion of all the experimental results with the predictions of the analytical model.

6.2 Proposed analytical approach based on an approximated strain distribution function

6.2.1 Strain Distribution function (SDF)

Having discussed the implications of modelling the tension stiffening effect, a method based on strain distribution along the bar is introduced here. In this method, the strain distribution function (SDF) is assumed to represent the strain along the bar between cracks in the bond development length. The bond development length (l_t) is defined as the length over which stress from the reinforcement is transferred to the concrete. By using the SDF together with equilibrium of forces, the contribution of concrete at each section can be determined. In general, it is assumed that the strain distribution between cracked sections consists of two components: the bond development length, which is characterised by the relative movement between concrete and reinforcement, and a composite length. However, in the proposed model, in addition to bond development length, l_t , and composite length , l_c , a damaged length (l_{di}) is introduced to account for bond deterioration at the crack section, which is evident in the experimental investigation. Accordingly, the length between cracks is generally divided into three segments. Fig. 6-1 shows the strain distribution assumed at different lengths between cracks. The strain distribution in the bar for the each of the three segments is represented by equations 6-2(a) to 6-2(c).

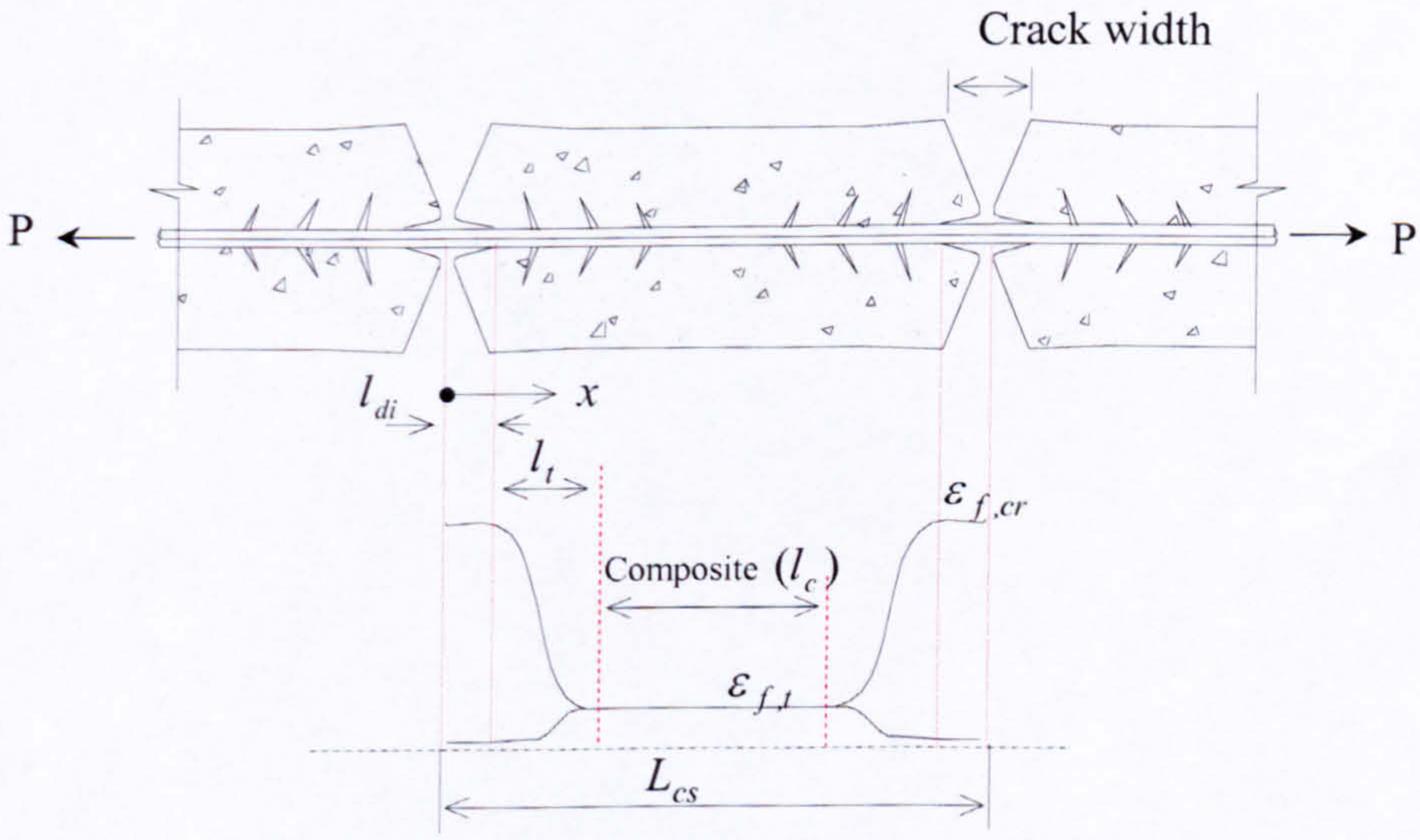

Fig. 6-1 Approximated strain distribution for different length between cracks

$$\varepsilon_f(x) = \frac{P}{A_f E_{f,cr}} \qquad 0 \le x \le l_{di} \qquad \text{(6-2a)}$$

$$\varepsilon_f(x) = 0.5\left(\cos\left(\frac{\pi(x - l_{di})}{l_t}\right) + 1\right)\left(\varepsilon_{f,cr} - \varepsilon_{f,t}\right) + \varepsilon_{f,t} \qquad l_{di} \le x \le l_{di} + l_t \qquad \text{(6-2b)}$$

$$\varepsilon_f(x) = \left(\frac{P}{A_f E_f + A_c E_c}\right) \qquad l_{di} + l_t \le x \le L_{cs}/2 \qquad \text{(6-2c)}$$

Considering equilibrium, stress and strain of the bar at the section of the crack and in the damage length $(0 \le x \le l_{di})$ can be found as $\sigma_f = P/A_f$ and $\varepsilon_f = P/A_f E_f$, respectively. For simplicity, the concrete is assumed to carry no stresses in the longitudinal direction along the damage length (l_{di}). Therefore, the strain and force carried by the concrete in this segment is equal to zero.

In the composite section ($l_{di} + l_t \le x \le L_{cs}/2$), if it exists at the load level considered, strain compatibility between concrete and bar is assumed. In this segment concrete and rebar support the applied force P in proportion to their stiffness. Therefore, strain in concrete and steel is equal to $\varepsilon_c = P/(A_f E_f + A_c E_c)$. From this strain the amount of load shared by the concrete at the composite section can be found as $P_c = P/(1 + \eta\rho)$, where n and ρ are the modular ratio and reinforcement ratio, respectively.

Although strain compatibility does not exist along the bond development length, the concrete contribution at any section in the bond development length can be found through force equilibrium. Force at any section should be equal to the force of the reinforcement at the crack section. As SDF dictates the force contribution of the bar at any section along the bond development length, the concrete contribution can be calculated by applying the force equilibrium between the crack section and the section in consideration. All of the above equations are based on the linear elastic behaviour of materials and uniform distribution of stresses across the section.

6.2.2 Length parameters: development length (l_t), damage lengths (l_{di}), composite length (l_c)

If the lengths l_t, l_{di} and l_c can be established, then the average concrete contribution (tension stiffening) of the control volume can also be determined. By introducing a criterion for concrete cracking, these calculations can be further extended to model the experimental results of direct tension tests of any length and, therefore, to model the tension stiffening effect of concrete in general.

Determination of bond development length l_t

The bond development length, l_t, can be found from equation 5-4 (ACI 2003) as discussed in chapter 5 ($l_t = k_p A_f f_{fu} / (f_c')^{0.5}$). Development length ($l_t$) proposed here is the length required to anchor a bar when the bar is stretched to its ultimate strength (f_{fu}). As there is not enough research on bond development length for a given stress level in the bar, it is assumed that the bond development length is linearly proportionate to the stresses in the bar (f_{fi}). With this assumption a generic solution for bond development for a given stress in the bar is now possible (see equation 6-3). In this relation, k_p is the only bond related parameter and can be determined by using the results of the pull-out tests using an assumed average bond stress as explained in chapter 5, equation 5-6.

$$l_t = k_p A_f f_{fi} / (f_c')^{0.5} \qquad (6\text{-}3)$$

Determination of damage length l_{di}

As long as strain compatibility is assumed between concrete and reinforcement, the total energy applied to the system can be determined from the internal energy stored. However, in reality strain compatibility between concrete and reinforcement exists only in the composite length. In the bond development length the force in the bar is gradually transferred to the concrete through bond stresses. This incompatibility of strain between concrete and reinforcement causes a certain amount of energy to be lost from the system known as energy loss due to slipping. From the experimental strain distribution in the bar between cracks, it is clear that a certain length close to the section of the crack is de-bonded (see Fig 4-8). These de-bonding actions also cause loss of energy from the

system. In this study, in modelling the tension stiffening effect, the loss of energy from the system is considered to be the result of de-bonding slipping and cracking of concrete. Slipping energy can be determined from the strain distribution on the bar. Equations to find the bond stress (τ) and bond slip (s) based on the proposed SDF are shown below, equation 6-4 and 6-5, along with typical results showing the bond stress and slip calculated from a strain profile, Fig. 6-2. In the calculation of slip, strain in the concrete is ignored for simplicity as the strain in the concrete is negligibly small compared to the strain in the bar (see also equation 4-2). The example shown is based on a de-bonded length of 25mm and a composite length of 80mm occurring between a 500mm cracked block. The figure only shows strain, stress and slip profiles of half the length between two adjacent cracks.

$$\tau(x) = \frac{E_f d_f}{4} \frac{d\varepsilon_f(x)}{dx} \tag{6-4}$$

$$s(x) = \int_0^x \varepsilon_f(x)dx \tag{6-5}$$

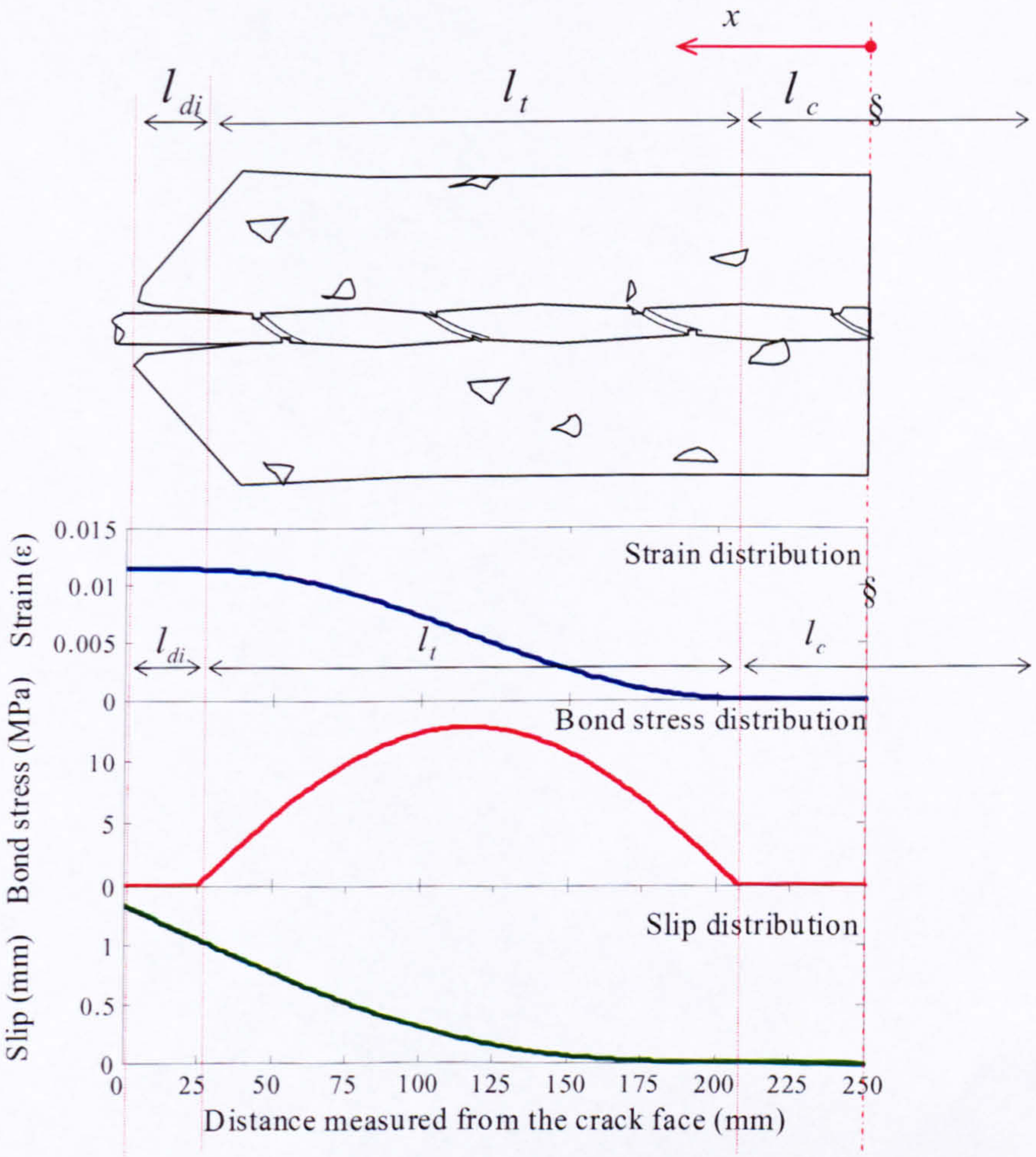

Fig. 6-2 Bond stress slip for the given strain profile

The de-bonded length for a given loading and cracking condition is the only unknown and can be found iteratively from the energy balance of the control volume during incremental changes in load, equation 6-6. Contributing parameters in equation 6-6 for the considered control volume are given in equations 6-7 to 6-11. With all other quantities known, by a proper estimate of the value for the de–bonded energy per unit area of interface between reinforcement and concrete, γ, it is possible to find the incremental increase in the de-bonded length iteratively by applying the energy conservation principles between successive loading steps. In absence of experimental data, the value of the coefficient for de-bonding, γ, which is essentially the energy required for creating a de-bonded surface around the reinforcement, is assumed to be the same as the energy spent on cracking a unit length of plain concrete(0.1 N/mm - 0.15N/mm (Maekawa et al. 2002)). Ouyang and Shah (1994) proposed the value of γ be determined by the analytical model itself, such that the experimental results of the tension test agree with the analytical results. In the calculation for the de-bonded length for a given load step, de-bonded length is varied. For each varied de-bonded length new strain profiles are established using equation 6-2 (a) to (c) and for each de-bonded length incremental energy from the previous loading step is calculated to check whether it satisfy the equation 6-6. The value that satisfy the equation 6-6 then becomes the new de-bonded length and the corresponding strain profiles that are calculated from equation 6-2(a) to (c) now becomes the strain distribution for the current loading step. With strain distribution now fully established, the concrete contribution in tension can now be established for the given loading level.

$$\Delta E_{external} - \Delta E_{debonding} - \Delta E_{slipping} = \Delta E_{bar} + \Delta E_{concrete} \tag{6-6}$$

Where, $$\Delta E_{external} = \frac{1}{2} \times T \times \Delta U_{system} \tag{6-7}$$

$$\Delta E_{slipping} = \int_{l_{di}}^{l_t} (\tau(x)_n s(x)_n - \tau(x)_{n-1} s(x)_{n-1}) dx \tag{6-8}$$

$$\Delta E_{debonding} = \gamma \times ((l_{di})_n - (l_{di})_{n-1}) \pi d \tag{6-9}$$

$$\Delta E_{bar} = \frac{1}{2} \times \int_0^v E_f ((\varepsilon_f(x)_n)^2 - (\varepsilon_f(x)_{n-1})^2) dv \tag{6-10}$$

$$\Delta E_{concrete} = \frac{1}{2} \times \int_0^v E_c ((\varepsilon_c(x)_n)^2 - (\varepsilon_c(x)_{n-1})^2) dv \tag{6-11}$$

In the above equation, the applied tensile force at the crack section is denoted by T and the overall change of displacement, calculated by integrating the strain profile of the bar between cracks, is denoted by ΔU_{system}. The subscript 'n' is used to refer to quantities in the current loading step whilst '$n-1$' is used to refer to the quantities in the previous loading step. Subscript 'c' is used to represent strains of concrete whilst subscript '*f*' is used for fibre reinforcement.

6.2.3 Criterion for Cracking

The spacing between cracks (i.e. the length of the control volume) at the given load is determined by the criterion for cracking which is often the tensile strength of concrete. Estimation of the tensile strength is therefore one of the crucial elements of modelling tension stiffening effect. In the model, the tensile strength of concrete in direct tension f_t' is assumed to be $0.33\sqrt{f_c'}$ (Vecchio and Collins 1986). It is known that the tensile strength of concrete increases with the decrease in length between cracks or, in other words, a decrease in length segment to cross sectional area. Equation 6-12 is used in this analysis to estimate this variable tensile strength f_{td}' which is commonly known as dynamic tensile strength of concrete. In the equation 6-12 change in the maximum concrete stress, $\sigma_{c,max}$, and average concrete stress, $\sigma_{c,ave}$, of the segment between cracks is used to model increasing tensile resistance to cracking with the decrease in crack spacing. This equation has also been used for similar estimation of increasing tensile strength (Chan et al. (1993), Hyo-Gyoung et al. 2002).

$$f_{td}' = \alpha f_t' \left(\frac{\sigma_{ct,max}}{\sigma_{ct,ave}} \right)^{\beta} \quad \alpha = 0.80 \quad \beta = 0.60 \tag{6-12}$$

Where $f_t' = 0.33\sqrt{f_c'}$, and α, β are dimension less experimental constants.

6.3 Implementation

The implementation of the model reflects the fact that tension stiffening has three distinct stages of response:

a) Pre crack stage: This is characterised by the composite action between the reinforcement and concrete for a major part of its length resulting in high stiffness compared to the bare bar response;

b) Cracking stage (Stage II): This stage is characterised by a relatively flat stiffness response, with even less incremental stiffness than that of the bare bar due to the large increases in strain in the bar during cracking;

c) Post cracking stage: This is characterised by an almost steady response that lies above the bare bar response (see Fig 3-13). In the analytical model these features are accounted by having three subroutines.

In the analysis, for each load increase, computation starts with the calculation of the bond development length (l_t). If two times the calculated l_t is greater than the current crack spacing, S, the composite strain of concrete is calculated and a check takes place to determine if a new crack can take place. If the cracking criterion is met, the response will be dealt by a subroutine for "Cracking", else it is dealt by a subroutine "Intermediate cracking". If the summation of two times the bond development length (l_t) and damage length is found to be less than the crack spacing, then the response is dealt by the subroutine "Post cracking response". This procedure goes on until the bar stress reaches its maximum strength ($P \geq P_u$). The complete algorithm used is shown in Fig 6-3.

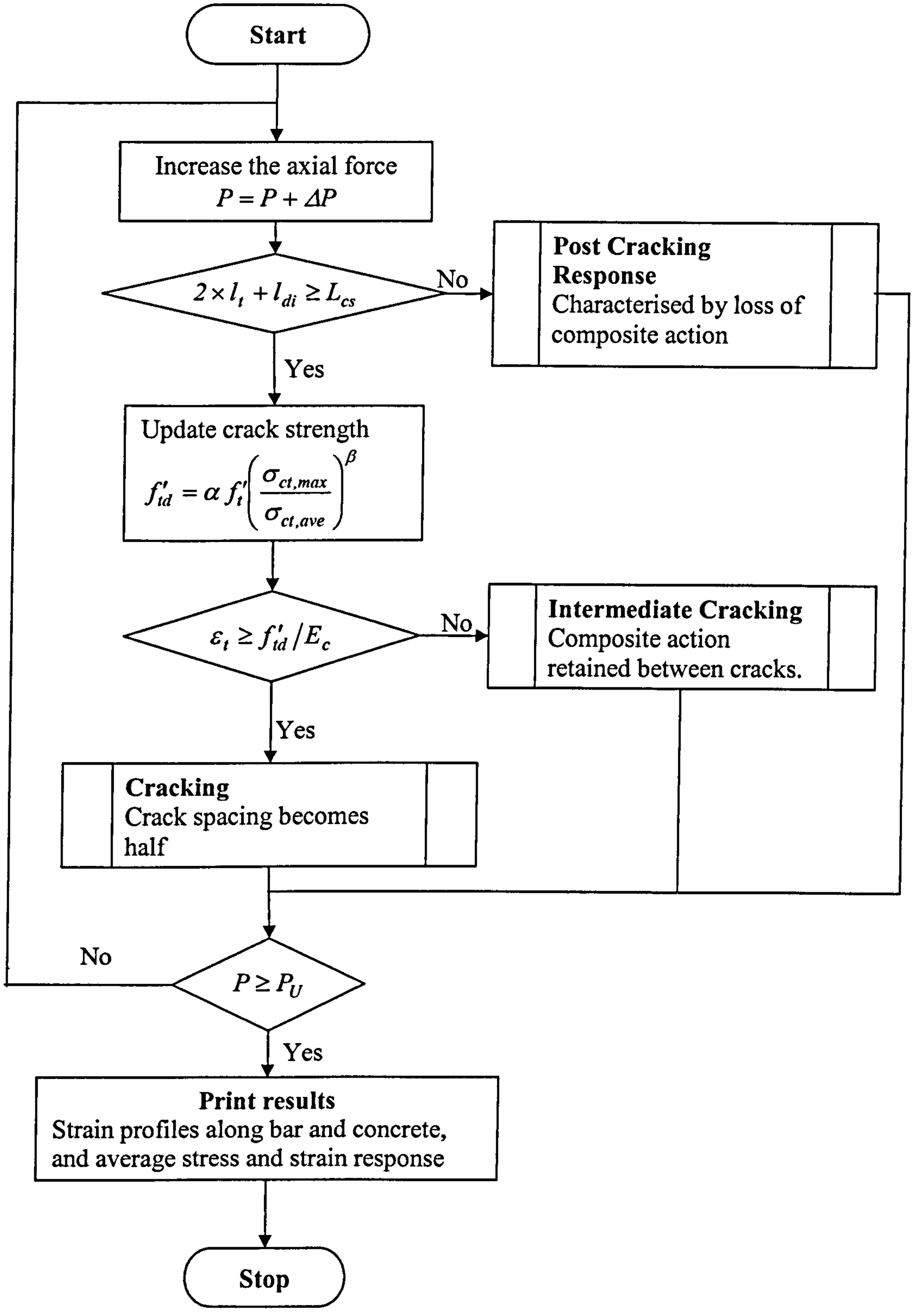

Fig. 6- 3 Algorithm used in the numerical computation of tension stiffening effect

In the subroutine "Intermediate cracking", it is assumed that the composite action between reinforcement and concrete is maintained at the middle between cracks.

In the subroutine "Cracking", since the crack spacing has halved, there is a need to check if there is still composite response. This depends on the new crack spacing and the bond development length (l_t) corresponding to that loading. With the exception of the "Cracking" subroutine, in the other two subroutines, the equation of conservation of energy is applied between the current and previous loading step. In the case of the "Cracking" subroutine the principle of conservation of energy is applied before and after the cracking for the same loading.

In the post cracking response, when composite action is lost, the bar strain at the middle of the cracked block (L_{cs} / 2) is calculated by using the bond development length, l_t, as shown in Fig 6-4. The strain distribution function remains the same sinusoidal function, but uses $\varepsilon_{f,m}$ for its minimum value. The full computer programme in MATLAB is given in Appendix 3.

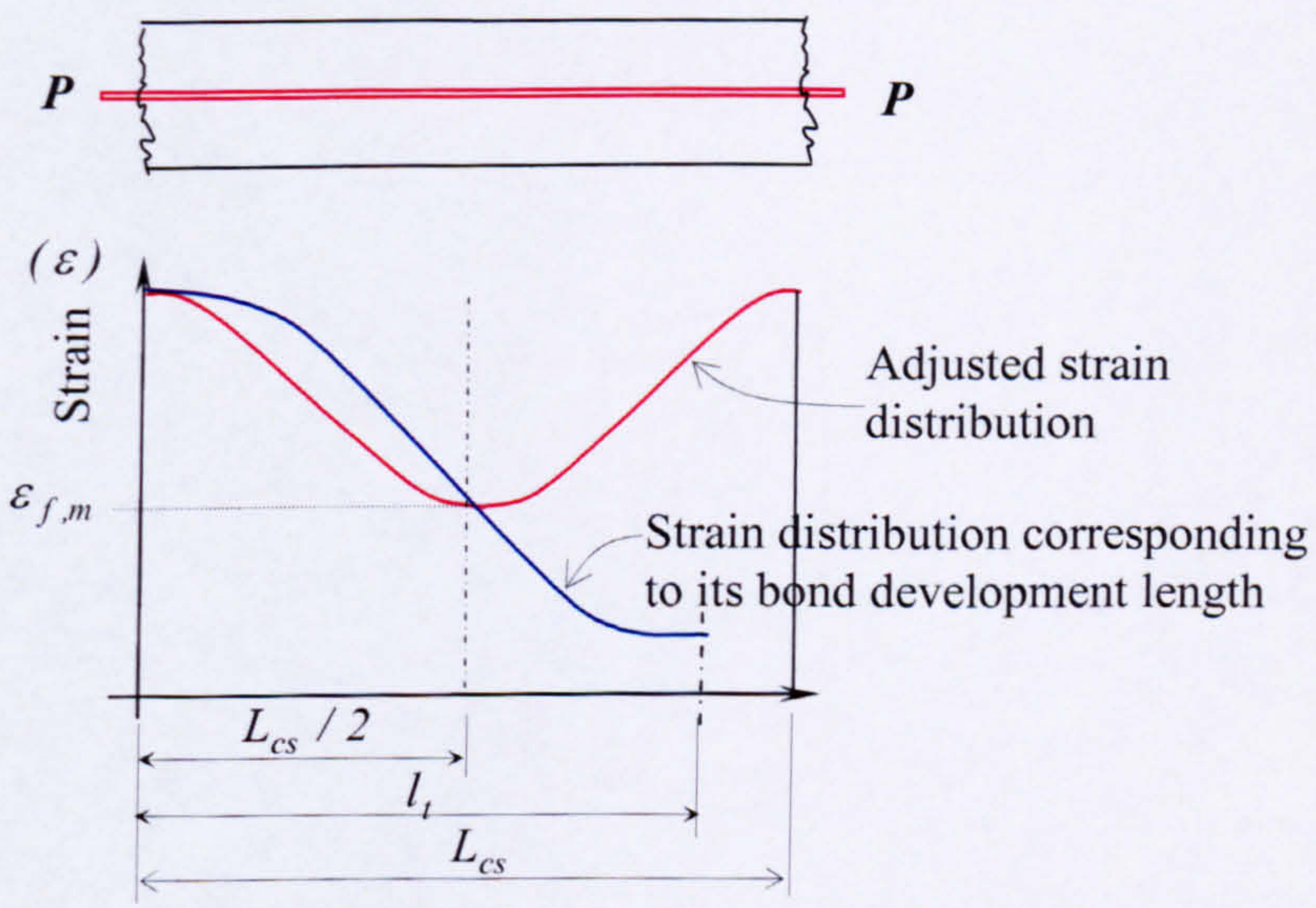

Fig. 6-4 Strain distribution in the post cracking stage

6.4 Comparison of results

In the experimental study four different reinforcement ratios, comprising two bar diameters and two concrete grades were studied. In Figs. 6-5 and 6-6 the experimental results are compared with the numerical predictions. Fig. 6-5 shows the results of the 19.1 mm diameter bar compared with analytical results, whilst Fig. 6-6 shows results of the 12.7 mm bar covering all test specimen (see also table 3.2).

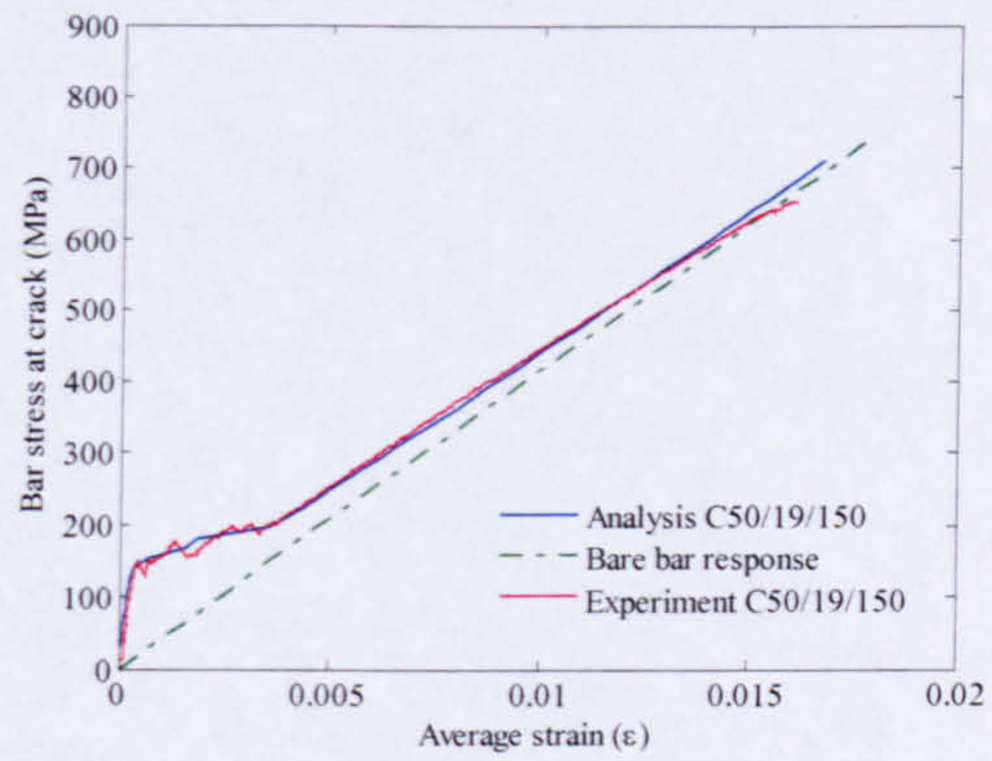

C50/19/150

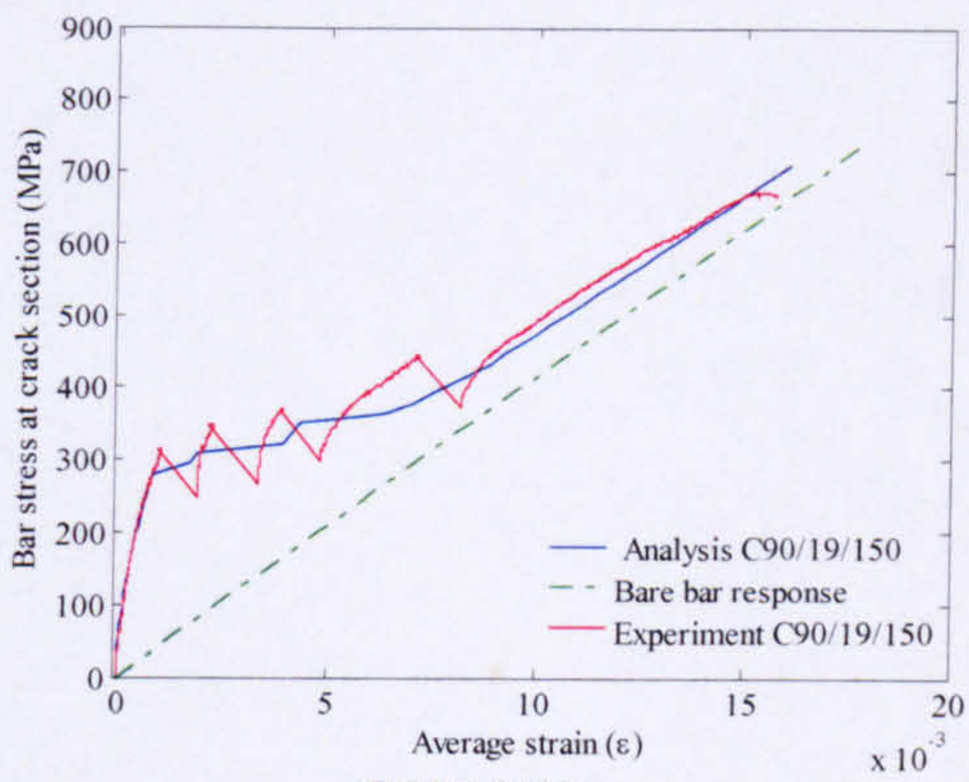

C90/19/150

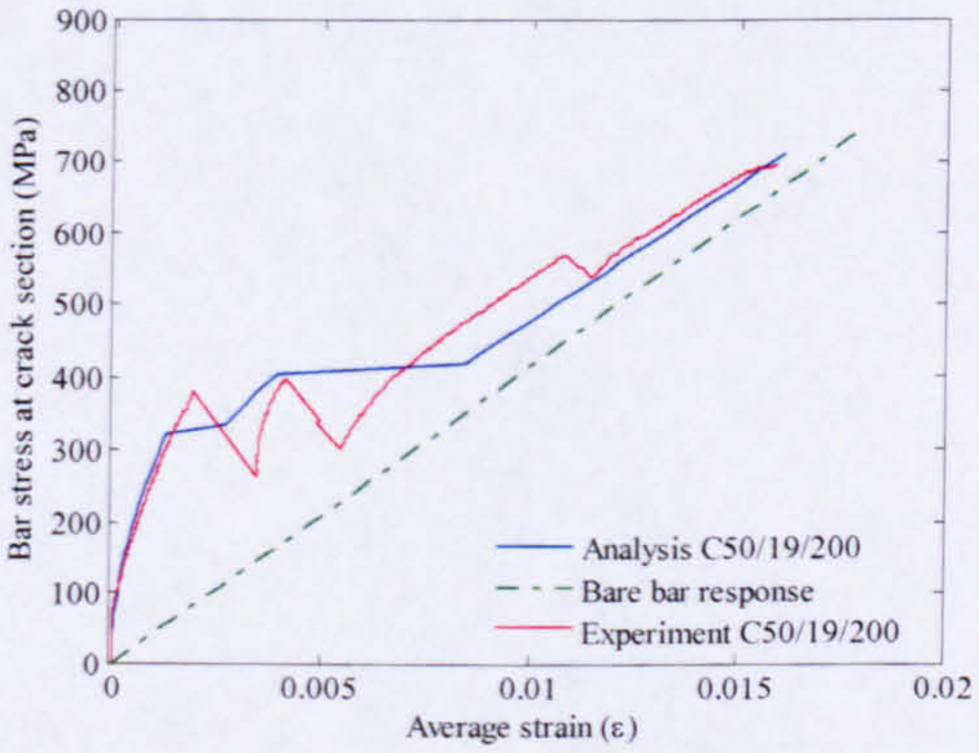

C50/19/200

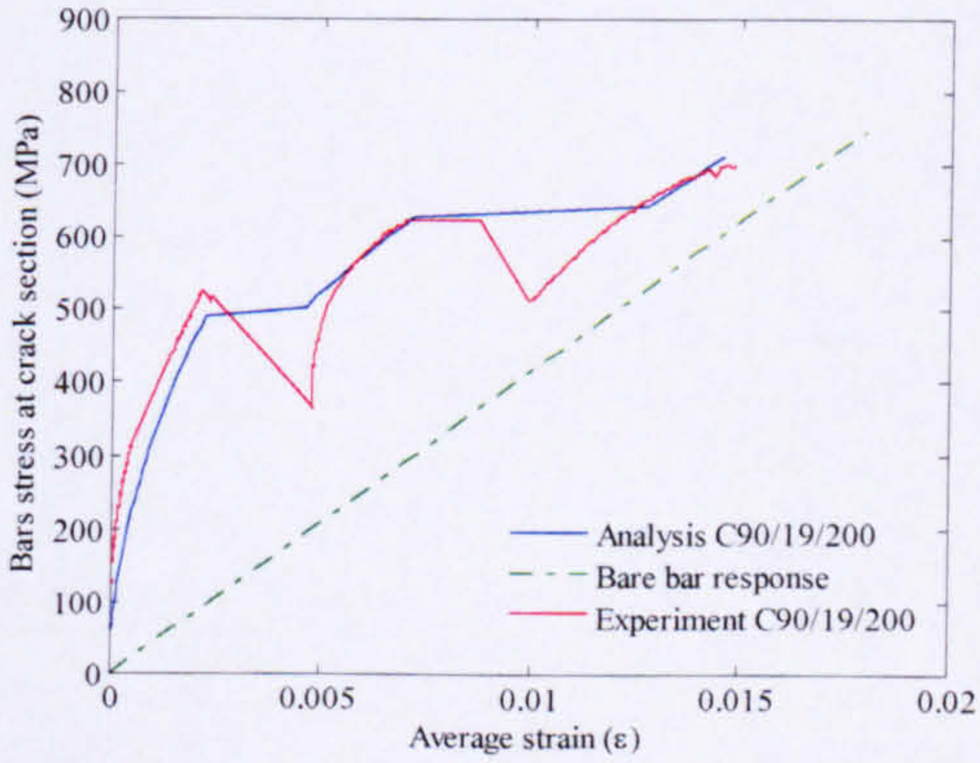

C90/19/200

Fig. 6-5 Experimental results of the 19.1 mm diameter bar compared with the results of the analytical model

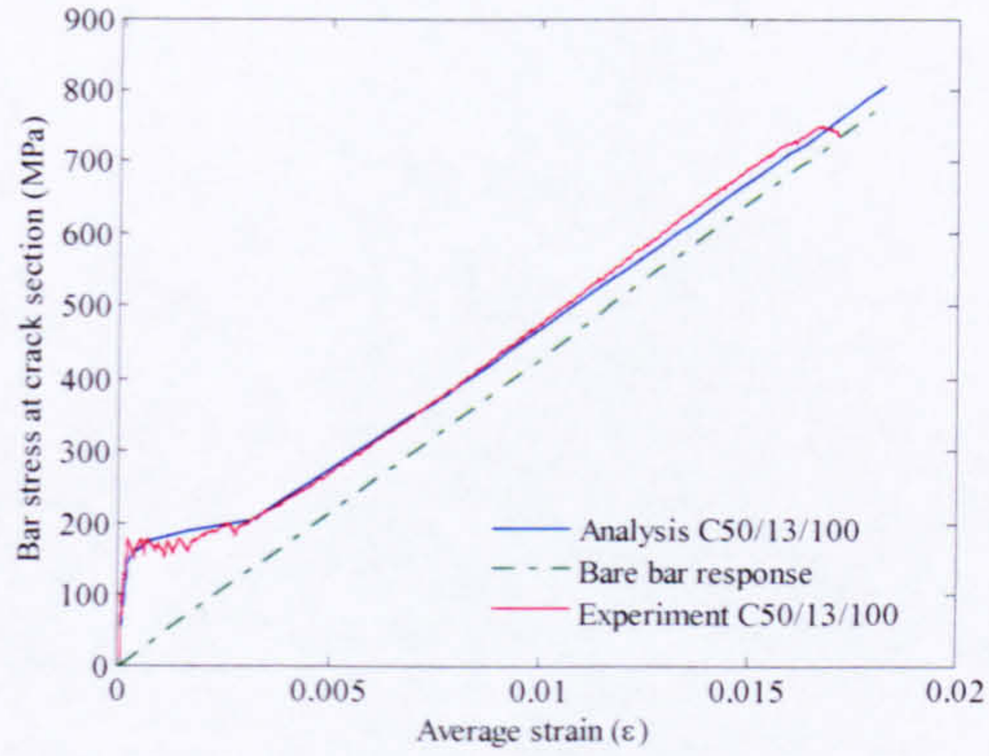

C50/13/100

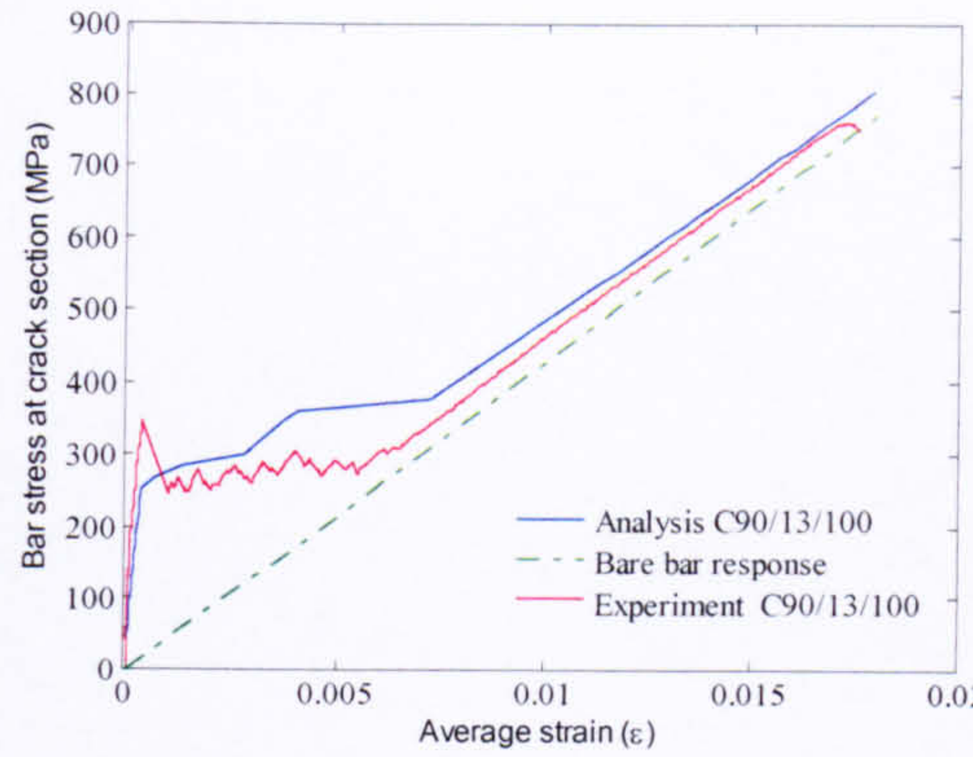

C90/13/100

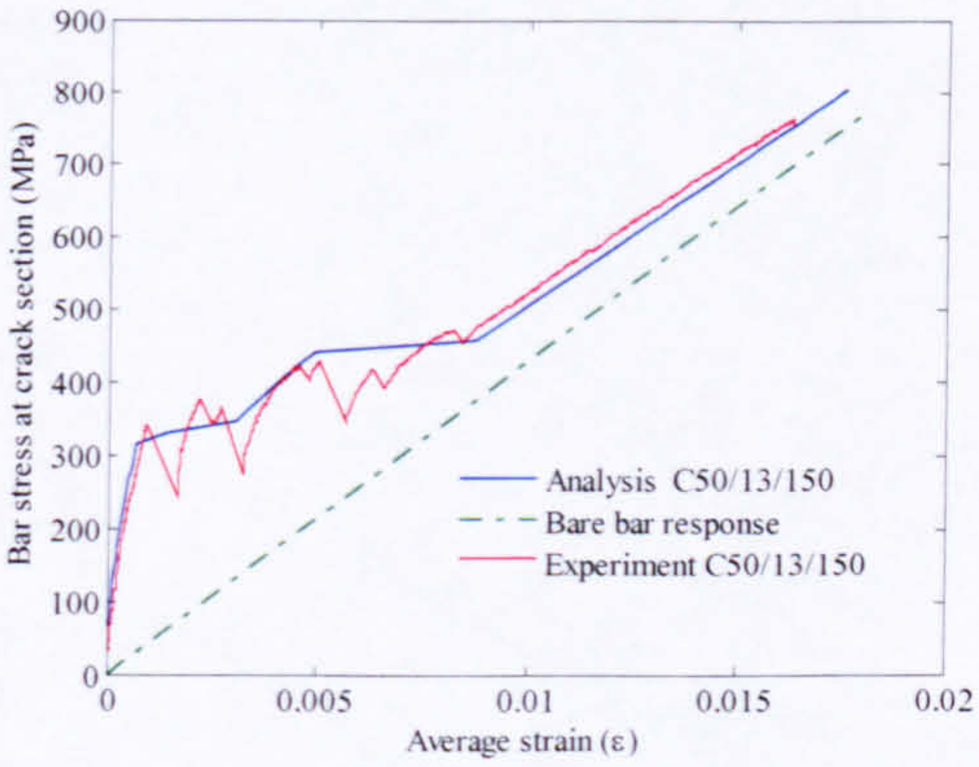

C50/13/150

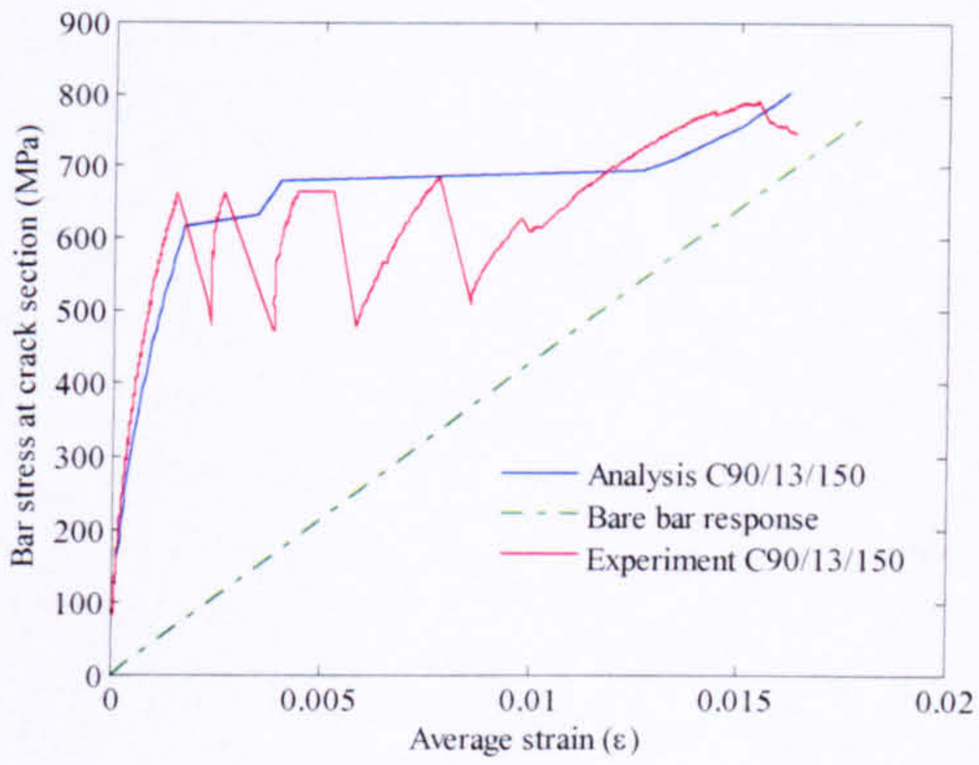

C90/13/150

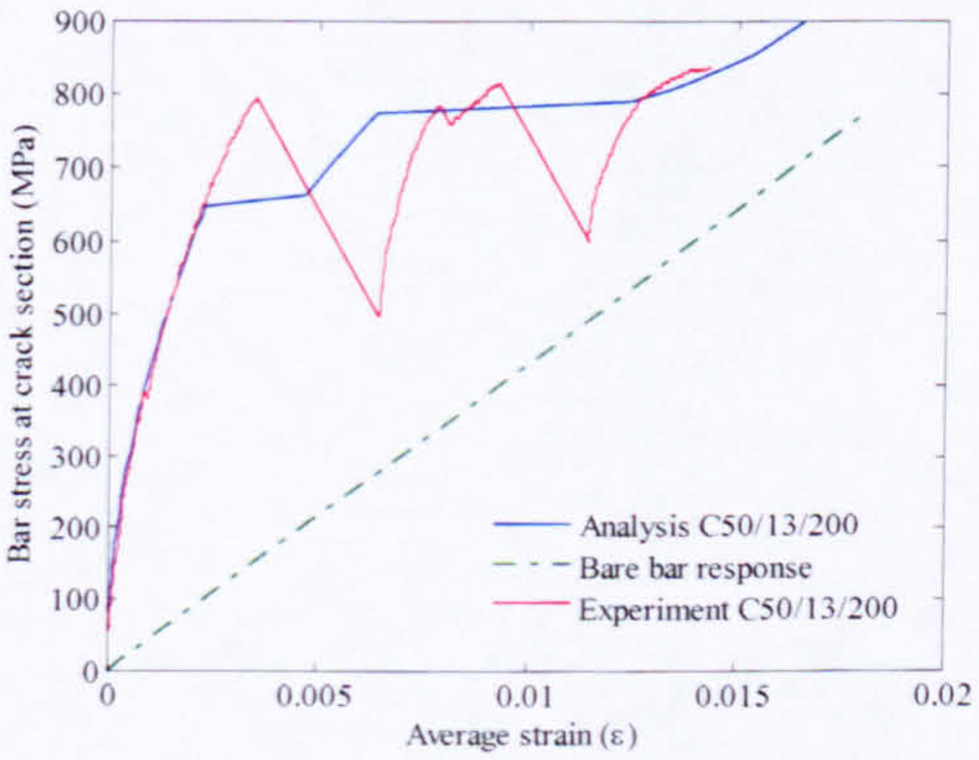

C50/13/200

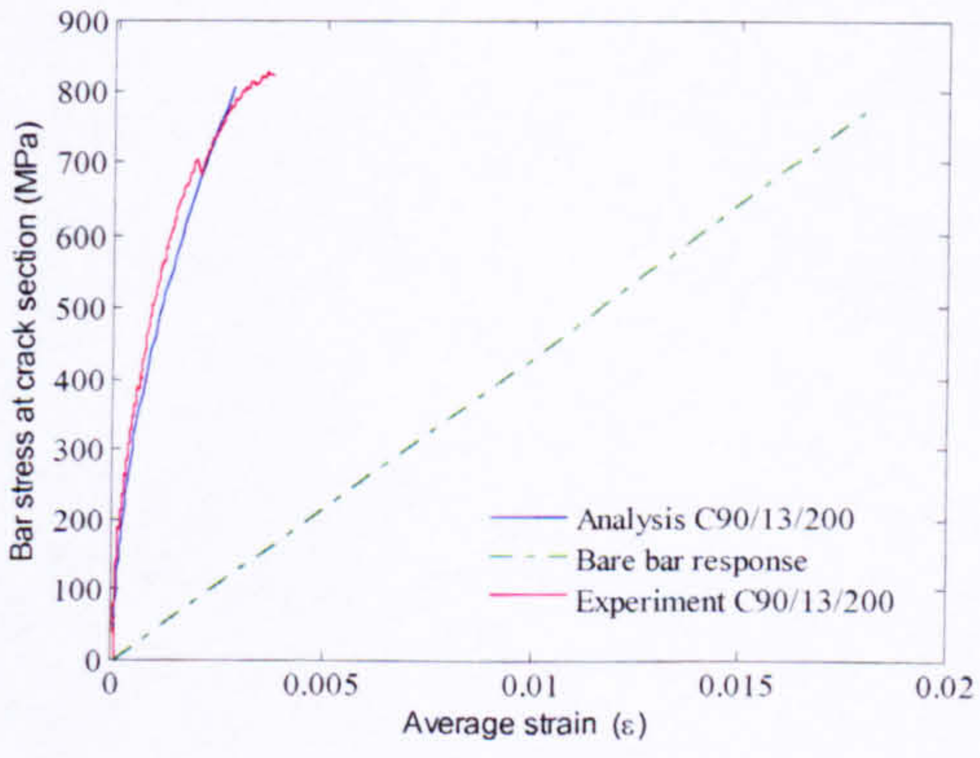

C90/13/200

Fig. 6-6 Experimental results of the 12.7 mm diameter bar compared with the results of the analytical model

Fig 6-7 shows the strain distribution in the bar during the analysis of C50/13/150. As the concrete strain is relatively low, the concrete contribution between cracks is not visible from this strain distribution diagram. Fig. 6-8 shows the force contribution of concrete and reinforcing bar along the specimen based on the analytical results of C50/13/200 at various stages of cracking. The first two figures (Figs. 6-8(a) & (b)) illustrate the change in force contribution before and after first cracking. In the latter stages of cracking the

degradation of the concrete contribution is evident as cracks mature and the distances between cracks are not sufficient for the bond development length (see Figs. 6-8(c) & (d)). After crack maturity, the model is showing the loss of composite action, as shown in Fig 6-8(d).

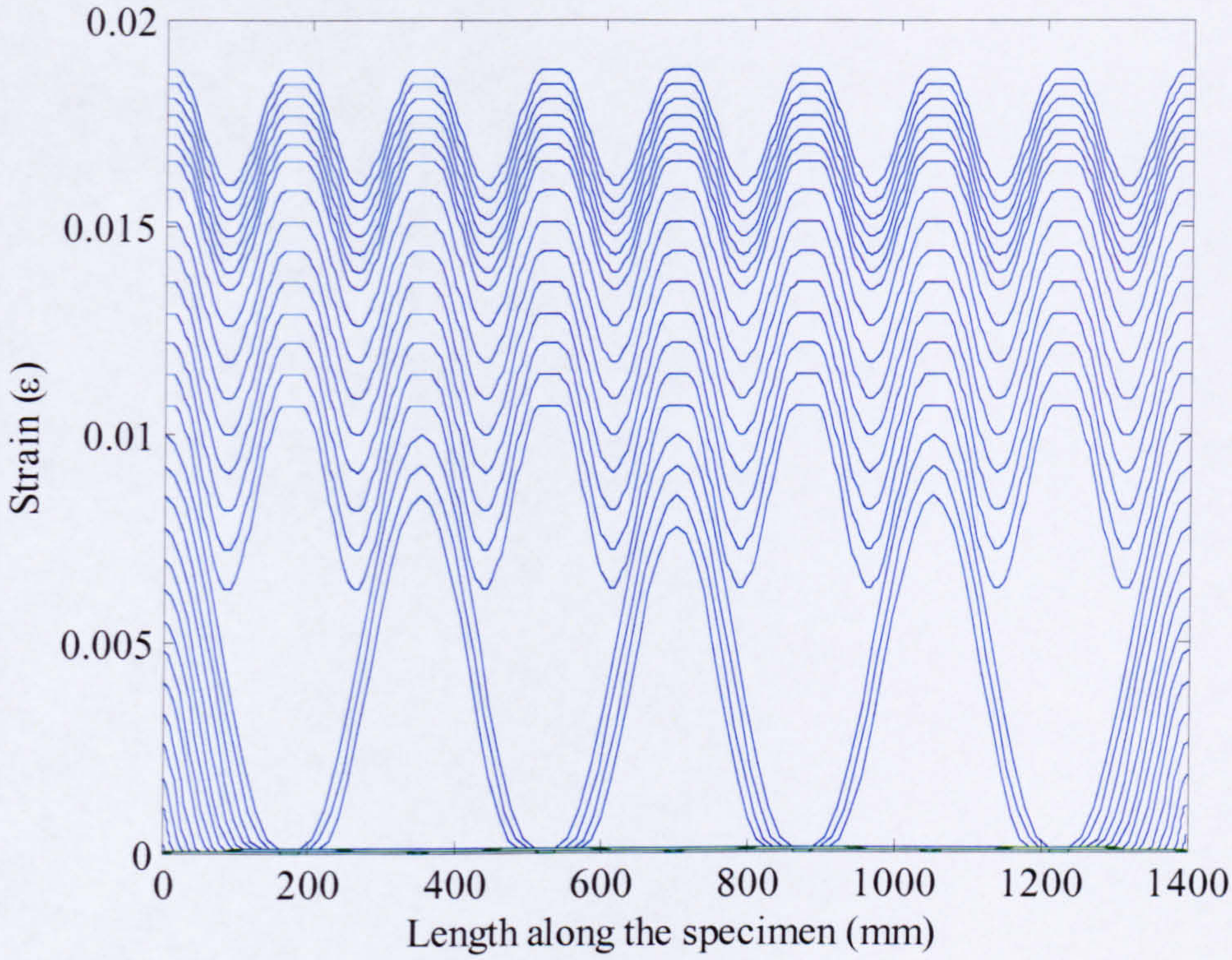

Fig. 6-7 Calculated strain distribution for the specimen C50/13/150

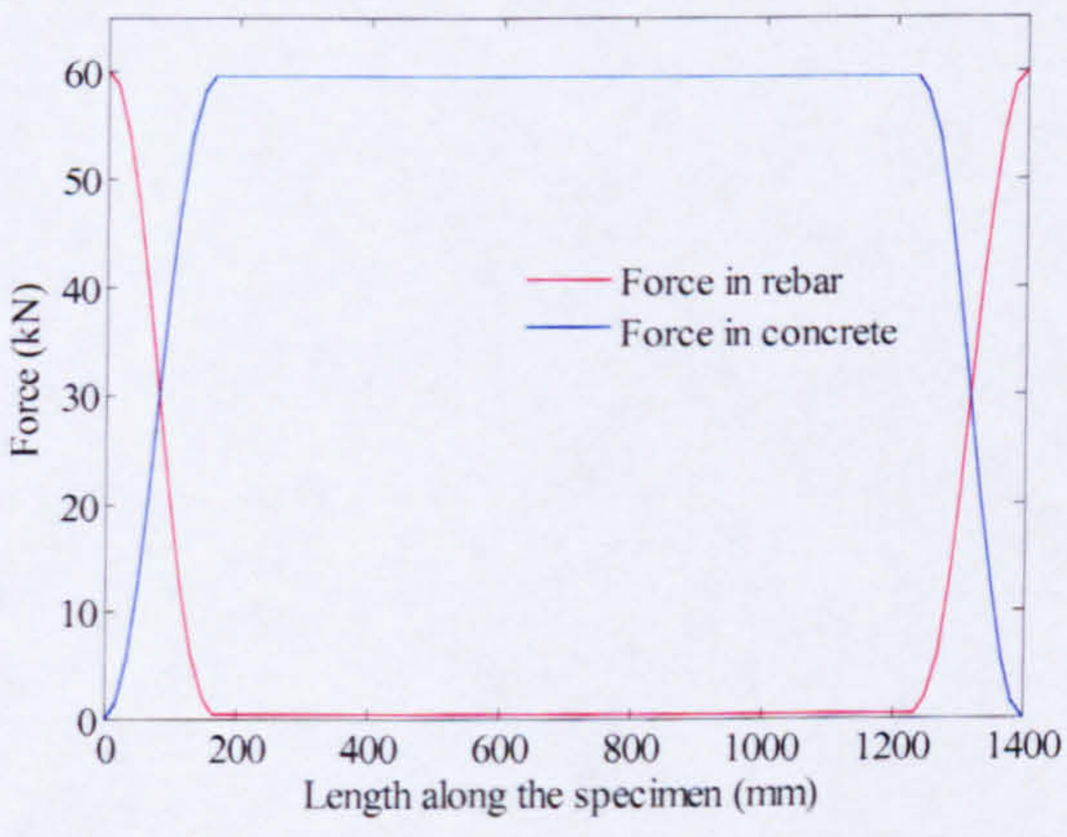

(a)

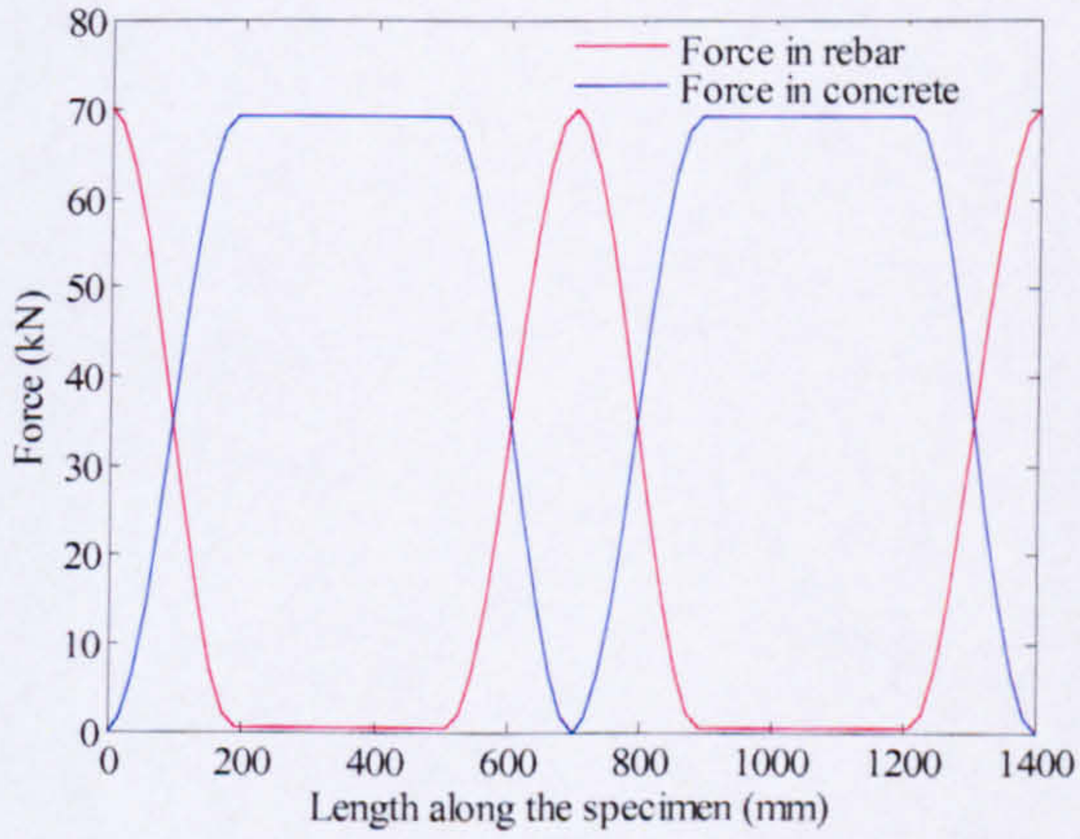

(b)

Fig. 6-8 Predicted force contribution of concrete and reinforcement for C50/13/200 (a) before first crack, (b) after first crack (c) after three cracks, and (d) after crack maturity

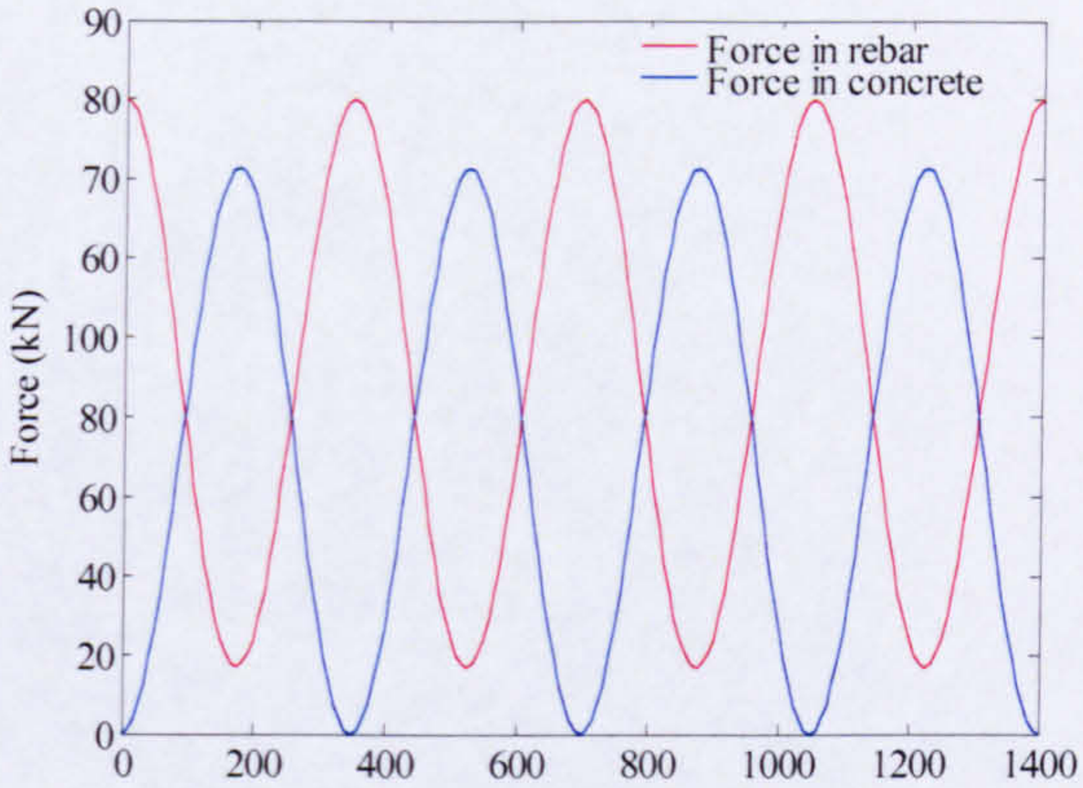

(c)

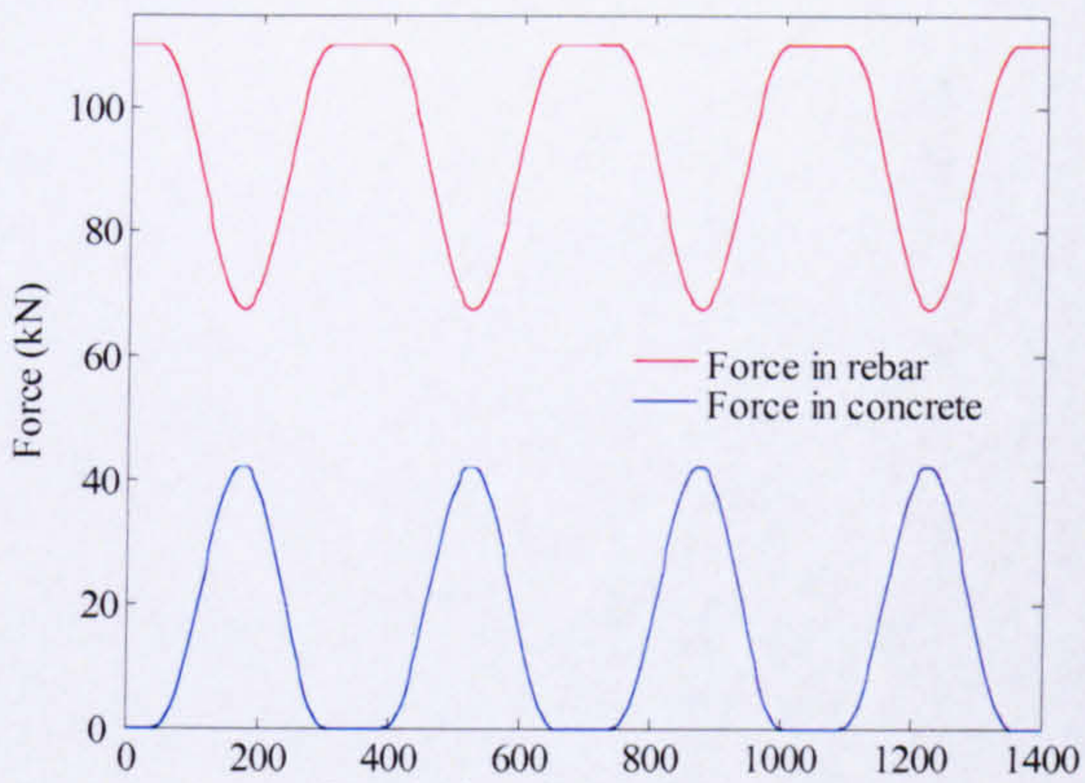

(d)

Fig. 6-9 Continued… Predicted force contribution of concrete and reinforcement for C50/13/200 (a) before first crack, (b) after first crack (c) after three cracks, and (d) after crack maturity

From the analyse of Figs. 6-5 and 6-6 it can be concluded that the strain distribution approach to model the tension stiffening behaviour is successful in modelling the tensile behaviour of GFRP reinforced concrete. The current model can benefit from having more refined equations for the bond development length as this can improve the predictions of strain distribution between cracks. The model relies on a cracking scheme that divides the crack span into two. This means that after the first crack, two simultaneous cracks take place, then four and so forth. However, during the experimental investigation simultaneous cracking was never encountered. An Incremental cracking scheme, that introduces only one crack at a time can further benefit the predictions of the model (Maekawa et al. 2002).

CHAPTER 7

DEFLECTIONS OF GFRP-RC

7.1 General

The work discussed in the previous chapters focus mainly on the development of a rational approach to model the tension stiffening behaviour of GFRP reinforced concrete. This chapter looks into the implementation of the tension stiffening model for predicting deflections of GFRP reinforced concrete flexural members. As GFRP is a softer material compared to conventional steel reinforcement, serviceability requirements in terms of deflections are generally the governing criterion for design. A proper estimate of the tension stiffening effect is therefore crucial for the accurate prediction of serviceability deflections. Moreover, since the smeared crack approach in FE analysis relies on the tension stiffening behaviour to model the interaction between concrete and reinforcement, the use of an accurate tension stiffening relation has become essential for FE modelling of GFRP RC.

This chapter presents the predictions of the tension stiffening model derived by modifying the CEB-FIP model (Chapter 3) and makes comparison with test results from beams and slabs reinforced with GFRP bars. Finally, this chapter presents a simple design oriented equation to accurately estimate the deflection of GFRP reinforced concrete.

7.2 Finite Element Analysis using ABAQUS

In this study numerical computation of deflections of flexural elements incorporating the tension stiffening effect is conducted using the ABAQUS FE package (Hibbit, Karlsson and Sorrensen Inc. 2001). ABAQUS is a general purpose FE code which has

several methods for simulating concrete; the more appropriate one for beams and slabs uses is the smeared crack approach. The section below briefly explains the concrete material modelling involved in ABAQUS.

7.2.1 Concrete material modelling

Modelling reinforced concrete in ABAQUS is done by combining standard elements, plain concrete elements with rebar element (– rods). Rebar elements can be defined singly or embedded in oriented surfaces and are modelled according to a one dimensional strain theory. This approach allows concrete to be considered separately from the reinforcing material and uses the tension stiffening to model the interaction of reinforcement and concrete (ABAQUS theory manual 2001).

The concrete model in ABAQUS consists of a compressive yield/ flow surface to model the concrete response in the predominantly compressive states of stress, together with damage elasticity to represent cracks that have occurred at the material calculation point. The occurrence of cracks is defined by the crack detection failure surface which is considered to be part of elasticity. Crack detection is an important feature for modelling of concrete both in tension and compression. Fig 7-1 and Fig. 7-2 show the crack detection surface used in ABAQUS in plain stress and *(p-q)* (deviatory stress) plane, respectively. Fig. 7-3 shows the uniaxial compression tension behaviour that needs to be calibrated for the successful use of the ABAQUS concrete model.

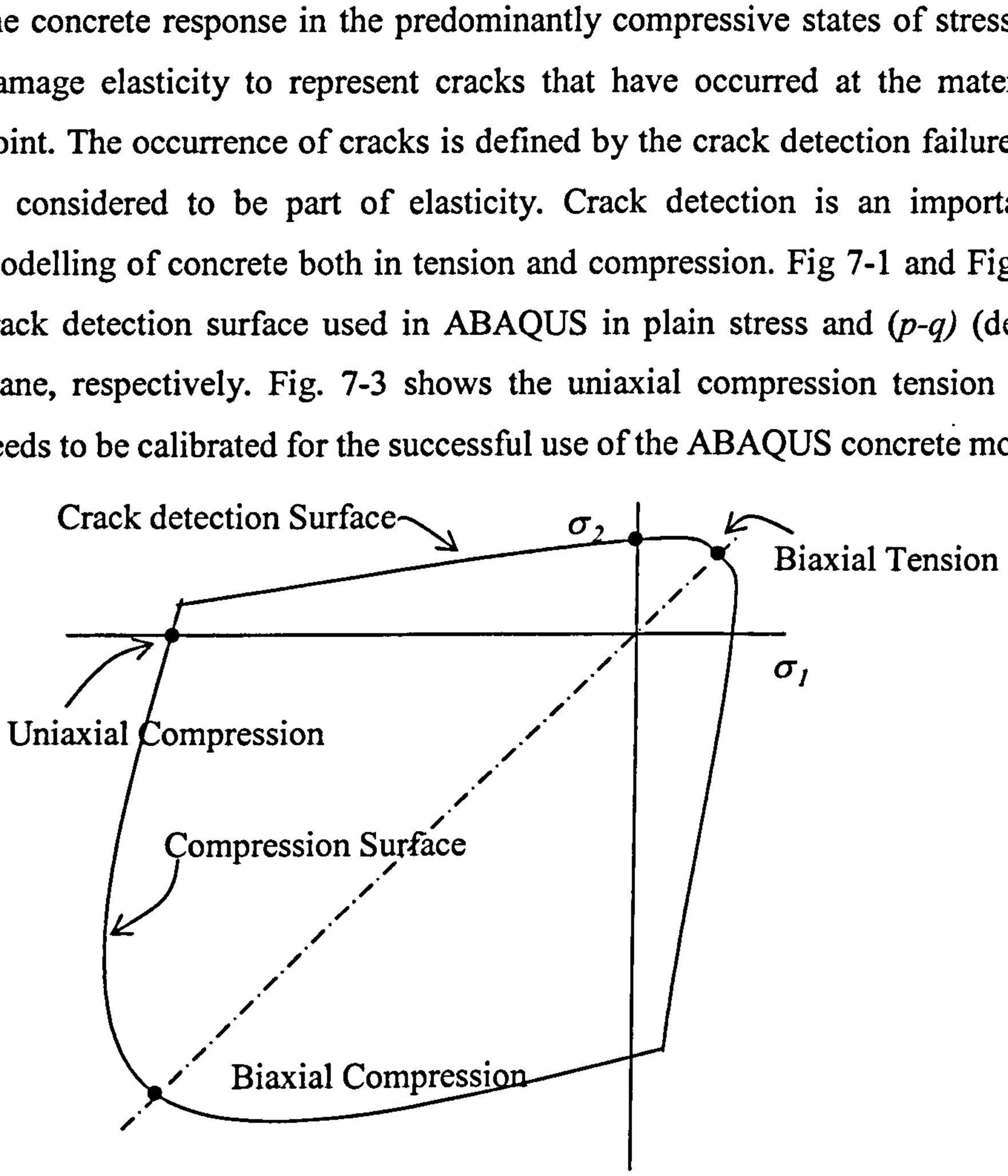

Fig. 7-1 Concrete failure surface in plane stress

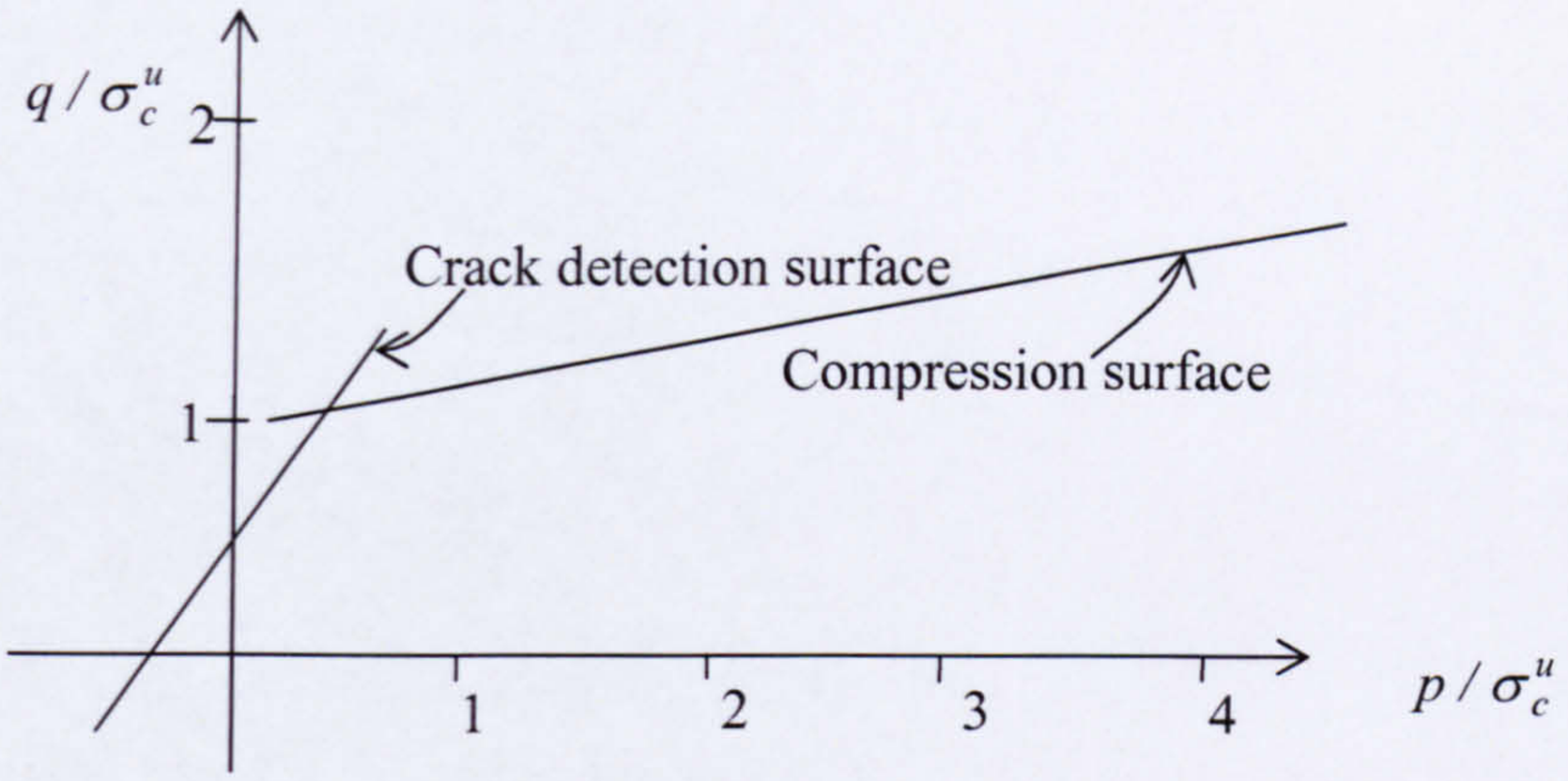

Fig. 7-2 Concrete failure surface in the *(p-q)* plane

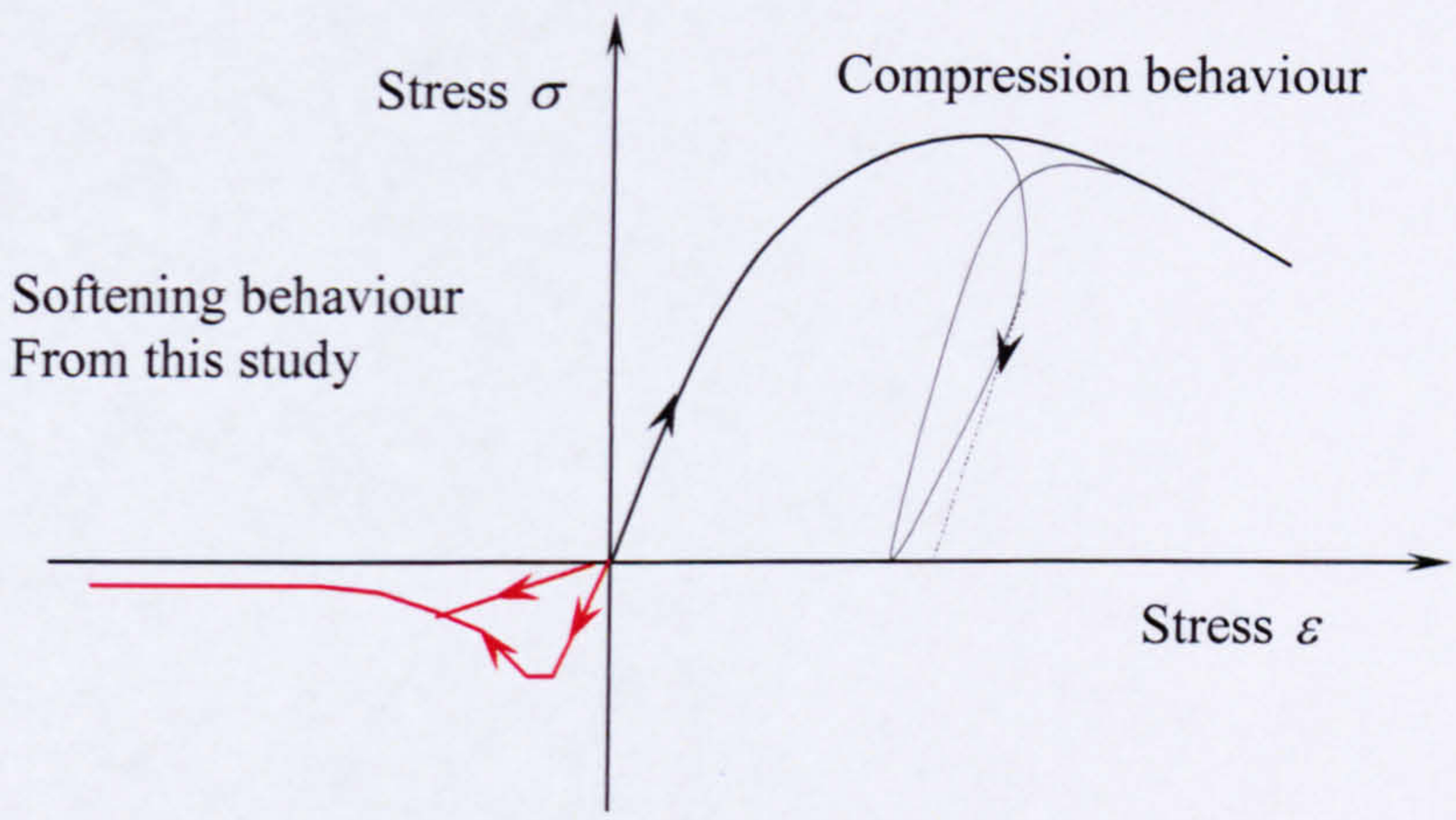

Fig. 7-3 Uni-axial behaviour of concrete

In the following analysis the compressive behaviour of concrete is based on the BS 8110 part II formulation. Modelling of tension behaviour is accomplished by the tension stiffening model proposed in Chapter 3 (Modified CEB-FIP model).

After initial trials, 2D Plane stress quadratic elements with 9 Gauss integration points (CPS8) were chosen to represent concrete in the slab and beam analysis. Following a mesh sensitivity analysis the mesh topology in the analysis was selected so that each element size was always kept close to 50-60 mm with aspect ratio close to 1. This mesh size was also adopted by Guadagnini (2002). The "Rebar" option was used to define the reinforcement in the element. As GFRP has a linear elastic relationship until failure, the stress-strain relationship derived from test was applied without any modification. Typical finite element meshes used to model the slabs and beams are shown in Fig. 7-4. Due to symmetry only half of the slab or beam is analysed. Full details of the

experimental and analytical results of the slabs and beams presented in Fig. 7-4 are discussed separately in sections 7.3.2, analysis of slabs, and 7.3.3, analysis of beams.

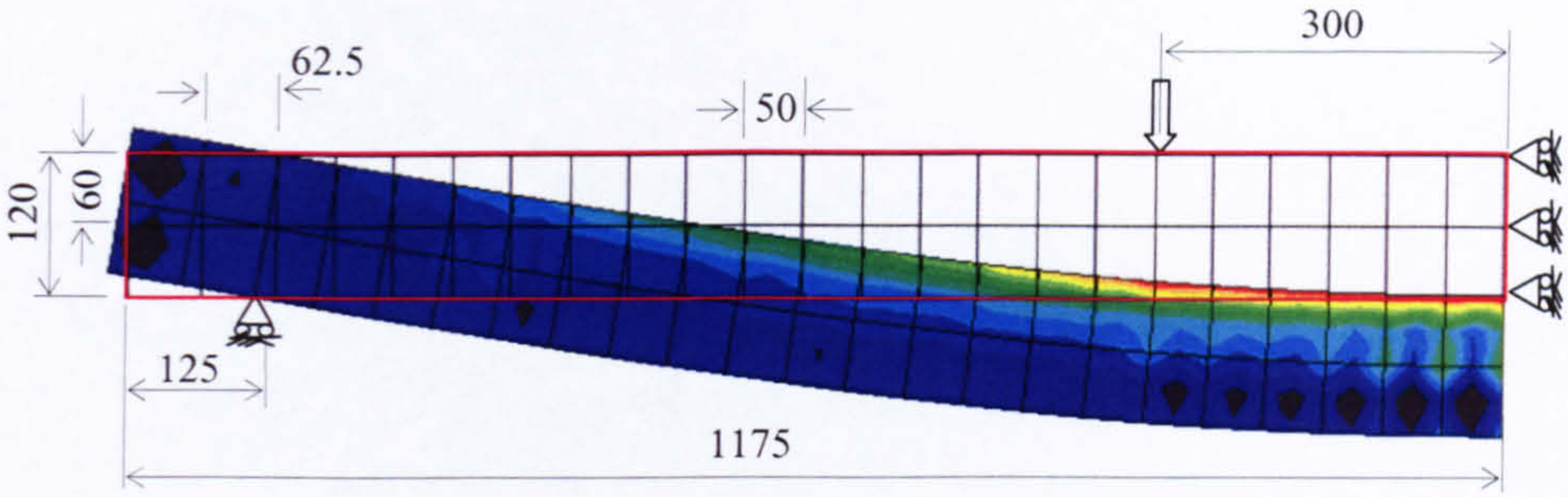

(a) FE mesh used for the slabs

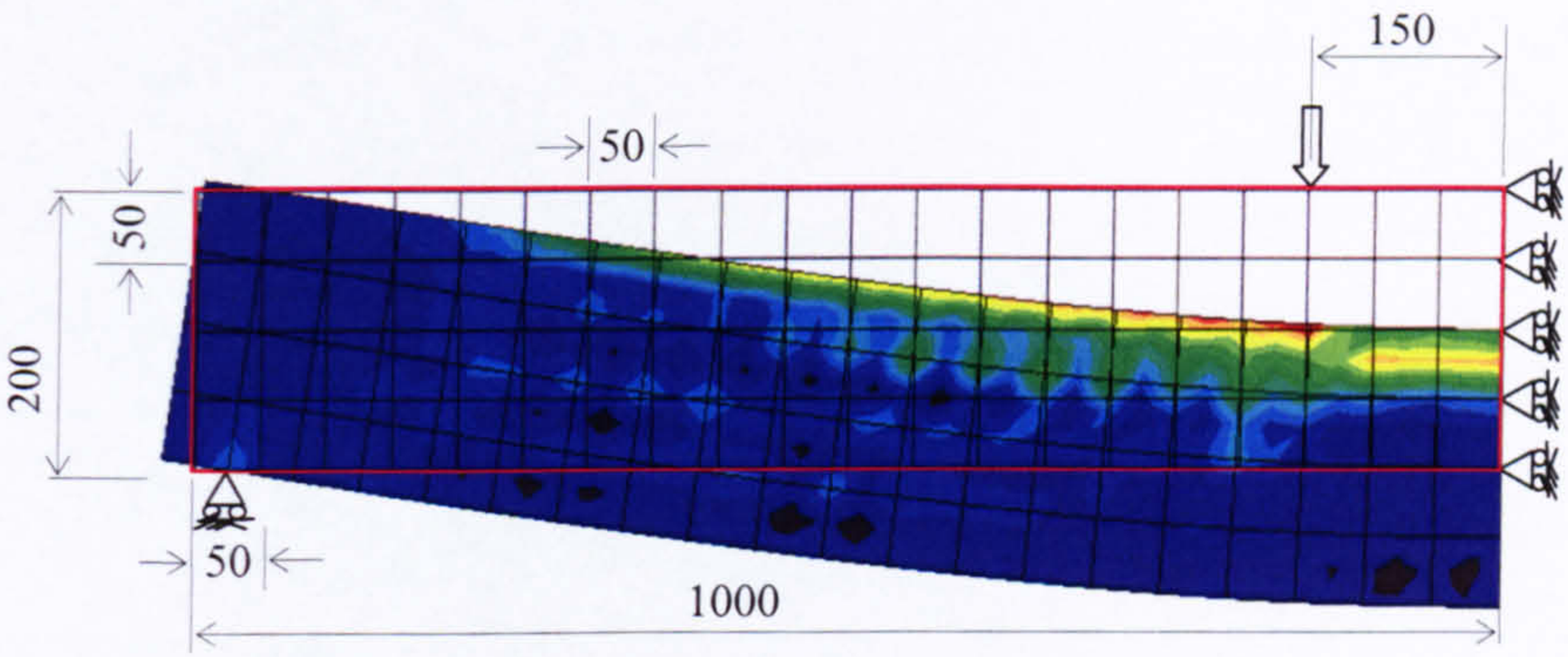

(b) FE mesh used for the beams

Fig. 7-4 Meshes used in the FE analysis

7.3 Deflection prediction of flexural elements

7.3.1 Determination of tension stiffening effect for flexural elements

Unlike in the case of direct tension members where axial strain distributes uniformly across a section, axial strain in the flexural members is proportional to the distance from the neutral axis. Since the reinforcement ratio remains important in evaluating the tension stiffening effect, an equivalent concrete area of uniform tension in the case of bending element needs to be decided first, before using tension stiffening models derived from direct tension tests. The closest guideline for determining the effective area in tension comes from the CEB-FIP model code 90 (1993). Fig 7-5 shows the recommended use of $A_{c.eff}$ for different sections due to different structural actions. However, the recommendations are limited and are intended to account for the non-uniform normal stress distribution of bond forces into the concrete cross section at the

ends of the transfer length. This approach can be considered to lead to a lower limit of effective area in the case of flexural elements.

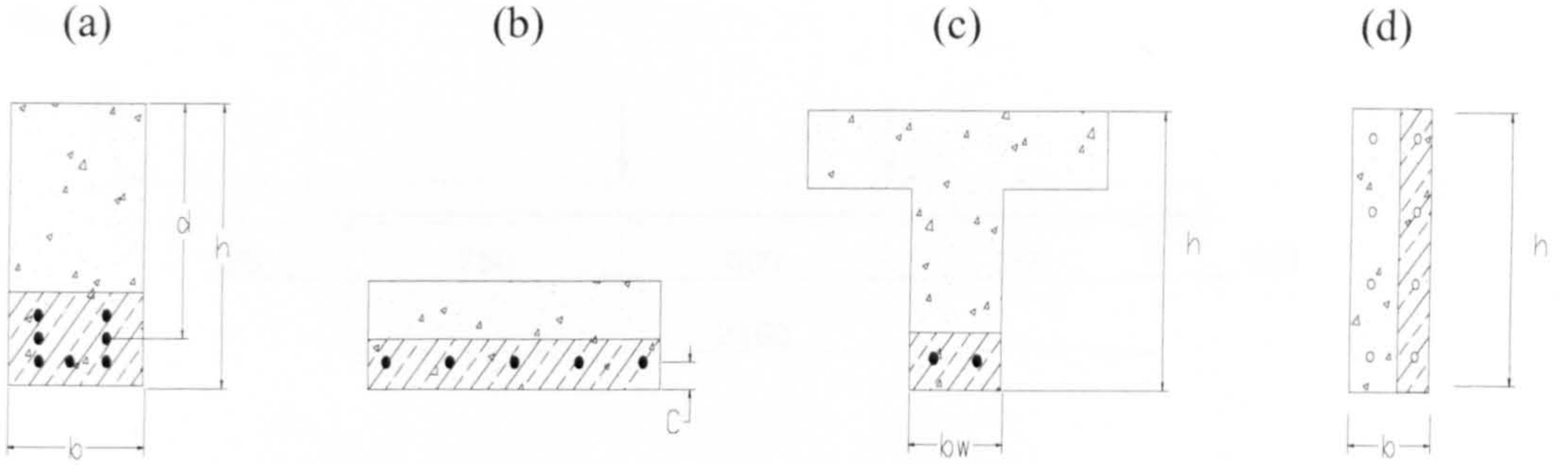

$A_{c,eff} = 2.5(h-d)b$ $<b(h-\bar{x})/3$

$A_{c,eff} = 2.5(c+\phi/2)b$ $<b(h-\bar{x})/3$

$A_{c,eff} = hb_w/3$

$A_{c,eff} = 2.5(c+\phi/2)b$ $<b/2$

Fig. 7-5 Effective tension area $A_{c,eff}$ according to (CEB-FIP) for: (a) Beams, (b) Slabs, (c) T Sections, and (d) members in tension

As the actual value of equivalent area of uniform tension in bending , $A_{c,eff}$, is complicated to calculate accurately, simple way and probably the most popular way is to assume it to be equal to $b(h-\bar{x})/2$, with h and x being the section height and depth to neutral axis respectively. This can be derived simply from the strain distribution alone if linear strain distribution in the bending section is assumed. Using this approach is consistent with interpretation of results of the direct tension test where non-uniform normal stress distribution by bond forces at the transfer length is not considered. In this study, in calibrating the tension stiffening model derived from direct tension tests to flexural elements $b(h-\bar{x})/2$ is used as the equivalent uniform tension in bending with x being the neutral axis depth of the cracked sections.

7.3.2 Analysis of slab

This section presents the deflection prediction of slabs using Finite Element analysis. Slabs used in this section are part of a detailed parametric study conducted on deflection of FRP reinforced slabs and beams (Al Sunna 2006) which used the same ASLAN 100 bar as in this study. Deflections of flexural elements with low reinforcement ratios, where deflection predictions using ACI equations have been found inadequate, are particularly selected for this discussion. In each of the analysis, along with the experimental and FE model results, deflection predictions based on ACI 440 equations are also presented for comparison purposes.

Fig. 7-6 shows the typical loading arrangement and reinforcement details of the experimental slabs used in this study. Table 1 shows the details of reinforcement used, cover of the bar, concrete strength and properties of the bar linked to the experimental study.

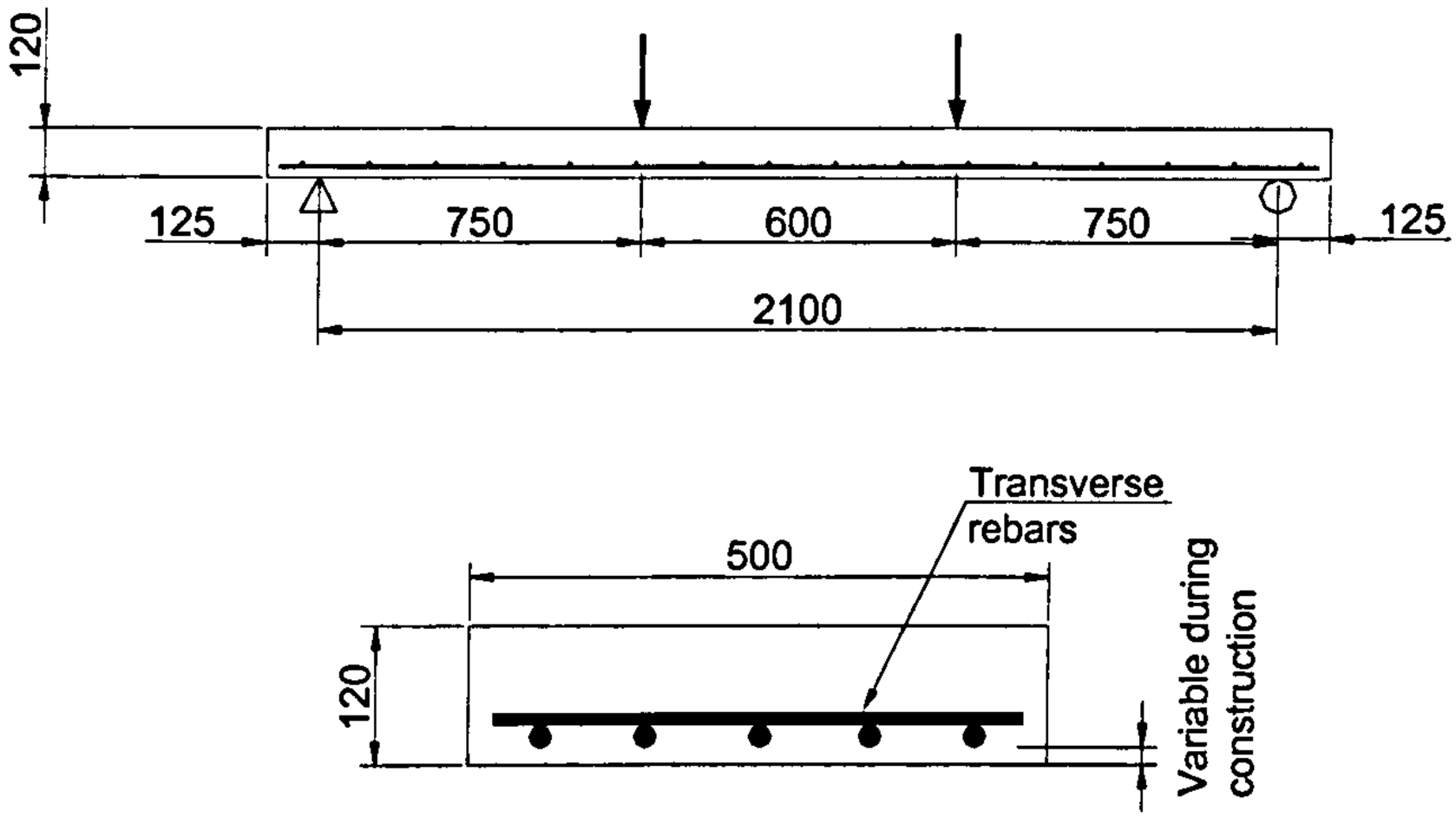

Fig. 7-6 Typical loading details and reinforcement details of the slabs

Table 7-1 Reinforcement details of slabs

Rebar type	Slab	Cover (mm)	Rebar used	$\rho = As / bh$ (%)	f_c' (MPa)
GFRP	S1	27.5	5Ø6mm	0.24	43
	S2	31	5Ø9.53mm	0.59	39
	S3	40	5Ø19.05mm	2.38	39

Fig 7-7 shows the tension stiffening values used for the 3 slabs calculated according to the effective area of concrete as discussed in the section above (see section 7.3.1). Detailed results of the slabs analysed are shown in Figs.7-8 to 7-10 starting from the slab with lowest reinforcement ratio, S1. The FE analysis always provided a good agreement with the experimental results whilst the ACI440.1R-03 prediction is shown to underestimate deflections at low reinforcement ratios. However, the ACI440.1R-03 prediction for the higher reinforcement ratio is in good agreement with the experimental results (see Fig 7-10). This confirms the trend also found by other researchers and reported in Chapter 1 and 2.

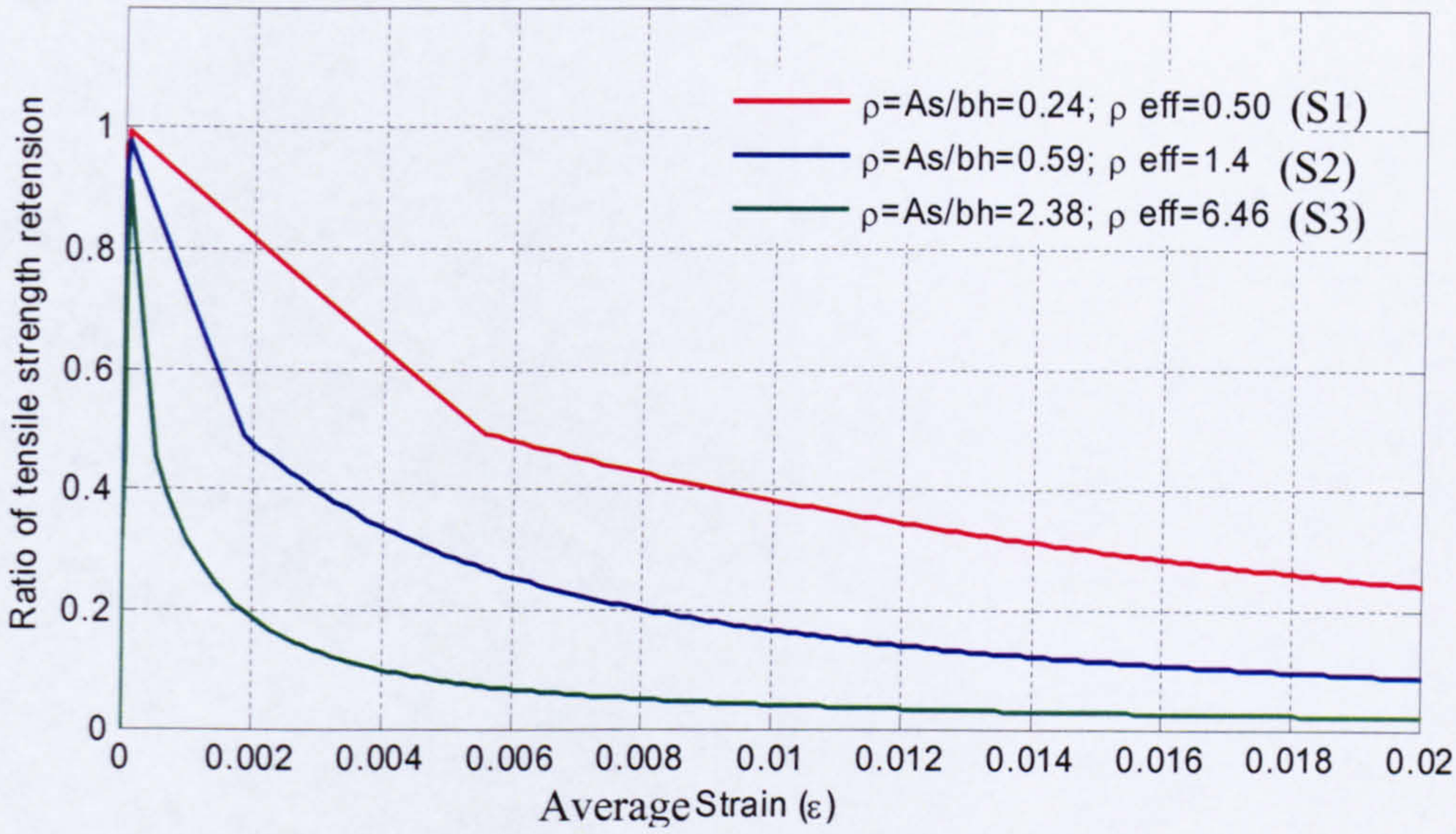

Fig. 7-7 Tension stiffening values for concrete for the three slabs S1-S3

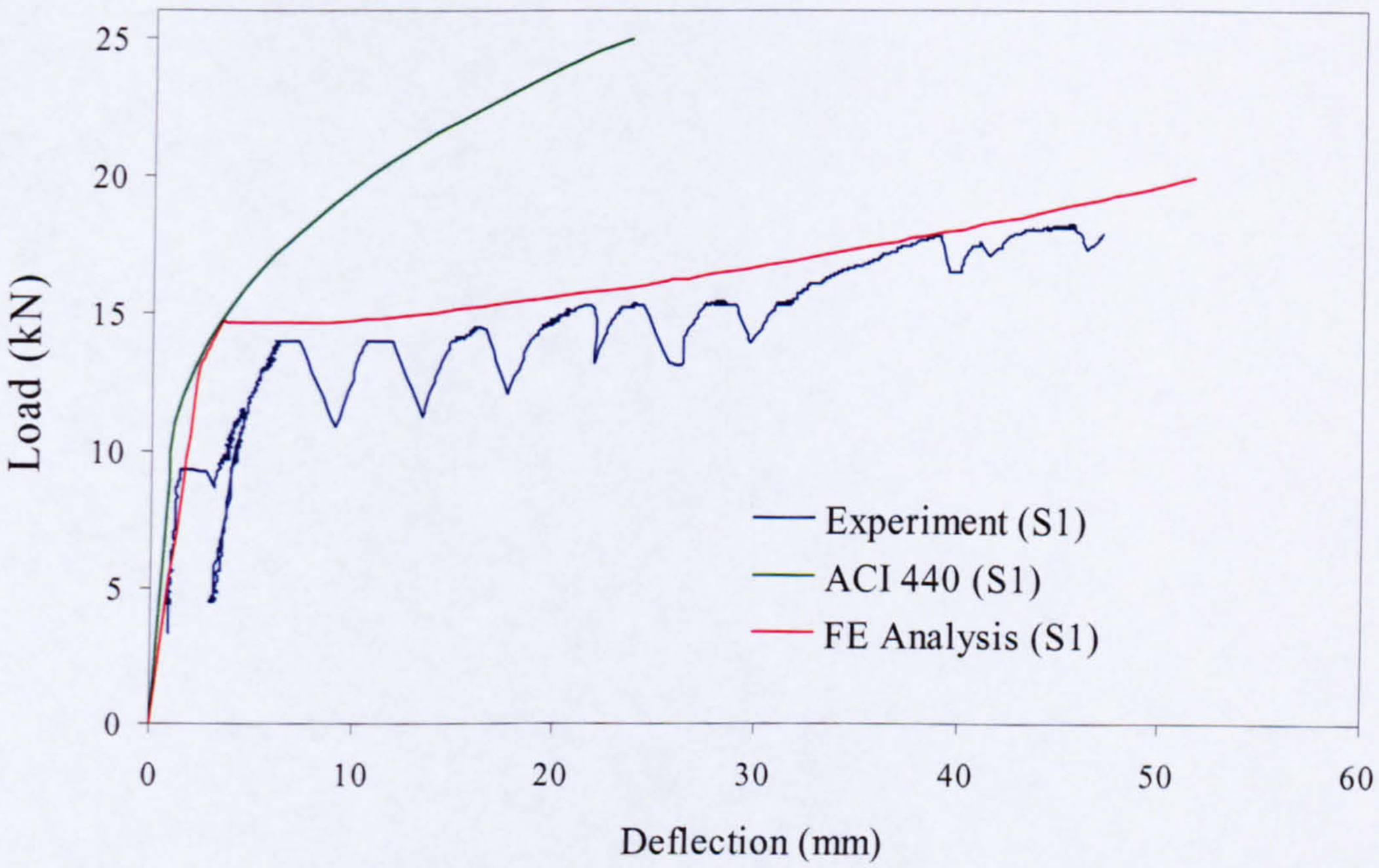

Fig. 7-8 FE prediction of central deflection of slab S1 plotted with experimental results and current ACI 440 (2003) prediction

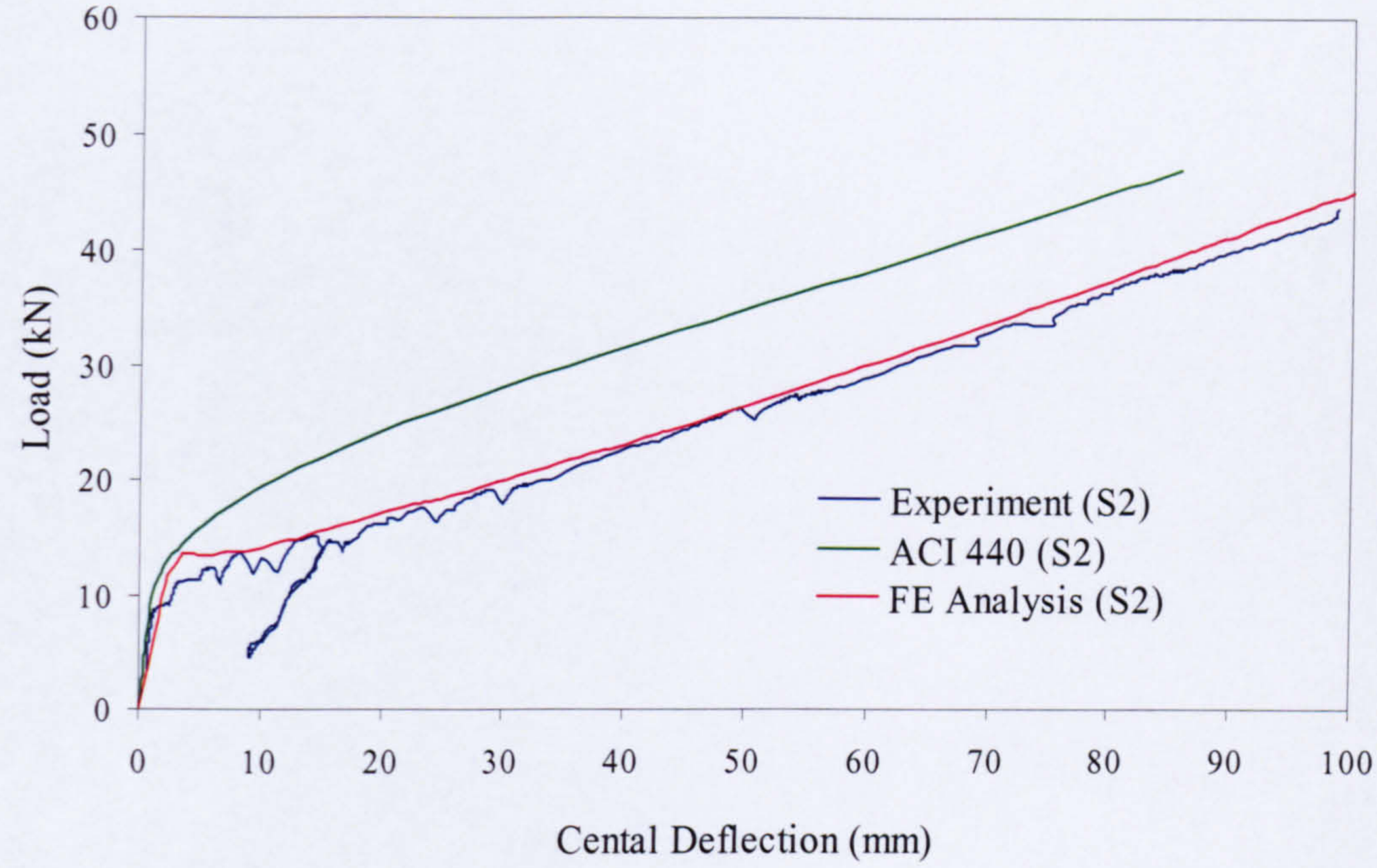

Fig. 7-9 FE prediction of central deflection for slab S2 plotted with experimental results and current ACI 440 (2003) prediction

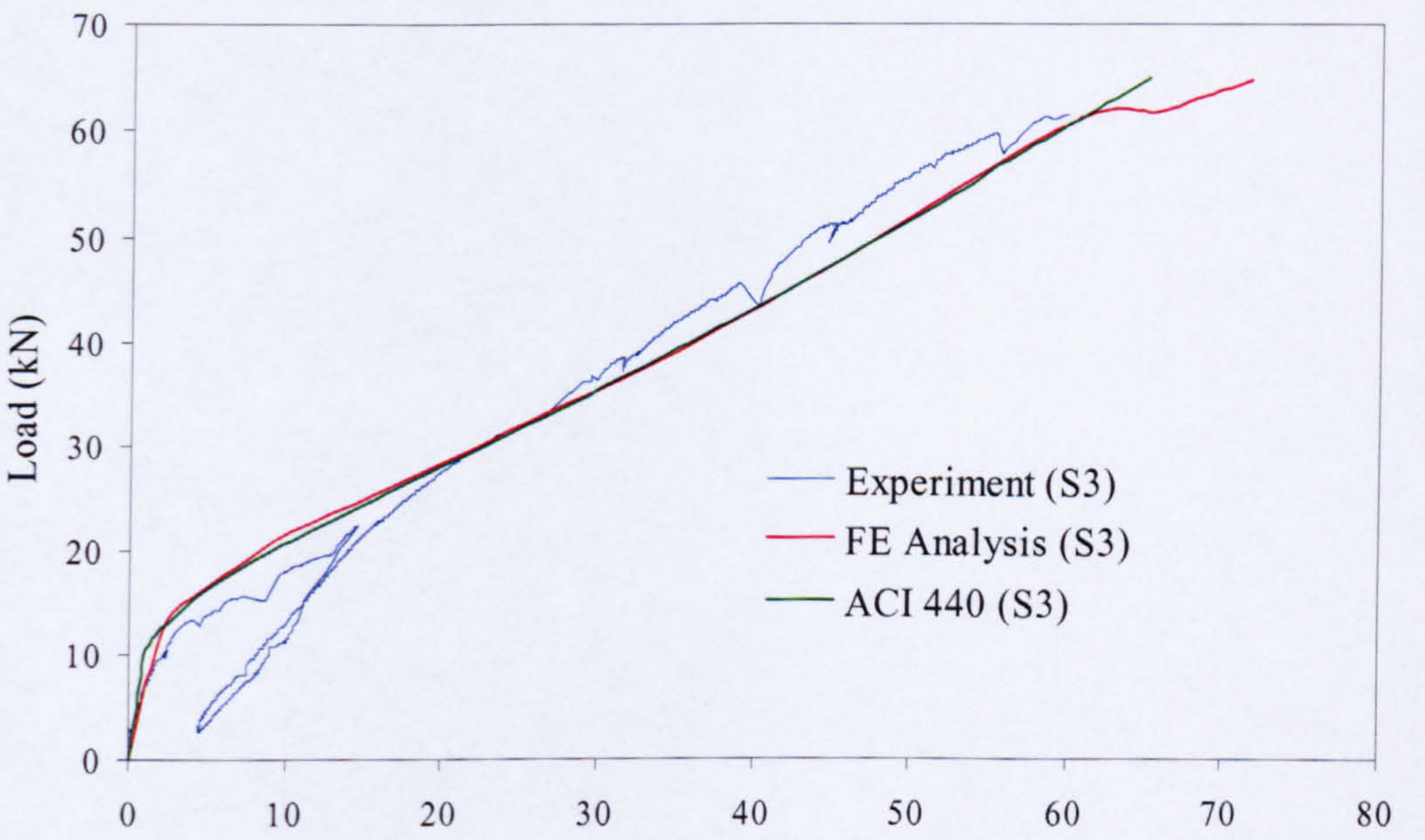

Fig. 7-10 FE prediction of central deflection for slab S3 plotted with experimental results and current ACI 440 (2003) prediction

7.3.3 Analysis of Beams

The Beams (B1-B3) that examined in this section were tested as part of the current study using the same concrete grades 50 and 90 used for the tension tests. Shear links for the beams were provided externally by wrapping the beam with steel bands at 80mm centres in the case of beam B1 and B3, and 120mm centres in the case of beam B2 to avoid shear failure. Fig. 7-11 shows the experimental set up and reinforcement details of the three beams. As failure due to rupture of the bar wanted to be explored, beams B1 and B2 were designed with the same reinforcement ratio, but different concrete strength aiming to achieve bar failure in one and concrete crushing failure in the other. All beams were cast and cured similar to the specimens for the direct tension tests. The external shear strips were applied only in the shear spans just before testing. Table 7-2 provides more detailed information such as reinforcement detail, cover concrete strength and the observed failure modes of each beam.

Failure of the bems B1 and B2 are shown in Figure 7-12 and 7-13 respectively.

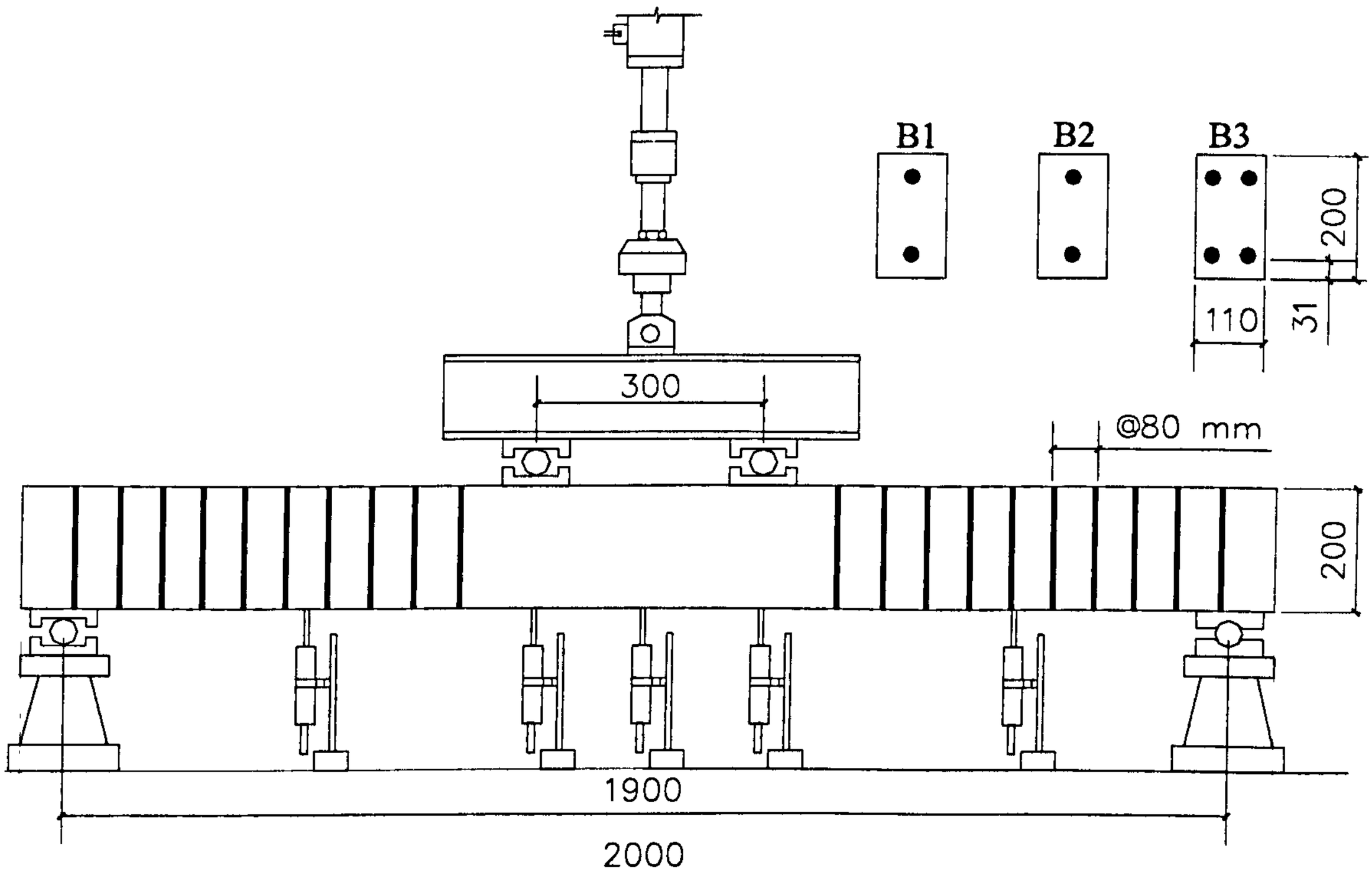

Fig. 7-11 Test set-up and the reinforcement details of the beams B1, B2 and B3

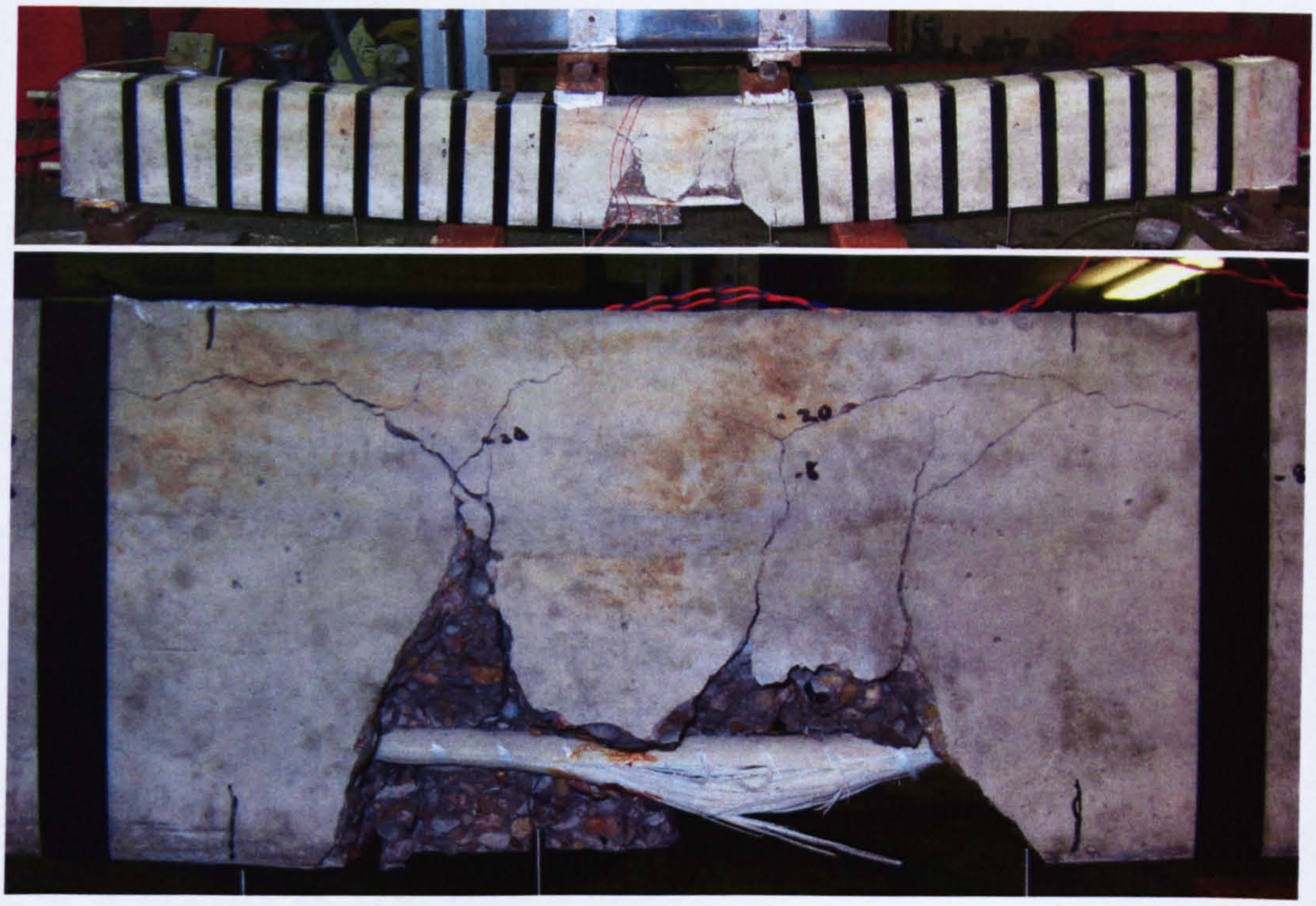

Fig. 7-12 Failure of Beam B1 triggered by reinforcement rupture

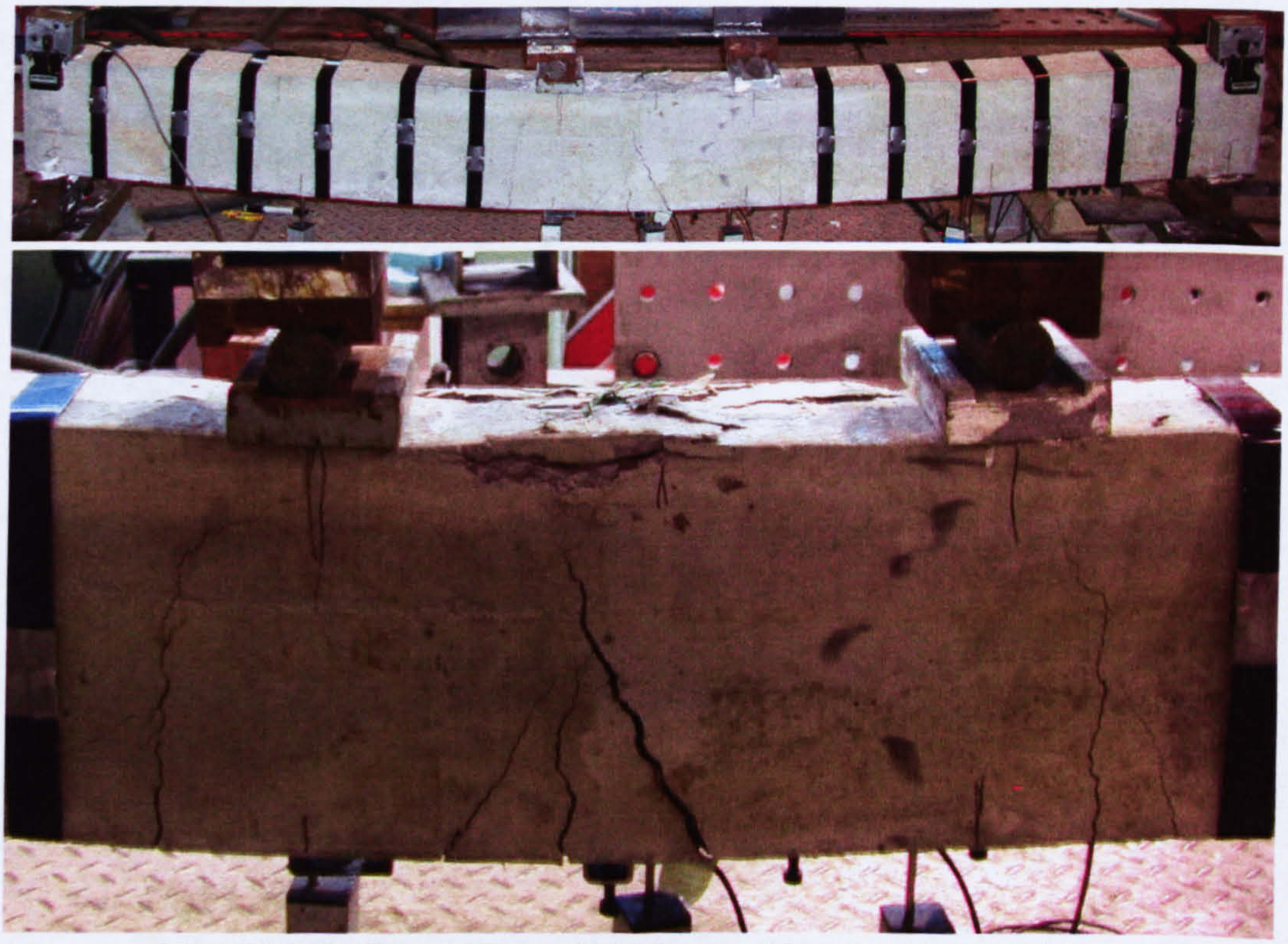

Fig. 7-13 Failure of Beam B2 triggered by concrete crushing

Table 7- 2 Details of the beams tested in this study

Type	Beam	Cover	Rebar use	$\rho = As / bh$ (%)	f_{cu}	Failure mode
GFRP	B1	31mm	1∅12.7 mm	0.57	91 MPa	Bar rupture
	B2	31mm	1∅12.7 mm	0.57	46 MPa	Con. Crushing
	B3	31mm	2∅12.7 mm	1.15	46 MPa	Con. Crushing

Fig 7-14 shows the tension stiffening characteristics used for the FEA of the beams. Fig 7-15 to Fig 7-17 show the load displacement relationships of beams B1 to B3, respectively along with the predictions according to the FE analysis and the ACI 440 (2003) approach (explained in section 2.2).

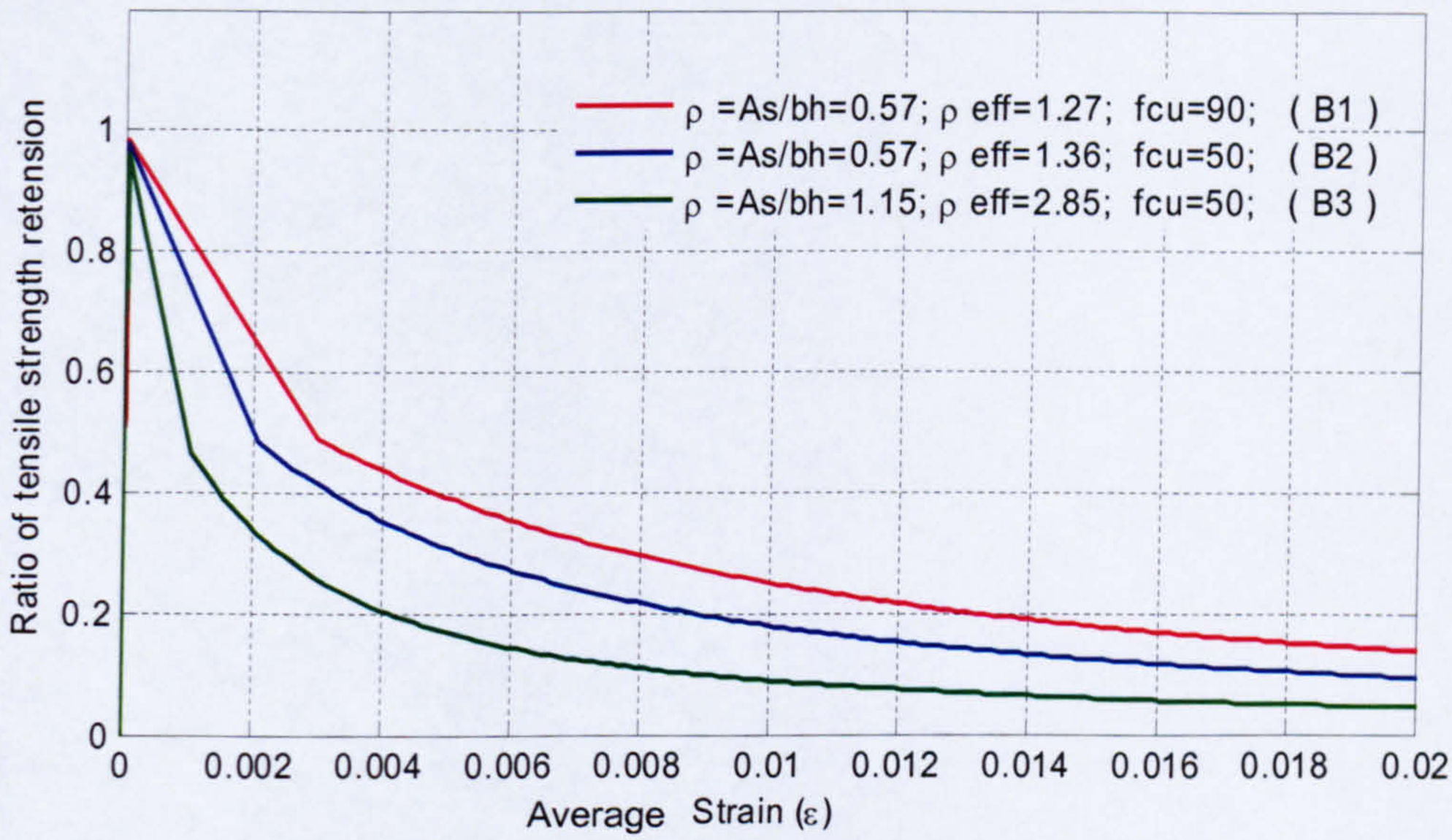

Fig. 7-14 Ratio of tension retention for the different beams used in the FE analysis

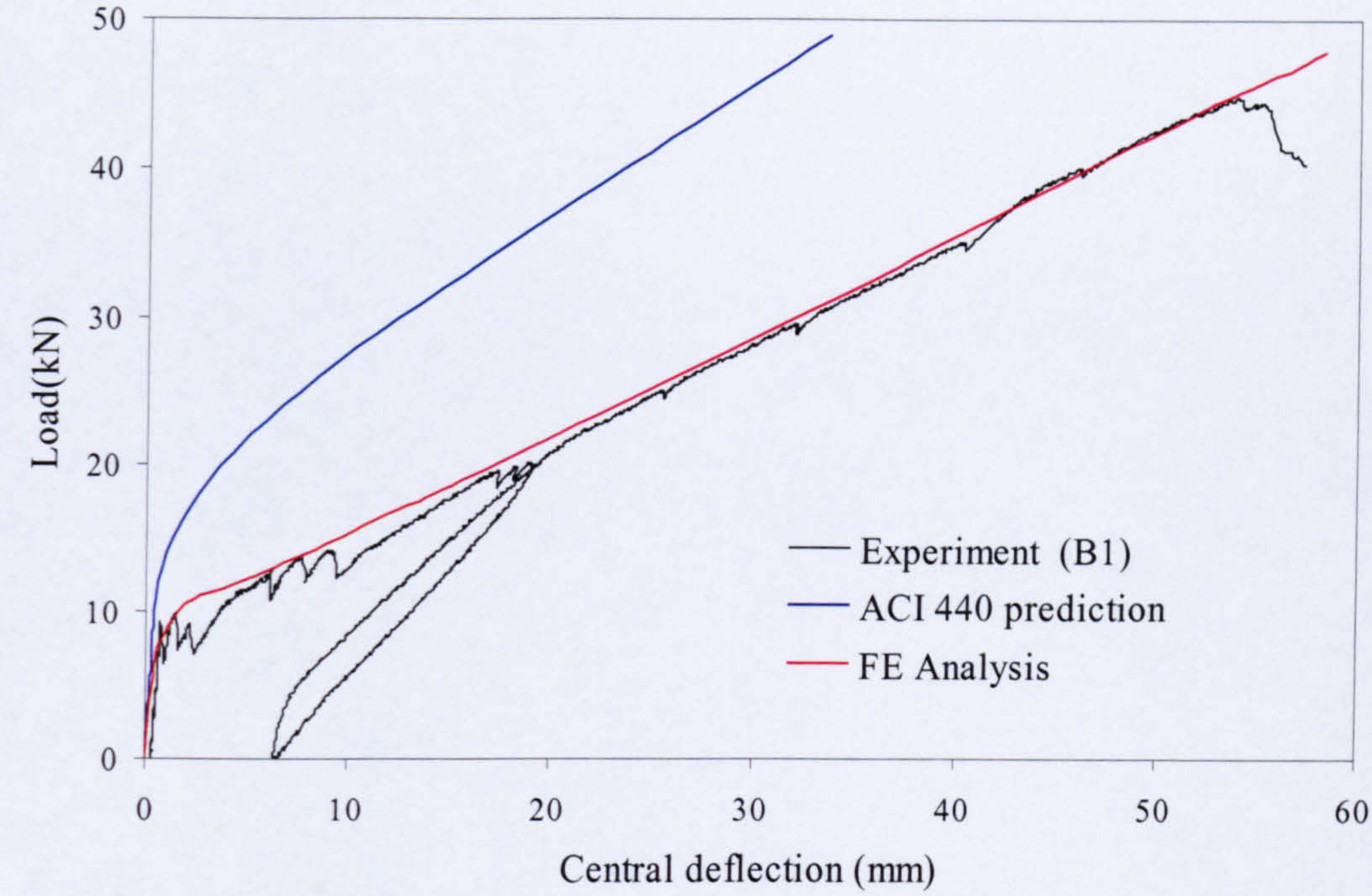

Fig. 7-15 FE prediction of central deflection of beam B1 plotted with experimental results and current ACI 440 (2003) prediction

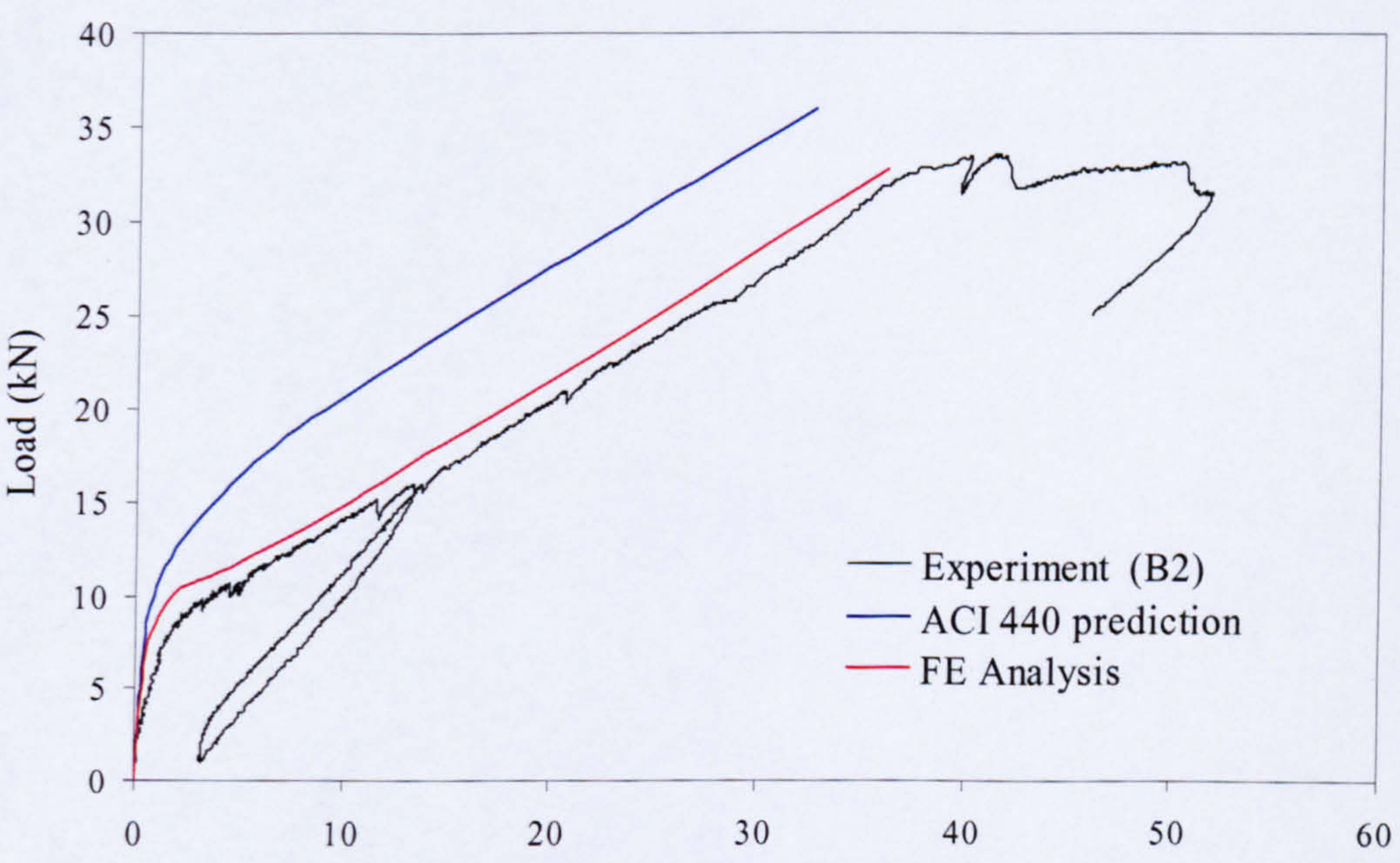

Fig. 7-16 FE prediction of central deflection of beam B2 plotted with experimental results and current ACI 440 (2003) prediction

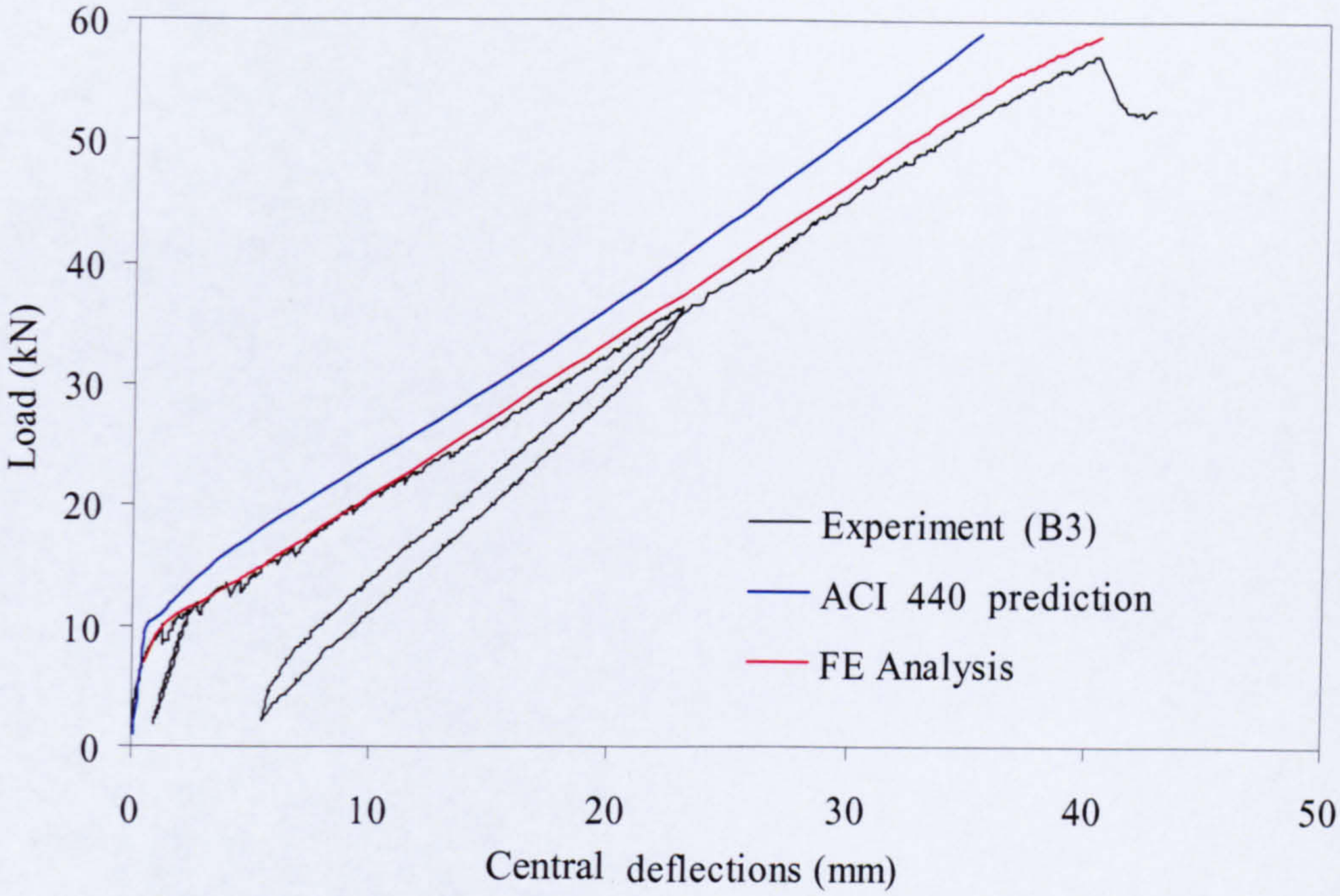

Fig. 7-17 FE prediction of central deflection of beam B3 plotted with experimental results and current ACI 440 (2003) prediction

The results are similar to the ones for the slabs. Whilst the FE analysis agrees quite well with the experimental results, the ACI predictions showed a similar trend of underestimating deflections at low reinforcement ratios. Furthermore, the ACI prediction shows less accuracy for beams with higher concrete strength, but similar reinforcement ratios (see Figs. 7-15 and 7-16).

From the above results of the slab and beam analysis, it is clear that accurate solutions for the structural behaviour of GFRP reinforced concrete can be achieved consistently with accurate modelling of the tension stiffening effect of concrete. It is also clear that the current ACI 440.1R-03 predictions fall far short in predicting experimental deflections of GFRP reinforced concrete, especially at low reinforcement ratios and high concrete strengths. This is attributable to the fact that the ACI equation significantly overestimates the tension stiffening behaviour at low reinforcement ratios. In the next section, a modification to the CEB-FIP model is proposed as a means of introducing an effective code based method for the prediction of deflections of GFRP reinforced concrete structures.

7.4 Concrete model code approach

7.4.1 General

Due to nonlinearity of reinforced concrete structural behaviour, nonlinear modelling is essential for predicting the structural behaviour of reinforced concrete elements (section 7.3.2 and 7.3.3). However, this should not prevent the engineers from having reliable and simplified techniques for design purposes. Since estimating deflections at service load is the governing criterion for design of GFRP RC flexural members, a reliable simplified model to predict deflection can hugely benefit the design process. As shown in the previous comparisons, the deflection predictions using ACI 440.1R-03 grossly underestimate deflections at low reinforcement ratios and therefore are unconservative, a view that is also supported by many other researchers (Faza et al. 1990, Alsayed et al. 2000, Abdullah 2002, Toutanji et al.2003).

The reduced cross sectional area method adopted in ACI for modelling the tension stiffening effect is part of the problem, since it overestimates the tension stiffening effect of direct tension members. A similar approach that uses a reduced cross sectional area to account for the effective inertia is equally ineffective and also underestimates deflection at lower reinforcement ratios. From the similarities of the two methods and their results, it appear that it is the over-estimation of the tension stiffening effect that causes the underestimation in deflections by the latter method. However, existing equations are reasonably good in predicting the behaviour for higher reinforcement ratios but not for lower reinforcement ratios. This suggests that reducing the effective area after cracking in the way it is currently done has no direct relationship to either the tension stiffening effect of direct tension elements or the deflections of bending elements.

7.4.2 Basis of deflection calculation according to the model code

The moment curvature relationship is a more fundamental and direct method to model the deflection behaviour of reinforced concrete. The CEB-FIP model code 90 recommendations for serviceability limit state of deflection are based on the moment-curvature relationship and account for the tension stiffening effect of cracked concrete by adopting an intermediate value of curvature by combining the cracked and un-cracked section curvatures. As curvature is directly responsible for flexural deflections,

this is a more fundamental and direct approach that can be adopted to account for the tension stiffening effect for deformation calculation of flexural elements. This method is also able to incorporate the effect of reinforcement, cracking, creep and shrinkage on deflection (CEB manual on Cracking and deformations 1983) (Favre and Carif 1994). Simplified form of the deflection formulae, derived by Favre and Carif from the moment curvature relationship as appeared in CEB-FIP model code 90 is shown below, equation 7-1a and 7-1b.

$$\Delta = (1 + \xi)\Delta_c \text{ for } M < M_{cr} \quad (7\text{-}1a)$$

$$\Delta = \left(\frac{h}{d}\right)^3 \eta(1 - 20\rho_{cm})\Delta_c \text{ for } M \geq M_{cr} \quad (7\text{-}1b)$$

Where, Δ=deflection, ξ= Creep coefficient, η= Correction factor based on the calculation percentage of tensile reinforcement, ρ_{cm}=Average compressive reinforcement ratio, Δ_c=Elastic deflection calculated with the rigidity $E_c I_c$ of the gross section

7.4.3 Theory underlying the CEB-FIP approach

Fig 7-18 shows a schematic representation of the general moment curvature relationship for the RC section with lines ψ_1 and ψ_2 representing the moment curvature relationship for the un-cracked section and the fully cracked section. Curvatures ψ_1 and ψ_2 in this model are calculated based on the elastic section analysis with the assumption that the plane sections remain plane. In the calculation of ψ_1 the un-cracked concrete section with the stiffness of the transformed section is used whilst in the calculation of ψ_2, the stiffness of the cracked concrete section ignoring the concrete contribution in tensile region is used. The continuous line represents typical moment curvature relationship for a section subjected to flexural action. Initially it follows the curve ψ_1 until cracking at moment M_{cr} or conveniently at moment $M_{cr,red}$, equation 7-2.

$$\psi_m = \psi_1 \text{ for } M < M_{cr} \quad (7\text{-}2)$$

The curvature then follows a path in-between ψ_1 and ψ_2 before it finally converges to the moment curvature relationship of the fully cracked section ψ_2. The intermediate curvature after cracking can be expressed as follows, equation 7-3.

$$\psi_m = \psi_2 - \Delta\psi_{TS} \quad (7\text{-}3)$$

$\Delta\psi_{TS}$ in equation 7-3 is the difference between the intermediate moment-curvature relationship, ψ_m, and the fully cracked curvature ,ψ_2, and it is attributed to the tension stiffening effect. Depending on the actual degradation of tension stiffening effect with the increase in curvature after cracking, a suitable function to reflect the actual moment curvature relationship can be employed. For example, inversely linear degradation of tension stiffening effect after cracking over the increasing curvature can be expressed as below.

$$\Delta\psi_{TS} = (\psi_{2r} - \psi_{1r}).\beta.\frac{M_{cr}}{M} \text{ for } M > M_{cr} \qquad (7\text{-}4)$$

Where ψ_{1r} and ψ_{2r} are the curvatures of cracked and un-cracked section at cracking moment M_{cr} and can be expressed in terms of ψ_1 and ψ_2 (curvatures at state 1 un-cracked and curvature at state 2 cracked respectively) as shown in equation 7-5.

$$\psi_{1r} = \psi_1 \frac{M_{cr}}{M} \qquad \psi_{2r} = \psi_2 \frac{M_{cr}}{M} \qquad (7\text{-}5)$$

The value of β represents the retention of curvature at M_{cr} and is a function of bond and load condition. For instantaneous deflections of steel RC elements, bars β is considered equal to one.

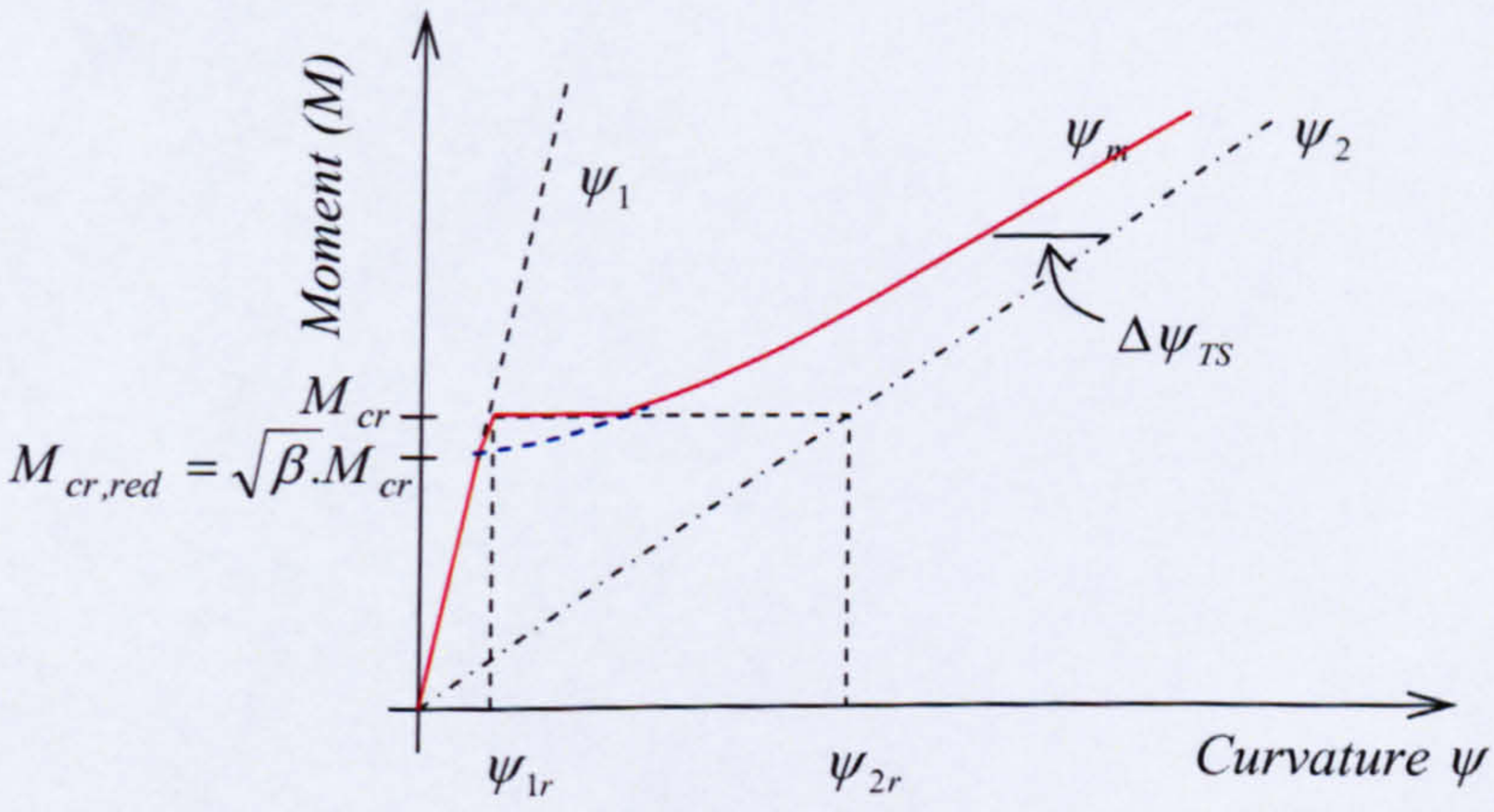

Fig. 7-18 Moment curvature relationship for the simple bending case (Favre and Carif 1994)

By substituting equation 7-5 into the equation 7-4, a simplified moment curvature relationship in terms of ψ_1 and ψ_2 is found, equation 7-6.

$$\psi_m = \psi_2 - (\psi_2 - \psi_1)\beta\left(\frac{M_{cr}}{M}\right)^2 \qquad (7\text{-}6)$$

$M_{cr} = z(f'_{tf})$ Cracking moment

z = Section modulus

f'_{tf} = Tensile strength of concrete in flexure

ψ_m = Mean curvature

By substituting $\psi_m = \psi_1$ in equation 7-6 above, a smooth transition to the deflection curve can be established with the same degradation of tension stiffening starting from $M_{cr,red} = \sqrt{\beta}.M_{cr}$ lower than the original cracking moment M_{cr}, also shown in Fig 7-18.

7.4.4 Simplified approach for prediction of deflections

The above governing moment-curvature relationship can be further simplified by considering the bilinear moment deflection relationship without significant compromise to the accuracy of the predictions. With this simplification, curvature in equations 7-6 is now replaced by deflections of un-cracked state, Δ_1, and cracked state, Δ_2, as shown in equation 7-7. This approach is also adopted in Euro code 2 (2001) (see equation 7-8).

$$\Delta = \Delta_2 - (\Delta_2 - \Delta_1)\beta\left(\frac{M_{cr}}{M}\right)^2 \qquad (7\text{-}7)$$

$$\Delta = \varsigma\Delta_2 + (1-\varsigma)\Delta_1 \qquad (7\text{-}8)$$

Where

$$\varsigma = 1 - \beta\left(\frac{\sigma_{sr}}{\sigma_s}\right)^2$$

σ_{sr} = Stress in the tension reinforcement calculated on the basis of cracked section under the loading conditions causing first crack

σ_s = Stress in tension reinforcement calculated on the basis of the cracked section

Note: σ_{sr}/σ_s can be replaced with M_{cr}/M for flexure where M_{cr} is the moment at which cracking starts.

As this research is dealing only with instantaneous deflections and modifying the existing equation to model the deflections of GFRP reinforced concrete, it is intended not to disturb the theoretical form of the above equation any further. A Full derivation of how this equation is reduced to the form which appears in CEB-FIP model code 90

(equation 7-1) can be found in CEB design manual on Cracking and deformations (1983) and work of Favre and Carif (1994).

7.4.5 Modification to model GFRP

By using the direct tension studies reported earlier in this thesis, the value of β for GFRP-RC is selected as 0.5 and a linear degradation is assumed for the decreasing tension stiffening effect with increasing deflections. The expression for the deflection of GFRP-RC flexural members can therefore be written as shown below.

$$\Delta = \Delta_2 - (\Delta_2 - \Delta_1)0.5\left(\frac{M_{cr}}{M}\right)^2 \qquad (7\text{-}9)$$

Fig. 7-19 and Fig. 7-20 shows experimental results compared with deflection predictions using equation 7-9 for the same slabs and beams discussed in section 7.3.3 and 7.3.2.

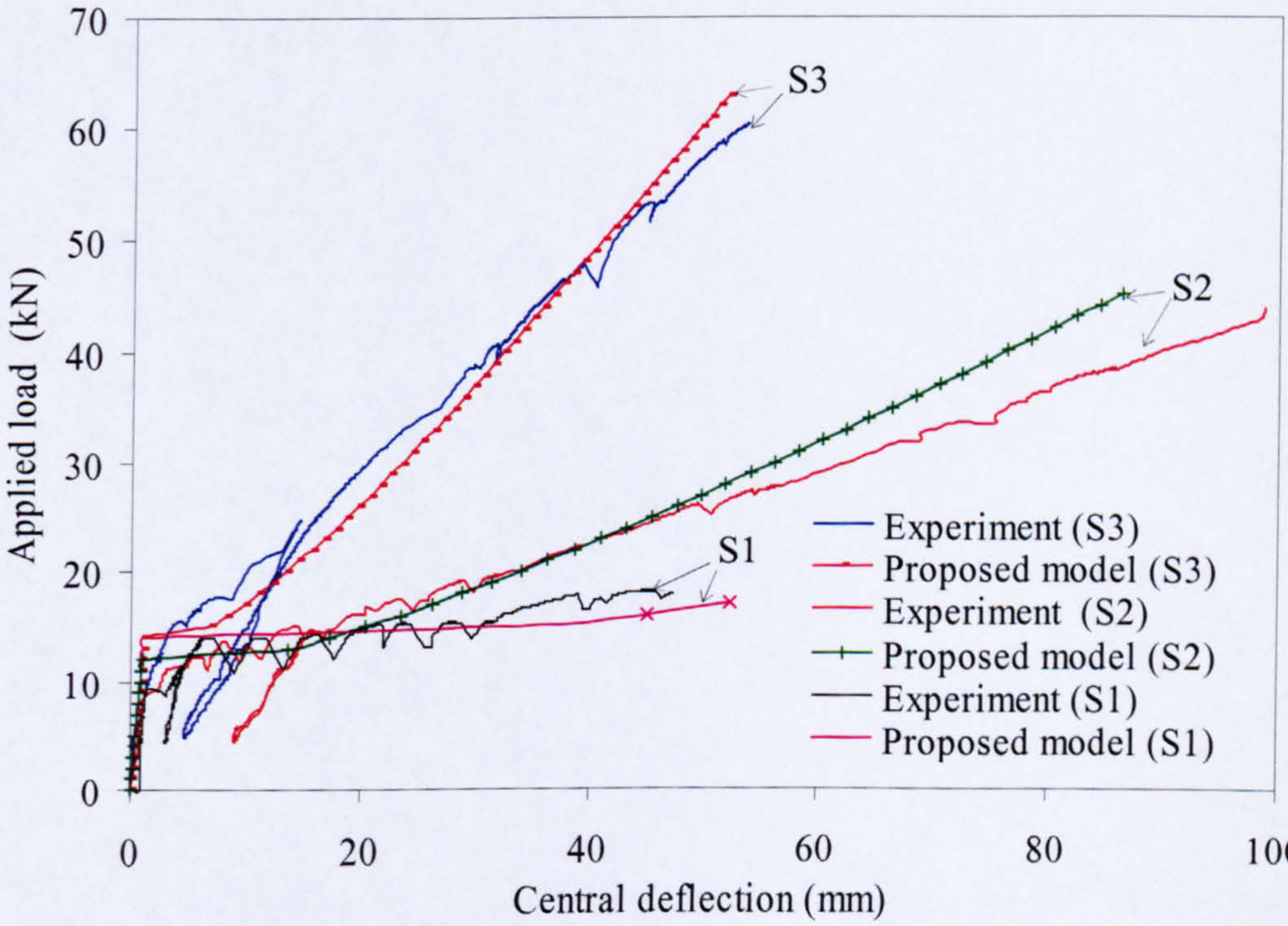

Fig. 7-19 Comparison of proposed model with experimental results of slabs

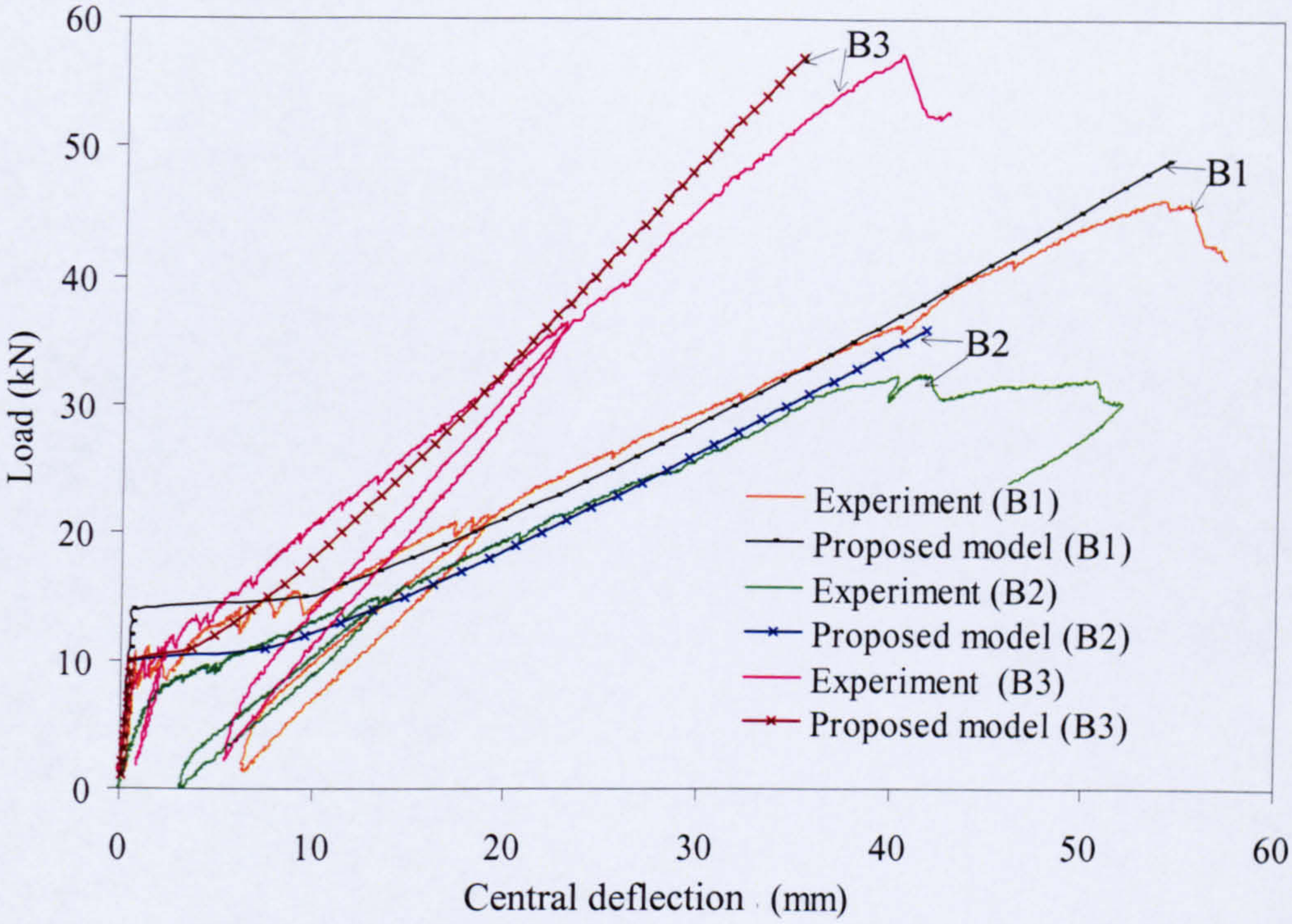

Fig. 7-20 Comparison of proposed model with experimental results of beams

Fig. 7-19 & Fig 7-20 show a good agreement of the estimated deflections with the experimental values especially at service loads where predictions of deflection are crucial from the design point of view. Compared to the ACI 440.1R-03 predictions discussed in the pervious section, predictions obtained according to the proposed method are more accurate and consistent. However, the prediction of deflections with this equation somewhat underestimate deflections near failure. This could be due to the deterioration to excessive slip in GFRP bars. Similar trends are observed in elements with partially bonded steel reinforcements.

CHAPTER 8

CONCLUSIONS AND RECOMMENDATIONS FOR FUTURE WORK

8.1 General

This study provides an insight into the tension stiffening behaviour of GFRP reinforced concrete. In this study tension stiffening is perceived as macroscopic bond modelling. The research extended from micro level examination of bond to macro level study of tension stiffening, thus providing a holistic approach for modelling the bond between concrete and reinforcement. Through the development of tension stiffening models, this study provides the essentials for modelling the behaviour GFRP RC in tension using the smeared crack approach in nonlinear Finite Element Analysis. Improper account of the tension stiffening effect is also found to be responsible for unreliable design equations, for example the ACI440.1R-03 recommendation for the prediction of deflections at service loads of GFRP reinforced concrete with low reinforcement ratios. Modifications to the CEB-FIP deflection equations are proposed and are shown to predict accurate serviceability limit deflections for a wide range of reinforcement ratios, including low reinforcement ratios.

8.2 Experimental investigations on tension stiffening effect

Direct tension tests were carried out to investigate the effect of: reinforcement ratio, concrete strength and bar diameter on the tension stiffening effect. Relatively low reinforcement ratios were selected for this study since concrete contribution is more

prominent on the overall structural behaviour at low reinforcement ratios than at high reinforcement ratios. From the parametric study it is found that reinforcement ratio and concrete strength have direct influence on tension stiffening behaviour while bar diameter has no significant influence.

The approach of representing tension stiffening effect of cracked concrete in ACI 224 as a reduction in effective area of the gross concrete section was found not to provide meaningful predictions for all reinforcement ratios.

The approach of decreasing the difference between the composite strain and bar strain at first crack to define subsequent average strain as adopted in CEB-FIP model, though in its current form overestimates the tension stiffening effect, is found to provided a better basis for predicting tension stiffening response. A modification to the CEB-FIP model based on the experimental evidence was proposed for modelling the tension stiffening effect of GFRP-RC, as shown below.

$$\varepsilon_m = \varepsilon_f \left[1 - 0.5 \left(\frac{f_{scr}}{f_f} \right)^2 \right] \qquad (8\text{-}1)$$

To understand the macroscopic behaviour of tension stiffening effect using bond as the building block, notched tension specimens with specially manufactured internal strain gauged bars were tested. Based on the strain readings, the bond stress distribution between cracks was determined. Bar strains at the middle section between cracks easily exceeded $10{,}000\mu\varepsilon$ before failure of the bar, suggesting loss of composite action between reinforcement and concrete. As the concrete can not sustain such strain and since there was no physical evidence of secondary cracks or appreciable loss of bond stresses, the predominant bond mechanism between concrete and reinforcement can be considered in all probability to be a "frictional pull-though mechanism". The deformed shape of the bar and its lower radial stiffness compared to concrete allow the bar to be pushed in the radial direction as it slips through the concrete. This allows sufficient bond to be developed and retained, with relatively little damage to the interface of the bar. However, the formation of secondary tensile cracks cannot be ruled out completely as they can still develop where high bond stresses are achieved due to better interlocking.

With a relatively large slip at the crack, bond deterioration is considered inevitable at some stage. From the detailed analysis carried out as part of this research programme, it is evident that the bond distribution between cracks of GFRP RC is different to that assumed for steel. Loss of bond at the crack section and migration of the peak shear stress away from the crack was found to be typical behaviour of the bond stress distribution of GFRP RC. Further analysis of bond stresses along the bar clearly suggests that there is no unique bond stress-slip relationship that is independent of bar strain.

Comparisons of average bond stress-slip relationship derived from the tension test and pull-out tests suggest that the pull-out test is never able to accurately represent the bond in the tension specimen. Pull-out tests produced average bond strengths of around 50% higher than the tension tests. It is believed that confinement is another important issue to consider before a unified bond model can be derived.

8.3 Tension stiffening Model

Numerical modelling of the tension stiffening effect based on a strain distribution function to represent strain between cracks was also proposed. The method was found to be very successful in predicting the experimental results. A further enhancement of the model could be achieved by adopting a more accurate model for the bond development length. The current prediction of the bond development length was derived using limited test results of pull-out tests which are not considered to be representative of direct tension. Furthermore the use of average bond strength to define the bond development length during the early stages of loading is bound to underestimate the development length.

8.4 Modelling deflection of flexural elements

It is shown that the ACI 440.1R-03 recommendations underestimate deflections at low reinforcement ratios.

Numerical studies using non-linear finite element analysis (ABAQUS) proved that accurate deflection predictions can be achieved consistently with the proposed tension stiffening model (equation 8-1).

An attempt is also made to develop simplified design equations to predict deflection of flexural elements. A modification to the CEB-FIP model code approach as proposed in equation 8-2 was found to be very effective in predicting deflections, especially at service loads.

$$\Delta = \Delta_2 - (\Delta_2 - \Delta_1)\, 0.5\left(\frac{M_{cr}}{M}\right)^2 \qquad (8\text{-}2)$$

The current research deals only with the instantaneous deflections of GFRP reinforced concrete. It is equally important to study the long term deflections of structures reinforced with FRP materials. Therefore concerted research effort is still required to investigate the long term deflections of structures subjected to sustained loading.

8.5 Recommendation for further work

Although bar diameter has little influence on the results of tension stiffness based on the direct tension tests, it is important to establish how the different bond characteristics of bars influence the tension stiffening. It is also important to look in more detail into the influence of reinforcement ratio on tension stiffening effect like number of bars used to achieve same reinforcement ratio has any significant influence on the tension stiffening effect.

Accurate modelling of bond between concrete and reinforcement has always been challenging for any reinforcement and GFRP is no different. This study fully acknowledges local variation of bond and has come up with a $\tau - s - \varepsilon$ relationship that can express the variation of local bond stress slip relationships. However, Influence of confinement is still a major variable to be included in the model. Therefore further research effort is required to quantify confining pressures and to couple confinement stresses with the $\tau - s - \varepsilon$ relationship to arrive at more generalised solutions for the bond stress slip relationship.

The development of a comprehensive constitutive relationship for bond is still needed. Models like the fracture mechanics based constitutive relationship with evolving failure surface proposed to model stress transfer at discrete cracks, "Normal/Shear cracking model" (Carol et al. 1997) can even be a starting point for more comprehensive accurate modelling of bond between concrete and reinforcements.

It is only the instantaneous tension stiffening effects that are looked at in this experimental and analytical study. It is also important to study the tension stiffening effect in the long term and during and after sustained and cyclic loading conditions.

The effective area around the reinforcement bar that contributes to the tension stiffening effect is another area that needs further examination.

Due to extensive slip and loss of composite action, the conventional frame work for calculation of deflections based on the assumption of plane section remain plane is not suitable for predicting deflections of GFRP RC. Therefore, a new approach that can accommodate the effect of excessive slip in the calculation of deflections is required.

Modelling tension stiffening effect with the use of SDF (Strain Distribution Function) can also benefit from more research into bond development length.

REFERENCES

Abdulla M.F., Thomas C. (1998), "Development of a model for the effective moment of inertia of one-way reinforced concrete elements," ACI Structural Journal, Vol. 95, No. 4, pp. 444-455.

Abdalla H.A. (2003), "Evaluation of Deflection in Concrete Members Reinforced with Fibre Reinforced Polymer (FRP) bars," Composite Structures, Vol.56, pp. 63-71.

Abrishami A.H., Mitchell D. (1996), "Influence of Splitting Cracks on Tension Stiffening." ACI Structural journal, V93, No.6, pp. 703-710

ACI Committee 440 (2003), "Guide for the Design and Construction of Concrete Reinforced with FRP Bars (ACI 440 .1R-03)," American Concrete Institute, Farmington Hill, Michigan, 42 pp.

ACI Committee 318 (2005), "Building Code Requirements for Structural Concrete (ACI 318-05) and Commentary (ACI 318R-05)," American Concrete Institute, Farmington Hills, Michigan, pp. 111-115.

ACI Committee 224 (1992), "Cracking of Concrete Members in Direct Tension (ACI 224.2R-92, Reapproved 1997)," American Concrete Institute, Detroit, 12 pp.

Achillides Z., Pilakoutas K. (2004) Bond behavior of fiber reinforced polymer bars under direct pullout conditions. Journal of Composites for Construction, 8 (2), April, pp. 173-181. I

Achillides Z. (1998), Bond and anchorage of FRP in concrete, PhD Thesis, Department of Civil and Structural Engineering University of Sheffield, 355 pp.

Alsayed S.H., Al-Saloum Y.A., Almusallam T.H. (2000), "Performance of glass fibre reinforced plastic bars as a reinforcing material for concrete structures", Composites: Part B: Engineering, Vol. 31, pp. 555-567.

Alsayed S.H. (1998), "Flexural behaviour of concrete beams reinforced with GFRP bars," Cement and concrete composites, Elsevier Science Ltd., Great Britain, 20, pp.1-11.

American society for testing materials (1985),"Concrete and mineral aggregates," Annual book of ASTM standards, ASTM, Philadelphia, vol. 04.02.

Anderson T.L. (1995), "Fracture Mechanics Fundamentals and Applications," CRC press LLC, USA, 689 pp.

ASCE (1982), "State of art report: Finite element analysis of reinforced concrete, American Society of Civil Engineers," New York, USA, pp. 505.

Al Sunna R. (2006), "Deflection behaviour of FRP reinforced concrete flexural members," PhD thesis, the University of Sheffield, June 2006, pp. 318.

Benmokarane B., Challal O., Masmoudi R, (1995), "Flexural response of concrete beams reinforced with FRP reinforcing bars," ACI Material Journal, Vol. 91, No. 2, pp. 46-55.

Belarbi A., Hsu T.T.C. (1994), "Constitutive laws of concrete in tension and reinforcing bars stiffened by concrete", ACI Structural Journal, Vol. 91, No. 4, pp. 465-473.

Branson D.E. (1977), "Deformation of concrete structures,"McGraw-Hill, New York.

British Standard Institute (2001), "BS 8110: Part I and Part II -Structural use concrete", BSI, London,

Carol I., Pere C.P., and Carols M.L. (1997), "Normal/Shear cracking model: Application to discrete crack analysis," Journal of Engineering Mechanics, V.123, No.8, pp. 765-773.

CEB (1978), "CEB-FIP Model Code for Concrete Structures," Comite Euro–International du Beton and Federation Internale de la Precontrainte, CEB, 348 pp.

CEB (1993), "CEB-FIP Model Code 90," Thomas Telford, London, 437 pp.

Choi C.K., Cheung S.H. (1995), "Tension stiffening model for planar reinforced concrete members", Computer and Structures, Elsevier Science Ltd., Vol. 59, No.1. pp. 179-190.

Chan H.C., Cheung Y.K., Huagn Y.P. (1993), "Crack Analysis of Reinforced concrete Tension Members", Journal of Structural Engineer, ASCE, Vol 118, No.8, pp. 2118-213

Comite Euro-International du Beton (CEB), (1983), CEB design manual on Cracking and Deformations, Swiss federal institute of Technology (EPFL), Lausanne, pp. 3.1-3.84

Cosenza E., Manfredi G., Realfonzo R. (1995), "Analytical modelling of bond between FRP reinforcing bars and concrete", Proceeding of the Second International RILEM Symppsium(FRPRCS-2), Ghent 23-25 August1995, edited by L. Taerwe, E & FN Spoon, London, pp 164-171.

Craig R.M., Razikalla, S.H., Tadros G., Benmokarane B.(1998), "Flexural behaviour of one- Way concrete slabs Reinforced by Fibre reinforced plastic reinforcements", ACI Structural Journal, pp. 353-365.

Dejke V., Tepfers R. (2001), "Durability and service life predication of GFRP for concrete reinforcement. FRPRC-5, Thomas Telford, London, pp. 505-514.

Dejke V. (2001), "Durability of FRP reinforcement in concrete" Department of building material, Chalmers University of Technology, Goteborg, Sweden, 211 pp.

Eurocrete Project (1997), "The development of non-ferrous reinforcement for concrete structures- final report," Prepared by Euro-Project (LTTC) ltd, 109 pp.

CEN (2004), "Eurocode 2: Design of concrete structures- Part 1-1: General rules and rules for buildings", Ref. No. EN 1992-1-1:2004, Comite Europeen de Normalisation, Brussels, 225 pp.

Favre R., Carif H. (1994), "Basic model and simplified calculations of deformations according to CEB-FIP model code 1990," ACI Structural Journal, pp. 169-177.

Federal Highway Administration (1997), "The Status of the Na-tion's Highway Bridges: Highway Bridge Replacement and Rehabilitation Program and National Bridge Inventory," Thirteenth Report to the United States Congress, Washington D.C.

Federation International de la Precontrainte (*fip*) (2000), State-of-art report: Bulletin 10: Bond of Reinforcement in Concrete, fib, Lausanne, 422 pp.

Floegl H., Mang A.H. (1982), "Tension stiffening concept based on bond slip", Journal of the structural Division, ASCE, Vol 108, No.ST12,pp. 2681-2699.

Foote R.M.L., Mai Y.W., Cotterell B. (1986), "Crack growth resistance curves in strain-softening materials," Journal of Mechanics Physics and Solids, Pergamon Journals Ltd., Vol34, No.6, pp 593.-607

Goto Y. (1971), "Cracks formed in concrete around deformed tension bars," ACI journal, Vol. 68, No. 4, April 1971, pp. 244-251.

Gere M.J., Timoshenko S.P. (1991), "Mechanics of Material",3rd Edition, Chapman and Hall, London, 807 pp.

Gerstle W., Ingraffera A.R., Gergely P. (1978) "Tension stiffening: Fracture mechanics approach", bond in concrete, London (UK), applied science publishers, pp. 97-106.

Gupta A.K., Maestini S.R. (1990), "Tension Stiffening model for reinforced concrete bars", Journal of Structural Engineer, ASCE, Vol 116, No. 3, pp. 769-790.

Gdoutos E.E, Pilakoutas K., Rodopoulos C.A. (2000), "Failure Analysis of Industrial Composite Material", McGraw-Hill, New York, USA, pp. 449-498.

Guadagnini M. (2002), "Shear behaviour and design of FRP RC beams," PhD thesis, the University of Sheffield, February 2002, 344 pp.

Hanselman D., Littlefield B. (2001), Mastering MATLAB 6, Prentice Hall, Inc., New Jersey, 744 pp.

Hillerborg A. (1983), "Analysis of one single crack", Fracture mechanics of concrete Edited by Wittmann FH., Elsevier Science Publishers, pp. 225-249.

Habbitt, karlsson and Sorensen, inc. (2001), ABAQUS User manual, Pawtucket, USA

Hsu T.T.C (1988), "Softened Truss Model Theory for Shear and Torsion," American Concrete Institute Structural Journal, Vol. 85, (6), pp. 624-634.

Hughes Brothers, Inc. (2003), USA, 27 Jan 2003, http://hughesbors.com.

Hyo-Gyoung Kwak, Jong-Young Song (2002), Cracking analysis of RC members using polynomial function", Engineering Structures, Elsevier Science Ltd, 24, pp. 455-468.

ISIS (2001), "Reinforcing Concrete Structures with Fibre Reinforced Polymers", Design Manual No. 3, Canadian Network of Centres of Excellence on Intelligent Sensing for Innovative Structures, Winnipeg, 158 pp.

JSCE (1997), "Recommendation for design and construction of concrete structures using continuous fibre reinforcing materials", Japan Society of Civil Engineers, October 1997

Kankam C.K. (1997), "Relationship of bond stress, Steel stress and slip in reinforced concrete", Journal of Structural Engineering, ASCE, Vol.123, No. 1, pp. 79-85.

Literland K.L., Oakley D.R., Proctor B.A. (1981), "The use of accelerated ageing procedure to predict the long term strength of GRC composites", Cement and Concrete Research –An International Journal, Vol. 11, No3, pp. 455-466.

Maekawa K., Pimanmas A., Okamura H. (2003), "Nonlinear Mechanics of Reinforced Concrete," Spon Press, London, 713 pp.

Kotsovos M.D. (1988), "Compressive force path concept: Basis for reinforce concrete ultimate limit state design", ACI Structural Journal, pp. 68-75.

Mirza S.M., Houde J. (1979), "Study of bond stress-slip relationships in reinforced concrete", ACI journal, January issue, pp. 19-46.

Ngo D., Scordelis A.C. (1967), "Finite element analysis of reinforced concrete beams", ACI journal. Vol 64, pp.152-163

Nilson A.H. (1968), "Non-Linear analysis of Reinforced concrete by Finite element method," ACI Journal, pp. 757-766

Nilson A.H. (1972), "Internal measurement of bond slip," ACI journal, Vol. 69, No. 7, July 1972, pp 439-441.

Neville A.M. (1996), "Properties of concrete", John Wiley & Sons, 4th edition, 844 pp.

Okamuna H., Maekawa K. (1991), Nonlinear Analysis and Constitutive Models of Reinforced Concrete, ,Tokyo, 182 pp.

Ouyang C., Mobasher B., Shah S.P. (1990), "An R-Curve approach for fracture of quasi brittle materials", Engineering Fracture Mechanics," Pergamon Press Plc., Vol.37, No. 4, pp. 901-913

Ouyang C., Shah S.P. (1991), "Geometry Dependent R-curve for quasi –brittle materials", Journal of American Ceramic society, 74(11), pp. 2831-2836.

Ouyang C., Shah S.P. (1994), "Fracture energy approach for predicting cracking of reinforced concrete tensile members", ACI Structural Journal, V91, No.1, pp. 69-78

Ouyang C., Wollrab E., Kulkarni M., Shah S.P. (1997), "Prediction of cracking response of Reinforcement concrete tensile member", Journal of Structural Engineering, ASCE, pp. 70-78.

Pang D., Hsu T.T.C. (1996), "Fixed angle softening truss model for reinforced concrete", ACI Structural Journal, V93, No2, pp.197-207

Pecce M., Manfredi G., Cosneza E. (2001), "Experimenal response and code models of GFRP RC beam in bending," Journal of Composite for Construction, Vol 4, No.4, ASCE, pp. 182-190.

Pilakoutas K., Guadagnini M., and Waldron P. (2001), "Design Philosophy for the Design of FRP RC Elements", The International Workshop on Structural Composites for Infrastructure Applications, Cairo, Egypt, The Arab Contractors Printing Company, pp. 275-291.

Rashid Y.R. (1968), "Analysis of pre-stressed concrete pressure vessels," Nuclear Engineering design, pp. 334-344

RILEM committee on fracture mechanics of concrete (1990), "Determination of Fracture parameters of plain concrete using Three point bending tests," Materrial and Structures, Research and testing , RILEM, Paris, V.23, 1990, pp. 457-460

Saint-Gbina Weber Ltd. (2003), "Product Manual: Epoxy plus: Thixotropic Anchor Grout (EPTAG)", Bedford, UK, pp. 2.100.

Shah S.P., Swartz S.E., Barr B. (1989), "Fracture of concrete and rock, recent development," Elsevier Applied Science, London,

Somayaji S., Shah S.P. (1981), "Bond stress versus slip relationship and cracking response of tension members," ACI Journal, pp. 217-225.

Sooriyaarachchi H., Pilakoutas K., Byars E. (2005). "Tension stiffening behaviour of GRP-reinforced concrete," 7th International Symposium for Fibre-Reinforced Polymer (FRP) Reinforcement for Concrete Structures – FRPRCS7, Shield et al. ed, American Concrete Institute SP-230, pp. 975-989

Tada H. (1985), "The stress analysis of cracks hand book", Paris Production Corporation, Missouri

Tighiourt B., Benmokrane B., Gao D. (1998), "Investigation of bond in concrete members with fibre reinforced polymer(FRP) bars", Construction and Building Materials, Elsevier Science Ltd., 12, pp. 453-462.

TMR "Development of Guidelines for the Design of Concrete Structures, Reinforced, Prestressed or Strengthened with Advanced Composites (ConFibreCrete)", Training and Mobility of Researchers, Research Network TMR "ConFibreCrete", http://www.shef.ac.uk/~tmrnet

Toutanji H., Deng Y. (2003), "Deflection and Crack Width Prediction of Concrete Beams Reinforced with Glass FRP Rods," Construction and Building Materials, Vol. 17, pp. 69-74.

Vecchio F.J., Collins M.P. (1986), "The modified compression field theory for reinforced concrete elements subjected to shear," American Concrete Institute Journal, Vol. 83, No.2., pp. 219- 231.

Vijay P.V., GangaRao V.S. (2001), "Accelerated and natural weathering of glass fibre reinforced plastic bars. Fibre Reinforced Polymer Reinforcement for Concrete Structures," SP-188-53, Detroit, American Concrete Institute, pp 605-613.

Wollrab E., Kullarni S.M., Ouyang C., Shah S.P. (1996), "Resoponse of reinforced concrete panels under uniaxial tension", ACI Structural Journal, V.93, No6, pp. 648-657.

Yang S., Chen J. (1988), "Bond slip and crack width calculations of tension members", ACI Structural Journal, July-August issue, pp. 414-422.

Zhao W., Pilakoutas K., Waldron P. (1997), "FRP reinforced concrete: calculations for deflections," In Third International Symposium on Non-metallic (FRP) Reinforcement for Concrete Structures, Japan Concrete Institute, Sapporo, Japan, Vol. 2, October 1997, pp. 511-518.

Zhao W. (1999), "Cracking and Deformation of FRP RC Elements," PhD Thesis, The Department of Civil and Structural Engineering, The University of Sheffield, 236 pp.

APPENDIX I

EXPERIMENTAL RESULTS OF TENSION TEST

Experimental results of C90/13/150

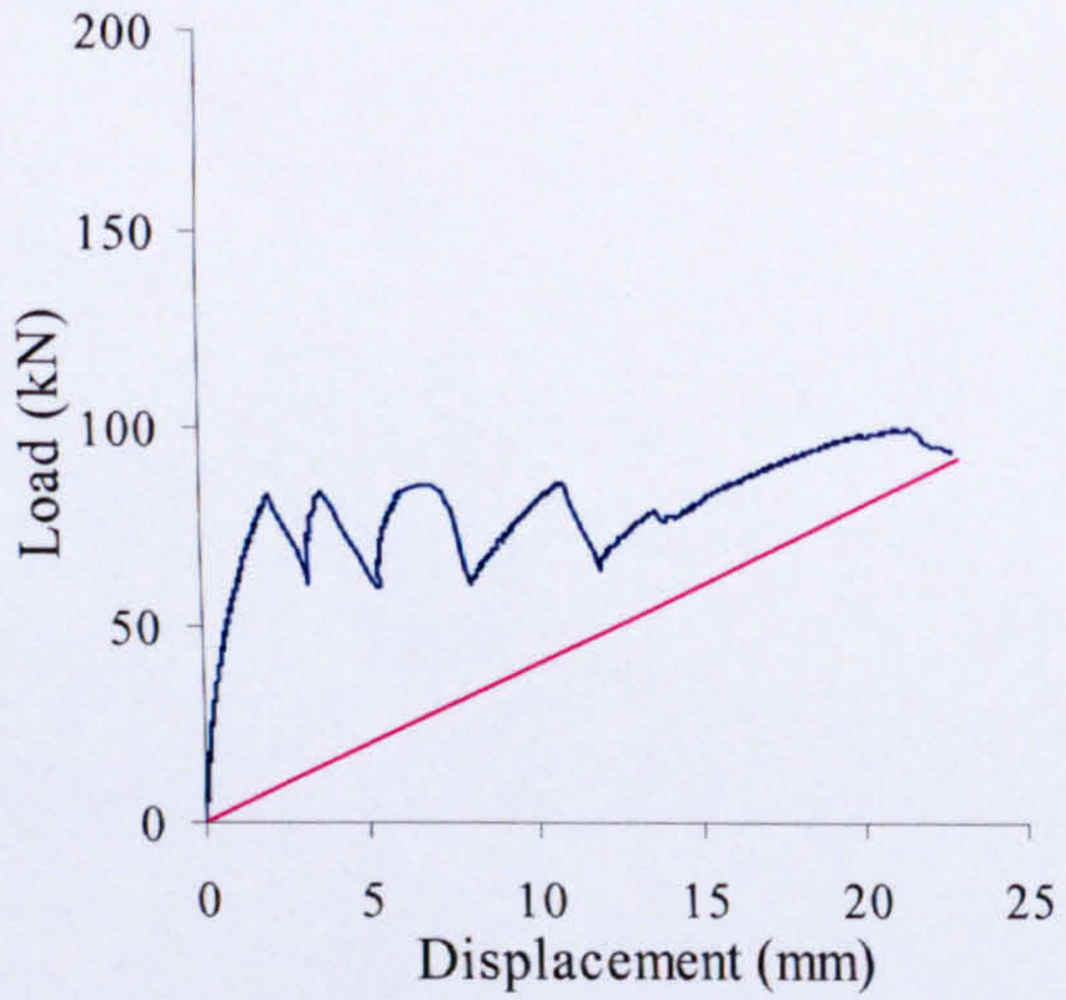

(a) Force displacement relationship

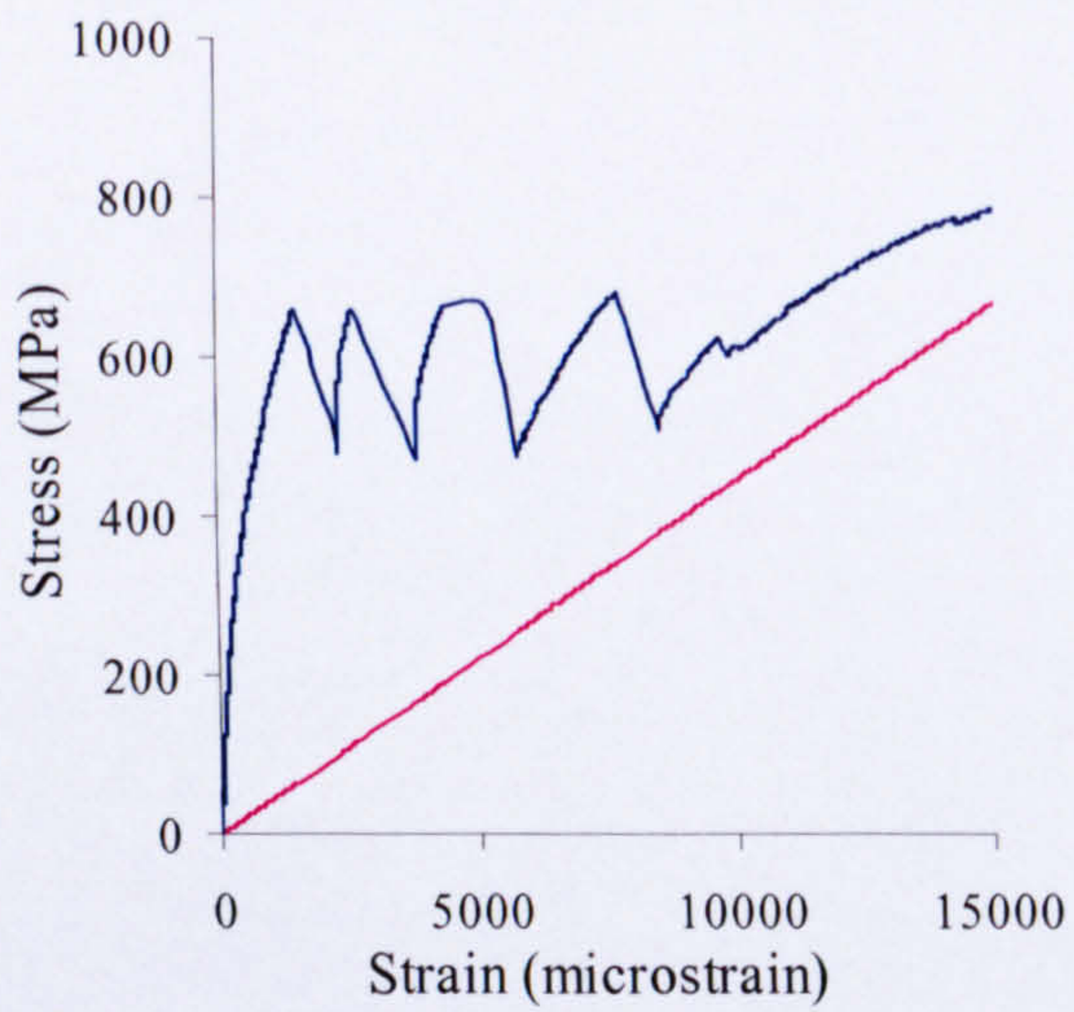

(b) Bar stress at crack section Vs total strain

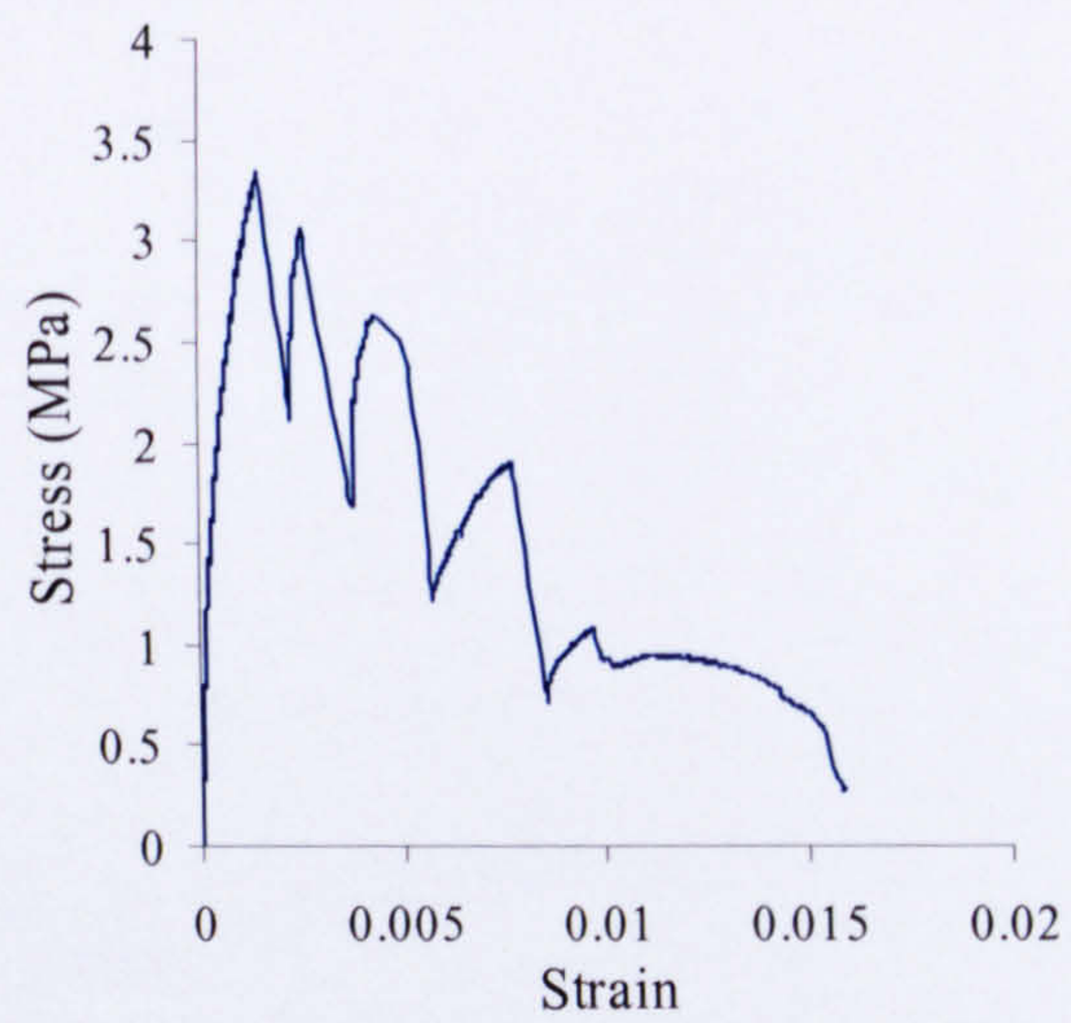

(c) Tension softening response of concrete

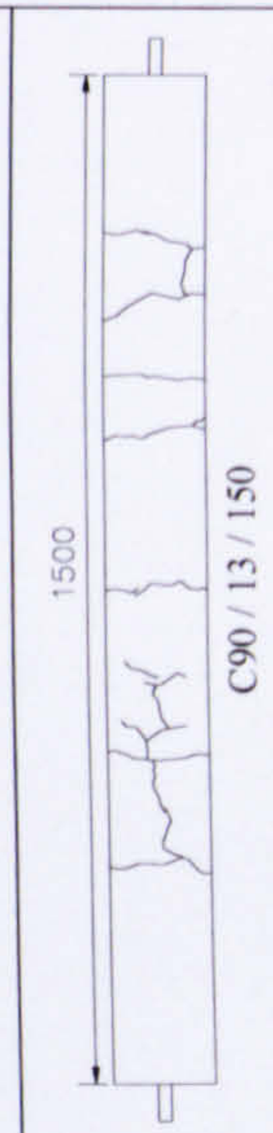

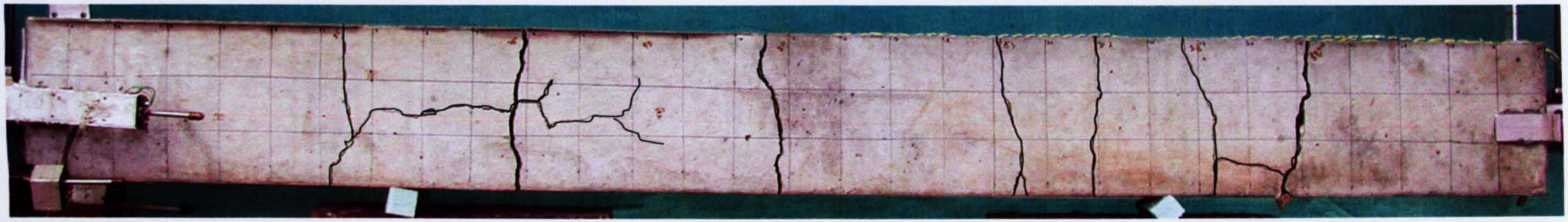

(a) Crack pattern of tested specimen

Experimental results of C50/13/150

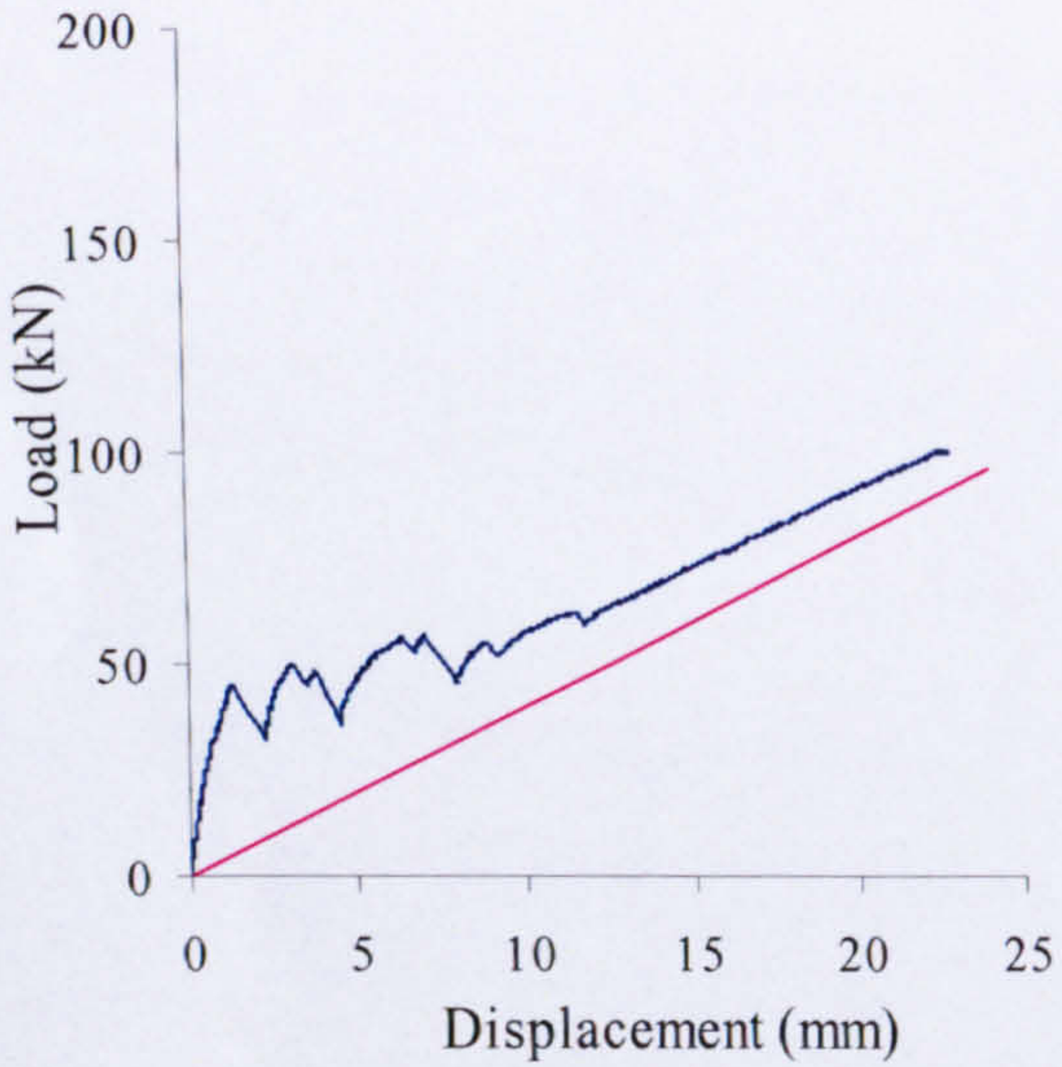

(a) Force displacement relationship

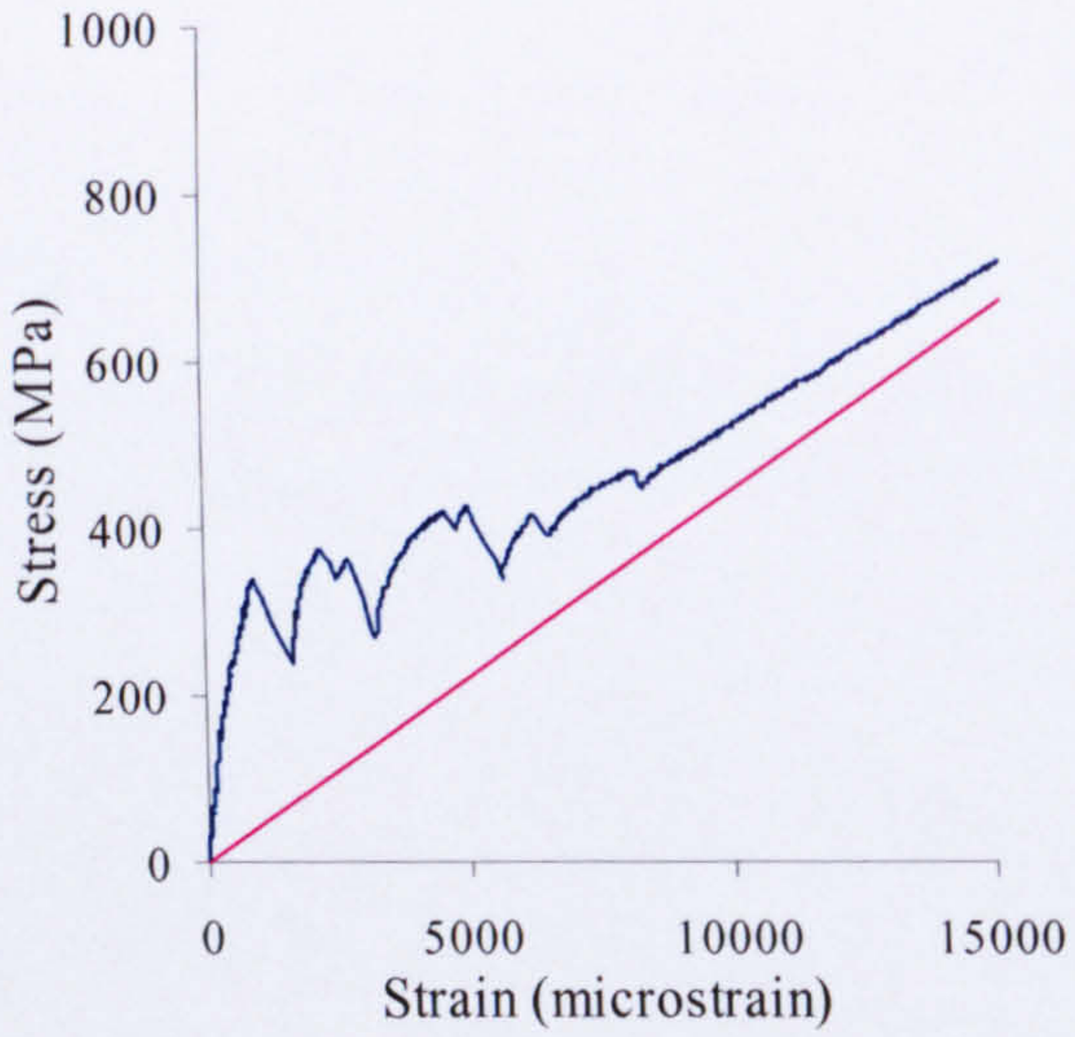

(b) Bar stress at crack section Vs total strain

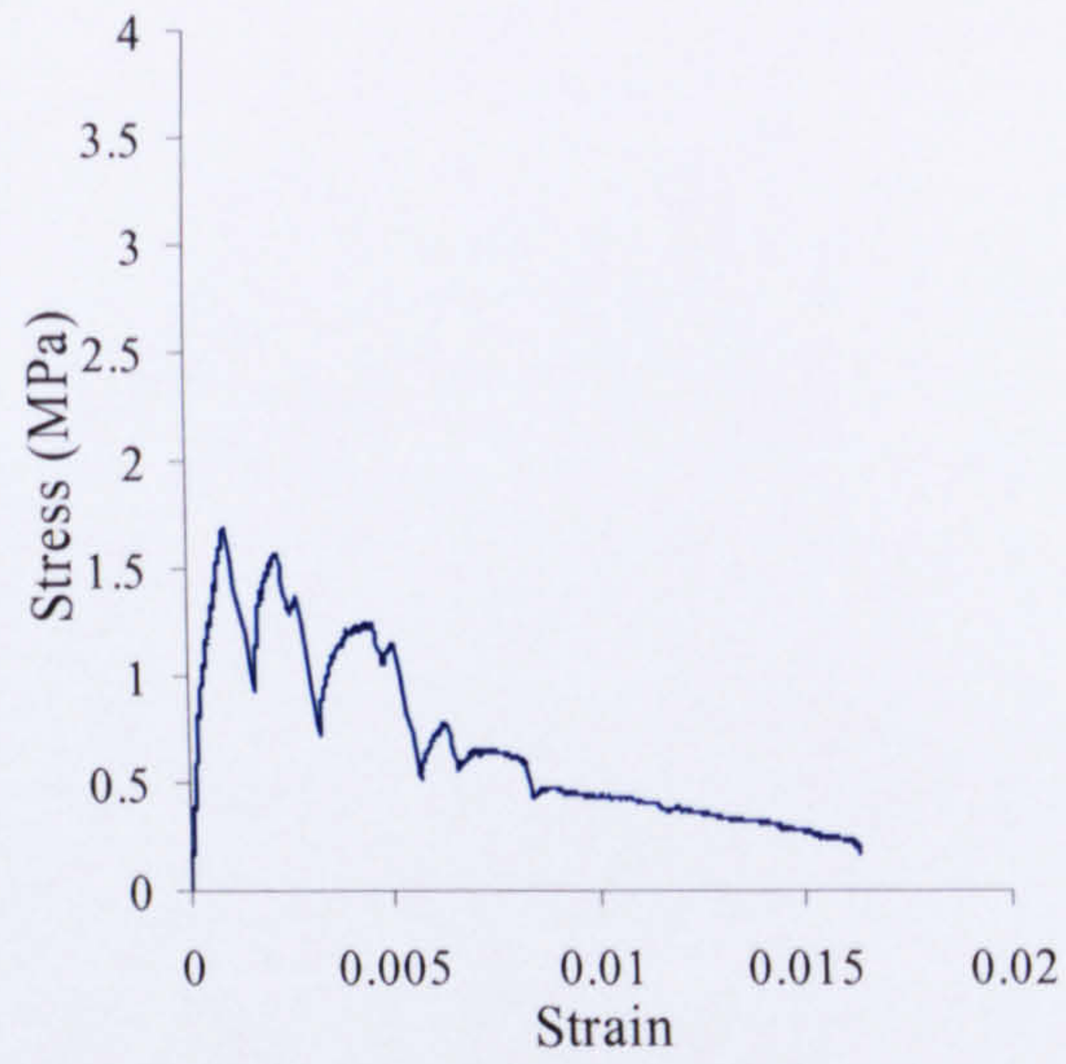

(c) Tension softening response of concrete

(a) Crack pattern of tested specimen

Experimental results of C90/19/150

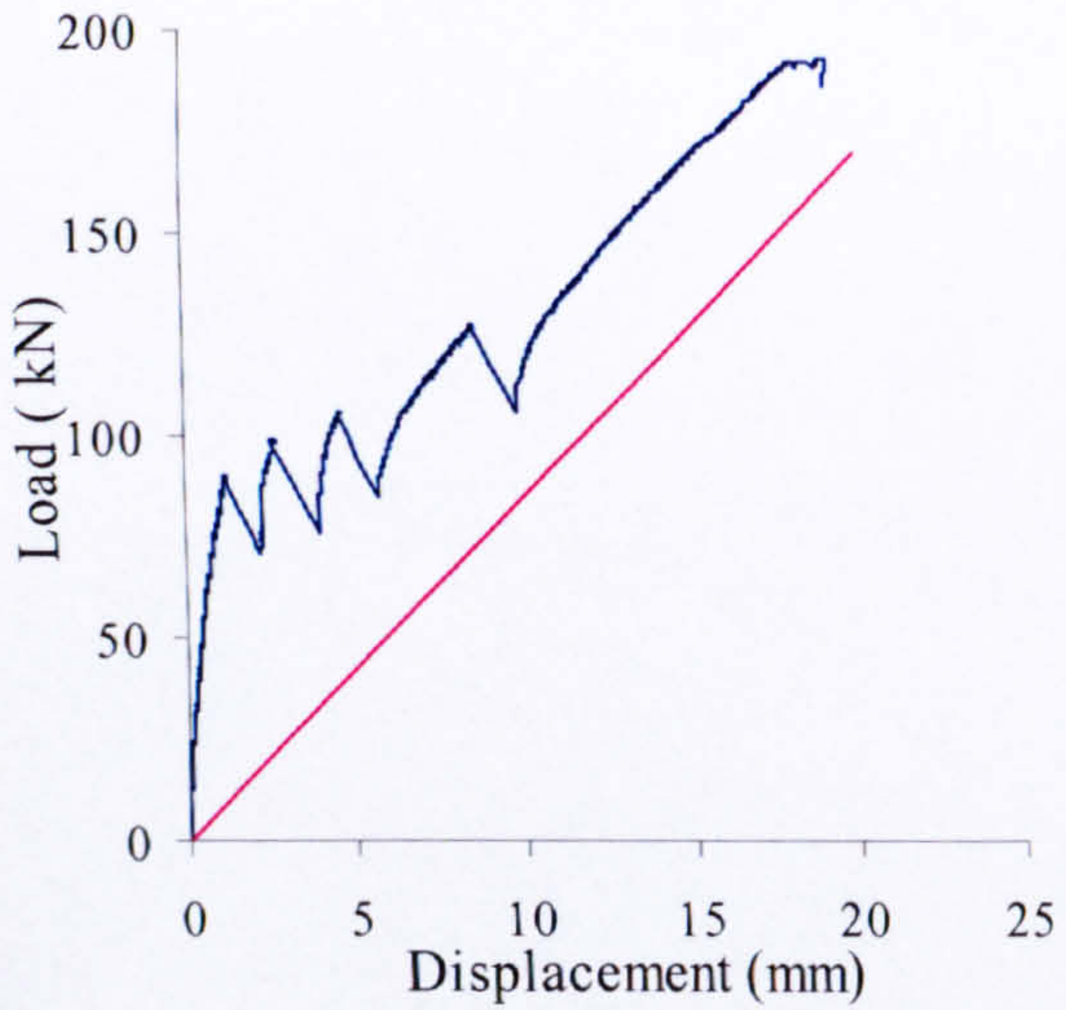

(a) Force displacement relationship

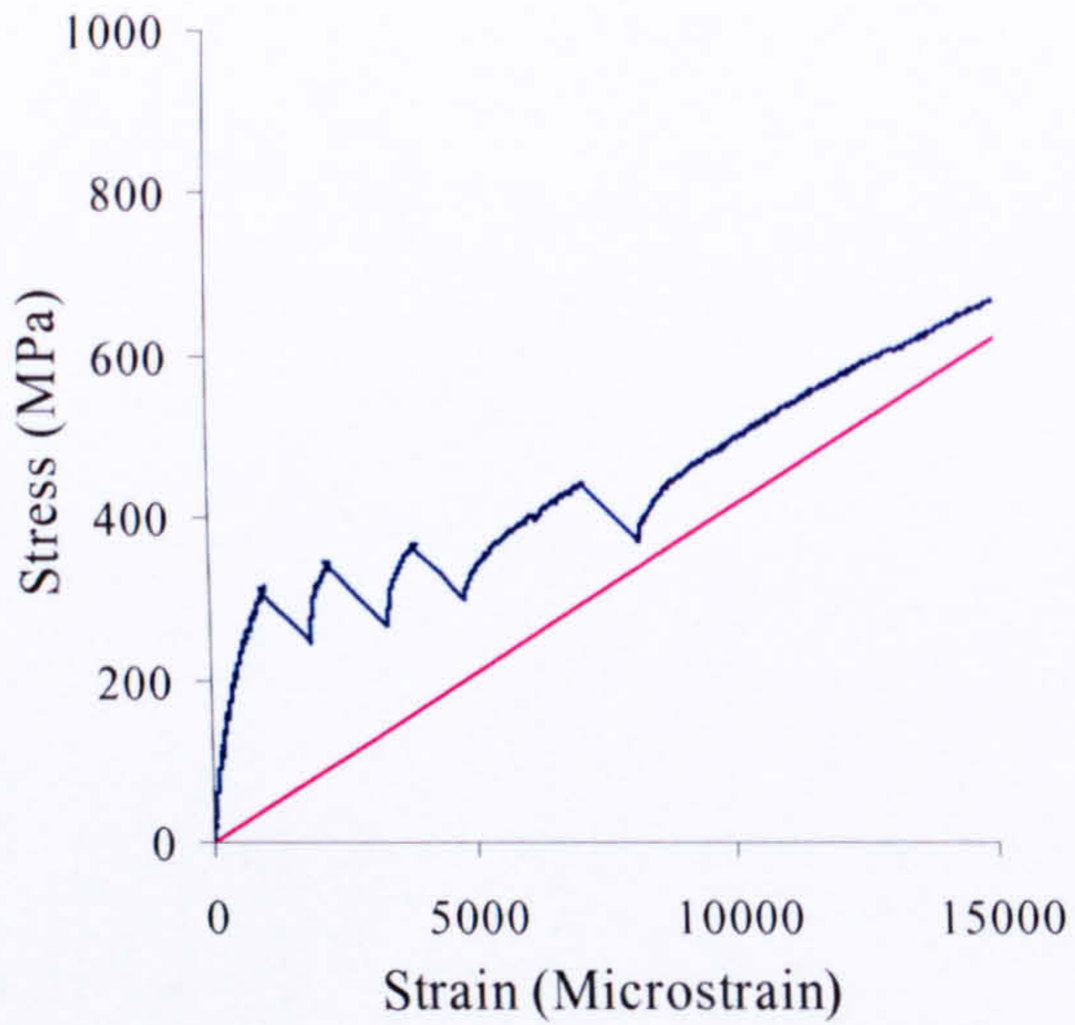

(b) Bar stress at crack section Vs total strain

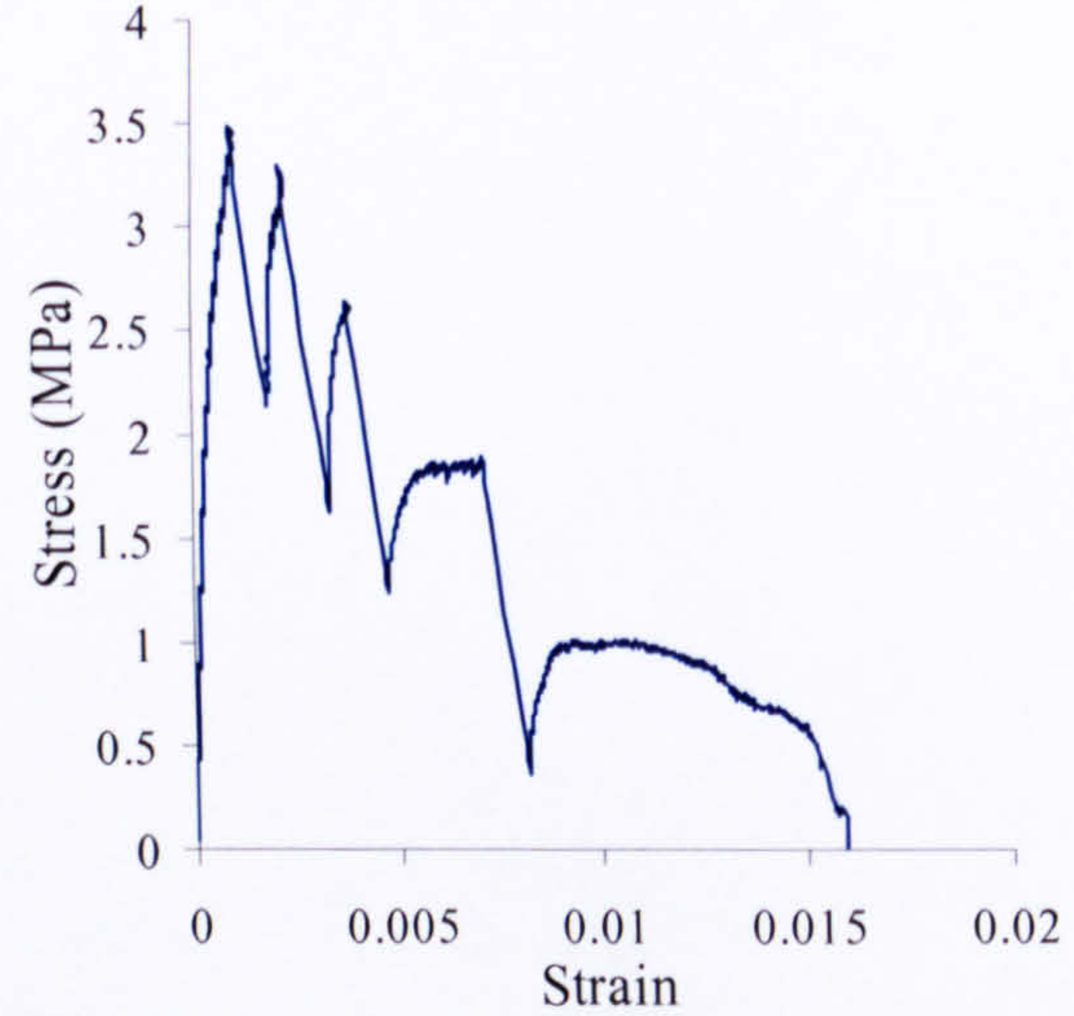

(c) Tension softening response of concrete

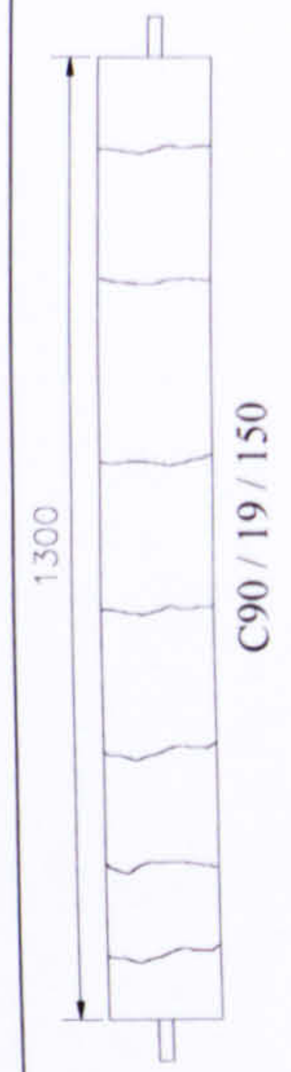

Experimental results of C50/19/150

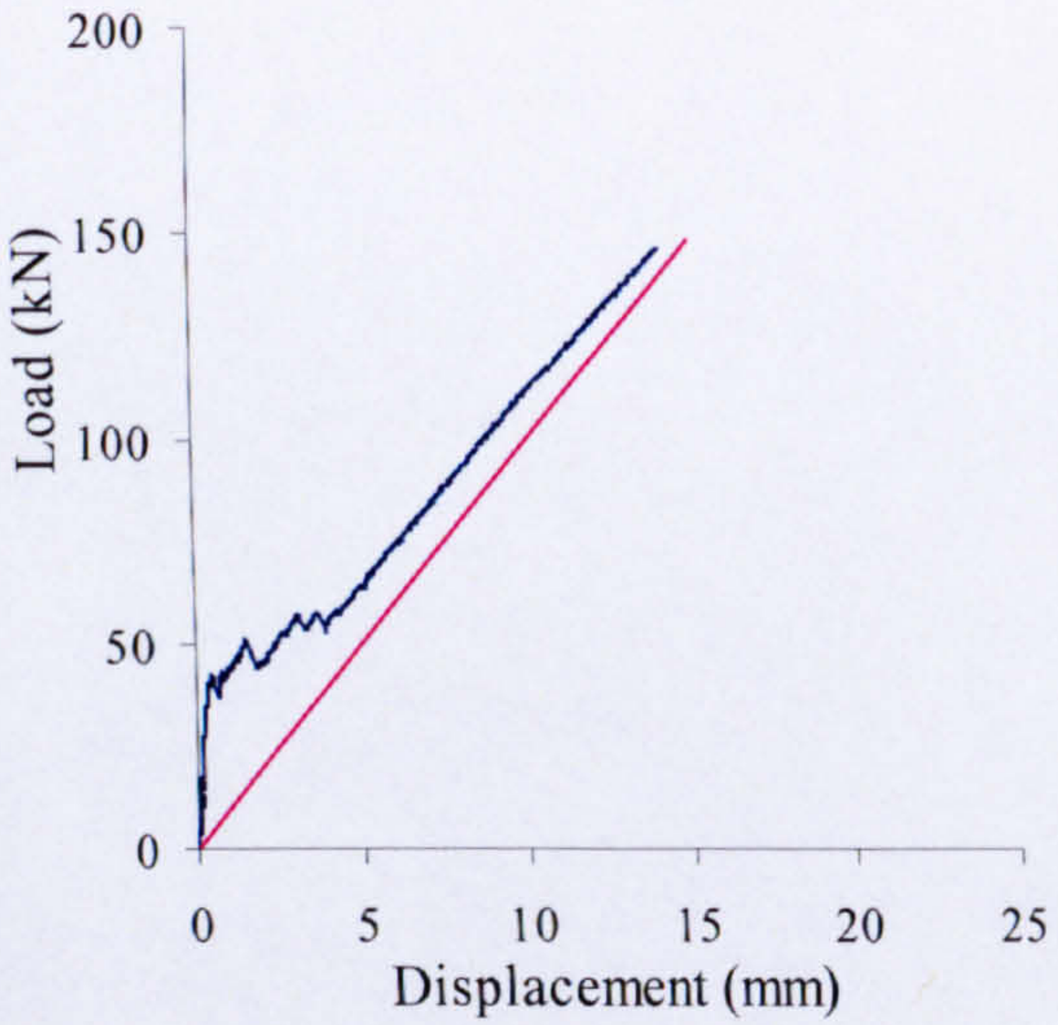

(a) Force displacement relationship

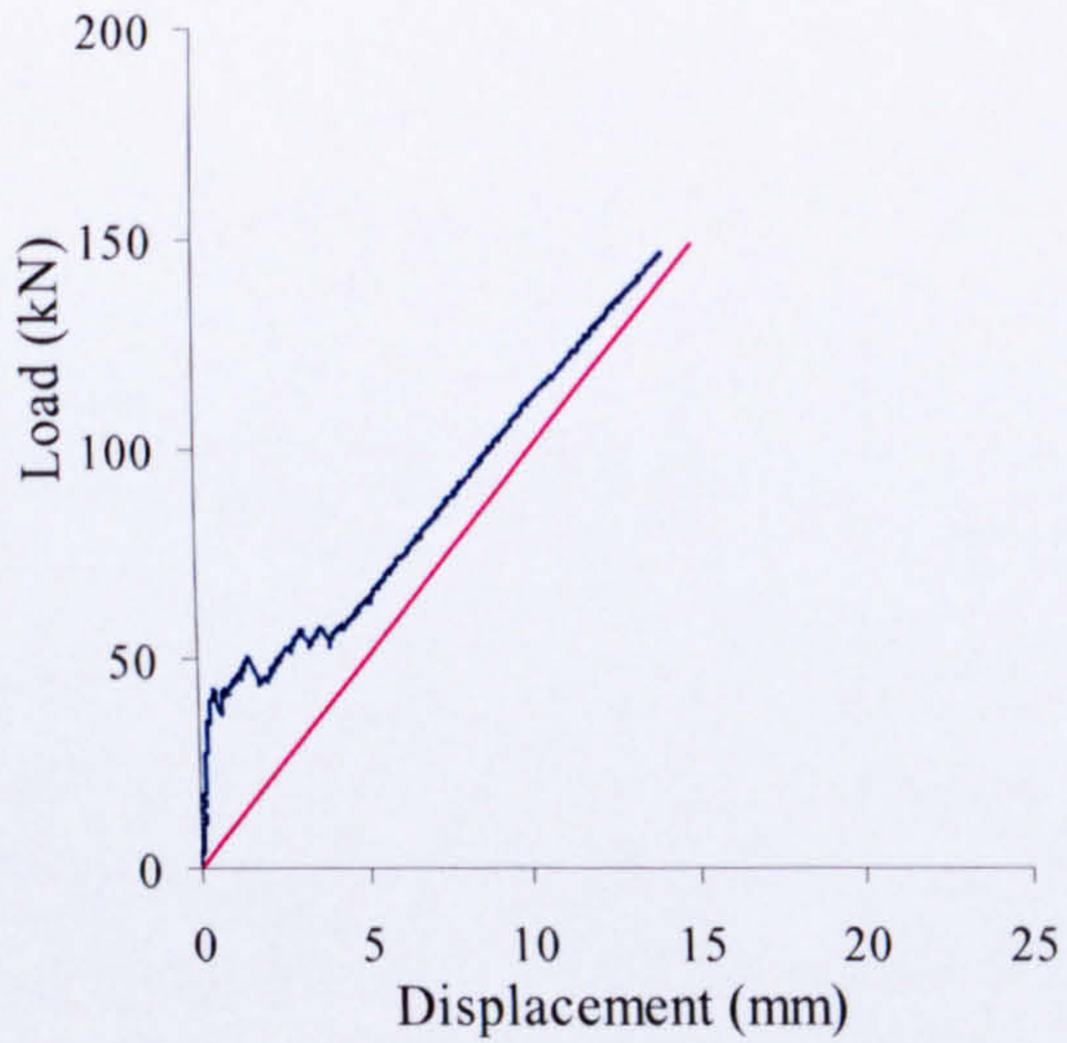

(b) Bar stress at crack section Vs total strain

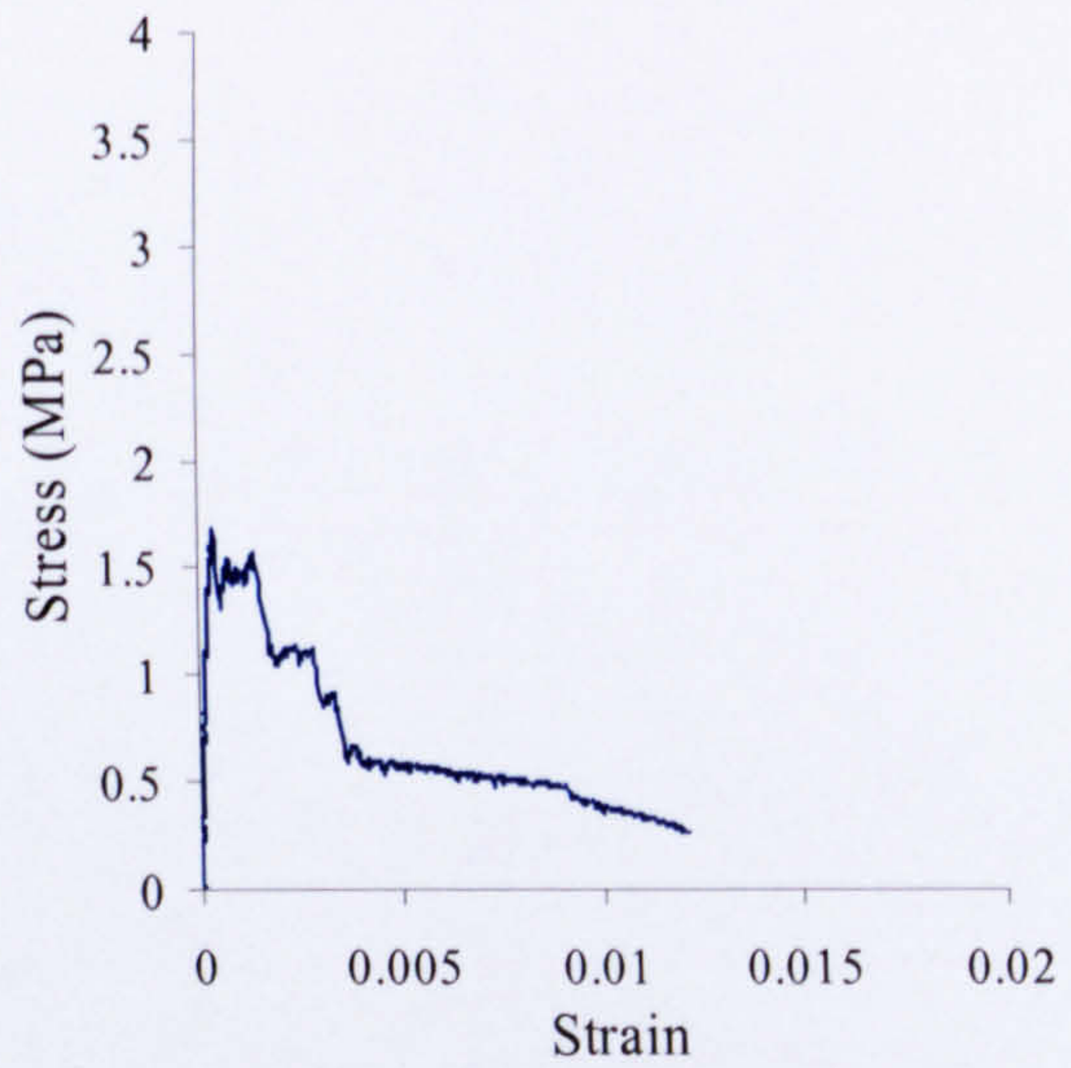

(c) Tension softening response of concrete

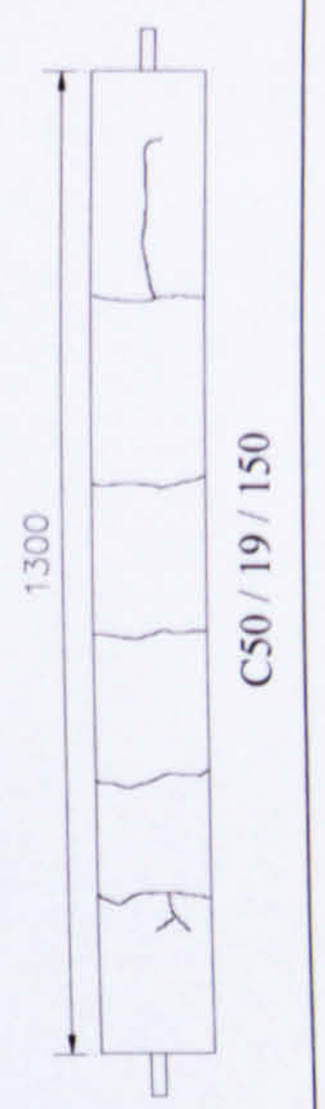

Experimental results of C50/13/100

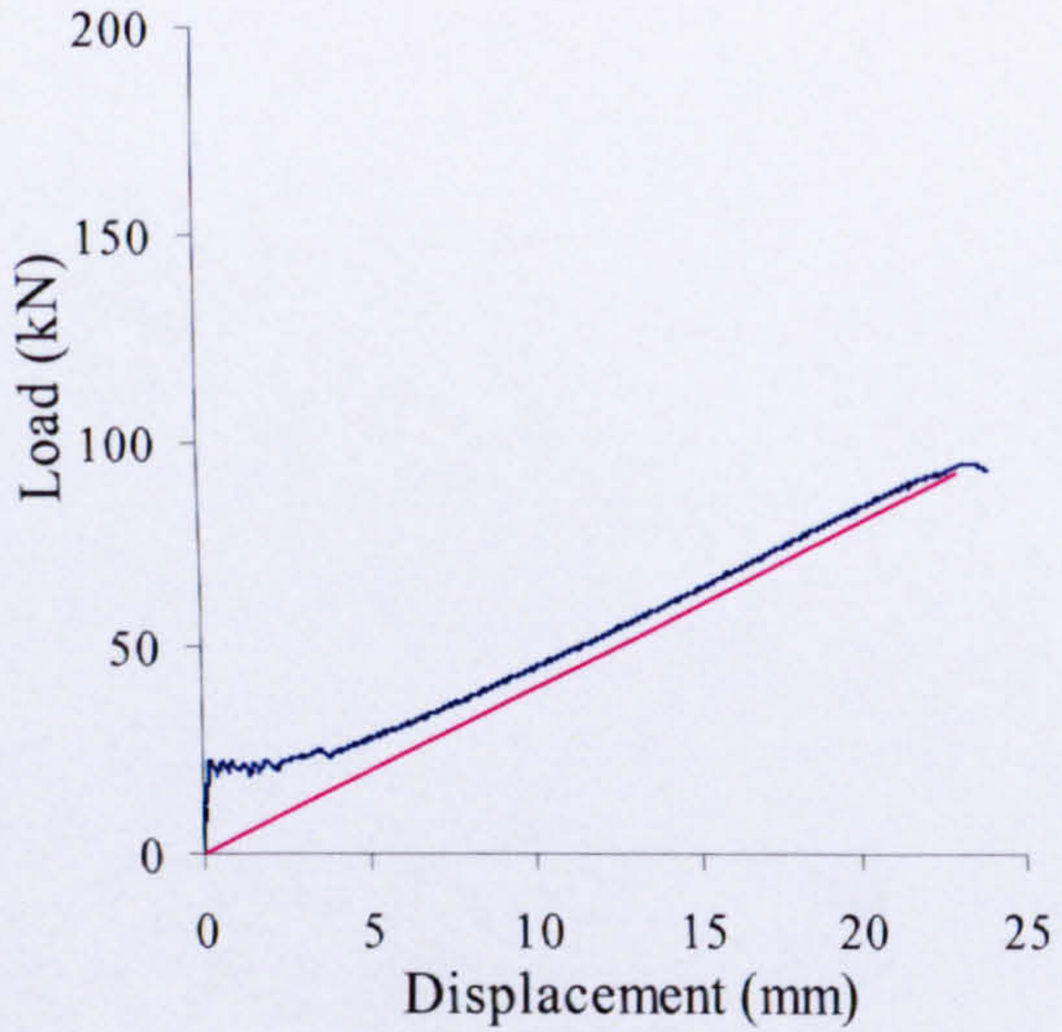

(a) Force displacement relationship

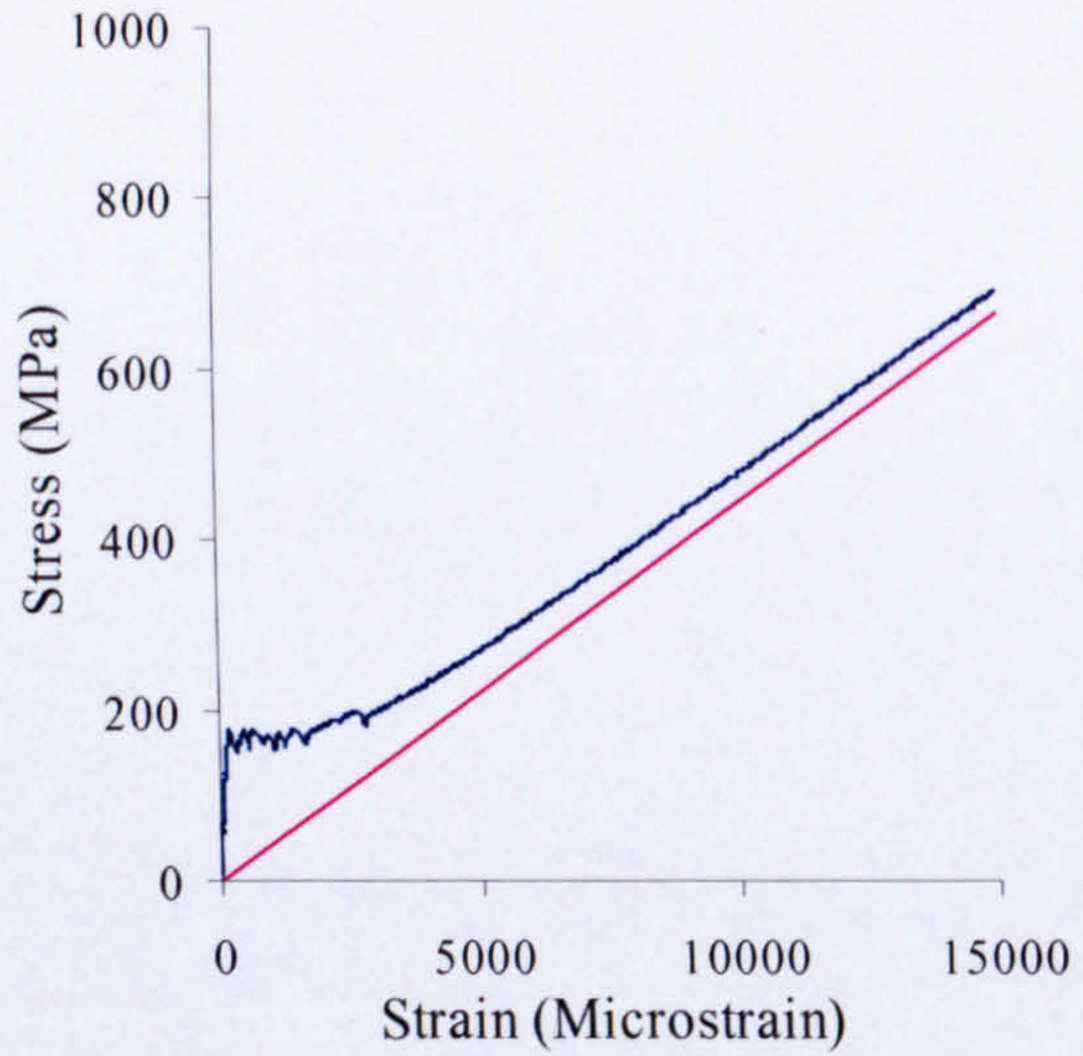

(b) Bar stress at crack section Vs total strain

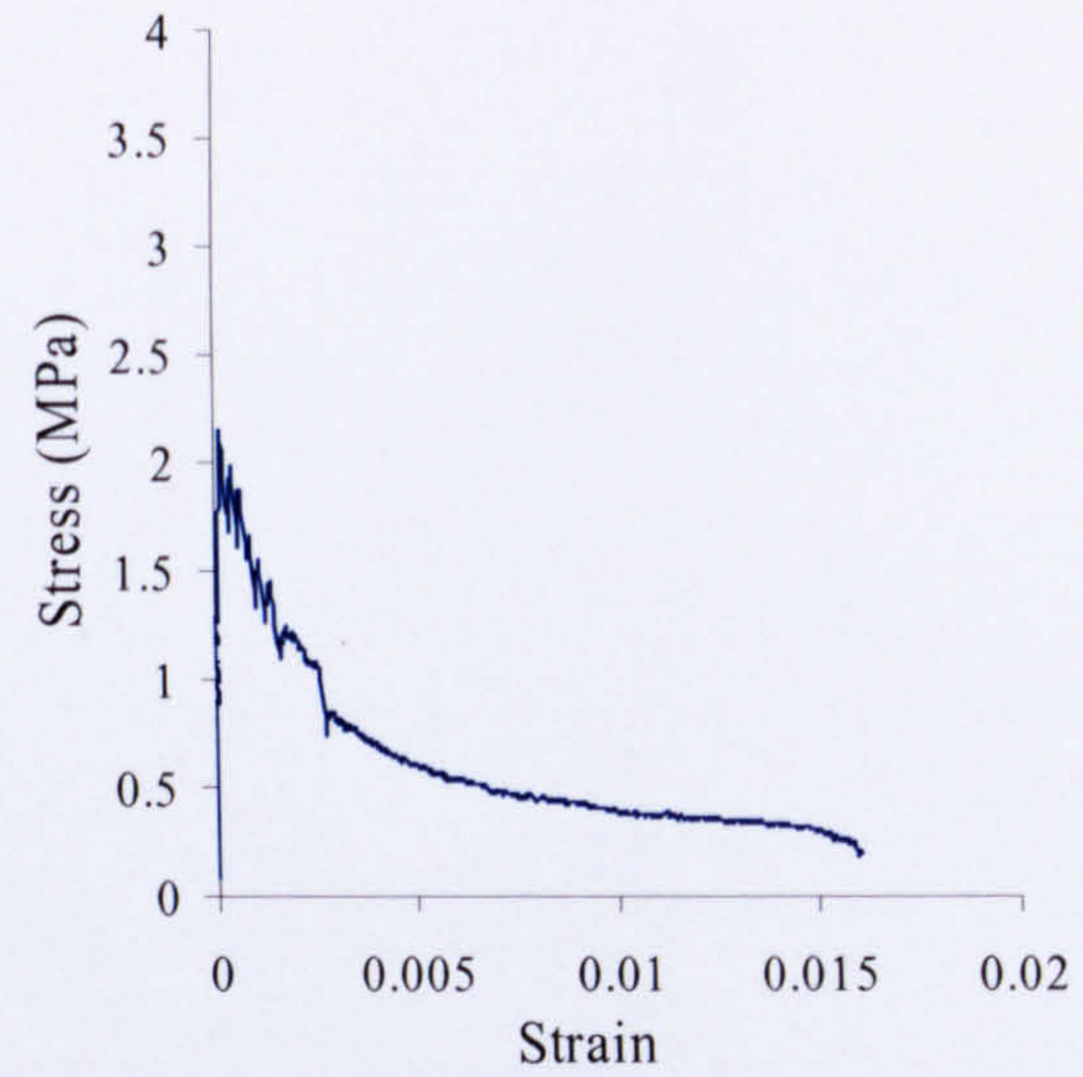

(c) Tension softening response of concrete

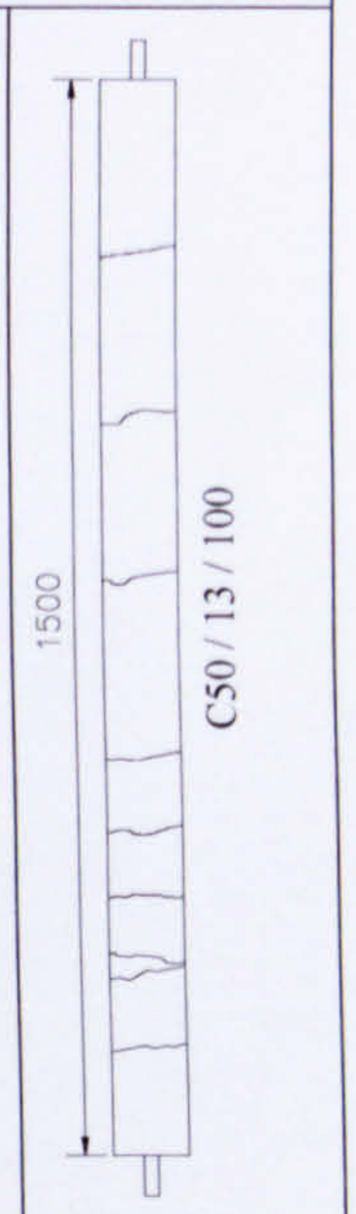

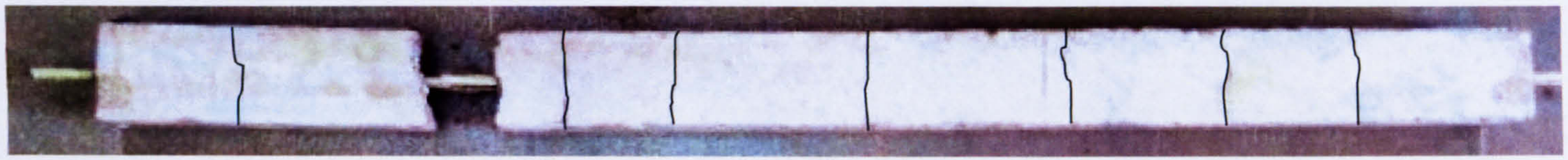

(a) Crack pattern of tested specimen

Experimental results of C90/13/100

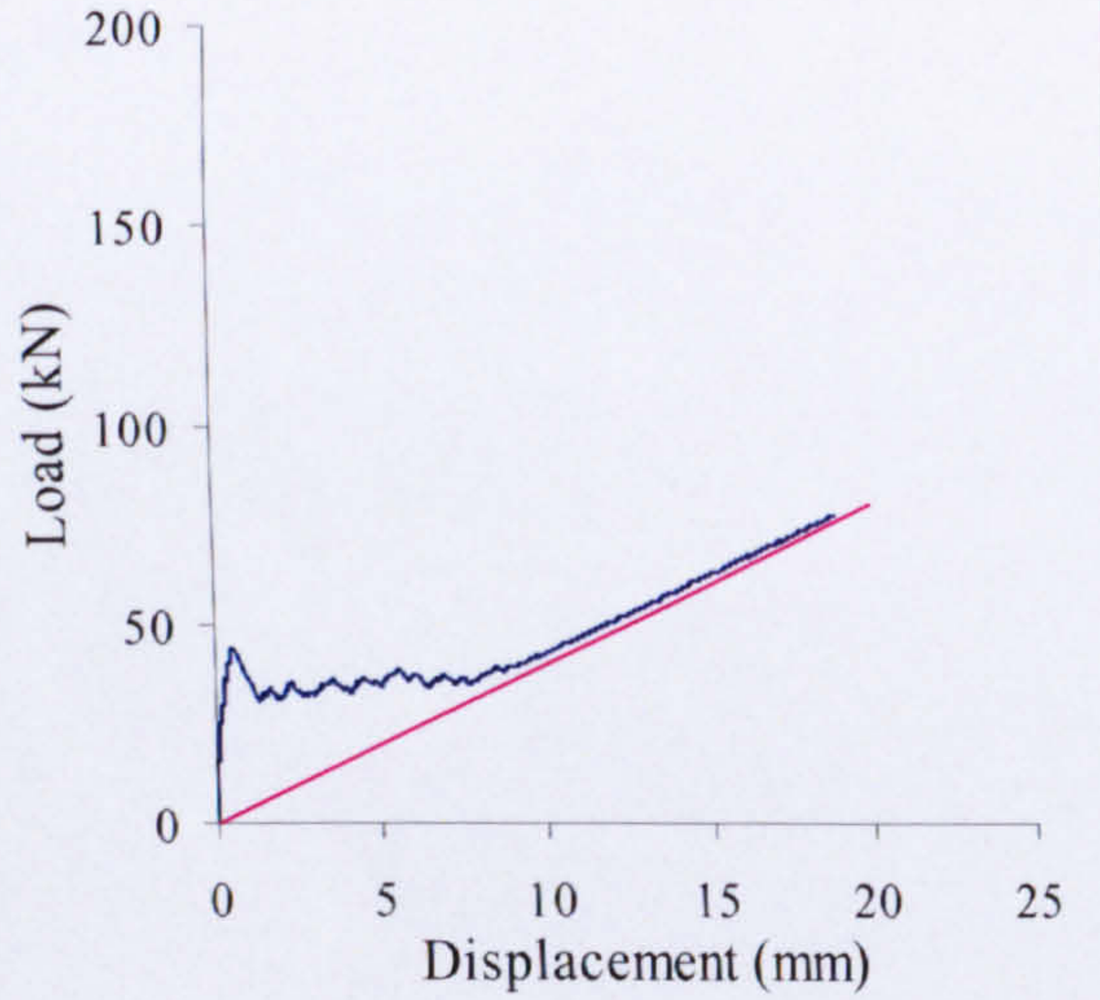

(a) Force displacement relationship

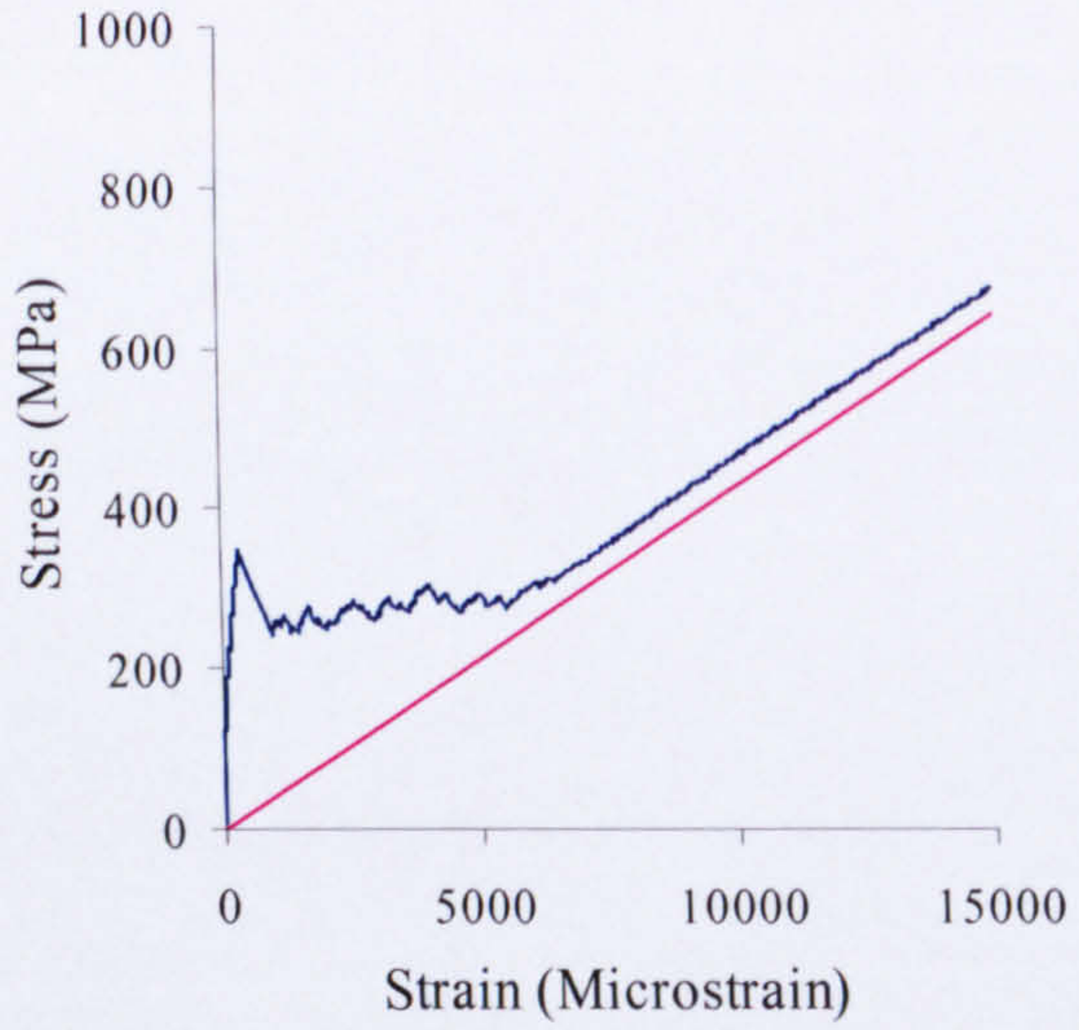

(b) Bar stress at crack section Vs total strain

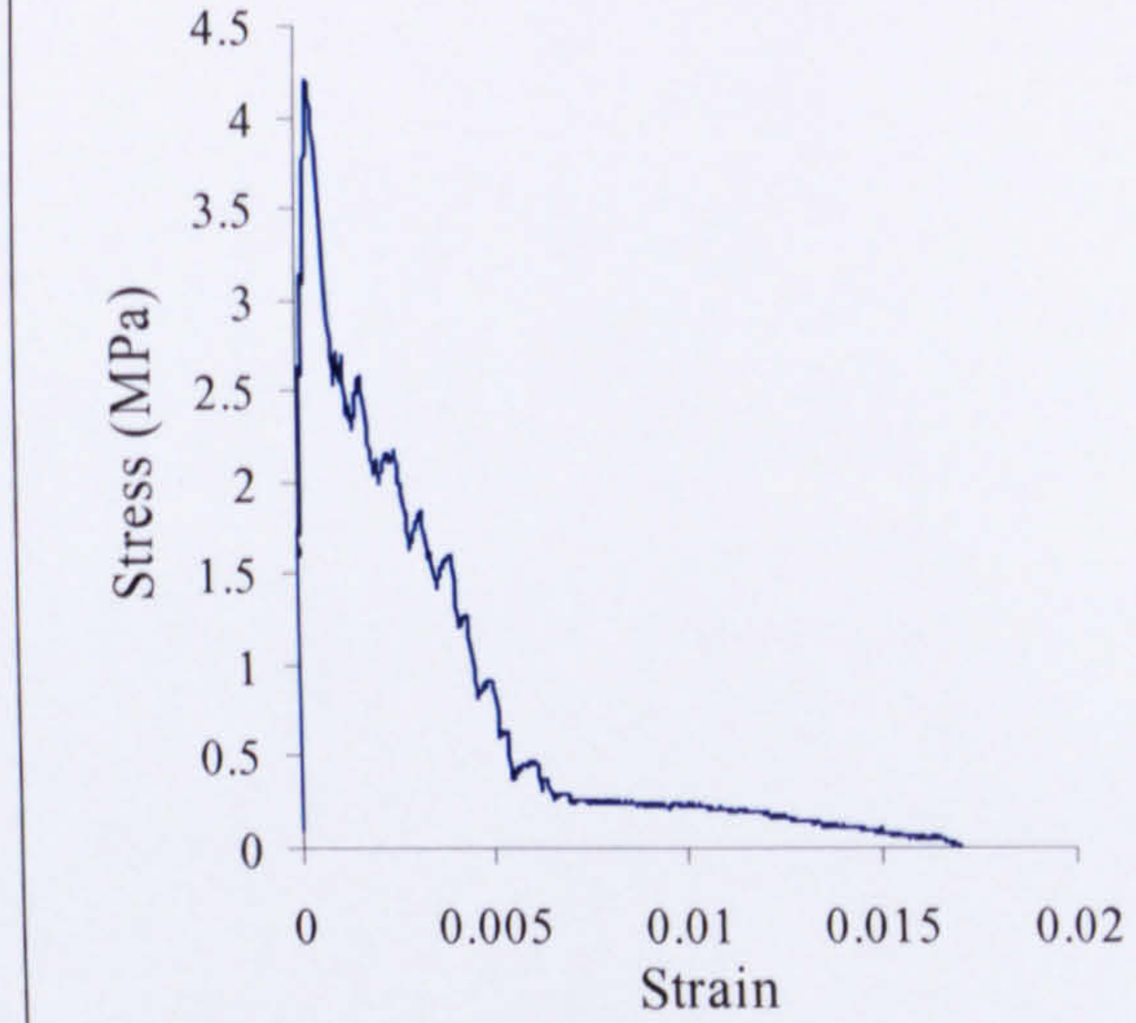

(c) Tension softening response of concrete

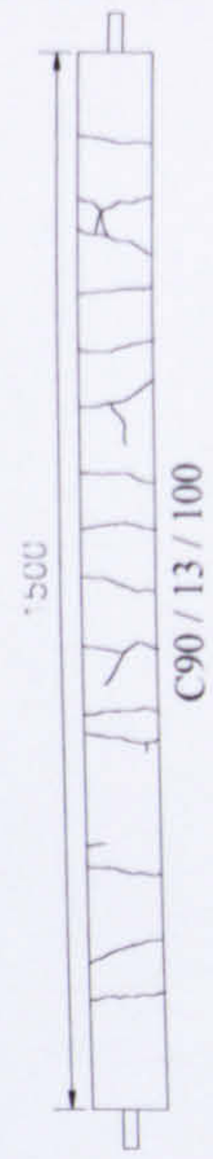

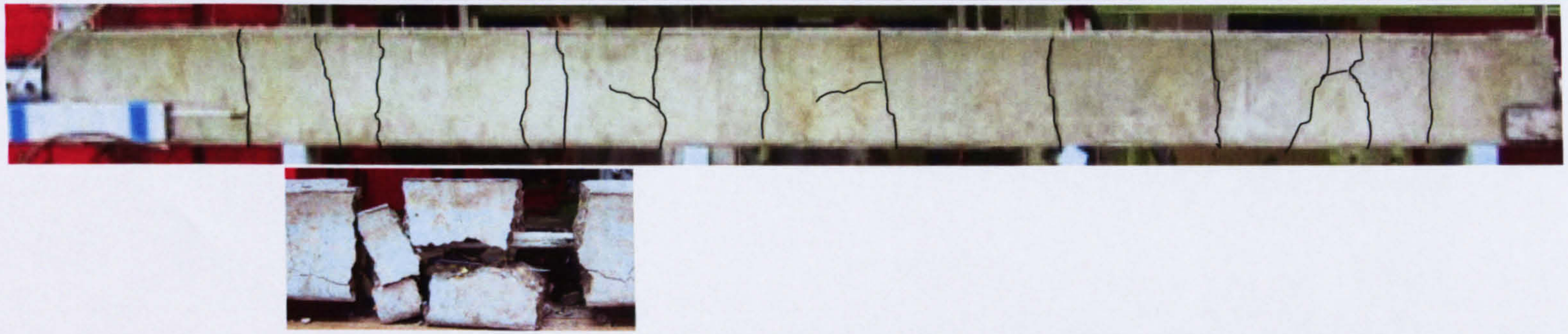

(a) Crack pattern of tested specimen & final fialure of the bar

Experimental results of C50/19/200

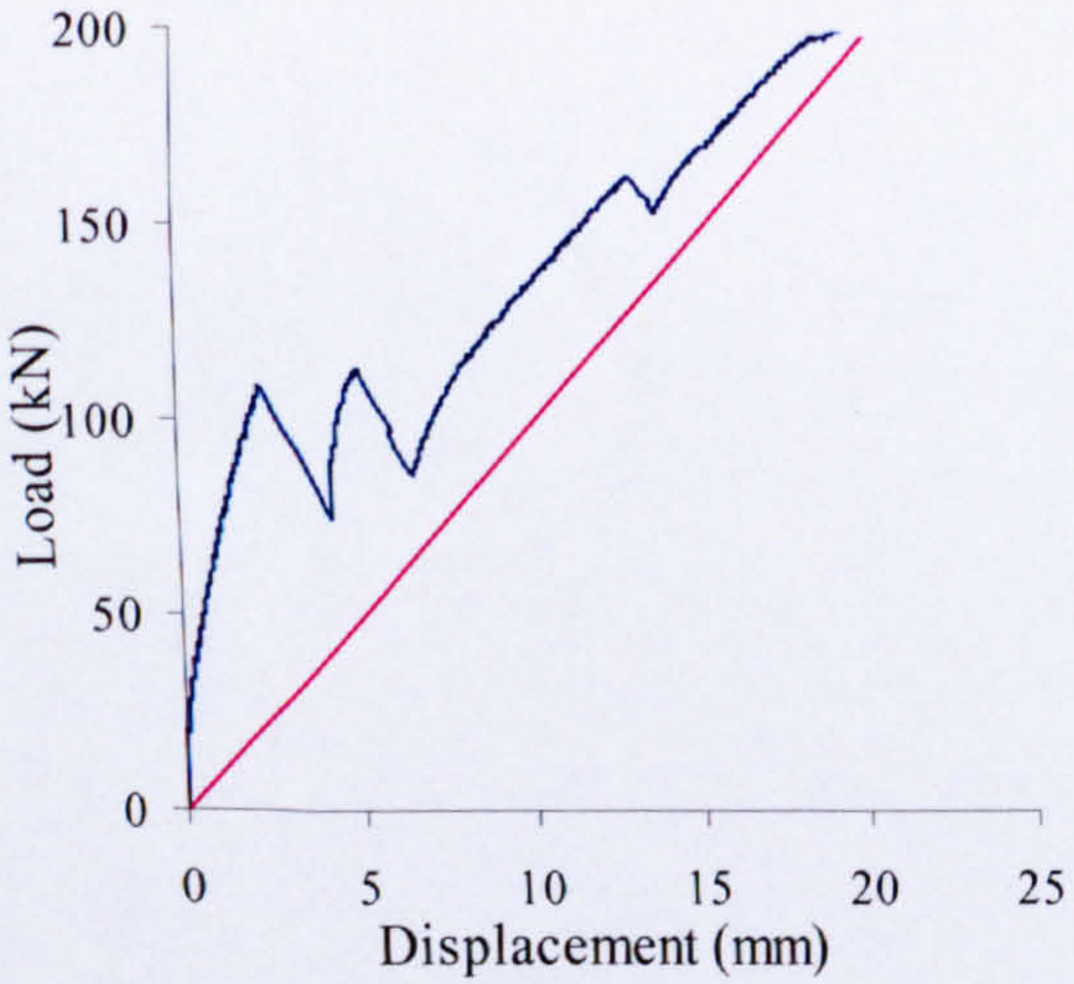

(a) Force displacement relationship

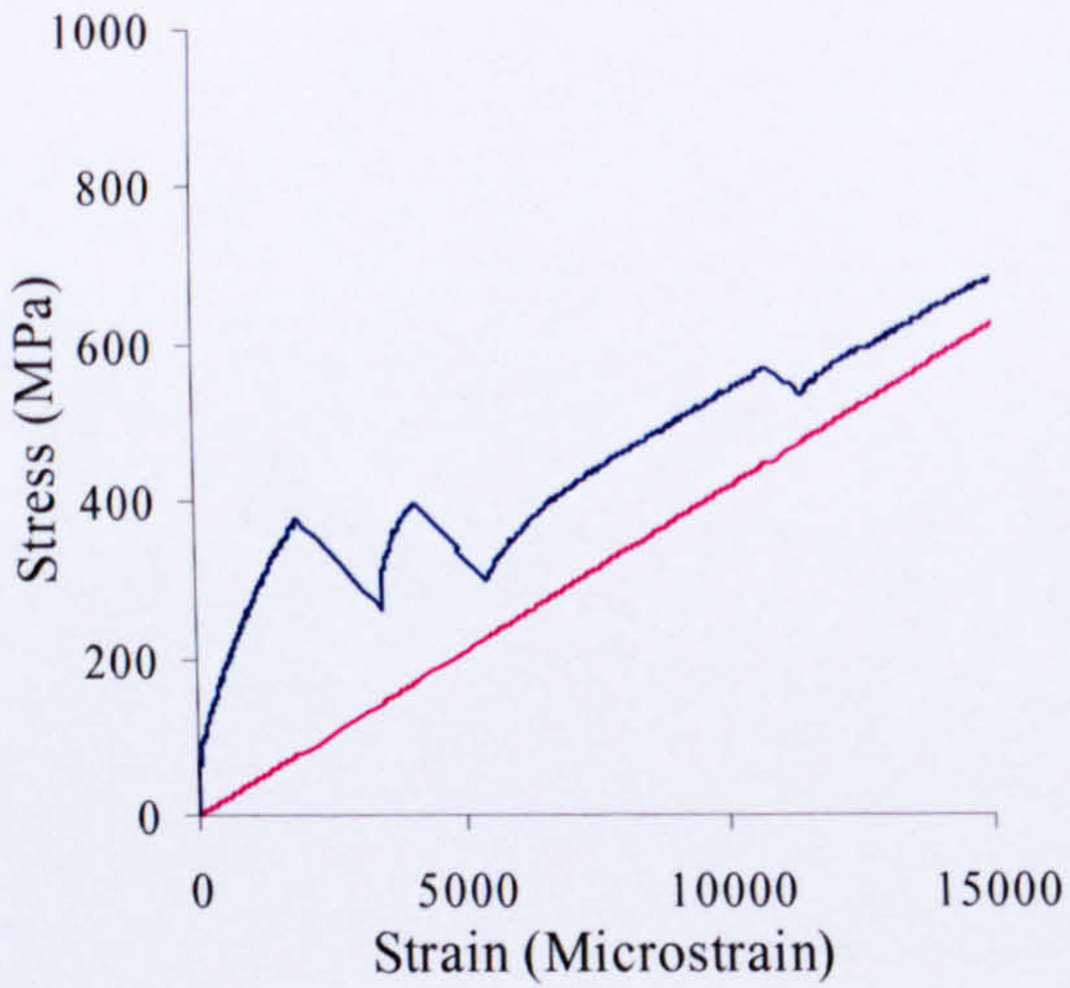

(b) Bar stress at crack section Vs total strain

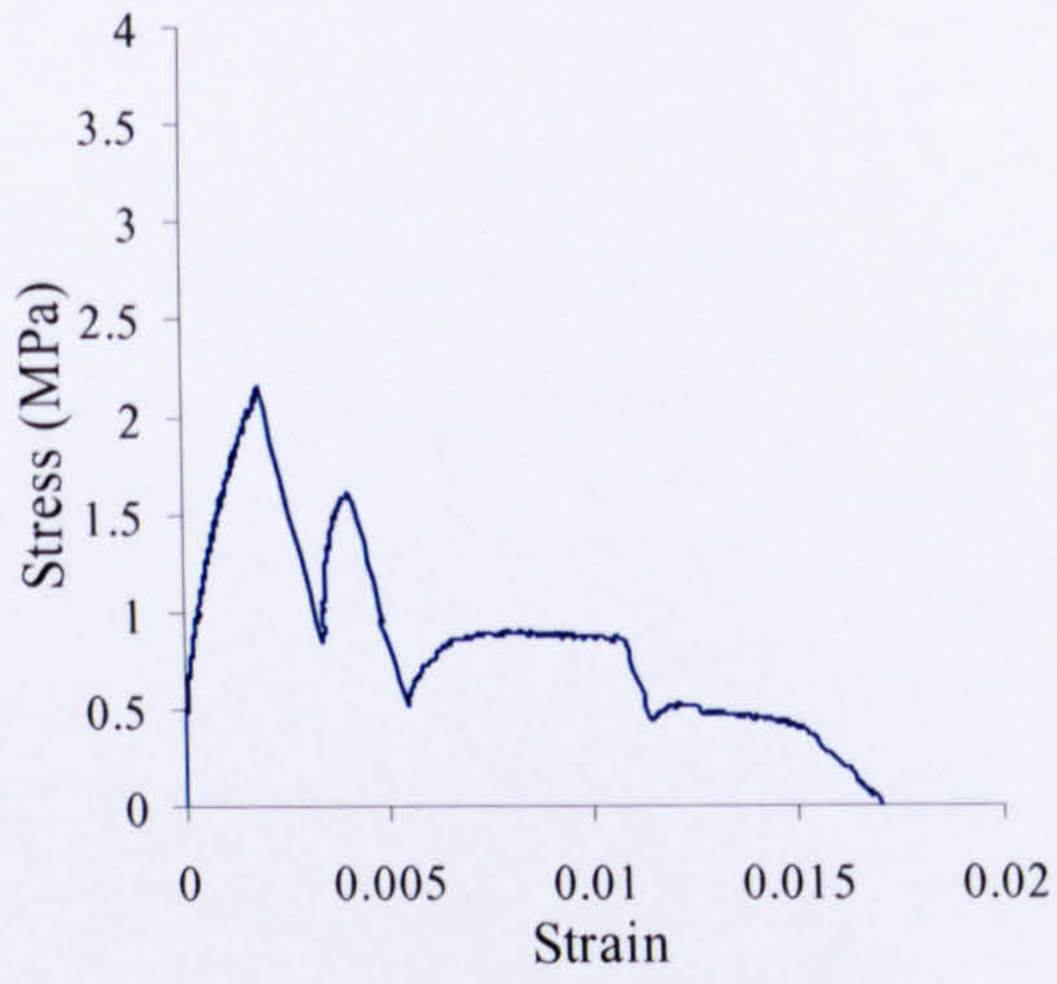

(c) Tension softening response of concrete

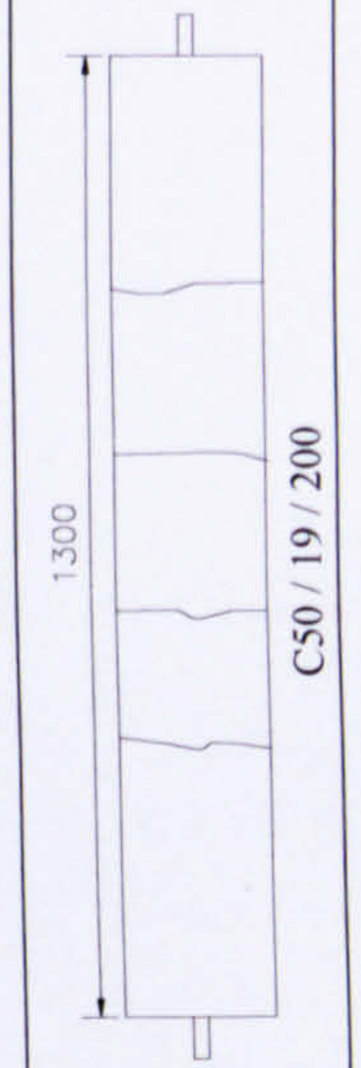

Experimental results of C90/19/200

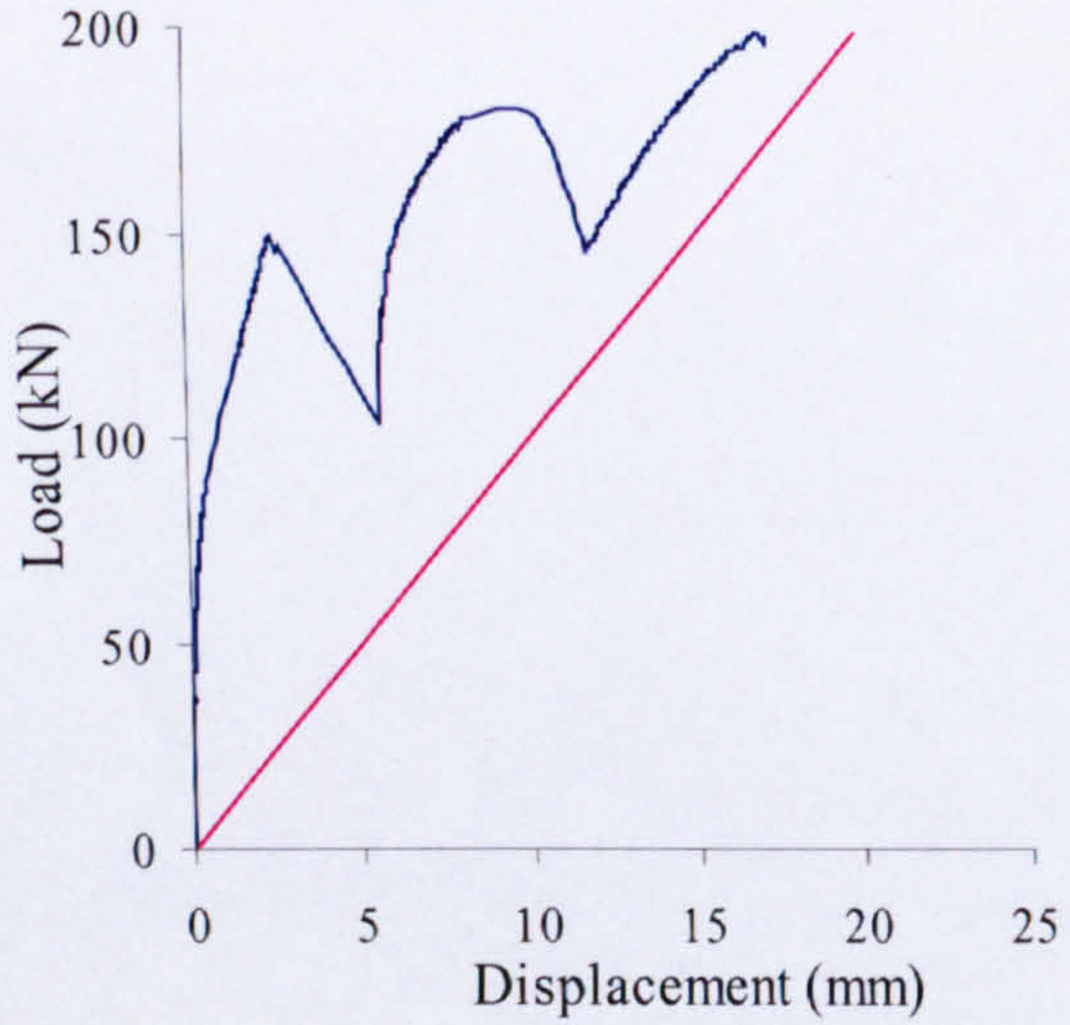

(a) Force displacement relationship

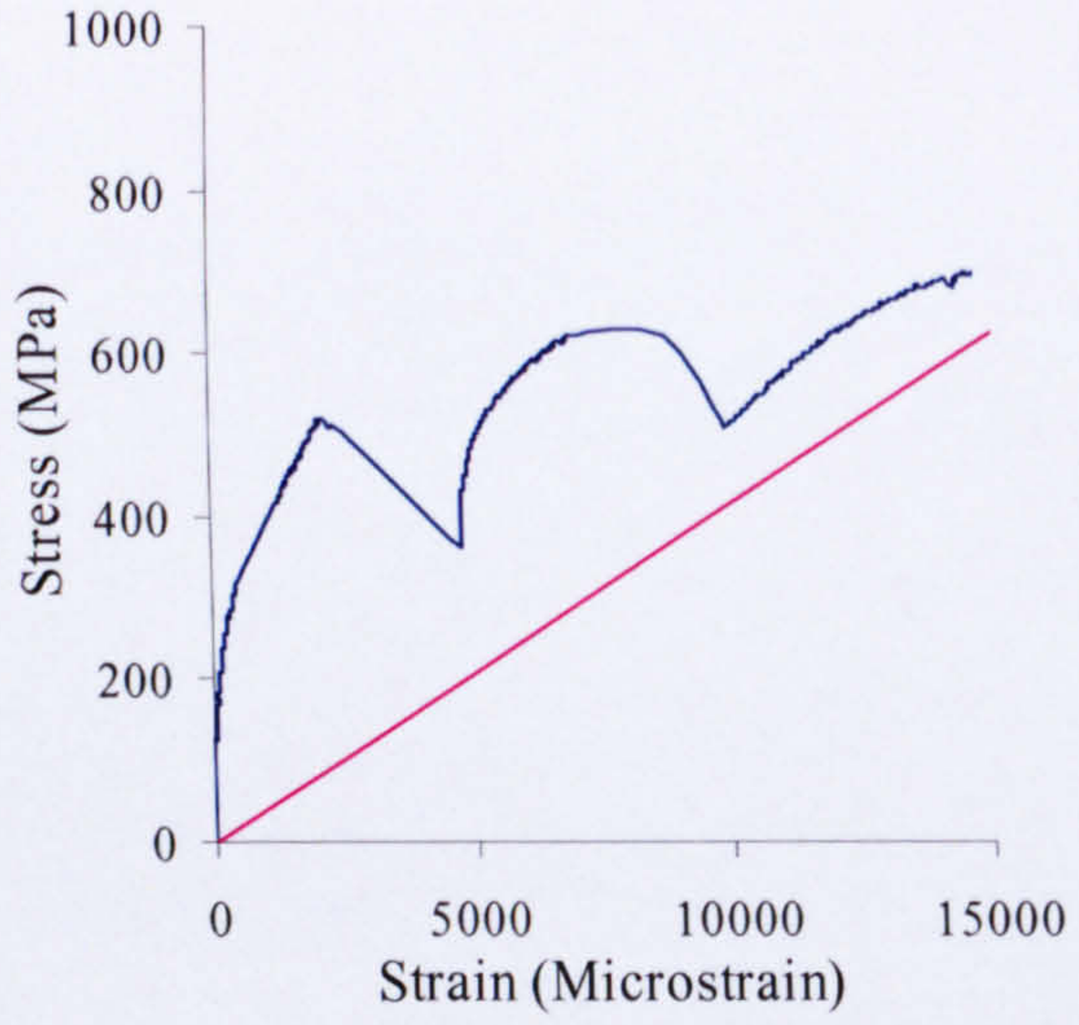

(b) Bar stress at crack section Vs total strain

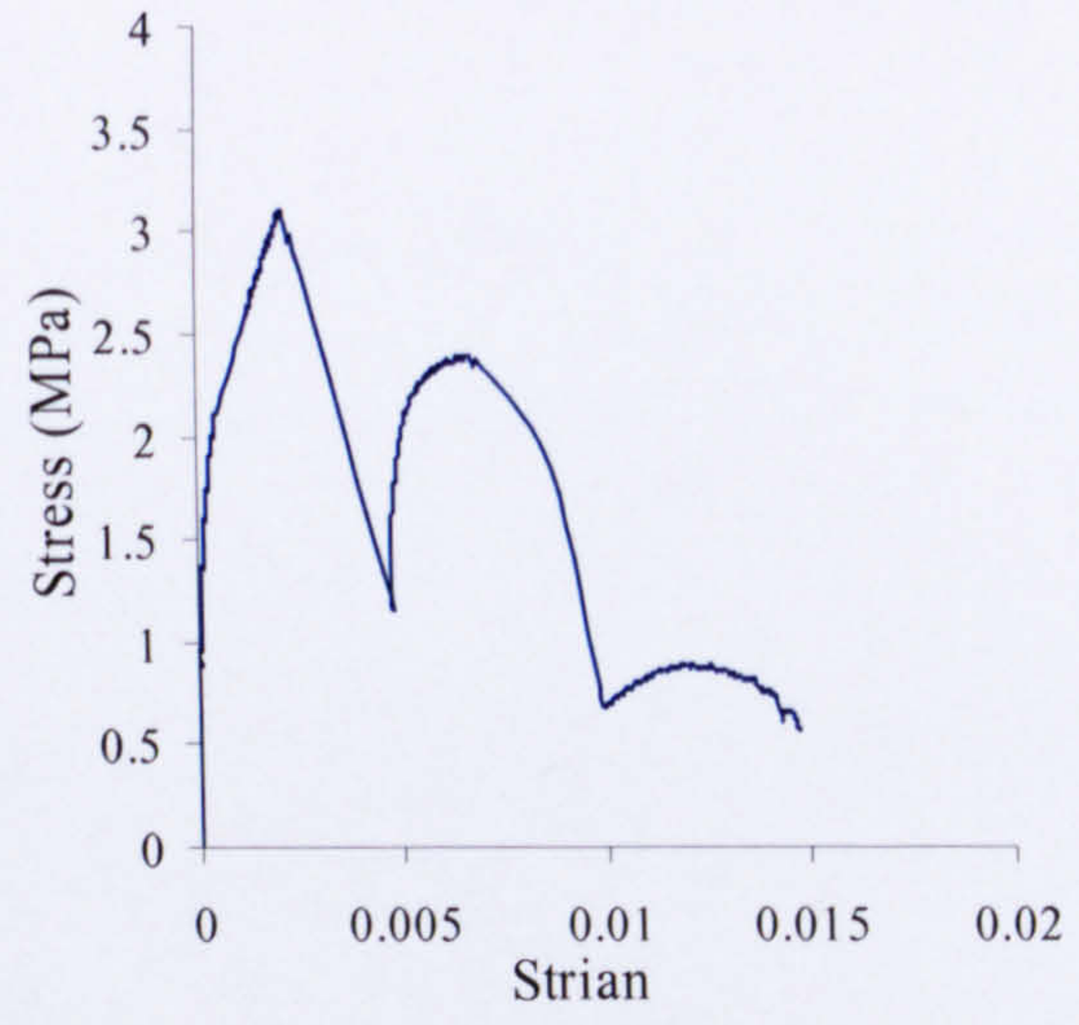

(c) Tension softening response of concrete

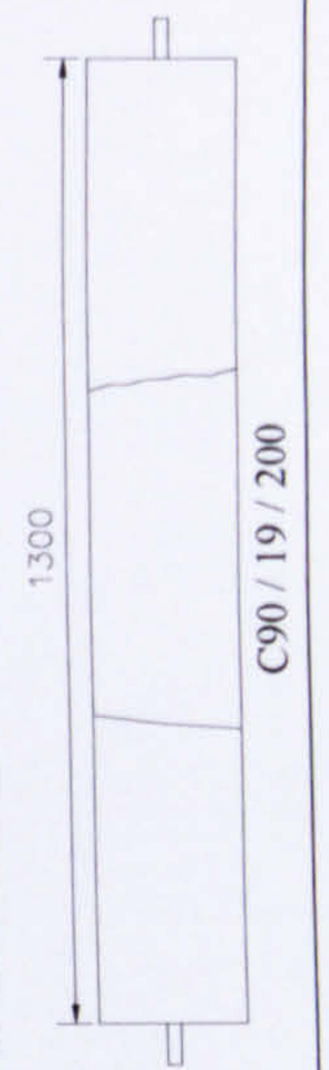

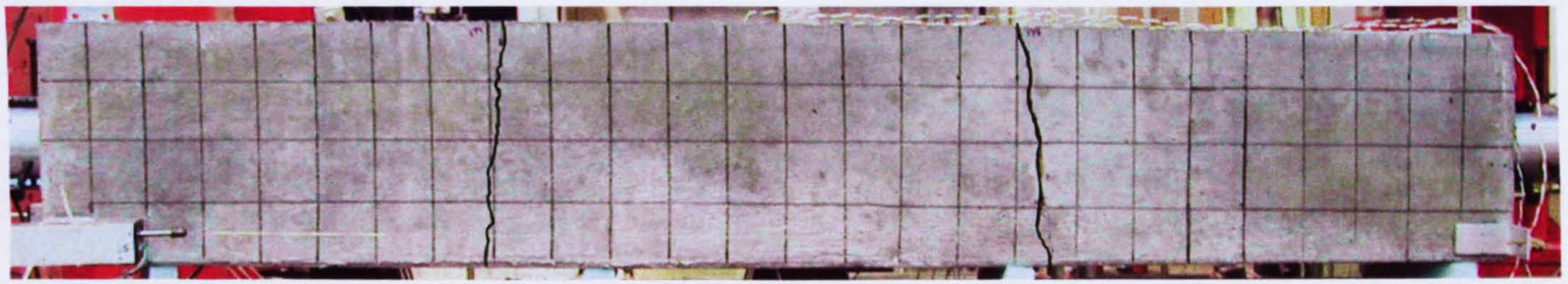

(a) Crack pattern of tested specimen

Experimental results of C50/13/200

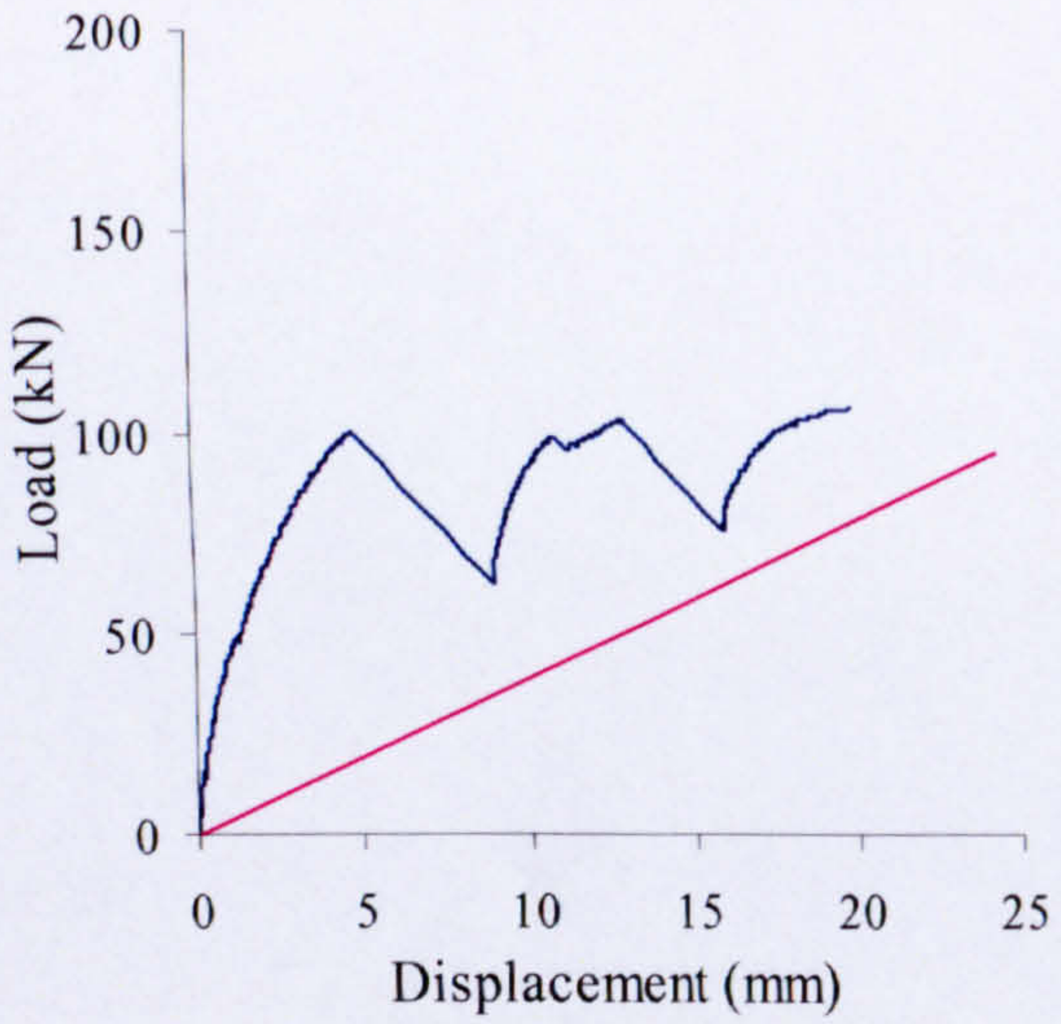

(a) Force displacement relationship

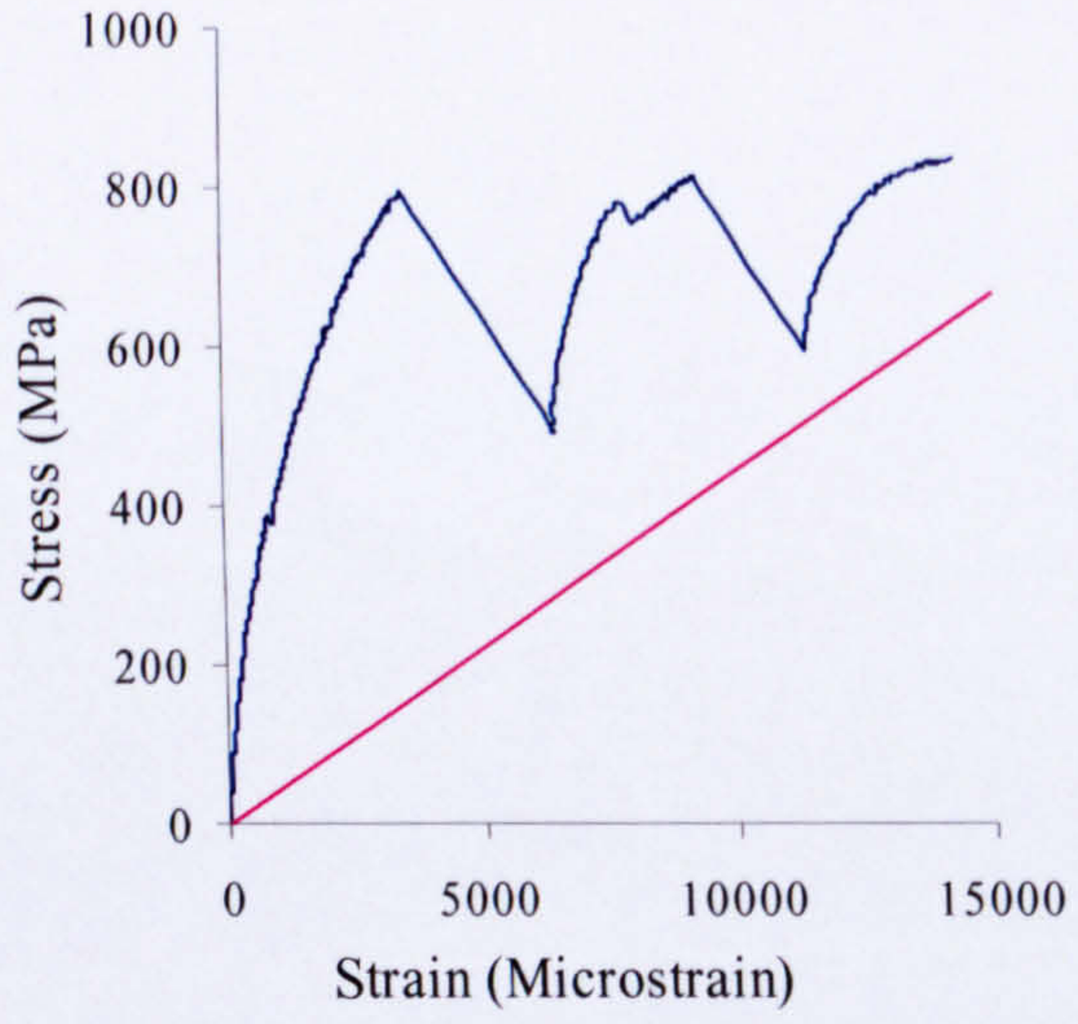

(b) Bar stress at crack section Vs total strain

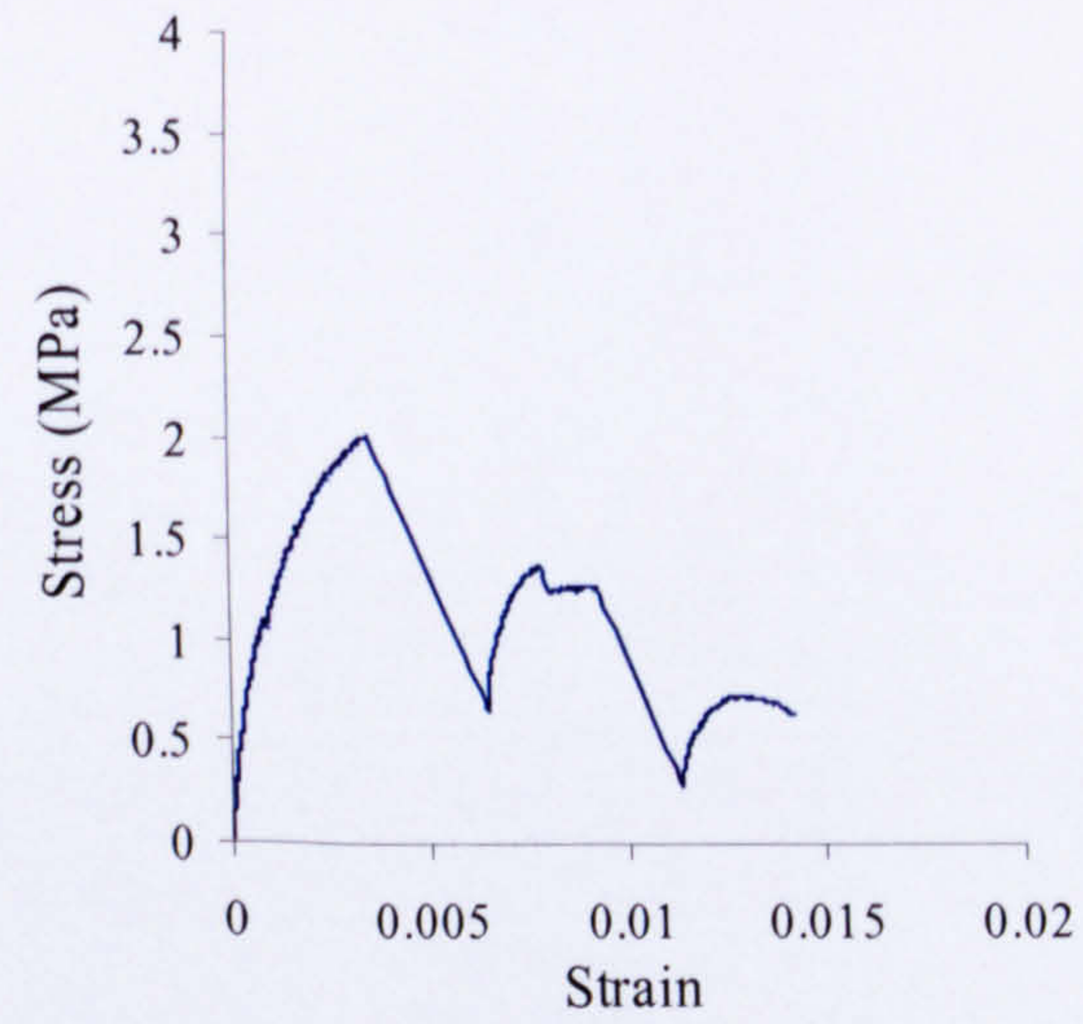

(c) Tension softening response of concrete

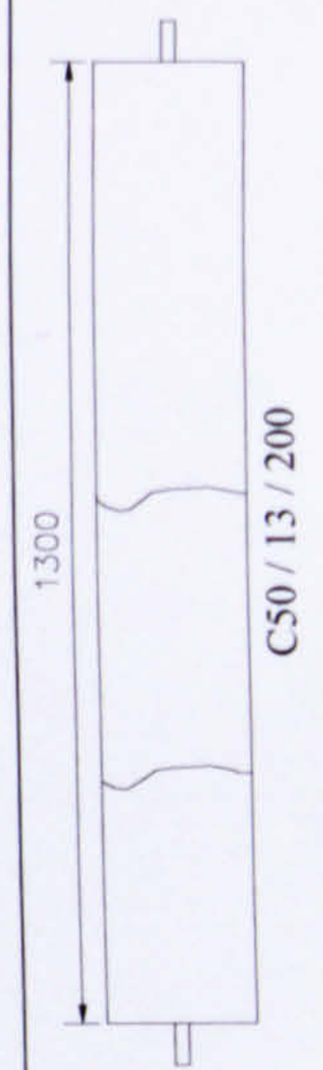

Experimental results of C90/13/200

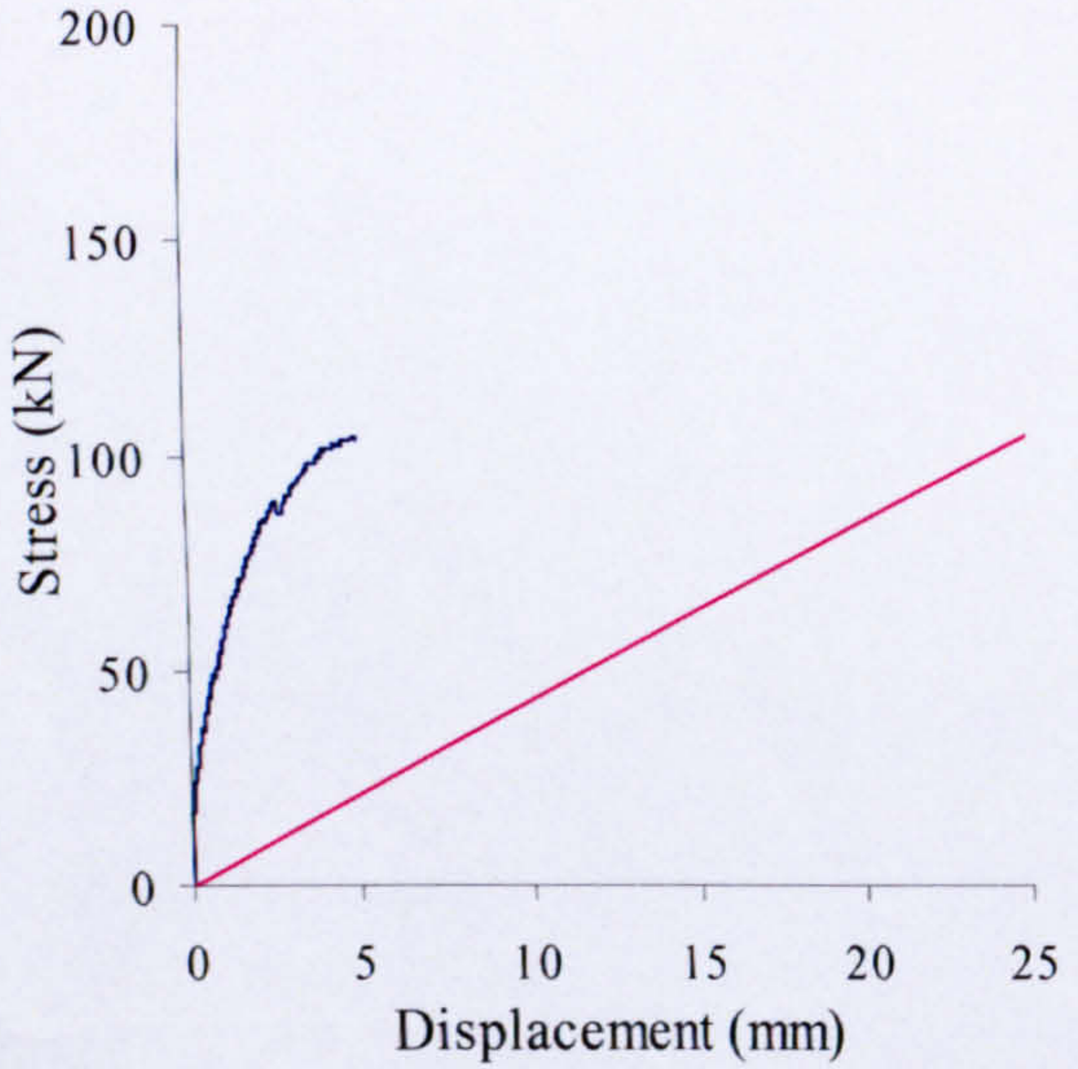

(a) Force displacement relationship

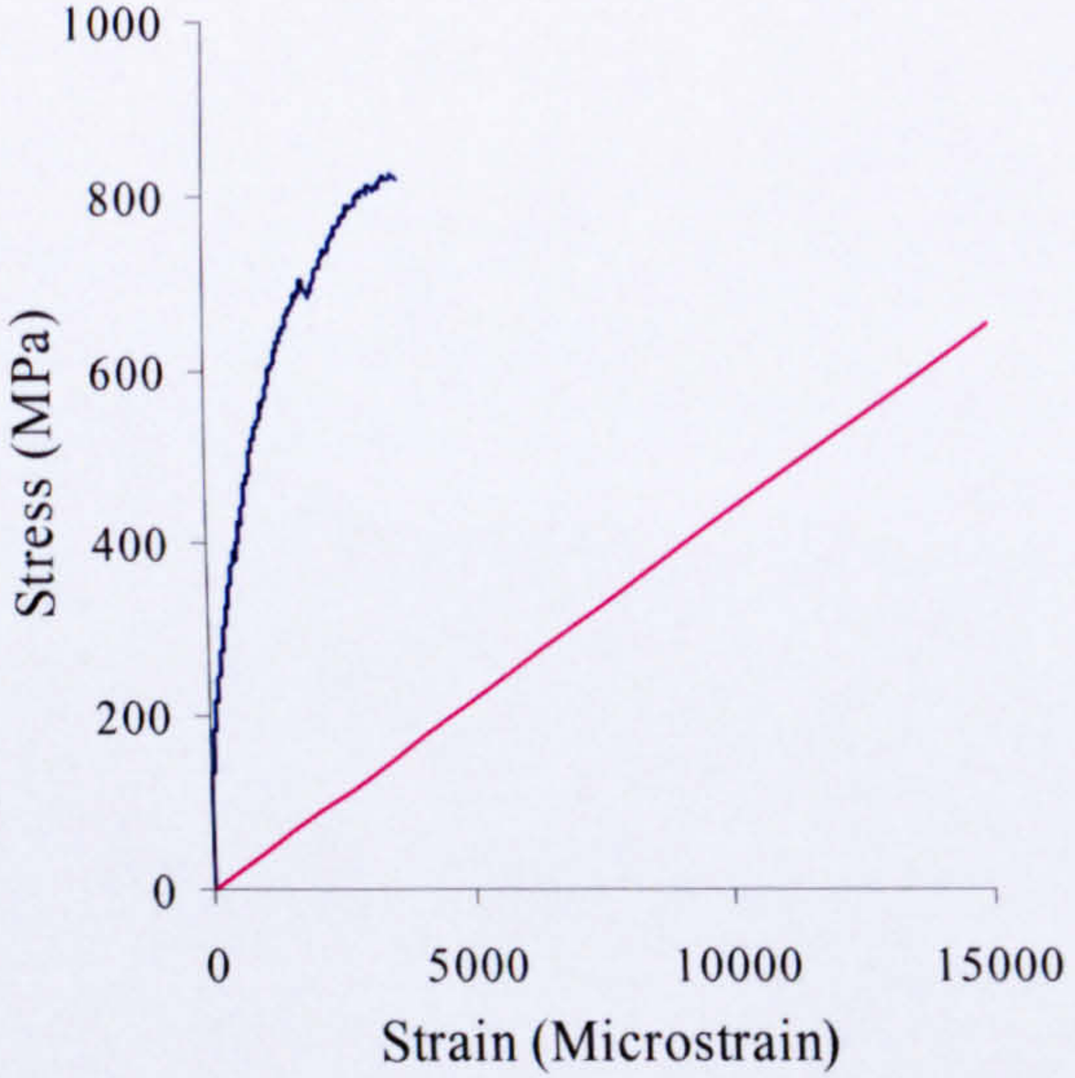

(b) Bar stress at crack section Vs total strain

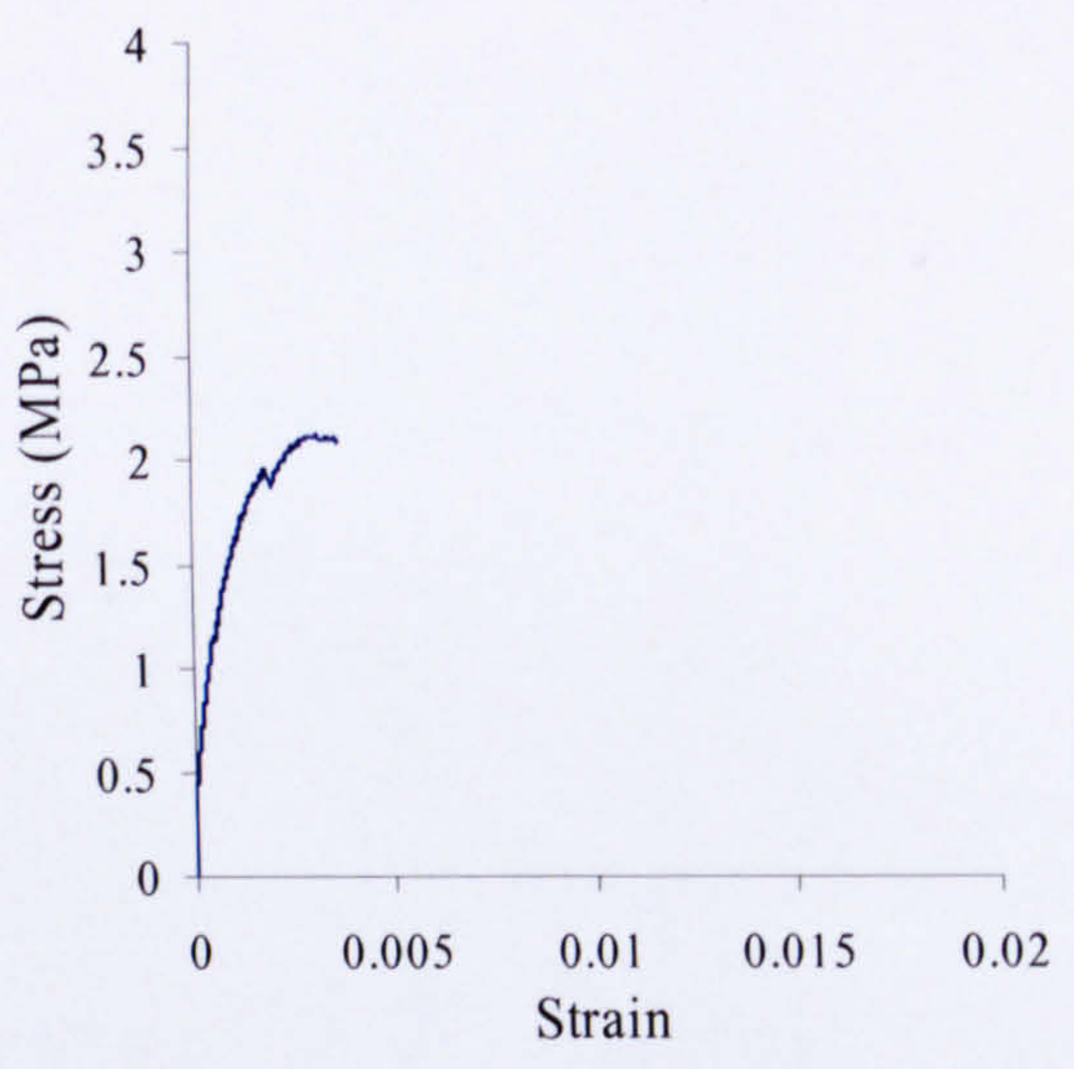

(c) Tension softening response of concrete

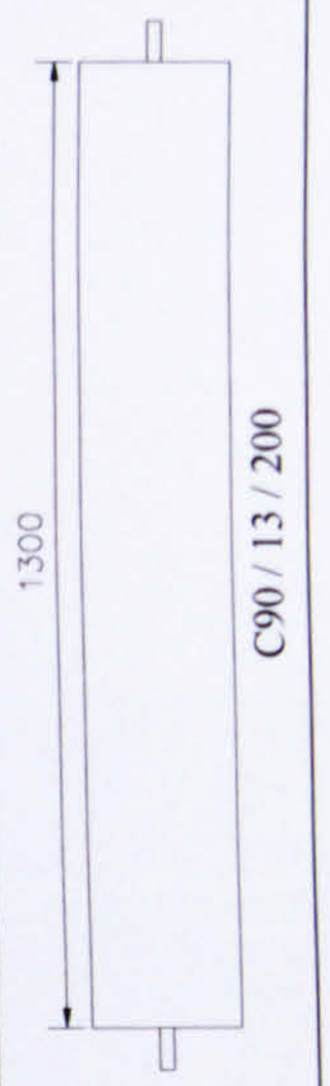

APPENDIX II

STRAIN DISTRIBUTION DIAGRAMS FROM THE PULL-OUT TESTS

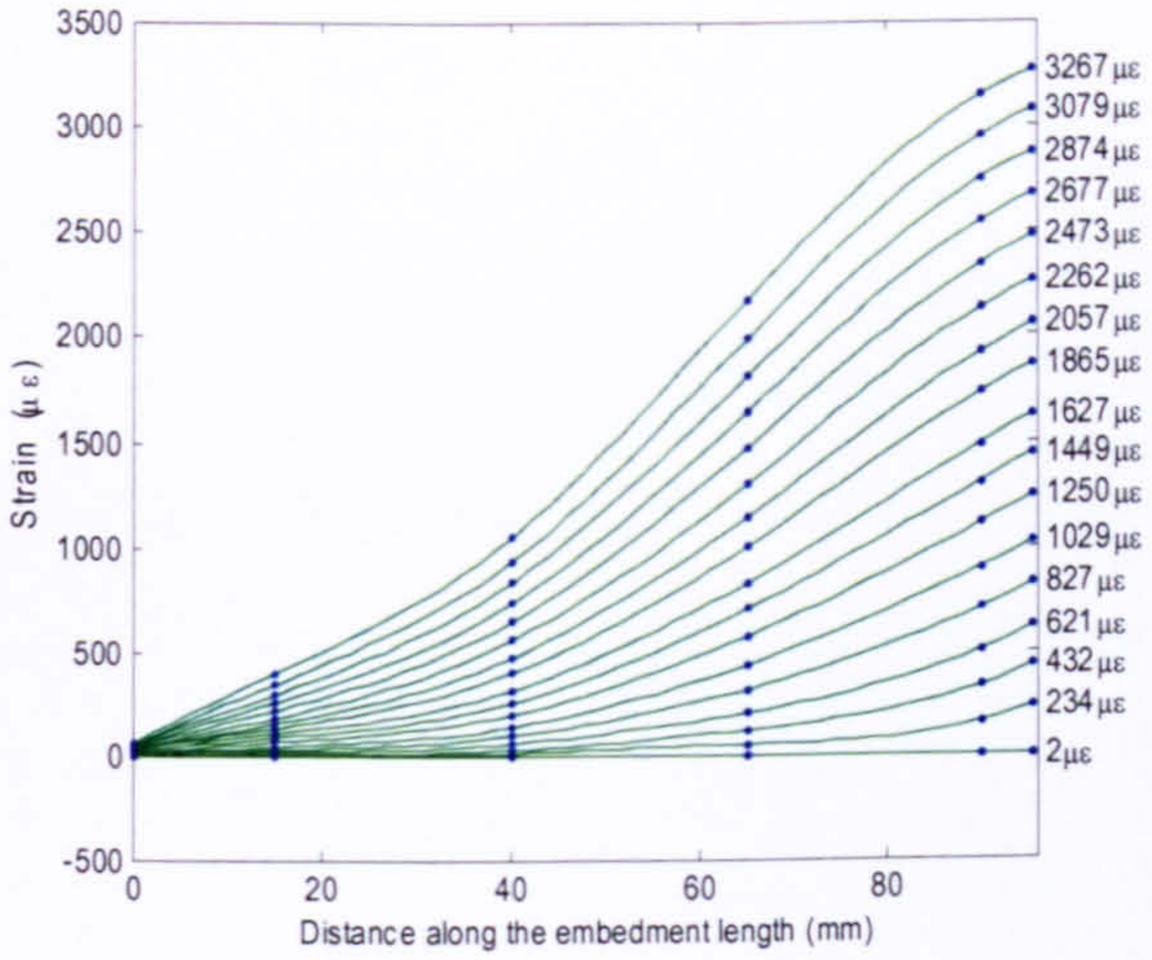

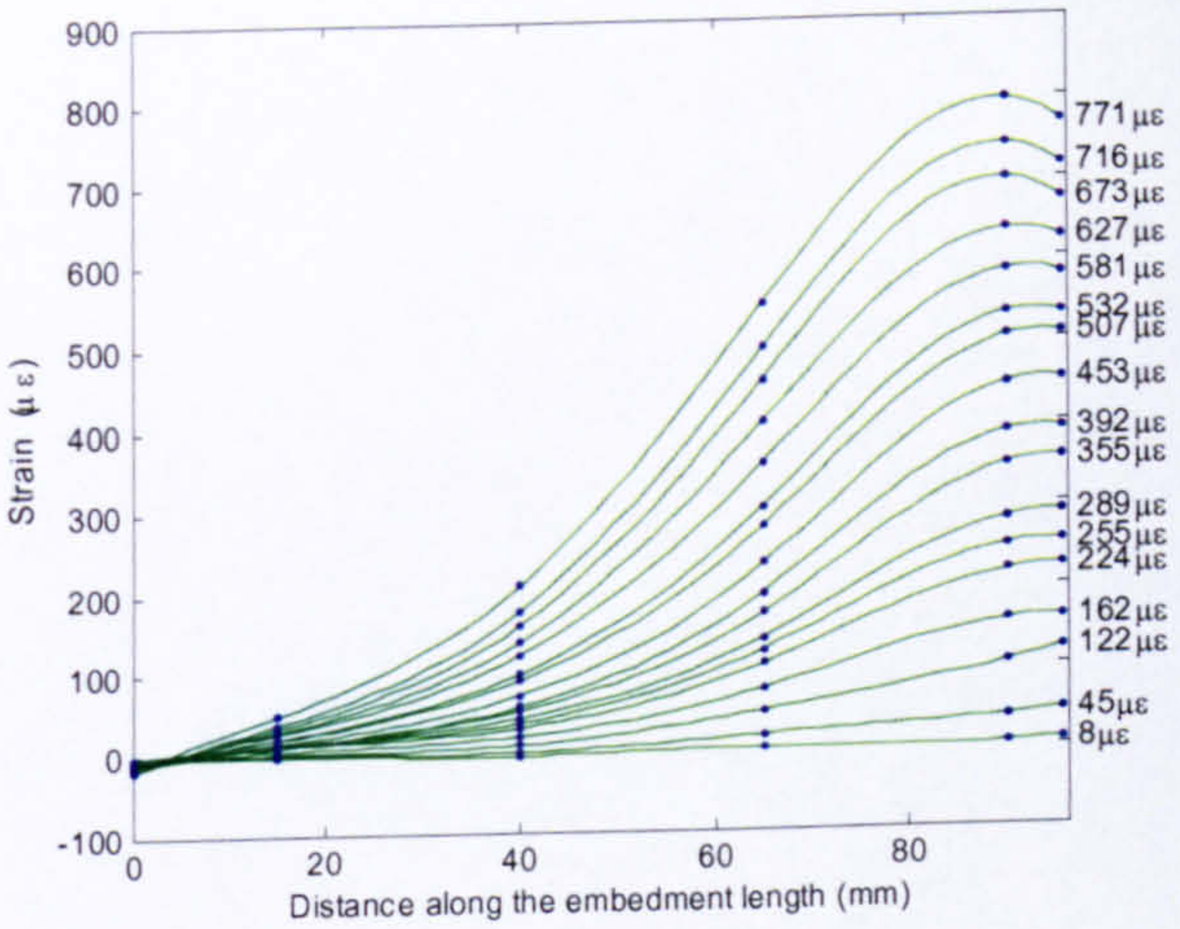

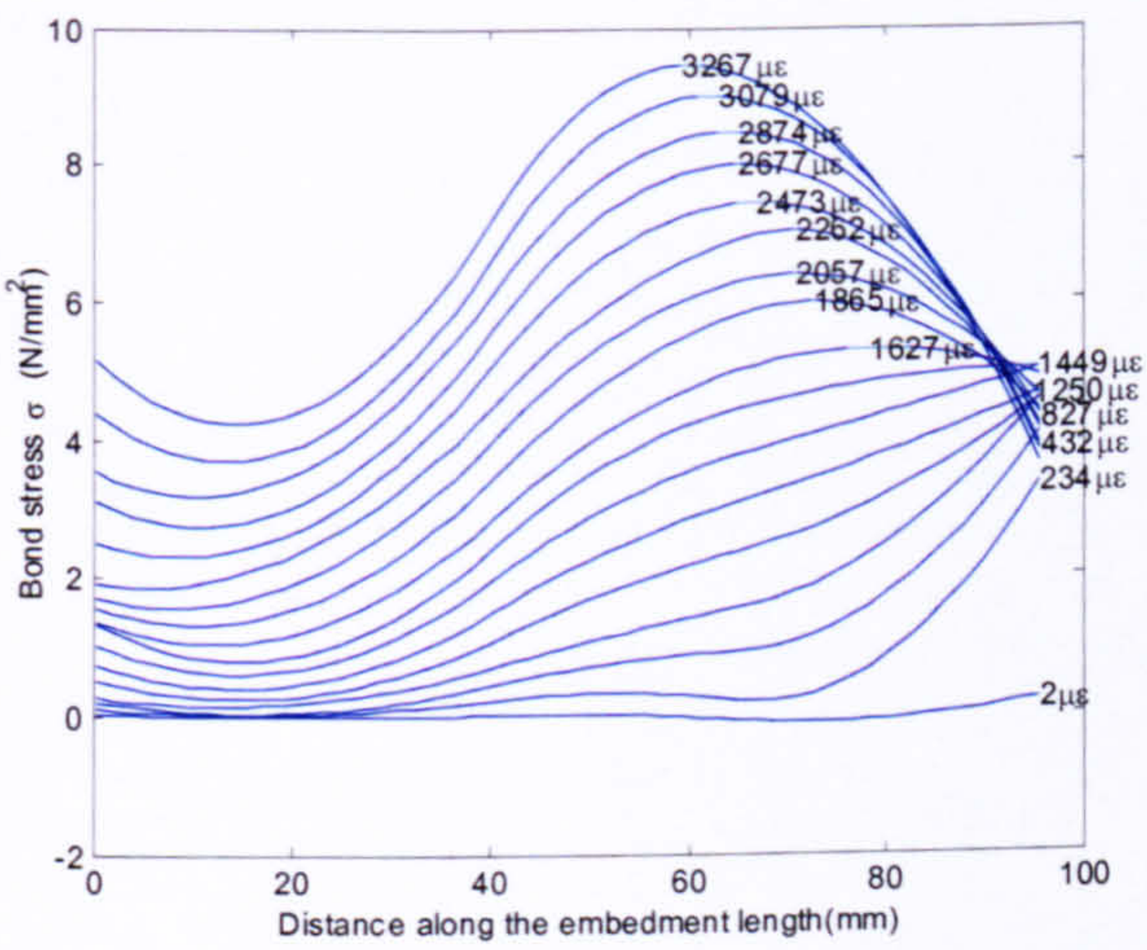

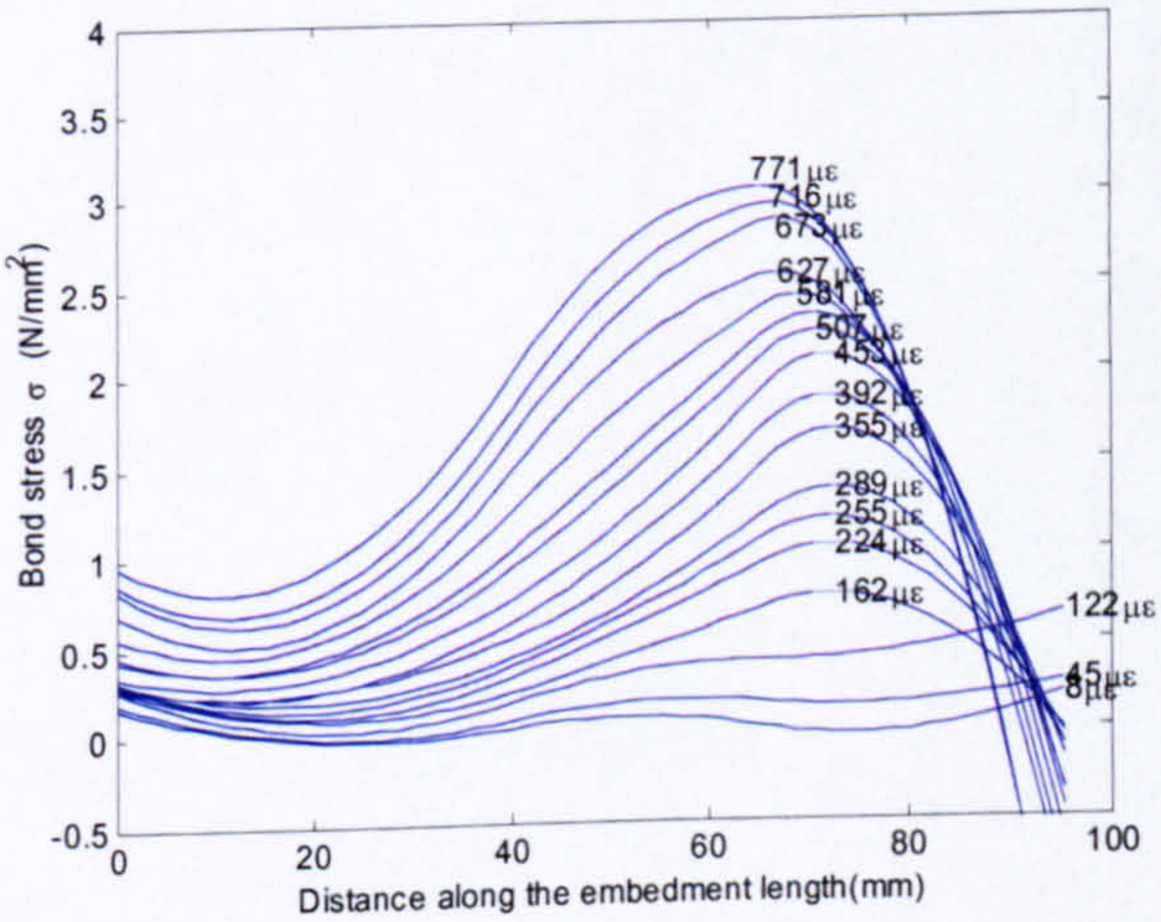

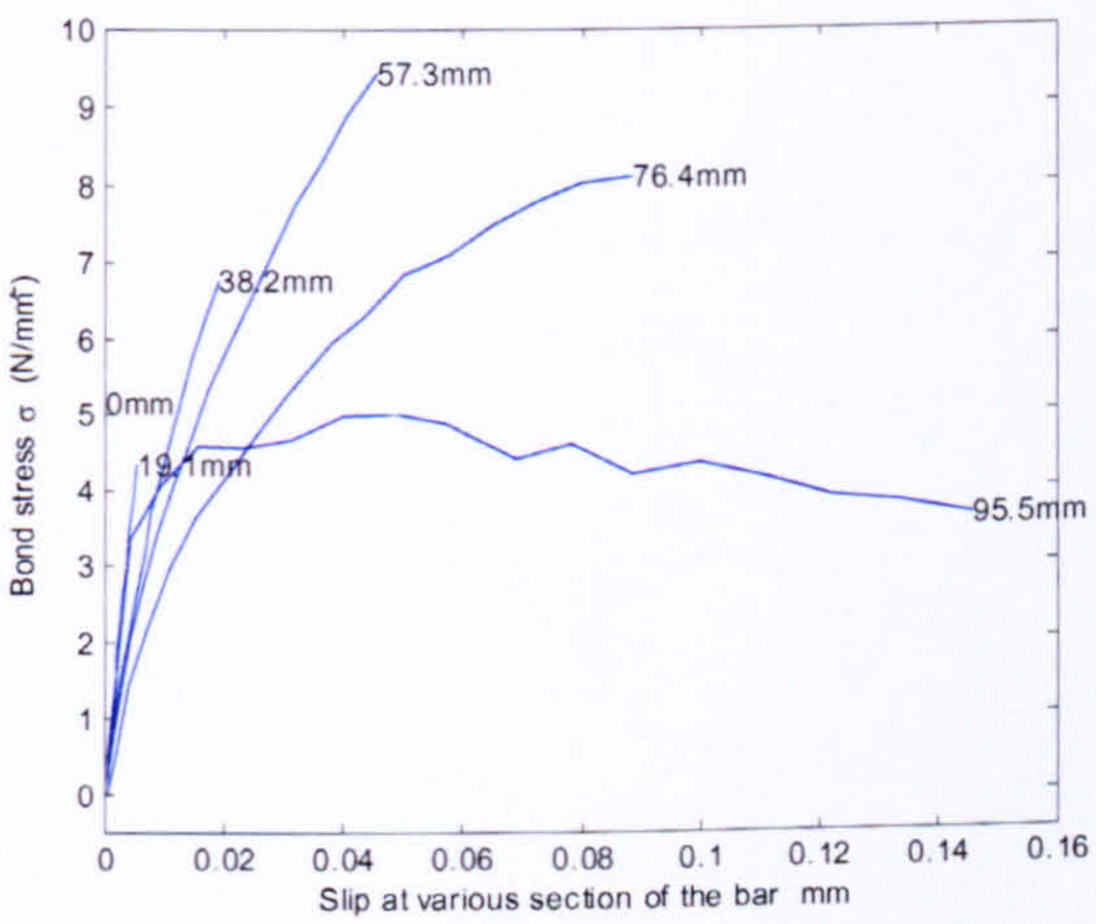

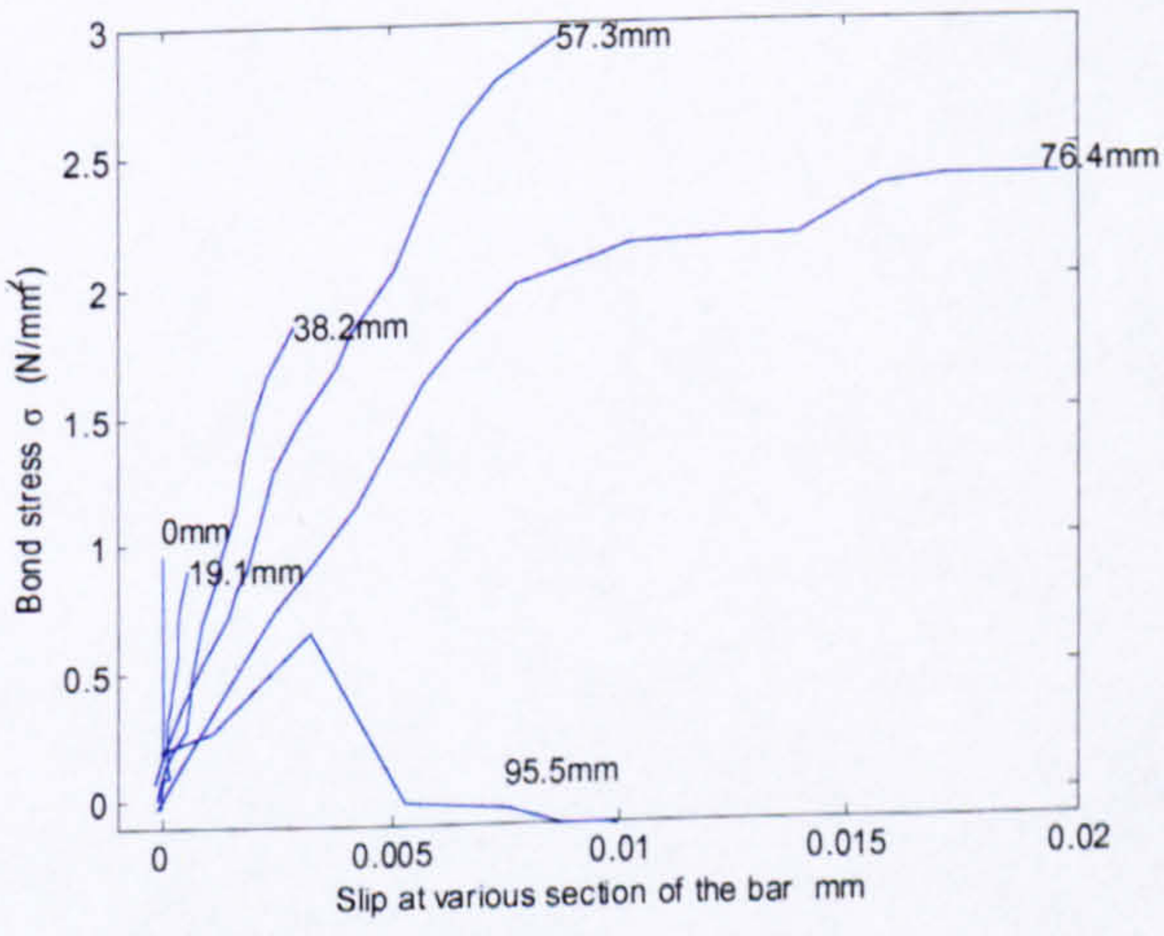

Fig. AII-1 Recorded strain distribution, bond stress distribution and local bond stress slip relationship at various positions in the bar for grade 90 (on the left) and grade 45 (on the right) concrete for embedment length of 5ϕ

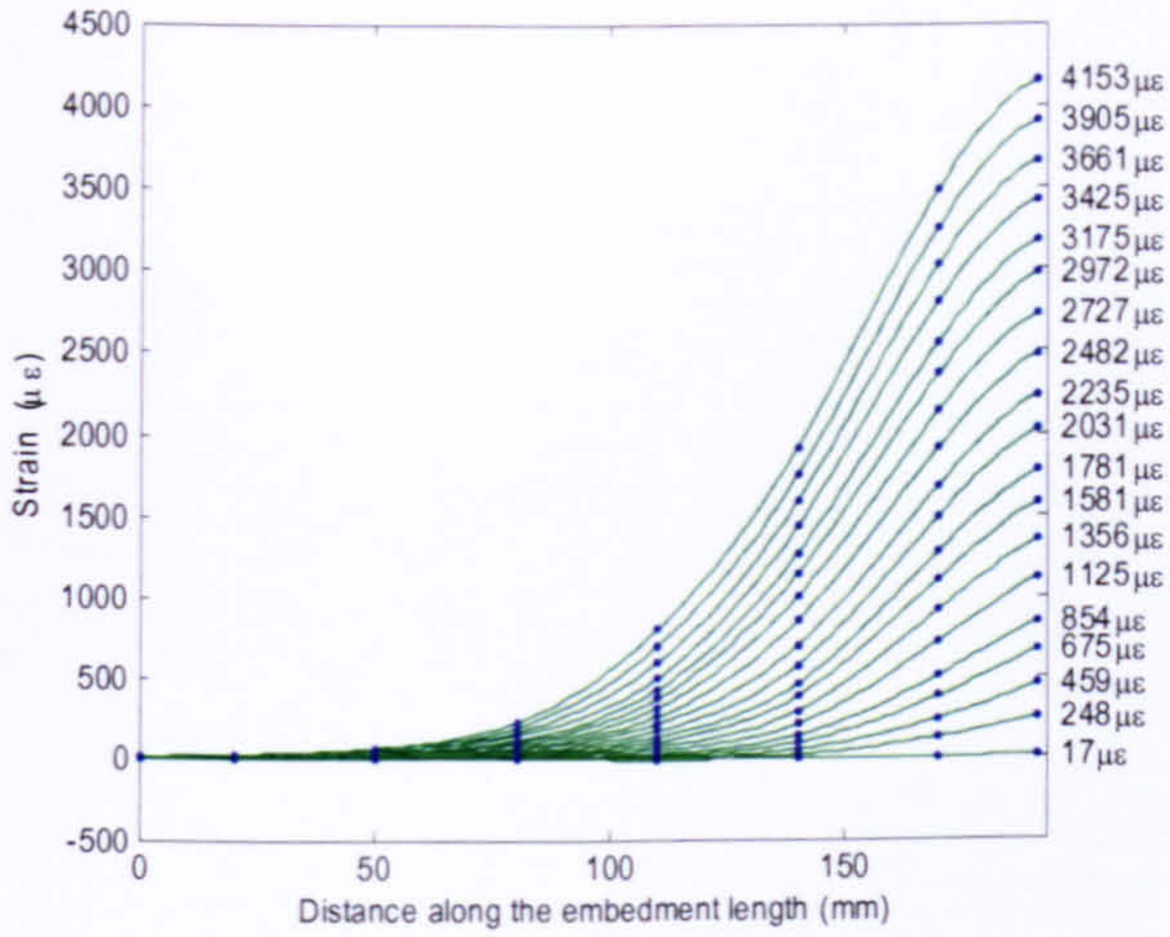

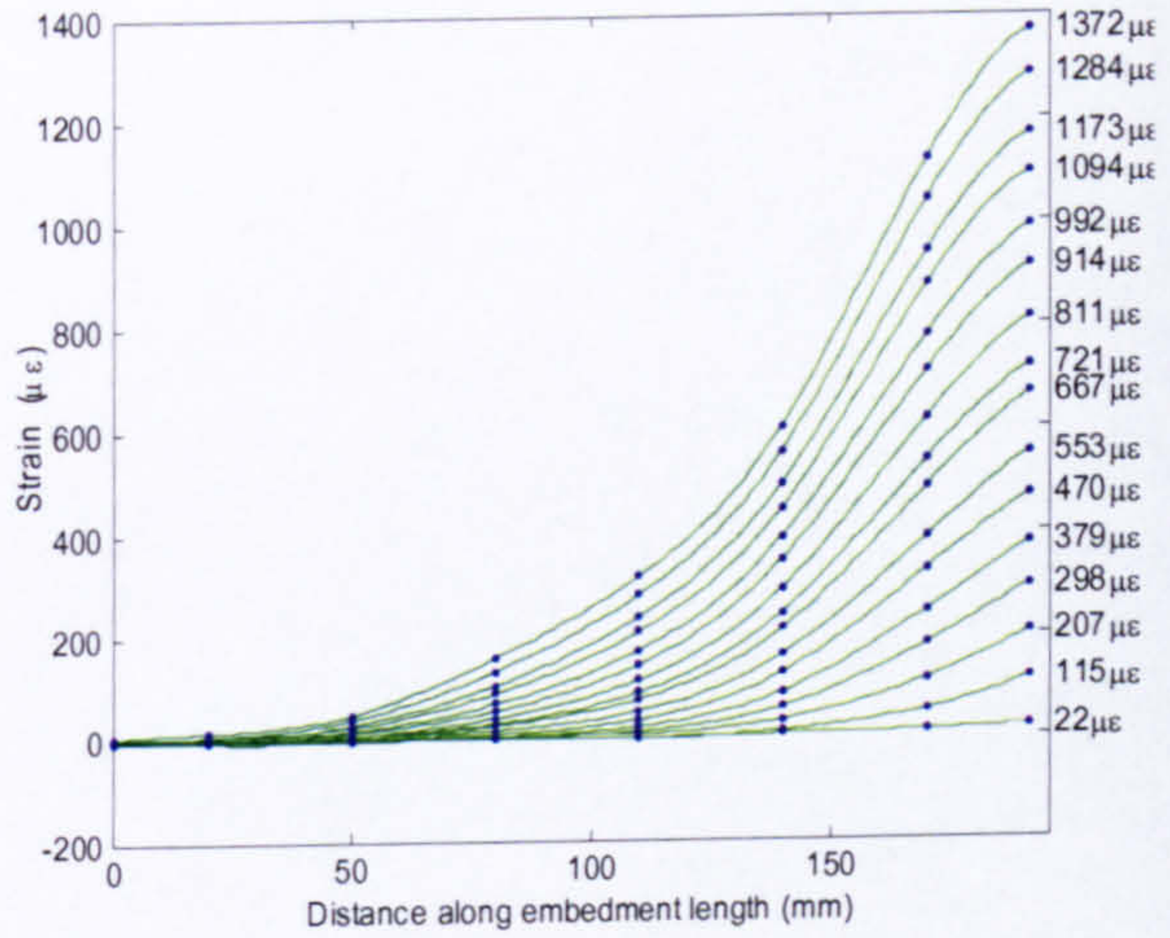

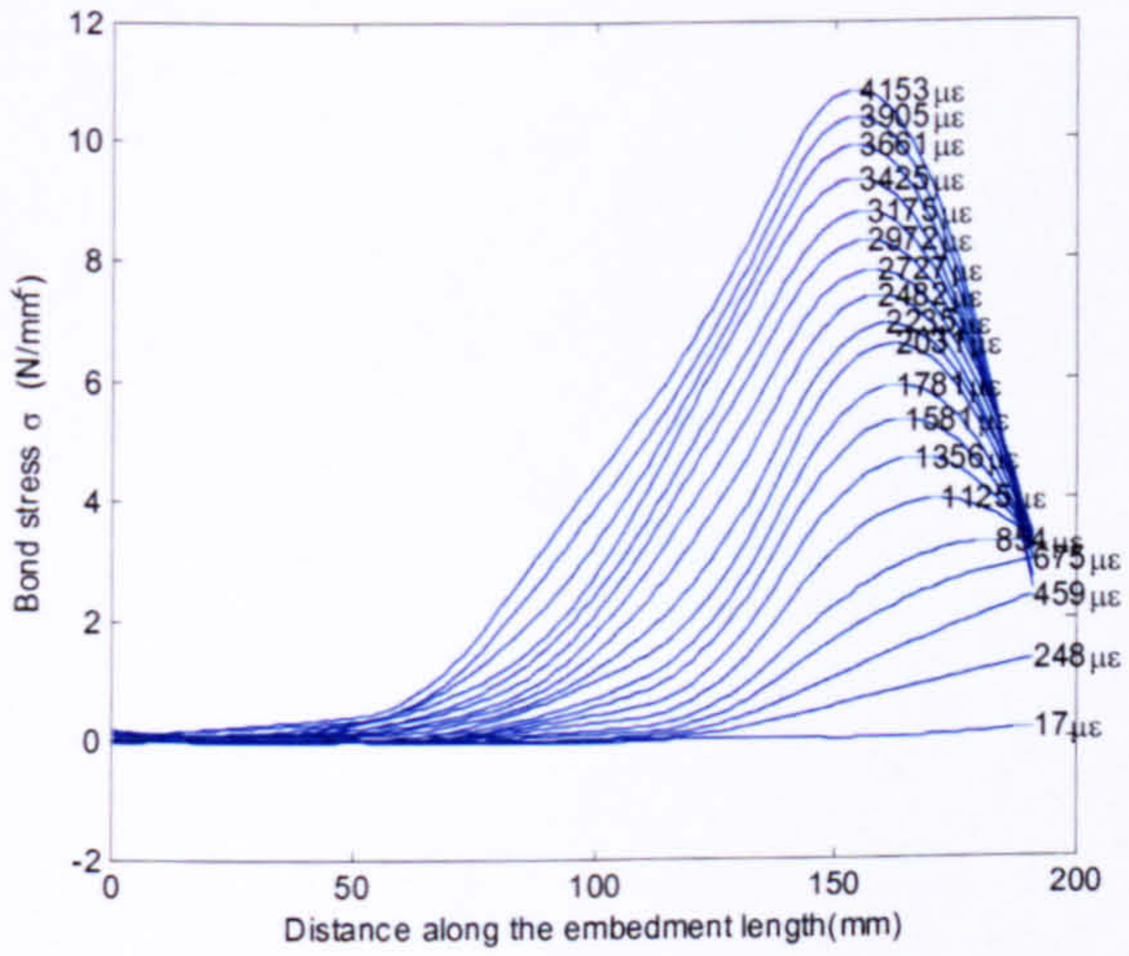

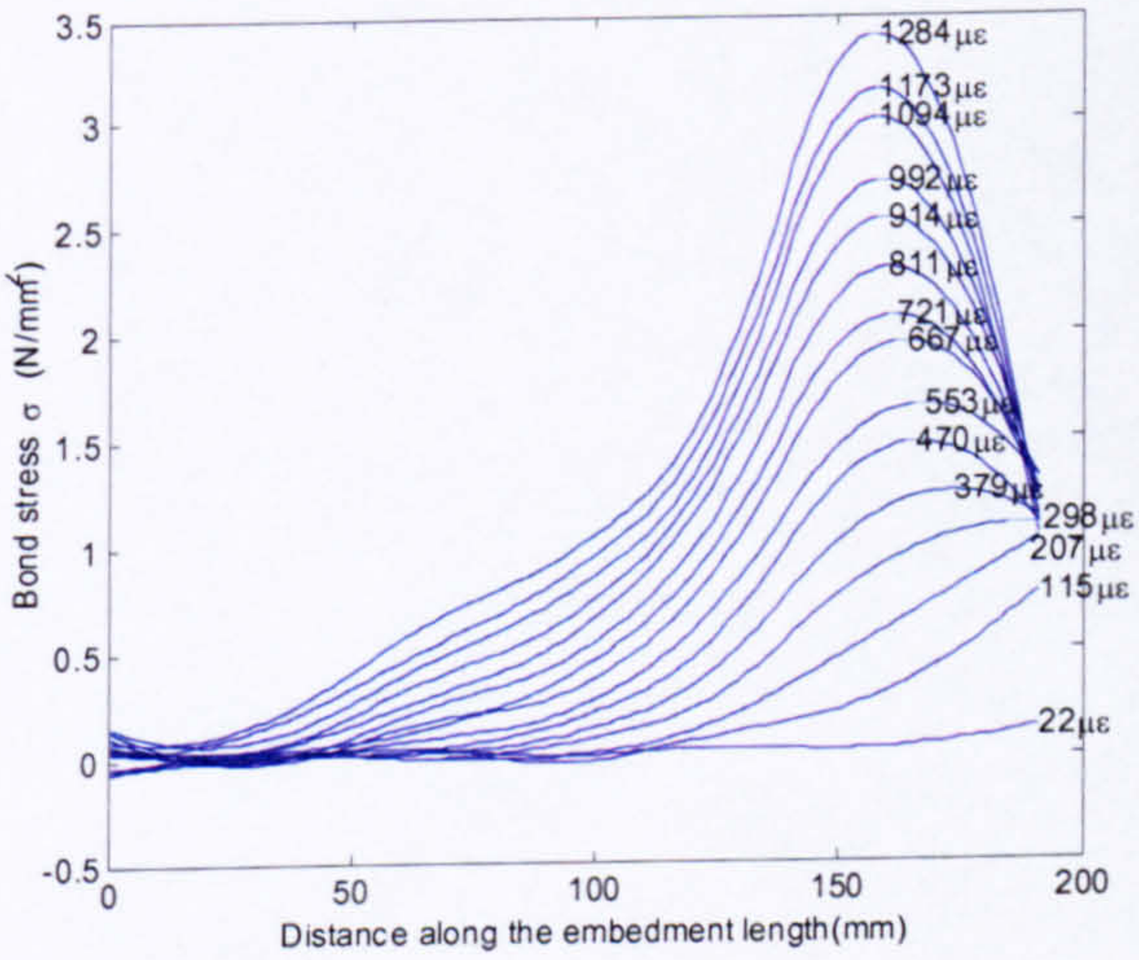

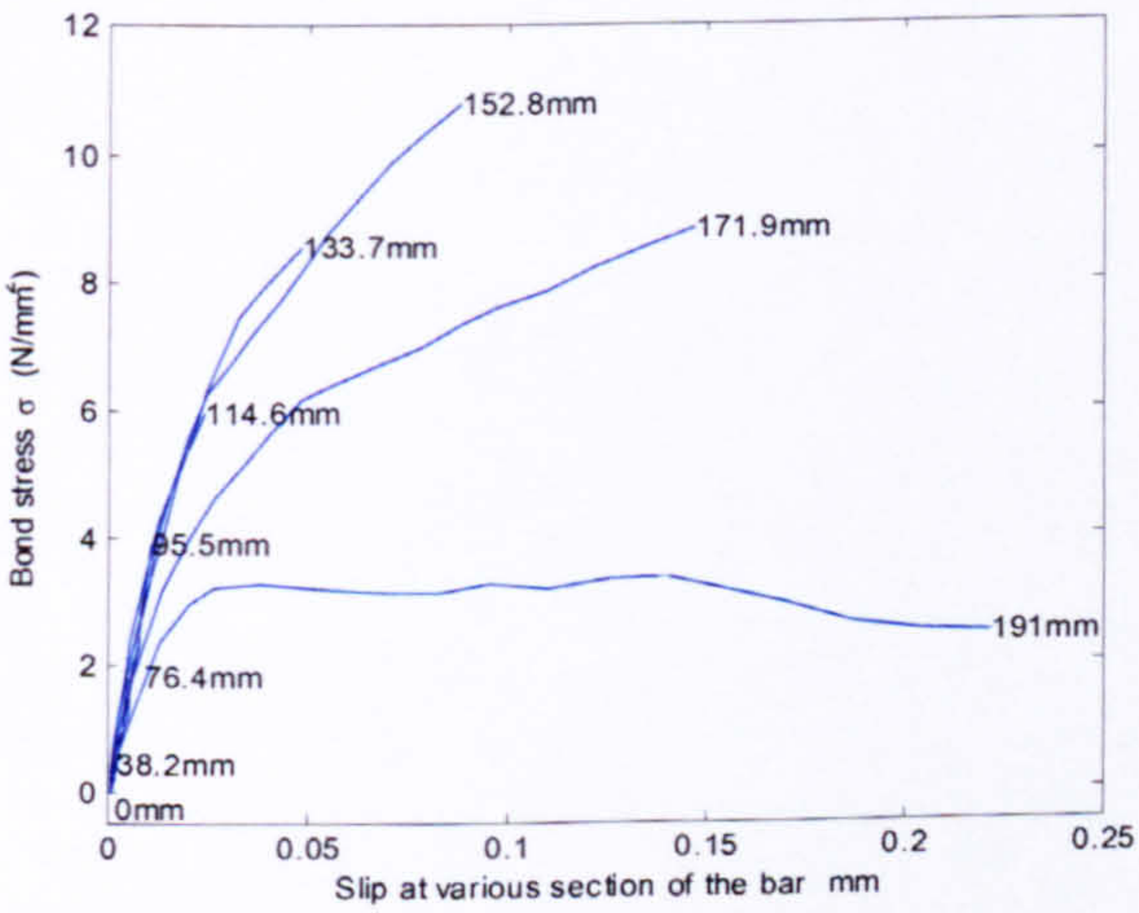

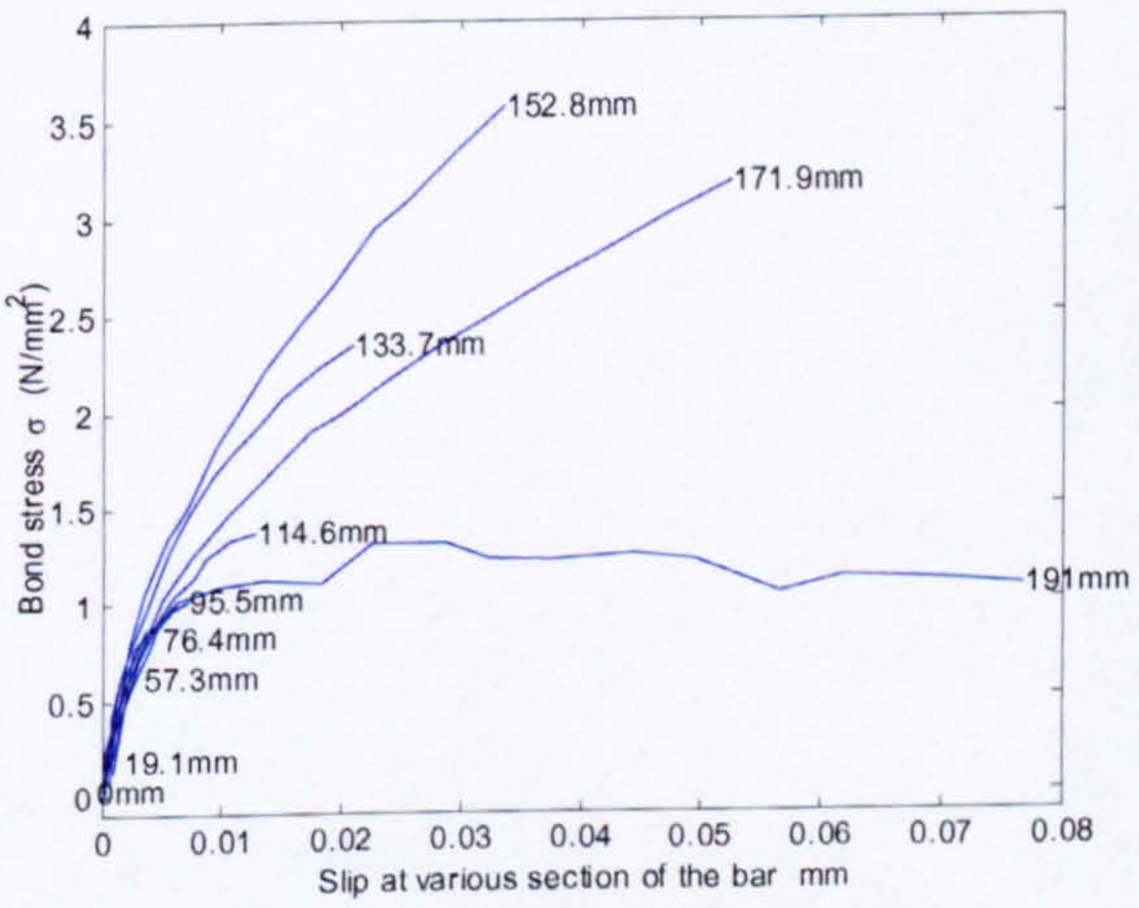

Fig. AII-2 Recorded strain distribution, bond stress distribution and local bond stress slip relationship at various positions in the bar for grade 90 (on the left) and grade 45 (on the right) concrete for embedment length of 10ϕ.

APPENDIX III

MATLAB PROGRAMME ROUTINE DEVISED FOR MODELLING TENSION STIFFENING EFFECT OF GFRP RC

```
%%%%%%%%%%%%%%%%%%%%%%%%%%%%%%%%%%%%%%%%%%%%%%%%%%%%%%%%%%%%%%%%
% MAIN PROGRAMME                                                       %
% Prediction of Tension stiffening effect of GFRP RC based on strain   %
% distribution function to approximate the strain between cracks       %
%%%%%%%%%%%%%%%%%%%%%%%%%%%%%%%%%%%%%%%%%%%%%%%%%%%%%%%%%%%%%%%%

clear all
load data                    % Read experimental results for final comparison
experiment=data
kp=0.011                     % mm2/kg Constant determined by pullout test (ACI)
es=42800.0;                  % N/mm2 Young's modulus of the bar
ec=28000.0 ;                 % N/mm2 Young's modulus of concrete
b=200.0;                     % mm Dimensions of the concrete specimen
d=200.0;                     % mm Dimensions of the concrete specimen
fcu=45.0;                    % N/mm2 Concrete cubic strength
bardia=12.7;                 % Diameter of the external reinforcement
length=1400.0;               % mm length of the test specimen
as=(bardia^2.0)*pi/4.0;      % mm2 Reinforcement area
ac=b*d;                      % mm2 Concrete area
p=as/ac;                     % Non dimensional (reinforcement ratio)
ne=es/ec;                    % Non dimensional(stiffness ratio)
s=length;                    % crack spacing
loadkn=0.0;                  % Initialising the load increment
ftt=0.33*sqrt(fcu*.8);       % Tensile strength of concrete
sysext=0.0;                  % Initialising Energy (work done by external forces)
sysbarint=0.0;               % Initialising Energy (energy stored in the bar)
sysconint=0.0;               % Initialising Energy (energy stored in concrete)
sysbond=0.0;                 % Initialising Energy (energy lost due to sliding)
damageindex=0.0;             % Initialising Energy (energy lost due to de-bonding)
loadincrement=2.0;           % Load steps (kN)
gama=.1;                     % N/mm De-bonding energy per unit length
cracknumber=0;               % Initialising crack number
i=0.0

kp=kp*(1+ne*p)*pi*bardia*9.81/(fcu*0.8)^0.5*1.5
for i=1:39
   loadkn=i*loadincrement*1000;
   Nc=loadkn/(1+ne*p);
   comstrain=loadkn/(as*es+ac*ec);
   lt=kp*Nc/(pi*bardia*9.81);
   if (2*lt>=(s-2*damageindex))
      [sysext,sysbarint,sysconint,sysbond,averagestress(i),...
      averagestrain(i),damageindex,straindisbar,straindiscon,...
      lengthbetcrack]=postcracking(sysext,sysbarint,sysconint,sysbond,...
      loadkn,p,ne,ft,as,b,d,ac,es,ec,lt,bardia,s,kp,gama,cracknumber,...
      damageindex,loadincrement)

 % Average stress calculation of the concrete
 else
    syms x
```

```
      g=int(loadkn-(0.5*(cos(pi*x/lt)+1)*(loadkn/(as*es)-comstrain)+....
        comstrain)*(es*as),x,0,lt)/ac;
      conaveragestress=(eval(g)*2+comstrain*(s-2*lt-2*damageindex)*ec)/...
        (s-2*damageindex)
      maxstress=loadkn/(as*es+ac*ec)*ec;
      ft=0.85*ftt*(maxstress/conaveragestress)^.6;

  % Cracking criterion
      if (comstrain >= ft/ec)
        [sysext,sysbarint,sysconint,sysbond,averagestress(i),...
          averagestrain(i),damageindex,s,cracknumber,ft,...
          straindisbar,straindiscon,lengthbetcrack]=cracking...
          (sysext,sysbarint,sysconint,sysbond,loadkn,p,ne,ft,as,b,...
          d,kp,ac,es,ec,lt,bardia,s,gama,cracknumber,damageindex,...
          loadincrement)

      else
        [sysext,sysbarint,sysconint,sysbond,averagestress(i),...
          averagestrain(i),damageindex,ft,straindisbar,...
          straindiscon,lengthbetcrack]=intermediatecracking...
          (sysext,sysbarint,sysconint,sysbond,loadkn,p,ne,kp,ft,...
          as,b,d,ac,es,ec,lt,bardia,s,gama,cracknumber,damageindex,...
          loadincrement)
      end
    end

%%%%%%%%%%%%%%%%%%%%%%%%%%%%%%%%%
% Plotting the results                                    %
%%%%%%%%%%%%%%%%%%%%%%%%%%%%%%%%%

    r=0.0
    straincon=[]
    strainbar=[]
    lengthalongbar=[]
    for j=1:2^(cracknumber)
      straincon=[straincon straindiscon]
      strainbar=[strainbar straindisbar]
      lengthalongbar=[lengthalongbar lengthbetcrack+r]
      r=s*j
    end
    plot(lengthalongbar,strainbar, lengthalongbar,straincon)
    hold on
ddmageindex(i)=damageindex
end
hold off
figure
% average stress strain dis bare bar stress strain distribution.
barebarstrain=linspace(0,0.018,50)
barebarstress=es*barebarstrain
plot(averagestrain, averagestress, barebarstrain, barebarstress,...
  experiment(2:end,20:20),experiment(2:end,21:21))
```

```
%%%%%%%%%%%%%%%%%%%%%%%%%%%%%%%%%%%%%%%%%%%%%%%%%%
% SUBROUTINE : INTERMEDIATE CRACKING                          %
%%%%%%%%%%%%%%%%%%%%%%%%%%%%%%%%%%%%%%%%%%%%%%%%%%

function [sysext,sysbarint,sysconint,sysbond,averagestress,averagestrain,...
        damageindex,ft,straindisbar,straindiscon,...
        lengthbetcrack]=intermediatecracking(sysext,sysbarint,...
        sysconint,sysbond,loadkn,p,ne,kp,ft,as,b,d,ac,es,ec,lt,...
        bardia,s,gama,cracknumber,damageindex,loadincrement)

Nc=loadkn/(1+ne*p)
comstrain=loadkn/(as*es+ac*ec)
Nclast=(loadkn-loadincrement*1000)/(1+ne*p)
loadknlast=loadkn-loadincrement*1000
comstrainlast=loadknlast/(as*es+ac*ec)
lt=kp*(Nc/(pi*bardia*9.81))
ltlast=kp*(Nclast/(pi*bardia*9.81))

i=0.0

for newdamageindex=linspace(damageindex,s/2-lt,50)
  i=i+1
  syms x

  % External work
  deltadistransfer1=(int(0.5*(cos(pi*x/lt)+1)*(loadkn/(as*es)-comstrain)...
     +comstrain,x,0,lt)+newdamageindex*loadkn/(as*es)+(s/2-lt-...
     newdamageindex)*comstrain)*.5*loadkn

  deltadistransfer2=(int(0.5*(cos(pi*x/ltlast)+1)*(loadknlast/(as*es)+...
     comstrainlast)+comstrainlast,x,0,ltlast)+(s/2-ltlast-damageindex)...
     *comstrainlast+damageindex*loadknlast/(as*es))*0.5*loadknlast

  deltasysext(i)=eval(deltadistransfer1-deltadistransfer2)


  % Steel internal work
  deltasysbar1=0.5*es*as*int((0.5*(cos(pi*x/lt)+1)*(loadkn/(as*es)-...
     comstrain)+comstrain)^2,x,0,lt)+0.5*es*as*newdamageindex*(loadkn/...
     (es*as))^2+0.5*as*es*(s/2-lt-newdamageindex)*comstrain^2

  deltasysbar2=0.5*es*as*int((0.5*(cos(pi*x/ltlast)+1)*(loadknlast/...
     (as*es)-comstrainlast)+comstrainlast)^2,x,0,ltlast)+0.5*es*as*...
     damageindex*(loadknlast/(es*as))^2+0.5*as*es*(s/2-ltlast-....
     damageindex)*comstrainlast^2

  deltasysbarint(i)=eval(deltasysbar1-deltasysbar2)


% Concrete internal work
  deltasyscon1=0.5*ec*ac*int(((loadkn-(0.5*(cos(pi*x/lt)+1)*(loadkn/...
```

```
    (as*es)-comstrain)+comstrain)*es*as)/(ac*ec))^2,x,0,lt)+0.5*ac*...
    ec*(s/2-lt-newdamageindex)*comstrain^2

deltasyscon2=0.5*ec*ac*int(((loadknlast-(0.5*(cos(pi*x/ltlast)+1)*...
    (loadknlast/(as*es)+comstrainlast)+comstrainlast)*es*as)/...
    (ac*ec))^2,x,0,ltlast)+0.5*ac*ec*(s/2-lt-damageindex)...
    *comstrainlast^2

deltasysconint(i)=eval(deltasyscon1-deltasyscon2)

 % Sliding
delslid1=0.5*pi*bardia*int(es*bardia/4*diff((0.5*(cos(pi*x/lt)+1))*...
    (loadkn/(as*es)-comstrain)+comstrain)*(int(0.5*(cos(pi*x/lt)+1)*...
    (loadkn/(as*es)-comstrain)+comstrain,x,0,lt)-int(0.5*(cos(pi*x/lt)...
    +1)*(loadkn/(as*es)-comstrain)+comstrain)),x,0,lt)

delslid2=0.5*pi*bardia*int(es*bardia/4*diff((0.5*(cos(pi*x/ltlast)+1)...
    *(loadknlast/(as*es)-comstrainlast)+comstrainlast))*(int(0.5*...
    (cos(pi*x/ltlast)+1)*(loadknlast/(as*es)-comstrainlast)+...
    comstrainlast,x,0,lt)-int(0.5*(cos(pi*x/ltlast)+1)*(loadknlast/...
    (as*es)-comstrainlast)+comstrainlast)),x,0,ltlast)

deltasliding(i)=-eval(delslid1-delslid2)

% Debonding
deltadebond(i)=gama*pi*bardia*(newdamageindex-damageindex)

% Energy balance before and after the load increment.
energydiff(i)=deltasysext(i)-(deltasysbarint(i)+deltasysconint(i))-...
    deltasliding(i)-deltadebond(i)
predamageindex(i)=newdamageindex
 end

 [value number]=min(abs(energydiff))
 for i=50:2
    if energydiff(i)>=0.0 & energydiff(i-1)<=0.0
       number=i-1
    elseif energydiff(i)<=0.0 & energydiff(i-1)>=0.0
       number=i-1
    end
 end

 damageindex=predamageindex(number)
 sysext=sysext+2^(cracknumber+1)*deltasysext(number)
 sysbarint=sysbarint+2^(cracknumber+1)*deltasysbarint(number)
 sysconint=sysconint+2^(cracknumber+1)*deltasysconint(number)
 sysbond=sysbond+2^(cracknumber+1)*deltasliding(number)
 totalstrain=2^(cracknumber+1)*(damageindex*loadkn/(as*es)+(s/2-lt-...
    damageindex)*loadkn/(as*es+ac*ec)+int(0.5*(cos(pi*x/lt)+1)*...
    (loadkn/(as*es)-comstrain)+comstrain,x,0,lt))
 length=2^(cracknumber+1)*s/2
```

```
averagestress=loadkn/as
averagestrain=eval(totalstrain)/length

% Recording the new state of stresses strain and damage length
damagelength1=linspace(0,damageindex,11)
damagelength2=linspace(s-damageindex,s,11)
transitionallength1=linspace(damageindex,(damageindex+lt),11)
transitionallength2=linspace(s-damageindex-lt,s-damageindex,11)
compositelength1=linspace(damageindex+lt,s/2,11)
compositelength2=linspace(s/2,s-lt-damageindex,11)
xi=linspace(0,lt,11)
xxi=linspace(lt,0,11)
strainbardambar(1:11)=loadkn/(es*as)
transitionalstrain1=0.5*(cos(pi*xi/lt)+1)*(loadkn/(as*es)-comstrain)...
   +comstrain,xi
transitionalstrain2=0.5*(cos(pi*xxi/lt)+1)*(loadkn/(as*es)-comstrain)...
   +comstrain,xxi
compositestrain(1:11)=loadkn/(as*es+ac*ec)
strainbardamcon(1:11)=0.0
transitionalstraincon1=(loadkn-(0.5*(cos(pi*xi/lt)+1)*(loadkn/(as*es)-...
   comstrain)+comstrain)*as*es)/(ac*ec),xi
transitionalstraincon2=(loadkn-(0.5*(cos(pi*xxi/lt)+1)*(loadkn/(as*es)-...
   comstrain)+comstrain)*as*es)/(ac*ec),xxi
compositestraincon(1:11)=loadkn/(as*es+ac*ec)
lengthbetcrack=[damagelength1 transitionallength1 compositelength1 ...
   compositelength2 transitionallength2 damagelength2]
straindisbar=[strainbardambar  transitionalstrain1  compositestrain ...
   compositestrain transitionalstrain2  strainbardambar]
straindiscon=[strainbardamcon transitionalstraincon1  compositestraincon...
   compositestraincon  transitionalstraincon2 strainbardamcon]
```

```
%%%%%%%%%%%%%%%%%%%%%%%%%%%%%%%%%%%%%%%%%%%%%%%%%%%%%%%
% SUBROUTINE: CRACKING                                  %
%%%%%%%%%%%%%%%%%%%%%%%%%%%%%%%%%%%%%%%%%%%%%%%%%%%%%%%

function[sysext,sysbarint,sysconint,sysbond,averagestress,averagestrain,...
    damageindex,s,cracknumber,ft,straindisbar,straindiscon,...
    lengthbetcrack]=cracking(sysext,sysbarint,sysconint,sysbond,...
    loadkn,p,ne,ft,as,b,d,kp,ac,es,ec,lt,bardia,s,gama,cracknumber,...
    damageindex,loadincrement)

Nc=loadkn/(1+ne*p)
comstrain=loadkn/(as*es+ac*ec)
lt=kp*Nc/(pi*bardia*9.81)
i=0.0
for newdamageindex=linspace(damageindex,s/4,50)
   i=i+1
% Composite action after cracking exist
   if ((s-4*newdamageindex)>=4*lt)
      syms x
       % External work
      deltadistransfer1=(int(0.5*(cos(pi*x/lt)+1)*(loadkn/(as*es)...
         -comstrain)+comstrain,x,0,lt)+newdamageindex*loadkn/...
         (as*es)+(s/4-lt-newdamageindex)*comstrain)*.5*loadkn*4

      deltadistransfer2=(int(0.5*(cos(pi*x/lt)+1)*(loadkn/(as*es)...
         -comstrain)+comstrain,x,0,lt)+damageindex*loadkn/(as*es)...
         +(s/2-lt-damageindex)*comstrain)*.5*loadkn*2

      deltasysex=eval(deltadistransfer1)-eval(deltadistransfer2)
      deltasysext(i)=deltasysex

      % Steel internal work
      deltasys=0.5*es*as*(int((0.5*(cos(pi*x/lt)+1)*(loadkn/...
         (as*es)-comstrain)+comstrain)^2,x,0,lt))*2
      deltasysbarint(i)=eval(deltasys)+0.5*es*as*newdamageindex*...
         (loadkn/(es*as))^2*4-0.5*es*as*damageindex*(loadkn/...
         (es*as))^2*2+0.5*as*es*(s-4*lt-4*newdamageindex)*...
         comstrain^2-0.5*as*es*(s-2*lt-2*damageindex)*comstrain^2

      % Concrete internal wrok
      deltasys=0.5*ec*ac*int(((loadkn-(0.5*(cos(pi*x/lt)+1)*...
         (loadkn/(as*es)-comstrain)+comstrain)*as*es)/...
         (ac*ec))^2,x,0,lt)*2
      deltasysconint(i)=eval(deltasys)+0.5*ac*ec*...
         (s-4*lt-4*newdamageindex)*comstrain^2-0.5*ac*ec*...
         (s-2*lt-2*damageindex)*comstrain^2


      % Sliding
      delslid=0.5*pi*bardia*int(es*bardia/4*diff...
         ((0.5*(cos(pi*x/lt)+1))*(loadkn/(as*es)-comstrain)...
```

```
    +comstrain)*(int(0.5*(cos(pi*x/lt)+1)*(loadkn/(as*es)...
    -comstrain)+comstrain,x,0,lt)-int(0.5*(cos(pi*x/lt)+1)*...
    (loadkn/(as*es)-comstrain)+comstrain)),x,0,lt)*2
deltasliding(i)=-eval(delslid)

% Debonding
deltadebond(i)=gama*pi*bardia*(4*newdamageindex-2*damageindex)

% Cracking
syms a
averageconstress=(int((loadkn-(0.5*(cos(pi*x/lt)+1)*...
  (loadkn/(as*es)-comstrain)+comstrain)*as*es)/ac,x,0,lt)*2+...
  comstrain*ec*(s-2*damageindex-2*lt))/(s-2*damageindex)
fa=(1.122-0.561*(a/d)-0.205*(a/d)^2+0.471*(a/d)^3-0.190*...
    (a/d)^4)/sqrt(1-a/d)
acf=10
facf=(1.22-0.561*(acf/d)-0.205*(acf/d)^2+0.471*(acf/d)^3-...
    0.190*(acf/d)^4)/sqrt(1-acf/d)
delcrack=b*(int(1/ec*averageconstress^2*a*fa^2,a,0,10)+1/ec*...
      averageconstress^2*10*facf^2*(d-acf))
  deltacrack(i)=eval(delcrack)

% Loss of composite action is consider between cracks.
else
    comstrains=0.5*(cos(pi*(s-4*newdamageindex)/...
      (4*lt))+1)*(loadkn/(as*es)-comstrain)+comstrain

    syms x
    deltadistransfer1=(int(0.5*(cos(pi*x/(s/4-newdamageindex))+1)...
      *(loadkn/(as*es)-comstrains)+comstrains,x,0,...
      (s/4-newdamageindex))+loadkn/(as*es)*newdamageindex)*4.0...
    *loadkn*0.5
        deltadistransfer2=(int(0.5*(cos(pi*x/lt)+1)*(loadkn/(as*es)...
    -comstrain)+comstrain,x,0,lt)+damageindex*loadkn/(as*es)...
    +(s/2-lt-damageindex)*comstrain)*0.5*loadkn*2.0
deltasysex=eval(deltadistransfer1)-eval(deltadistransfer2)
deltasysext(i)=deltasysex

 % Steel internal work
deltabar= 0.5*es*as*int((0.5*(cos(pi*x/(s/4-newdamageindex))...
    +1) *(loadkn/(as*es)-comstrains)+comstrains)^2,x,0,...
    (s/4-newdamageindex))*4-0.5*es*as*int((0.5*(cos(pi*x/lt)...
    +1)*(loadkn/(as*es)-comstrain)+comstrain)^2,x,0,lt)*2+...
    0.5*es*as*(4*newdamageindex-2*damageindex)*...
    (loadkn/(as*es))^2-0.5*comstrain^2*es*as*...
    (s-2*damageindex-2*lt)
deltasysbarint(i)=eval(deltabar)

 % Concrete internal work
 deltaconcrete=0.5*ec*ac*(int(((loadkn-(0.5*(cos(pi*x/...
    (s/4-newdamageindex))+1)*(loadkn/(as*es)-comstrains)...
```

```
    +comstrains)*as*es)/(ac*ec))^2,x,0,(s/4-newdamageindex)))...
    *4-0.5*ec*ac*int(((loadkn-(0.5*(cos(pi*x/lt)+1)*...
    (loadkn/(as*es)+comstrain)+comstrain)*as*es)/(ac*ec))...
    ^2,x,0,lt)*2-0.5*comstrain^2*ac*ec*(s-2*lt-2*damageindex)
deltasysconint(i)=eval(deltaconcrete)

% Sliding
 delslid1=0.5*pi*bardia*int(es*bardia/4*diff((0.5*(cos(pi*x/...
    (s/4-newdamageindex))+1)*(loadkn/(as*es)-comstrains))...
    +comstrains)*(int((0.5*(cos(pi*x/(s/4-newdamageindex))+1)...
    *(loadkn/(as*es)-comstrains)+comstrains),x,0,....
    (s/4-newdamageindex))-int(0.5*(cos(pi*x/(s/4-...
    newdamageindex))+1)*(loadkn/(as*es)-comstrains)+...
    comstrains)),x,0,(s/4-newdamageindex))*4

 delslid2=0.5*pi*bardia*int(es*bardia/4*diff((0.5*...
    (cos(pi*x/lt)+1)*(loadkn/(as*es)-comstrain))+comstrain)...
    *(int(0.5*(cos(pi*x/lt)+1)*(loadkn/(as*es)-comstrain)...
    +comstrain,x,0,lt)-int(0.5*(cos(pi*x/lt)+1)*(loadkn/...
    (as*es)-comstrain)+comstrain)),x,0,lt)*2
 delslid1=eval(delslid1)
 delslid2=eval(delslid2)

 if abs(delslid1)>abs(delslid2)
     deltasliding(i)=-(delslid1-delslid2)
 else
     deltasliding(i)=0.0
 end

 % Debonding
 deltadebond(i)=gama*pi*bardia*(4*newdamageindex-2*damageindex)

 % Cracking
 syms a
 averageconstress=(int((loadkn-(0.5*(cos(pi*x/lt)+1)*...
    (loadkn/(as*es)-comstrain)+comstrain)*as*es)/ac,x,0,lt)...
    *2+comstrain*ec*(s-2*damageindex-2*lt))/(s-2*damageindex)
 fa=(1.122-0.561*(a/d)-0.205*(a/d)^2+0.471*(a/d)^3-0.190*...
    (a/d)^4)/sqrt(1-a/d)
 acf=10
 facf=(1.22-0.561*(acf/d)-0.205*(acf/d)^2+0.471*(acf/d)^3...
    -0.190*(acf/d)^4)/sqrt(1-acf/d)
 delcrack=b*(int(1/ec*averageconstress^2*a*fa^2,a,0,10)+1/ec*...
        averageconstress^2*acf*facf^2*(d-acf))
     deltacrack(i)=eval(delcrack)
 end

 energydiff(i)=deltasysext(i)-(deltasysbarint(i)+deltasysconint(i))...
    -deltasliding(i)-deltadebond(i)-deltacrack(i)
 predamageindex(i)=newdamageindex
end
```

```
[value number]=min(abs(energydiff))
for i=50:2
   if energydiff(i)>=0.0 & energydiff(i-1)<=0.0
      number=i-1
   elseif energydiff(i)<=0.0 & energydiff(i-1)>=0.0
      number=i-1
   end
end

damageindex=predamageindex(number)
sysext=sysext+2^(cracknumber)*deltasysext(number)
sysbarint=sysbarint+2^(cracknumber)*deltasysbarint(number)
sysconint=sysconint+2^(cracknumber)*deltasysconint(number)
sysbond=sysbond+2^(cracknumber+1)*deltasliding(number)

% Recording the new state of stresses strain and crack spacing
if(s-4*damageindex>=4*lt)
   comstrain=loadkn/(as*es+ac*ec)
   totalstrain=4*(int(0.5*(cos(pi*x/lt)+1)*(loadkn/(as*es)-comstrain)+...
      comstrain,x,0,lt)+damageindex*loadkn/(as*es)+(s/4-lt-damageindex)...
      *comstrain)
else
   comstrains=0.5*(cos(pi*(s-4*damageindex)/(4*lt))+1)*(loadkn/(as*es)-...
      comstrain)+comstrain
   totalstrain=4*(int(0.5*(cos(pi*x/(s/4-damageindex))+1)*(loadkn/(as*es)...
      -comstrains)+comstrains,x,0,(s/4-damageindex))+damageindex*...
      loadkn/(as*es))
end

averagestrain=eval(totalstrain)/s
averagestress=loadkn/as
cracknumber=cracknumber+1
s=s/2

if (s-2*damageindex>=2*lt)
   damagelength1=linspace(0,damageindex,11)
   damagelength2=linspace(s-damageindex,s,11)
   transitionallength1=linspace(damageindex,(damageindex+lt),11)
   transitionallength2=linspace(s-damageindex-lt,s-damageindex,11)
   compositelength1=linspace(damageindex+lt,s/2,11)
   compositelength2=linspace(s/2,s-lt-damageindex,11)
   xi=linspace(0,lt,11)
   xxi=linspace(lt,0,11)
   strainbardambar(1:11)=loadkn/(es*as)
   transitionalstrain1=0.5*(cos(pi*xi/lt)+1)*(loadkn/(as*es)-comstrain)+...
      comstrain,xi
   transitionalstrain2=0.5*(cos(pi*xxi/lt)+1)*(loadkn/(as*es)-comstrain)+...
      comstrain,xxi
   compositestrain(1:11)=loadkn/(as*es+ac*ec)
   strainbardamcon(1:11)=0.0
```

```
    transitionalstraincon1=(loadkn-(0.5*(cos(pi*xi/lt)+1)*(loadkn/(as*es)-...
       comstrain)+comstrain)*as*es)/(ac*ec),xi
    transitionalstraincon2=(loadkn-(0.5*(cos(pi*xxi/lt)+1)*(loadkn/(as*es)...
       -comstrain)+comstrain)*as*es)/(ac*ec),xxi
    compositestraincon(1:11)=loadkn/(as*es+ac*ec)

else
    damagelength1=linspace(0,damageindex,11)
    damagelength2=linspace(s-damageindex,s,11)
    transitionallength1=linspace(damageindex,s/2,22)
    transitionallength2=linspace(s/2,s-damageindex,22)
    xi=linspace(0,s/2-damageindex,22)
    xxi=linspace(s/2-damageindex,0,22)
    strainbardambar(1:11)=loadkn/(es*as)
    transitionalstrain1=(0.5*(cos(pi*xi/(s/2-damageindex))+1)*(loadkn/...
       (as*es)-comstrains)+comstrains),xi
    transitionalstrain2=(0.5*(cos(pi*xxi/(s/2-damageindex))+1)*(loadkn/...
       (as*es)-comstrains)+comstrains),xxi
    strainbardamcon(1:11)=0.0
    transitionalstraincon1=(loadkn-(0.5*(cos(pi*xi/(s/2-damageindex))+1)*...
       (loadkn/(as*es)-comstrains)+comstrains)*as*es)/(ac*ec),xi
    transitionalstraincon2=(loadkn-(0.5*(cos(pi*xxi/(s/2-damageindex))+1)*...
       (loadkn/(as*es)-comstrains)+comstrains)*as*es)/(ac*ec),xxi
end

if (s-2*damageindex>=2*lt)
    lengthbetcrack=[damagelength1 transitionallength1 compositelength1 ....
       compositelength2 transitionallength2 damagelength2]
    straindisbar=[strainbardambar transitionalstrain1  compositestrain ....
       compositestrain transitionalstrain2 strainbardambar]
    straindiscon=[strainbardamcon transitionalstraincon1  compositestraincon ....
       compositestraincon  transitionalstraincon2 strainbardamcon]
else
    lengthbetcrack=[damagelength1 transitionallength1 transitionallength2 ...
       damagelength2]
    straindisbar=[strainbardambar transitionalstrain1 transitionalstrain2...
       strainbardambar]
    straindiscon=[strainbardamcon transitionalstraincon1 ...
       transitionalstraincon2 strainbardamcon]
end
```

```
%%%%%%%%%%%%%%%%%%%%%%%%%%%%%%%%%%%%%%%%%%%%%%%%
% SUBROUTINE : POST CRACKING                                %
%%%%%%%%%%%%%%%%%%%%%%%%%%%%%%%%%%%%%%%%%%%%%%%%

function [sysext,sysbarint,sysconint,sysbond,averagestress,averagestrain,...
     damageindex,straindisbar,straindiscon,lengthbetcrack]=postcracking...
     (sysext,sysbarint,sysconint,sysbond,loadkn,p,ne,ft,as,b,d,ac,es,...
     ec,lt,bardia,s,kp,gama,cracknumber,damageindex,loadincrement)

Nc=loadkn/(1+ne*p)
Nclast=(loadkn-loadincrement*1000)/(1+ne*p)
lt=kp*(Nc/(pi*bardia*9.81))
ltlast=kp*(Nclast/(pi*bardia*9.81))
comstrain=loadkn/(as*es+ac*ec)
comstrainlast=(loadkn-1000*loadincrement)/(ac*ec+as*es)
loadknlast=loadkn-1000*loadincrement
newstraindiff=loadkn/(as*es)-loadkn/(as*es+ac*ec)
oldstraindiff=loadknlast/(as*es)-loadknlast/(as*es+ac*ec)
if 2*ltlast<=(s-2*damageindex)%previous composite section
   midstrainlast=comstrainlast
else
   midlast=0.5*(cos(pi*(s/2-damageindex)/ltlast)+1)*(loadknlast/(as*es)-...
     comstrainlast)+comstrainlast
   midstrainlast=midlast
end

i=0.0
for newdamageindex=linspace(damageindex,s/2,50)
  i=i+1
  syms x
  % External work
  mid=0.5*(cos(pi*(s/2-newdamageindex)/lt)+1)*(newstraindiff)+comstrain
       midstrain=mid
  deltadis1=int(0.5*(cos(pi*x/(s/2-newdamageindex))+1)*(loadkn/(as*es)-...
    midstrain)+midstrain,x,0,(s/2-newdamageindex))*loadkn*0.5+ loadkn/...
    as*es)*newdamageindex*loadkn*0.5

  if 2*ltlast<=(s-2*damageindex)
    deltadis2=(int(0.5*(cos(pi*x/ltlast)+1)*(loadknlast/(as*es)-...
    comstrainlast)+comstrainlast,x,0,ltlast)+loadknlast/(as*es)*...
    damageindex+comstrainlast*(s/2-damageindex-ltlast))*loadknlast*0.5
  else
    deltadis2=(int(0.5*(cos(pi*x/(s/2-damageindex))+1)*(loadknlast/(as*es)-...
    midstrainlast)+midstrainlast,x,0,(s/2-damageindex))+loadknlast/(as*es)*...
    damageindex)*loadknlast*0.5
  end

  deltasysex= deltadis1-deltadis2
  deltasysext(i)=eval(deltasysex)

  % Steel internal work
```

```
deltasysbar1=0.5*es*as*int((0.5*(cos(pi*x/(s/2-newdamageindex))+1)*...
(loadkn/(as*es)-midstrain)+midstrain)^2,x,0,(s/2-newdamageindex))
deltasysbar1=deltasysbar1+0.5*es*as*newdamageindex*(loadkn/(as*es))^2

if 2*ltlast<=(s-2*damageindex)
   deltasysbar2=0.5*es*as*int((0.5*(cos(pi*x/ltlast)+1)*...
      (loadknlast/(as*es)-comstrainlast)+comstrainlast)^2,x,0,ltlast)
   deltasysbar2=deltasysbar2+0.5*es*as*damageindex*(loadknlast/...
      (es*as))^2+0.5*es*as*(s/2-damageindex-ltlast)*(loadknlast/...
      (es*as+ec*ec))^2
else
   deltasysbar2=0.5*es*as*int((0.5*(cos(pi*x/(s/2-damageindex))+1)*...
   (loadknlast/(as*es)-midstrainlast)+midstrainlast)^2,x,0,(s/2-...
   damageindex))
   deltasysbar2=deltasysbar2+0.5*es*as*damageindex*(loadknlast/(es*as))^2
end
deltasysbar=deltasysbar1-deltasysbar2
deltasysbarint(i)=eval(deltasysbar)

%concrete internal wrok
deltasyscon1=0.5*ec*ac*int(((loadkn-(0.5*(cos(pi*x/(s/2-...
   newdamageindex))+1)*(loadkn/(ac*ec)-midstrain)+midstrain)*as*es)...
   /(ac*ec))^2,x,0,(s/2-newdamageindex))

if 2*ltlast<=(s-2*damageindex)
   deltasyscon2=0.5*ac*ec*int(((loadknlast-(0.5*(cos(pi*x/ltlast)+1)*...
      (loadknlast/(as*es)-comstrainlast)+comstrainlast)*es*as)/...
      (ec*ac))^2,x,0,ltlast)
   deltasyscon2=deltasyscon2+0.5*es*as*(s/2-damageindex-ltlast)*...
      (comstrainlast)^2
else
   deltasyscon2=0.5*ac*ec*int(((loadknlast-(0.5*(cos(pi*x/(s/2-...
      damageindex))+1)*(loadknlast/(as*es)-midstrainlast)+...
      midstrainlast)*es*as)/(ac*ec))^2,x,0,(s/2-damageindex))
   deltasyscon2=deltasyscon2
end
deltasyscon=deltasyscon1-deltasyscon2
deltasysconint(i)=eval(deltasyscon)

% Sliding
delslid1=0.5*pi*bardia*int(es*bardia/4*diff(0.5*(cos(pi*x/(s/2-...
   newdamageindex))+1)*(loadkn/(as*es)-midstrain))*(int(0.5*...
   (cos(pi*x/(s/2-newdamageindex))+1)*(loadkn/(as*es)-midstrain)+...
      midstrain,x,0,(s/2-newdamageindex))-int(0.5*(cos(pi*x/(s/2-...
      newdamageindex))+1)*(loadkn/(as*es)-midstrain)+midstrain))...
      ,x,0,(s/2-newdamageindex))

if  (2*ltlast<=(s-2*damageindex))
            delslid2=0.5*pi*bardia*int(es*bardia/4*diff(0.5*(cos(pi*x/...
      ltlast)+1)*(oldstraindiff))*(int(0.5*(cos(pi*x/ltlast)+1)*...
      (oldstraindiff)+loadknlast/(as*es+ac*ec),x,0,ltlast)-...
```

```
        int(0.5*(cos(pi*x/ltlast)+1)*(oldstraindiff)+loadknlast/...
        (as*es+ac*ec))),x,0,ltlast)
else
   delslid2=0.5*pi*bardia*int(es*bardia/4*diff(0.5*(cos(pi*x/...
      (s/2-damageindex))+1)*(loadknlast/(as*es)-midstrainlast))*...
      (int(0.5*(cos(pi*x/(s/2-damageindex))+1)*(loadknlast/(as*es)-...
      midstrainlast)+midstrainlast,x,0,s/2-damageindex)-...
      int(0.5*(cos(pi*x/(s/2-damageindex))+1)*(loadknlast/(as*es)-...
      midstrainlast)+midstrainlast)),x,0,(s/2-damageindex))
end
delslid1=eval(delslid1)
delslid2=eval(delslid2)

if abs(delslid1)>abs(delslid2)
   deltasliding(i)=-(delslid1-delslid2)
else
   deltasliding(i)=0.0
end

   % Debonding
   deltadebond(i)=gama*pi*bardia*(newdamageindex-damageindex)

   % Energy balance
   energydiff(i)=deltasysext(i)-(deltasysbarint(i)+deltasysconint(i))-deltasliding(i)...
      -deltadebond(i)
   predamageindex(i)=newdamageindex
end

[value number]=min(abs(energydiff))
for i=50:2
   if energydiff(i)>=0.0 & energydiff(i-1)<=0.0
      number=i-1
   elseif energydiff(i)<=0.0 & energydiff(i-1)>=0.0
      number=i-1
   end
end

damageindex=predamageindex(number)
sysext=sysext+2^(cracknumber+1)*deltasysext(number)
sysbarint=sysbarint+2^(cracknumber+1)*deltasysbarint(number)
sysconint=sysconint+2^(cracknumber+1)*deltasysconint(number)
sysbond=sysbond+2^(cracknumber+1)*deltasliding(number)

midstrain=(loadkn/(as*es)-comstrain)*0.5*(cos(pi*(s/2-damageindex)/lt)+1)...
   +comstrain
totalstrain=2^(cracknumber+1)*(damageindex*loadkn/(as*es)+...
   int(0.5*(cos(pi*x/(s/2-damageindex))+1)* ...
(loadkn/(as*es)-midstrain)+midstrain,x,0,(s/2-damageindex)))
length=2^(cracknumber+1)*s/2
averagestrain=eval(totalstrain)/length
averagestress=loadkn/as
```

```
midstrain=(loadkn/(as*es)-comstrain)*0.5*(cos(pi*(s/2-damageindex)/lt)+1)...
   +comstrain
damagelength1=linspace(0,damageindex,11)
damagelength2=linspace(s-damageindex,s,11)
transitionallength1=linspace(damageindex,s/2,22)
transitionallength2=linspace(s/2,s-damageindex,22)

xi=linspace(0,s/2-damageindex,22)
xxi=linspace(s/2-damageindex,0,22)
strainbardambar(1:11)=loadkn/(es*as)
transitionalstrain1=0.5*(cos(pi*xi/(s/2-damageindex))+1)*...
   (loadkn/(as*es)-midstrain)+midstrain,xi
transitionalstrain2=0.5*(cos(pi*xxi/(s/2-damageindex))+1)*(loadkn/(as*es)...
   -midstrain)+midstrain,xxi
strainbardamcon(1:11)=0.0
transitionalstraincon1=(loadkn-(0.5*(cos(pi*xi/(s/2-damageindex))+1)*...
   (loadkn/(as*es)-midstrain)+midstrain)*as*es)/(ac*ec),xi
transitionalstraincon2=(loadkn-(0.5*(cos(pi*xxi/(s/2-damageindex))+1)*...
   (loadkn/(as*es)-midstrain)+midstrain)*as*es)/(ac*ec),xxi
lengthbetcrack=[damagelength1 transitionallength1 transitionallength2 ...
   damagelength2 ]
straindisbar=[strainbardambar  transitionalstrain1  transitionalstrain2 ...
   strainbardambar ]
straindiscon=[strainbardamcon transitionalstraincon1  ...
   transitionalstraincon2 strainbardamcon ]
```